

## **INFORMATION TO USERS**

This manuscript has been reproduced from the microfilm master. UMI films the text directly from the original or copy submitted. Thus, some thesis and dissertation copies are in typewriter face, while others may be from any type of computer printer.

**The quality of this reproduction is dependent upon the quality of the copy submitted.** Broken or indistinct print, colored or poor quality illustrations and photographs, print bleedthrough, substandard margins, and improper alignment can adversely affect reproduction.

In the unlikely event that the author did not send UMI a complete manuscript and there are missing pages, these will be noted. Also, if unauthorized copyright material had to be removed, a note will indicate the deletion.

Oversize materials (e.g., maps, drawings, charts) are reproduced by sectioning the original, beginning at the upper left-hand corner and continuing from left to right in equal sections with small overlaps.

Photographs included in the original manuscript have been reproduced xerographically in this copy. Higher quality 6" x 9" black and white photographic prints are available for any photographs or illustrations appearing in this copy for an additional charge. Contact UMI directly to order.

**ProQuest Information and Learning  
300 North Zeeb Road, Ann Arbor, MI 48106-1346 USA  
800-521-0600**

**UMI<sup>®</sup>**



**Effect of Interfacial Characteristics on Phase Inversion**

By

Kazem Seidshazileh

a Thesis Submitted to the  
Faculty of Engineering  
in Partial Fulfillment of the Requirements  
for the Degree of

**DOCTOR OF PHILOSOPHY**

Major Subject

Chemical Engineering

APPROVED:

\_\_\_\_\_  
A.M. Al Taweel

\_\_\_\_\_  
F. Hamdullahpur

\_\_\_\_\_  
M. Fels

\_\_\_\_\_  
P. Gregson

\_\_\_\_\_  
R. Pal (External Examiner)

**DALHOUSIE UNIVERSITY - DALTECH**

Halifax, Nova Scotia

1999



**National Library  
of Canada**

**Acquisitions and  
Bibliographic Services**

395 Wellington Street  
Ottawa ON K1A 0N4  
Canada

**Bibliothèque nationale  
du Canada**

**Acquisitions et  
services bibliographiques**

395, rue Wellington  
Ottawa ON K1A 0N4  
Canada

*Your file Votre référence*

*Our file Notre référence*

**The author has granted a non-exclusive licence allowing the National Library of Canada to reproduce, loan, distribute or sell copies of this thesis in microform, paper or electronic formats.**

**The author retains ownership of the copyright in this thesis. Neither the thesis nor substantial extracts from it may be printed or otherwise reproduced without the author's permission.**

**L'auteur a accordé une licence non exclusive permettant à la Bibliothèque nationale du Canada de reproduire, prêter, distribuer ou vendre des copies de cette thèse sous la forme de microfiche/film, de reproduction sur papier ou sur format électronique.**

**L'auteur conserve la propriété du droit d'auteur qui protège cette thèse. Ni la thèse ni des extraits substantiels de celle-ci ne doivent être imprimés ou autrement reproduits sans son autorisation.**

0-612-63484-1

**Canada**

DALTECH LIBRARY

AUTHORITY TO DISTRIBUTE MANUSCRIPT THESIS

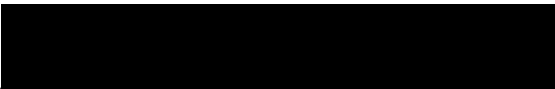
TITLE:

Effect of interfacial characteristics on phase inversion of liquid dispersion

The above library may make available or authorize another library to make available individual photo/microfilm copies of this thesis without restrictions.

Full Name of Author: Kazem Seidshazileh

Signature of Author:



Date:

August 1999 *OCT 15 1999*

**Dedicated to:**

**My beloved country:**

**The Islamic Republic of Iran**

# TABLE OF CONTENTS

<b>TABLE OF CONTENTS</b> .....	<b>IV</b>
<b>LIST OF TABLES</b> .....	<b>VII</b>
<b>LIST OF FIGURES</b> .....	<b>XI</b>
<b>LIST OF FIGURES</b> .....	<b>XI</b>
<b>NOMENCLATURE</b> .....	<b>XXX</b>
<b>ACKNOWLEDGEMENTS</b> .....	<b>XXXIII</b>
<b>ABSTRACT</b> .....	<b>XXXIV</b>
<b>1 INTRODUCTION</b> .....	<b>1</b>
<b>2 LITERATURE REVIEW</b> .....	<b>4</b>
2.1 PHASE INVERSION OF LIQUID DISPERSION .....	4
2.1.1 <i>Phenomenological Interpretation of Phase Inversion</i> .....	4
2.1.2 <i>Phase Inversion Delay Time</i> .....	7
2.1.3 <i>Effect of Hydrodynamic Factors on Phase Inversion</i> .....	9
2.1.4 <i>Effect of Interfacial Factors on Phase Inversion</i> .....	17
2.1.5 <i>Phase Inversion Experiments</i> .....	19
2.2 EFFECT OF INTERFACIAL CHARACTERISTICS ON DROP COALESCENCE.....	23
2.2.1 <i>Introduction</i> .....	23
2.2.2 <i>Effect of Mixing Time</i> .....	25
2.2.3 <i>Film Drainage</i> .....	25
2.2.4 <i>Equilibrium Interfacial Tension</i> .....	29
2.2.5 <i>Equilibrium Interfacial Concentration</i> .....	30
2.2.6 <i>Viscoelasticity</i> .....	31
2.2.7 <i>Elasticity</i> .....	35
2.2.8 <i>Diffusivity</i> .....	36
2.2.9 <i>Charge Effect</i> .....	37
2.2.10 <i>Mass Transfer Effect</i> .....	39

<b>3</b>	<b>EXPERIMENTAL</b> .....	<b>40</b>
3.1	EXPERIMENTAL SETUP.....	40
3.2	EXPERIMENTAL PROCEDURE.....	43
3.3	PHASE INVERSION MEASUREMENT .....	45
3.4	DROP SIZE MEASUREMENT .....	47
3.4.1	<i>Image Processing</i> .....	47
3.4.2	<i>Accuracy of drop size measurement</i> .....	48
3.5	REPRODUCIBILITY OF DROP SIZE MEASUREMENT .....	50
3.6	MEASUREMENT OF INTERFACIAL TENSION .....	50
3.7	DATA TREATMENT.....	51
3.7.1	<i>Drop Size Calculation</i> .....	51
3.7.2	<i>Calculation of the Equilibrium Interfacial Concentration</i> .....	56
3.7.3	<i>Diffusivity Calculation</i> .....	57
3.7.4	<i>Elasticity Calculation</i> .....	57
3.8	SYSTEMS EXAMINED.....	58
<b>4</b>	<b>RESULTS AND DISCUSSIONS</b> .....	<b>64</b>
4.1	EFFECT OF INTERFACIAL CHARACTERISTICS ON COALESCENCE .....	64
4.1.1	<i>Drop-Size Distribution</i> .....	66
4.1.1.1	Effect of Mixing Time .....	67
4.1.1.2	Effect of Gravity Forces.....	68
4.1.1.3	Number Density .....	69
4.1.1.4	Volume Density .....	71
4.1.1.5	Transient Drop Size Distribution .....	75
4.1.1.6	Self-Similarity.....	77
4.1.2	<i>Average Drop Size</i> .....	82
4.1.3	<i>Coalescence Rate</i> .....	88
4.2	PHASE INVERSION .....	92
4.2.1	<i>Effect of Hydrodynamics on Phase Inversion</i> .....	99
4.2.2	<i>Effect of Surface Active Agents on Phase Inversion</i> .....	101
4.3	INTERFACIAL CHARACTERISTICS .....	106
4.3.1	<i>Equilibrium Interfacial Tension</i> .....	106
4.3.2	<i>Equilibrium Interfacial Concentration</i> .....	107
4.3.3	<i>Dynamic Interfacial Tension</i> .....	109
4.3.4	<i>Diffusivity</i> .....	112
4.3.5	<i>Marangoni Elasticity</i> .....	119



4.4	EFFECT OF INTERFACIAL CHARACTERISTICS ON COALESCENCE AND PHASE INVERSION .....	119
4.4.1	<i>Effect of Equilibrium Interfacial Tension on Quasi-equilibrium Drop Size</i> .....	121
4.4.2	<i>Effect of Interfacial Characteristics on Coalescence Rate</i> .....	123
4.4.3	<i>Effect of Interfacial Characteristics on Phase Inversion of Systems Containing Surfactant</i> 129	
4.4.4	<i>Effect of Interfacial Characteristics on Phase Inversion of Industrial Systems</i> .....	135
5	<b>CONCLUSIONS AND RECOMMENDATIONS</b> .....	138
6	<b>REFERENCES</b> .....	148
	<b>APPENDIX A</b> .....	159
	<b>APPENDIX B</b> .....	178
	<b>APPENDIX C</b> .....	188
	<b>APPENDIX D</b> .....	199
	<b>APPENDIX E</b> .....	210
	<b>APPENDIX F</b> .....	226
	<b>APPENDIX G</b> .....	237
	<b>APPENDIX H</b> .....	242

## LIST OF TABLES

Table 1. Some phase inversion investigations in the literature.....	11
Table 2. Number of drops to make a sample used in literature .....	47
Table 3. Reproducibility of drop size measurement (0.75% acetophenon/0.05M aq. NaCl/0.1 mmole/m <sup>3</sup> at 300 rpm).....	50
Table 4. Example of drop size calculation.....	52
Table 5. Physical properties of chemical investigated at 25°C.....	59
Table 6. Physical properties of surfactants at 25°C .....	59
Table 7. Systems and condition investigated in coalescence experiments .....	61
Table 8. Synthetic systems investigated in phase-inversion experiments.....	61
Table 9. Industrial streams investigated in phase inversion experiments .....	62
Table 10. Effect of mixing time on average quasi-steady state drop size.....	68
Table 11. Regression analysis of the normalized cumulative-volume density for (0.75% acetophenon/ 0.05 molar aq. NaCl/ Triton).....	79
Table 12. Regression analysis of fitting normalized cumulative-volume density to Schwartz-Bezmer distribution .....	81
Table 13. Regression analysis of normalized cumulative-volume-densities obtained under transient condition (300→200 rpm).....	81
Table 14. Regression analysis of transient Sauter mean diameter (Eq. 28).....	87
Table 15. Quasi-equilibrium Sauter mean diameter (0.75% acetophenon / 0.05 M aq. NaCl / Triton systems).....	88

Table 16. Effect of concentration and molecular weight of surfactants on coalescence rate of the systems studied .....	90
Table 17. Parameters of Langmuir isotherm Equation for systems investigated.....	108
Table A18. The mean and the standard deviations of the quasi-steady drop-number-density. ....	159
Table A19. The correlation coefficients of the quasi-steady number density.....	159
Table A20. The mean and the standard deviations of the quasi-steady drop-volume density. ....	160
Table A21. The correlation coefficients of the quasi-steady state volume density.....	160
Table A22. The transient mean and the standard deviations of (0.75% acetophenon/ 0.05 molar aq. NaCl) .....	161
Table A23. The correlation coefficients of (0.75% acetophenon/ 0.05 molar aq. NaCl).....	161
Table A24. The transient mean and the standard deviations of (0.75% acetophenon / 0.05 molar aq. NaCl / 0.1 mmole/m <sup>3</sup> Triton X100).....	162
Table A25. The correlation coefficients of (0.75% acetophenon/ 0.05 molar aq. NaCl/ 0.1 mmole/m <sup>3</sup> Triton X100) .....	162
Table A26. The transient mean and the standard deviations of (0.75% acetophenon/ 0.05 molar aq. NaCl/ 0.2 mmole/m <sup>3</sup> Triton X100).....	163
Table A27. The correlation coefficients of fitting transient drop size to normal and log-normal distribution (0.75% acetophenon/ 0.05 molar aq. NaCl/ 0.2 mmole/m <sup>3</sup> Triton X100).....	163
Table A28. The transient mean and the standard deviations of (0.75% acetophenon / 0.05 molar aq. NaCl / 1.0 mmole/m <sup>3</sup> Triton X100).....	164
Table A29. The correlation coefficients of (0.75% acetophenon / 0.05 molar aq. NaCl /1.0 mmole/m <sup>3</sup> Triton X100) .....	164

Table A30. The transient mean and the standard deviations of (0.75% acetophenon / 0.05 molar aq. NaCl / 0.1 mmole/m <sup>3</sup> Triton X165).....	165
Table A31. The correlation coefficients of (0.75% acetophenon/ 0.05 molar aq. NaCl / 0.1 mmole/m <sup>3</sup> Triton X165) .....	165
Table A32. The transient mean and the standard deviations of (0.75% acetophenon / 0.05 molar aq. NaCl / 0.2 mmole/m <sup>3</sup> Triton X165) .....	166
Table A33. The correlation coefficients of (0.75% acetophenon / 0.05 molar aq. NaCl / 0.2 mmole/m <sup>3</sup> Triton X165) .....	166
Table A34. The transient mean and the standard deviations of (0.75% acetophenon / 0.05 molar aq. NaCl / 0.1 mmole/m <sup>3</sup> Triton X305).....	167
Table A35. The correlation coefficients of (0.75% acetophenon / 0.05 molar aq. NaCl / 0.1 mmole/m <sup>3</sup> Triton X305) .....	167
Table A36. The transient mean and the standard deviations of (0.75% acetophenon / 0.05 molar aq. NaCl / 0.2 mmole/m <sup>3</sup> Triton X305).....	168
Table A37. The correlation coefficients of (0.75% acetophenon / 0.05 molar aq. NaCl / 0.2 mmole/m <sup>3</sup> Triton X305) .....	168
Table A38. The transient mean and the standard deviations of (0.75% acetophenon / 0.05 molar aq. NaCl / 0.1 mmole/m <sup>3</sup> Triton X405).....	169
Table A39. The correlation coefficients of (0.75% acetophenon / 0.05 molar aq. NaCl / 0.1 mmole/m <sup>3</sup> Triton X405) .....	169
Table A40. The transient mean and the standard deviations of (0.75% acetophenon / 0.05 molar aq. NaCl / 0.2 mmole/m <sup>3</sup> Triton X405).....	170
Table A41. The correlation coefficients of (0.75% acetophenon / 0.05 molar aq. NaCl / 0.2 mmole/m <sup>3</sup> Triton X405) .....	170

Table A42. The correlation coefficients of normalized cumulative volume at transient condition (300→200 rpm) shown in Table 13 .....	171
Table A43. The correlation coefficients (R) of adsorption model approximation.....	172
Table A44. Is the R-value reported in Table A43, significant, at 95% confidence level?.....	174
Table A45. Regression analysis of fitting data (expanding-drop technique) into approximation model of surfactant adsorption equation. ....	176
Table A46. Linear correlation of the interfacial characteristic (x) in form of $y = a + b.x$ for (acetophenon/ 0.05 molar aq. NaCl/ 0.0-1.0 mmole/m <sup>3</sup> Triton).....	177
Table A47. Linear correlation of the interfacial characteristic (x) in form of $y = a + b.x$ for (Bayol oil/ water/ 0.0-300 mole/m <sup>3</sup> Triton, 600-1300 rpm).....	177
Table A48. Linear correlation of the interfacial characteristic (x) in form of $y = a + b.x$ for (gasoline/ industrial caustic, 600-1300 rpm). Dispersed flow rate of drop formation was 0.0316 mL/min) .....	177

## LIST OF FIGURES

Figure 1. Schematic diagram of inclusion and escape processes.....	6
Figure 2. Dynamic conductivity trace as an aqueous phase dispersed in immiscible oil inverts to oil in water (Pacek et al., 1994).....	10
Figure 3. Schematic diagram of experimental setup.....	40
Figure 4. Mixing vessel and impeller design (dimensions in inches) .....	41
Figure 5. Samples of drops imaged. ....	44
Figure 6. Impeller speed calibration curve .....	46
Figure 7. Torque calibration curve .....	46
Figure 8. Microscope calibration curve .....	49
Figure 9. Schematic diagram of the "Inverse doctor treatment" for removing elemental sulfur from gasoline in Esso Canada unit, Vancouver, BC. ....	63
Figure 10. Schematic diagram of shifting drop-size distribution due to decrease in impeller speed.....	66
Figure 11. Bimodality in volume density (0.75% acetophenon/ 0.05 molar aq. NaCl, 300→200 rpm, after 120 minutes).....	73
Figure 12. Bimodality in cumulative-volume density (0.75% acetophenon/ 0.05 molar aq. NaCl, 300→200 rpm, after 120 minutes) .....	73
Figure 13. Effect of surfactant concentration on Sauter mean diameter of (0.75% acetophenon/ 0.05 molar aq. NaCl / Triton X100) .....	84
Figure 14. Effect of surfactant molecular weight/length on Sauter mean diameter of (0.75% acetophenon / 0.05 molar aq. NaCl/ 0.1 mmole/m <sup>3</sup> Triton) .....	84
Figure 15. Effect of surfactant molecular weight/length on Sauter mean diameter of (0.75% acetophenon/0.05 molar aq. NaCl/ 0.2 mmole/m <sup>3</sup> Triton) .....	85

Figure 16. Effect of surfactant concentration on the coalescence rate of (0.75% acetophenon/ 0.05 molar aq. NaCl / Triton X100, 200 rpm).....	91
Figure 17. Effect of surfactant molecular weight/length on the coalescence rate of (0.75% acetophenon/ 0.05 molar aq. NaCl / 0.1 mmole/m <sup>3</sup> Triton, 200 rpm).....	91
Figure 18. Effect of surfactant molecular weight/length on the coalescence rate of (0.75% acetophenon/ 0.05 molar aq. NaCl / 0.2 mmole/m <sup>3</sup> Triton, 200 rpm).....	92
Figure 19. A typical example of conductivity signal during phase inversion.....	93
Figure 20. Inclusion of continuous droplets in dispersed drops (10% water/ Irving kerosene).....	95
Figure 21. High packing of droplets in drop (30% water / Irving kerosene) .....	95
Figure 22. Long dispersed drops (45% water / Irving kerosene).....	95
Figure 23. Dispersed drops of Irving kerosene in water (45% holdup).....	97
Figure 24. Effect of dispersed phase holdup on phase inversion delay time of (water/Irving gasoline system, 700 rpm).....	97
Figure 25. Effect of ( $\Phi_{\text{Catastrophic}} - \Phi_{\text{initial}}$ ) on phase inversion of (water / Irving gasoline system, 700 rpm). 99	99
Figure 26. Effect of agitation intensity on phase-inversion holdup of gasoline/water and gasoline/20%(w/w) Caustic solution.....	100
Figure 27. Effect of surfactant concentration on phase-inversion holdup of (Bayol oil/ water/ Triton X100) .....	102
Figure 28. Effect of surfactant molecular weight/length on phase-inversion holdup of (Bayol oil/ water/ Triton) .....	103
Figure 29. Effect of capacity number on phase-inversion holdup of industrial systems .....	105
Figure 30. Effect of gasoline type on phase inversion of gasoline/water .....	105

Figure 31. Effect of surfactant concentration on equilibrium interfacial tension of (Bayol oil/ water/ Triton X100) .....	107
Figure 32. Effect of surfactant concentration on equilibrium interfacial concentration of (Bayol oil/ water/ Triton X100). .....	109
Figure 33. Effect of surfactant concentration on the dynamic interfacial tension of (acetophenon / water / Triton X100, drop-volume technique) .....	111
Figure 34. Effect of surfactant concentration on the dynamic interfacial tension of (acetophenon/ water / Triton X100, maximum-drop-pressure technique).....	111
Figure 35. Effect of surfactant concentration on the Triton diffusivity in (acetophenon / water/ Triton X100) .....	115
Figure 36. Effect of surfactant molecular weight/length on the Triton diffusivity in (Bayol oil/ water/ 0.1 mole/m <sup>3</sup> Triton, drop-volume technique).....	117
Figure 37. Effect of capacity number of the industrial caustic on the apparent diffusivity of the SAA on (gasoline/ industrial caustic, expanding-drop technique).....	118
Figure 38. Effect of surfactant concentration on Marangoni interfacial elasticity of (Bayol oil/ water/ Triton X100, dispersed phase flow rate = 0.0316 mL, expanding-drop technique).....	120
Figure 39. Effect of molecular weight/length on Marangoni interfacial elasticity of (Bayol oil/ water/ 0.1 mole/m <sup>3</sup> Triton, dispersed phase flow rate = 0.0316 mL, expanding-drop technique) .....	120
Figure 40. Effect of equilibrium interfacial tension on quasi-equilibrium Sauter mean diameter of (0.75% acetophenon / water / Triton systems, 300 rpm) .....	122
Figure 41. Effect of equilibrium interfacial tension on quasi-equilibrium Sauter mean diameter for (0.75% acetophenon / water/ Triton systems, 200 rpm) .....	122
Figure 42. Effect of equilibrium interfacial tension on coalescence rate (0.75% acetophenon / 0.05 molar aq. NaCl / Triton, 200 rpm).....	123



Figure 43. Effect of equilibrium interfacial concentration on coalescence rate (0.75% acetophenon / 0.05 molar aq. NaCl / Triton, 200 rpm) .....	125
Figure 44. Effect of surfactant diffusivity on coalescence rate (0.75% acetophenon / 0.05 molar aq. NaCl / Triton, 200 rpm, drop-volume technique) .....	125
Figure 45. Effect of surfactant diffusivity on coalescence rate (0.75% acetophenon / 0.05 molar aq. NaCl / Triton, 200 rpm, maximum-drop-pressure technique) .....	126
Figure 46. Effect of Marangoni interfacial elasticity on coalescence rate (0.75% acetophenon/ 0.05 molar aq. NaCl / Triton, 200 rpm).....	128
Figure 47. Diagram of film thinning. a) surfactant soluble in the continuous phase; b) surfactant soluble in the dispersed phase (Krawczyk, et al., 1991).....	128
Figure 48. Effect of equilibrium interfacial tension on the phase inversion of (Bayol oil / water / Triton systems).....	130
Figure 49. Effect of equilibrium interfacial concentration on the phase inversion of (Bayol oil / water / Triton systems).....	131
Figure 50. Effect of surfactant diffusivity on the phase inversion of (Bayol oil / water / Triton systems).	133
Figure 51. Effect of Marangoni interfacial elasticity on the phase inversion of (Bayol oil / water / Triton X100) .....	134
Figure 52. Effect of Marangoni interfacial elasticity on the phase inversion of (Bayol oil / water / Triton) .....	134
Figure 53. Effect of equilibrium interfacial tension on phase-inversion holdup (gasoline / industrial caustic, 1000 rpm).....	136
Figure 54. Effect of SAA diffusivity on the phase inversion of (industrial systems, maximum-drop-pressure technique).....	136
Figure 55. Effect of Marangoni interfacial elasticity on the phase inversion of (industrial systems, maximum-drop-pressure technique) .....	137

Figure B56. Effect of mixing time on drop-number-density of (0.5% CLB-Bayol oil/ water/ 1.0 mmole/m <sup>3</sup> Triton X100, 250 rpm) .....	178
Figure B57. Effect of mixing time on drop-volume density of (0.5% CLB-Bayol oil/ water/ 1.0 mmole/m <sup>3</sup> Triton X100, 250 rpm) .....	178
Figure B58. Effect of mixing time on cumulative-volume density of (0.5% CLB-Bayol oil/ water/ 1.0 mmole/m <sup>3</sup> Triton X100, 250 rpm).....	179
Figure B59. Effect of mixing time on average drop size of (0.5% CLB-Bayol oil/ water/ 1.0 mmole/m <sup>3</sup> Triton X100, 250 rpm) .....	179
Figure B60. Effect of gravity on evolution of number density of (0.5% Bayol oil / water, 500→250 rpm) .....	180
Figure B61. Effect of gravity on evolution of volume density of (0.5% Bayol oil / water, 500→250 rpm) .....	180
Figure B62. Effect of gravity on evolution of cumulative-volume density of (0.5% Bayol oil / water, 500→250 rpm).....	181
Figure B63. Effect of gravity on evolution of drop mean diameter of (0.5% Bayol oil / water, 500→250 rpm).....	181
Figure B64. Effect of gravity on evolution of number density of (0.5% Bayol oil / water/ 0.25 mmole/m <sup>3</sup> Triton X100, 500→250 rpm) .....	182
Figure B65. Effect of gravity on evolution of volume density of (0.5% Bayol oil / water/ 0.25 mmole/m <sup>3</sup> Triton X100, 500→250 rpm) .....	182
Figure B66. Effect of gravity on evolution of cumulative-volume density of (0.5% Bayol oil/ water/ 0.25 mmole/m <sup>3</sup> Triton X100, 500→250 rpm) .....	183
Figure B67. Effect of gravity on evolution of drop mean diameter of (0.5% Bayol oil / water / 0.25 mmole/m <sup>3</sup> Triton X100, 500→250 rpm) .....	183

Figure B68. Effect of gravity on evolution of number density of (0.5% Bayol oil / water / 1.0 mmole/m <sup>3</sup> Triton X100, 500→250 rpm) .....	184
Figure B69. Effect of gravity on evolution of volume density of (0.5% Bayol oil/ water/ 1.0 mmole/m <sup>3</sup> Triton X100, 500→250 rpm) .....	184
Figure B70. Effect of gravity on evolution of cumulative-volume density of (0.5% Bayol oil / water / 1.0 mmole/m <sup>3</sup> Triton X100, 500→250 rpm) .....	185
Figure B71. Effect of gravity on evolution of drop mean diameter of (0.5% Bayol oil / water / 1.0 mmole/m <sup>3</sup> Triton X100, 500→250 rpm) .....	185
Figure B72. Effect of gravity on evolution of number density of (0.5% Bayol oil / water / 4.5 mmole/m <sup>3</sup> Triton X100, 500→250 rpm) .....	186
Figure B73. Effect of gravity on evolution of cumulative-volume density of (0.5% Bayol oil / water / 4.5 mmole/m <sup>3</sup> Triton X100, 500→250 rpm) .....	186
Figure B74. Effect of gravity on evolution of volume density of (0.5% Bayol oil / water / 4.5 mmole/m <sup>3</sup> Triton X100, 500→250 rpm) .....	187
Figure B75. Effect of gravity on evolution of mean drop diameter of (0.5% Bayol oil / water / 4.5 mmole/m <sup>3</sup> Triton X100, 500→250 rpm) .....	187
Figure C76. Effect of impeller speed on drop-number distribution of (0.5% CLB-Bayol oil / water).....	188
Figure C77. Effect of impeller speed on cumulative drop-number distribution of (0.5% CLB-Bayol oil / water) .....	188
Figure C78. Effect of impeller speed on drop-number distribution of (0.75% acetophenon / 0.05 molar aq. NaCl).....	189
Figure C79. Effect of impeller speed on cumulative drop-number distribution of (0.75% acetophenon / 0.05 molar aq. NaCl).....	189

Figure C80. Effect of impeller speed on drop-number-density of (0.75% acetophenon / 0.05 molar aq. NaCl / 0.1 mmole/m <sup>3</sup> Triton X100) .....	190
Figure C81. Effect of impeller speed on cumulative drop-number-density of (0.75% acetophenon / 0.05 molar aq. NaCl / 0.1 mmole/m <sup>3</sup> Triton X100).....	190
Figure C82. Effect of impeller speed on drop-number-density of (0.75% acetophenon / 0.05 molar aq. NaCl / 0.2 mmole/m <sup>3</sup> Triton X100) .....	191
Figure C83. Effect of impeller speed on cumulative drop-number- density of (0.75% acetophenon / 0.05 molar aq. NaCl / 0.2 mmole/m <sup>3</sup> Triton X100).....	191
Figure C84. Effect of impeller speed on drop-number- density of (0.75% acetophenon / 0.05 molar aq. NaCl / 1.0 mmole/m <sup>3</sup> Triton X100).....	192
Figure C85. Effect of impeller speed on cumulative drop-number- density of (0.75% acetophenon / 0.05 molar aq. NaCl / 1.0 mmole/m <sup>3</sup> Triton X100).....	192
Figure C86. Effect of impeller speed on drop-number- density of (0.75% acetophenon / 0.05 molar aq. NaCl / 0.1 mmole/m <sup>3</sup> Triton X165).....	193
Figure C87. Effect of impeller speed on cumulative drop-number- density of (0.75% acetophenon / 0.05 molar aq. NaCl / 0.1 mmole/m <sup>3</sup> Triton X165).....	193
Figure C88. Effect of impeller speed on drop-number-density of (0.75% acetophenon / 0.05 molar aq. NaCl / 0.2 mmole/m <sup>3</sup> Triton X165) .....	194
Figure C89. Effect of impeller speed on cumulative drop-number-density of (0.75% acetophenon / 0.05 molar aq. NaCl / 0.2 mmole/m <sup>3</sup> Triton X165).....	194
Figure C90. Effect of impeller speed on drop-number-density of (0.75% acetophenon / 0.05 molar aq. NaCl / 0.1 mmole/m <sup>3</sup> Triton X305) .....	195
Figure C91. Effect of impeller speed on cumulative drop-number-density of (0.75% acetophenon / 0.05 molar aq. NaCl / 0.1 mmole/m <sup>3</sup> Triton X305).....	195

Figure C92. Effect of impeller speed on drop-number-density of (0.75% acetophenon / 0.05 molar aq. NaCl / 0.2 mmole/m <sup>3</sup> Triton X305) .....	196
Figure C93. Effect of impeller speed on cumulative drop-number-density of (0.75% acetophenon / 0.05 molar aq. NaCl / 0.2 mmole/m <sup>3</sup> Triton X305).....	196
Figure C94. Effect of impeller speed on drop-number-density of (0.75% acetophenon / 0.05 molar aq. NaCl / 0.1 mmole/m <sup>3</sup> Triton X405) .....	197
Figure C95. Effect of impeller speed on cumulative drop-number-density of (0.75% acetophenon / 0.05 molar aq. NaCl / 0.1 mmole/m <sup>3</sup> Triton X405).....	197
Figure C96. Effect of impeller speed on drop-number-density of (0.75% acetophenon / 0.05 molar aq. NaCl / 0.2 mmole/m <sup>3</sup> Triton X405) .....	198
Figure C97. Effect of impeller speed on cumulative drop-number-density of (0.75% acetophenon / 0.05 molar aq. NaCl / 0.2 mmole/m <sup>3</sup> Triton X405).....	198
Figure D98. Effect of impeller speed on volume-density-distribution of (0.5% CLB-Bayol oil/water) ....	199
Figure D99. Effect of impeller speed on cumulative-volume density distribution of (0.5% CLB-Bayol oil / water) .....	199
Figure D100. Effect of impeller speed on volume-density-distribution of (0.75% acetophenon/ 0.05 molar aq. NaCl).....	200
Figure D101. Effect of impeller speed on cumulative-volume density distribution of (0.75% acetophenon / 0.05 molar aq. NaCl).....	200
Figure D102. Effect of impeller speed on volume-density-distribution of (0.75% acetophenon/ 0.05 molar aq. NaCl/ 0.1 mmole/m <sup>3</sup> Triton X100).....	201
Figure D103. Effect of impeller speed on the cumulative-volume density distribution of (0.75% acetophenon / 0.05 molar aq. NaCl / 0.1 mmole/m <sup>3</sup> Triton X100) .....	201
Figure D104. Effect of impeller speed on volume-density-distribution of (0.75% acetophenon/ 0.05 molar aq. NaCl/ 0.2 mmole/m <sup>3</sup> Triton X100).....	202

Figure D105. Effect of impeller speed on the cumulative-volume density distribution of (0.75% acetophenon / 0.05 molar aq. NaCl / 0.2 mmole/m <sup>3</sup> Triton X100) .....	202
Figure D106. Effect of impeller speed on volume-density-distribution of (0.75% acetophenon/ 0.05 molar aq. NaCl/ 1.0 mmole/m <sup>3</sup> Triton X100).....	203
Figure D107. Effect of impeller speed on the cumulative-volume density distribution of (0.75% acetophenon / 0.05 molar aq. NaCl / 1.0 mmole/m <sup>3</sup> Triton X100) .....	203
Figure D108. Effect of impeller speed on volume-density-distribution of (0.75% acetophenon/ 0.05 molar aq. NaCl/ 0.1 mmole/m <sup>3</sup> Triton X165).....	204
Figure D109. Effect of impeller speed on cumulative-volume density distribution of (0.75% acetophenon / 0.05 molar aq. NaCl / 0.1 mmole/m <sup>3</sup> Triton X165) .....	204
Figure D110. Effect of impeller speed on volume-density-distribution of (0.75% acetophenon / 0.05 molar aq. NaCl / 0.2 mmole/m <sup>3</sup> Triton X165).....	205
Figure D111. Effect of impeller speed on cumulative-volume density distribution of (0.75% acetophenon / 0.05 molar aq. NaCl / 0.2 mmole/m <sup>3</sup> Triton X165) .....	205
Figure D112. Effect of impeller speed on volume-density-distribution of (0.75% acetophenon/ 0.05 molar aq. NaCl / 0.1 mmole/m <sup>3</sup> Triton X305).....	206
Figure D113. Effect of impeller speed on the cumulative-volume density distribution of (0.75% acetophenon / 0.05 molar aq. NaCl / 0.1 mmole/m <sup>3</sup> Triton X305) .....	206
Figure D114. Effect of impeller speed on volume-density-distribution of (0.75% acetophenon/ 0.05 molar aq. NaCl / 0.2 mmole/m <sup>3</sup> Triton X305).....	207
Figure D115. Effect of impeller speed on the cumulative-volume density distribution of (0.75% acetophenon / 0.05 molar aq. NaCl / 0.2 mmole/m <sup>3</sup> Triton X305) .....	207
Figure D116. Effect of impeller speed on volume-density-distribution of (0.75% acetophenon/ 0.05 molar aq. NaCl / 0.1 mmole/m <sup>3</sup> Triton X405).....	208

Figure D117. Effect of impeller speed on the cumulative-volume density distribution of (0.75% acetophenon / 0.05 molar aq. NaCl / 0.1 mmole/m <sup>3</sup> Triton X405) .....	208
Figure D118. Effect of impeller speed on volume-density-distribution of (0.75% acetophenon/ 0.05 molar aq. NaCl / 0.2 mmole/m <sup>3</sup> Triton X405).....	209
Figure D119. Effect of impeller speed on the cumulative-volume density distribution of (0.75% acetophenon / 0.05 molar aq. NaCl / 0.2 mmole/m <sup>3</sup> Triton X405) .....	209
Figure E120. Evolution of number density of (0.75% acetophenon / 0.05 molar aq. NaCl, 300 → 200 rpm) .....	210
Figure E121. Evolution of number density of (0.75% acetophenon / 0.05 molar aq. NaCl / 0.1 mmole/m <sup>3</sup> Triton X100, 300 → 200 rpm) .....	210
Figure E122. Evolution of number density of (0.75% acetophenon / 0.05 molar aq. NaCl / 0.2 mmole/m <sup>3</sup> Triton X100, 300 → 200 rpm) .....	211
Figure E123. Evolution of number density of (0.75% acetophenon / 0.05 molar aq. NaCl / 1.0 mmole/m <sup>3</sup> Triton X100, 300 → 200 rpm) .....	211
Figure E124. Evolution of number density of (0.75% acetophenon / 0.05 molar aq. NaCl / 0.1 mmole/m <sup>3</sup> Triton X165, 300 → 200 rpm) .....	212
Figure E125. Evolution of number density of (0.75% acetophenon / 0.05 molar aq. NaCl / 0.2 mmole/m <sup>3</sup> Triton X165, 300 → 200 rpm) .....	212
Figure E126. Evolution of number density of (0.75% acetophenon / 0.05 molar aq. NaCl / 0.1 mmole/m <sup>3</sup> Triton X305, 300 → 200 rpm) .....	213
Figure E127. Evolution of number density of (0.75% acetophenon / 0.05 molar aq. NaCl / 0.2 mmole/m <sup>3</sup> Triton X305, 300 → 200 rpm) .....	213
Figure E128. Evolution of number density of (0.75% acetophenon / 0.05 molar aq. NaCl / 0.1 mmole/m <sup>3</sup> Triton X405, 300 → 200 rpm) .....	214

Figure E129. Evolution of number density of (0.75% acetophenon / 0.05 molar aq. NaCl / 0.2 mmole/m <sup>3</sup> Triton X405, 300 → 200 rpm) .....	214
Figure E130. Evolution of volume density of (0.75% acetophenon / 0.05 molar aq. NaCl, 300 → 200 rpm) .....	215
Figure E131. Evolution of volume density of 0.75% acetophenon / 0.05 molar aq. NaCl / 0.1 mmole/m <sup>3</sup> Triton X100, 300 → 200 rpm) .....	216
Figure E132. Evolution of volume density of 0.75% acetophenon / 0.05 molar aq. NaCl / 0.2 mmole/m <sup>3</sup> Triton X100, 300 → 200 rpm) .....	216
Figure E133. Evolution of volume density of 0.75% acetophenon / 0.05 molar aq. NaCl / 1.0 mmole/m <sup>3</sup> Triton X100, 300 → 200 rpm) .....	217
Figure E134. Evolution of volume density of 0.75% acetophenon / 0.05 molar aq. NaCl / 0.1 mmole/m <sup>3</sup> Triton X165, 300 → 200 rpm) .....	217
Figure E135. Evolution of volume density of 0.75% acetophenon / 0.05 molar aq. NaCl / 0.2 mmole/m <sup>3</sup> Triton X165, 300 → 200 rpm) .....	218
Figure E136. Evolution of volume density of 0.75% acetophenon / 0.05 molar aq. NaCl / 0.1 mmole/m <sup>3</sup> Triton X305, 300 → 200 rpm) .....	218
Figure E137. Evolution of volume density of 0.75% acetophenon / 0.05 molar aq. NaCl / 0.2 mmole/m <sup>3</sup> Triton X305, 300 → 200 rpm) .....	219
Figure E138. Evolution of volume density of 0.75% acetophenon / 0.05 molar aq. NaCl / 0.1 mmole/m <sup>3</sup> Triton X405, 300 → 200 rpm) .....	219
Figure E139. Evolution of volume density of 0.75% acetophenon / 0.05 molar aq. NaCl / 0.2 mmole/m <sup>3</sup> Triton X405, 300 → 200 rpm) .....	220
Figure E140. Evolution of cumulative-volume density of (0.75% acetophenon / 0.05 molar aq. NaCl, 300→200 rpm).....	221



Figure E141. Evolution of cumulative-volume density of (0.75% acetophenon / 0.05 molar aq. NaCl / 0.1 mmole/m <sup>3</sup> Triton X100, 300→200 rpm).....	221
Figure E142. Evolution of cumulative-volume density of (0.75% acetophenon / 0.05 molar aq. NaCl / 0.2 mmole/m <sup>3</sup> Triton X100, 300→200 rpm).....	222
Figure E143. Evolution of cumulative-volume density of (0.75% acetophenon / 0.05 molar aq. NaCl / 1.0 mmole/m <sup>3</sup> Triton X100, 300→200 rpm).....	222
Figure E144. Evolution of cumulative-volume density of (0.75% acetophenon / 0.05 molar aq. NaCl / 0.1 mmole/m <sup>3</sup> Triton X165, 300→200 rpm).....	223
Figure E145. Evolution of cumulative-volume density of (0.75% acetophenon / 0.05 molar aq. NaCl / 0.2 mmole/m <sup>3</sup> Triton X165, 300→200 rpm).....	223
Figure E146. Evolution of cumulative-volume density of (0.75% acetophenon / 0.05 molar aq. NaCl / 0.1 mmole/m <sup>3</sup> Triton X305, 300→200 rpm).....	224
Figure E147. Evolution of cumulative-volume density of (0.75% acetophenon / 0.05 molar aq. NaCl / 0.2 mmole/m <sup>3</sup> Triton X305, 300→200 rpm).....	224
Figure E148. Evolution of cumulative-volume density of (0.75% acetophenon / 0.05 molar aq. NaCl / 0.1 mmole/m <sup>3</sup> Triton X405, 300→200 rpm).....	225
Figure E149. Evolution of cumulative-volume density of (0.75% acetophenon / 0.05 molar aq. NaCl / 0.2 mmole/m <sup>3</sup> Triton X405, 300→200 rpm).....	225
Figure F150. Self-similarity behavior of (0.5% CLB-Bayol oil/water) at quasi-steady .....	226
Figure F151. Similarity behavior of (0.5 Bayol oil/water/ Triton) at quasi-steady .....	226
Figure F152. Self-similarity behavior of (0.75% acetophenon/ 0.05 molar aq. NaCl/ Triton, 300 rpm) at quasi-steady.....	227
Figure F153. Self-similarity behavior of (0.75% acetophenon/ 0.05 molar aq. NaCl/ Triton, 200 rpm) at quasi-steady.....	227

Figure F154. Self-similarity behavior of all systems studied at quasi-steady.....	228
Figure F155. Self-similarity behavior of temporal size distribution of (0.5% CLB-Bayol oil/ water/ 1.0 mmole/m <sup>3</sup> Triton X100, 250 rpm).....	229
Figure F156. Self-similarity behavior of temporal size distribution of (0.5% Bayol oil/ water, 500→250 rpm).....	229
Figure F157. Self-similarity behavior of temporal size distribution of 0.5% Bayol oil/ water/ 0.25 mmole/m <sup>3</sup> Triton X100, 500→250 rpm).....	230
Figure F158. Self-ilarity behavior of temporal size distribution of 0.5% Bayol oil/ water/ 1.0 mmole/m <sup>3</sup> Triton X100, 500→250 rpm) .....	230
Figure F159. Self-similarity behavior of temporal size distribution of (0.5% Bayol oil/ water/ 4.5 mmole/m <sup>3</sup> Triton X100, 500→250 rpm) .....	231
Figure F160. Self-similarity behavior of temporal size distribution of (0.75% acetophenon/ 0.05 molar aq. NaCl, 300→200 rpm).....	232
Figure F161. Self-similarity behavior of temporal size distribution (0.75% acetophenon/ 0.05 molar aq. NaCl / 0.1 mmole/m <sup>3</sup> Triton X100, 300→200 rpm).....	232
Figure F162. Self-similarity behavior of temporal size distribution (0.75% acetophenon/ 0.05 molar aq. NaCl / 0.2 mmole/m <sup>3</sup> Triton X100, 300→200 rpm).....	233
Figure F163. Self-similarity behavior of temporal size distribution (0.75% acetophenon/ 0.05 molar aq. NaCl / 1.0 mmole/m <sup>3</sup> Triton X100, 300→200 rpm).....	233
Figure F164. Self-similarity behavior of temporal size distribution (0.75% acetophenon/ 0.05 molar aq. NaCl / 0.1 mmole/m <sup>3</sup> Triton X165, 300→200 rpm).....	234
Figure F165. Self-similarity behavior of temporal size distribution (0.75% acetophenon/ 0.05 molar aq. NaCl / 0.2 mmole/m <sup>3</sup> Triton X165, 300→200 rpm).....	234

Figure F166. Self-similarity behavior of temporal size distribution (0.75% acetophenon/ 0.05 molar aq. NaCl / 0.1 mmole/m <sup>3</sup> Triton X305, 300→200 rpm).....	235
Figure F167. Self-similarity behavior of temporal size distribution (0.75% acetophenon/ 0.05 molar aq. NaCl / 0.2 mmole/m <sup>3</sup> Triton X305, 300→200 rpm).....	235
Figure F168. Self-similarity behavior of temporal size distribution (0.75% acetophenon/ 0.05 molar aq. NaCl / 0.1 mmole/m <sup>3</sup> Triton X405, 300→200 rpm).....	236
Figure F169. Self-similarity behavior of temporal size distribution (0.75% acetophenon/ 0.05 molar aq. NaCl / 0.2 mmole/m <sup>3</sup> Triton X405, 300→200 rpm).....	236
Figure G170. Transient average drop size of (0.75% acetophenon / 0.05 molar aq. NaCl, 300→200 rpm) .....	237
Figure G171. Transient average drop size of (0.75% acetophenon / 0.05 molar aq. NaCl / 0.1 mmole/m <sup>3</sup> Triton X100, 300→200 rpm) .....	237
Figure G172. Transient average drop size of (0.75% acetophenon/ 0.05 molar aq. NaCl / 0.2 mmole/m <sup>3</sup> Triton X100, 300→200 rpm) .....	238
Figure G173. Transient average drop size of (0.75% acetophenon/ 0.05 molar aq. NaCl / 1.0 mmole/m <sup>3</sup> Triton X100, 300→200 rpm) .....	238
Figure G174. Transient average drop size of (0.75% acetophenon/ 0.05 molar aq. NaCl / 0.1 mmole/m <sup>3</sup> Triton X165, 300→200 rpm) .....	239
Figure G175. Transient average drop size of (0.75% acetophenon/ 0.05 molar aq. NaCl / 0.2 mmole/m <sup>3</sup> Triton X165, 300→200 rpm) .....	239
Figure G176. Transient average drop size of (0.75% acetophenon / 0.05 molar aq. NaCl / 0.1 mmole/m <sup>3</sup> Triton X305, 300→200 rpm) .....	240
Figure G177. Transient average drop size of (0.75% acetophenon / 0.05 molar aq. NaCl / 0.2 mmole/m <sup>3</sup> Triton X305, 300→200 rpm) .....	240

Figure G178. Transient average drop size of (0.75% acetophenon / 0.05 molar aq. NaCl / 0.1 mmole/m <sup>3</sup> Triton X405, 300→200 rpm) .....	241
Figure G179. Transient average drop size of (0.75% acetophenon / 0.05 molar aq. NaCl / 0.2 mmole/m <sup>3</sup> Triton X405, 300→200 rpm) .....	241
Figure H180. Effect of surfactant concentration on equilibrium interfacial tension of (acetophenon/ water/ Triton) .....	242
Figure H181. Effect of surfactant concentration on equilibrium interfacial tension of (Bayol Oil/ water/ Triton) .....	242
Figure H182. Equilibrium interfacial tension of gasoline/industrial caustics) .....	243
Figure H183. Effect of molecular weight/length on interfacial concentration of acetophenon/ water/ 0.1 mmole/m <sup>3</sup> Triton).....	244
Figure H184. Effect of molecular weight/length on equilibrium interfacial concentration of (Bayol oil/ water/ 0.1 mmole/m <sup>3</sup> Triton).....	244
Figure H185. Effect of surfactant molecular weight/length on the dynamic Interfacial tension of (acetophenon / water / 0.1 mmole/m <sup>3</sup> Triton, drop-volume technique).....	245
Figure H186. Effect of surfactant molecular weight/length on the dynamic interfacial tension of (acetophenon / water / 0.1 mmole/m <sup>3</sup> Triton, maximum-drop-pressure-technique).....	245
Figure H187. Effect of surfactant molecular weight/length on the dynamic interfacial tension of (acetophenon / water / 0.2 mmole/m <sup>3</sup> Triton, drop-volume technique).....	246
Figure H188. Effect of surfactant molecular weight/length on the dynamic interfacial tension of (acetophenon / water / 0.2 mmole/m <sup>3</sup> Triton, maximum-drop-pressure-technique).....	246
Figure H189. Effect of surfactant concentration on the dynamic interfacial tension of (acetophenon / water / Triton X165, drop-volume technique) .....	247
Figure H190. Effect of surfactant concentration on the dynamic interfacial tension of (acetophenon / water / Triton X165, maximum-drop-pressure-technique) .....	247

Figure H191. Effect of surfactant concentration on the dynamic interfacial tension of (acetophenon / water / Triton X305, drop-volume technique) .....	248
Figure H192. Effect of surfactant concentration on the dynamic interfacial tension of (acetophenon / water / Triton X305, maximum-drop-pressure technique).....	248
Figure H193. Effect of surfactant concentration on the dynamic interfacial tension of (acetophenon / water / Triton X405, drop-volume technique) .....	249
Figure H194. Effect of surfactant concentration on the dynamic interfacial tension of (acetophenon / water / Triton X405, maximum-drop-pressure technique).....	249
Figure H195. Effect of surfactant concentration on the dynamic interfacial tension of (Bayol oil / water / Triton X100, drop-volume technique) .....	250
Figure H196. Effect of surfactant concentration on the dynamic interfacial tension of (Bayol oil / water / Triton X100, maximum-drop-pressure-technique) .....	250
Figure H197. Effect of surfactant molecular weight /length on the dynamic interfacial tension of (Bayol oil / water / 0.1 mole/m <sup>3</sup> Triton, drop-volume technique) .....	251
Figure H198. Effect of surfactant molecular weight/length on the dynamic interfacial tension of (Bayol oil / water / 0.1 mole/m <sup>3</sup> Triton, maximum-drop-pressure technique).....	251
Figure H199. Effect of surfactant concentration on the dynamic interfacial tension of (Bayol oil / water / Triton X165, drop-volume technique) .....	252
Figure H200. Effect of surfactant concentration on the dynamic interfacial tension of (Bayol oil / water / Triton X165, maximum-drop-pressure technique).....	252
Figure H201. Effect of surfactant concentration on the dynamic interfacial tension of (Bayol oil / water / Triton X305, drop-volume technique) .....	253
Figure H202. Effect of surfactant concentration on the dynamic interfacial tension of (Bayol oil / water / Triton X305, maximum-drop-pressure technique).....	253

Figure H203. Effect of surfactant concentration on the dynamic interfacial tension of (Bayol oil / water / Triton X405, drop-volume technique) .....	254
Figure H204. Effect of surfactant concentration on the dynamic interfacial tension of (Bayol oil / water / Triton X405, maximum-drop-pressure technique).....	254
Figure H205. Effect of capacity number on the dynamic interfacial of (Irving gasoline/ industrial caustics, drop-volume technique) .....	255
Figure H206. Effect of capacity number on the dynamic interfacial of (Irving gasoline/ industrial caustics, maximum-drop-pressure technique) .....	255
Figure H207. Effect of gasoline type on the dynamic interfacial tension of (gasoline/ aqueous phase, drop-volume technique).....	256
Figure H208. Effect of gasoline type on the dynamic interfacial tension of (gasoline/ aqueous phase, maximum-drop-pressure technique) .....	256
Figure H209. Effect of surfactant molecular weight/ length on the dynamic interfacial tension of (acetophenon/ water/ 0.1 mmole/m <sup>3</sup> Triton, dispersed phase flow rate = 0.042 mLiter/min, expanding-drop technique) .....	257
Figure H210. Effect of surfactant molecular weight/ length on the dynamic interfacial tension of (Bayol oil / water / 0.1 mole/m <sup>3</sup> Triton, dispersed phase flow rate = 0.0316 mLiter/min, expanding-drop technique).....	257
Figure H211. Effect of surfactant concentration on the dynamic interfacial tension of (Bayol oil/ water/ Triton X100, dispersed phase flow rate = 0.0316 mLiter/min, expanding-drop technique) .....	258
Figure H212. Effect of capacity number on the dynamic interfacial tension of (Irving gasoline/ industrial caustics, dispersed phase flow rate = 0.0316 mLiter/min, expanding-drop technique).....	258
Figure H213. Effect of surfactant molecular weight/ length on the initial slope of dynamic interfacial tension vs. time of (acetophenon/ water/0.1 mmole/m <sup>3</sup> Triton, expanding-drop technique).....	259
Figure H214. Effect of surfactant molecular weight/ length on the initial slope of dynamic interfacial tension vs. time of (Bayol oil/ water/ 0.1 mole/m <sup>3</sup> Triton, expanding-drop technique).....	259

Figure H215. Effect of capacity number of the industrial caustic on the initial slope of the interfacial tension vs. time of (gasoline/ industrial caustic, expanding-drop technique).....	260
Figure H216. Effect of surfactant concentration on the Triton diffusivity in (Bayol oil/ water/ Triton X100) .....	261
Figure H217. Effect of surfactant molecular weight/length on the Triton diffusivity in (acetophenon/ water system, drop-volume technique) .....	262
Figure H218. Effect of surfactant molecular weight/length on the Triton diffusivity in (acetophenon/water/Triton, maximum drop-pressure-technique) .....	262
Figure H219. Effect of surfactant molecular weight/length on the Triton diffusivity in (Bayol oil/ water/ 0.1 mmole/m <sup>3</sup> Triton, drop-volume technique) .....	263
Figure H220. Effect of surfactant molecular weight/length on the Triton diffusivity in (Bayol oil/water .1 mole/m <sup>3</sup> Triton, maximum-drop-pressure technique) .....	263
Figure H221. Effect of capacity number of the industrial caustic on the apparent SAA diffusivity in (Irving gasoline/ industrial caustic, maximum-drop-pressure-technique).....	264
Figure H222. Effect of gasoline type on the apparent SAA diffusivity in (gasoline/ aqueous solutions, maximum-drop-pressure-technique).....	264
Figure H223. Effect of concentration on the SAA diffusivity in (Bayol oil / water / Triton X100, expanding-drop technique).....	265
Figure H224. Effect of molecular weight/length on the SAA diffusivity of (acetophenon/ water/ 0.1mmole/m <sup>3</sup> Triton, expanding-drop technique) .....	265
Figure H225. Effect of molecular weight/length on SAA diffusivity in (Bayol oil/ water/ 0.1 mole/m <sup>3</sup> Triton, expanding-drop technique).....	266
Figure H226. Effect of surfactant concentration on Marangoni interfacial elasticity of (acetophenon/ water/ Triton X305, dispersed phase flow rate = 0.0316 mL/min, expanding-drop technique).....	267

Figure H227. Effect of molecular weight/length on Marangoni interfacial elasticity of (acetophenon/ water / 0.1 mmole/m<sup>3</sup> Triton, expanding-drop technique) ..... 267

Figure H228. Effect of capacity number on the Marangoni interfacial elasticity of (Irving gasoline/ industrial caustics, dispersed phase flow rate = 0.0316 mLiter, expanding-drop technique)..... 268



## NOMENCLATURE

$\bar{s}$	=surface-number mean	[mm <sup>2</sup> ]
$\bar{v}$	=volume-number mean	[mm <sup>3</sup> ]
A	= Aqueous	[-]
Ca	= capillary number $\left(\frac{G\mu_c d}{2\sigma}\right)$ ;	[-]
d	= drop diameter	[mm]
D	= impeller diameter	[mm]
d <sub>32</sub>	= Sauter mean diameter;	[mm]
d <sub>pq</sub>	= mean diameter;	[mm]
Em	=Marangoni elasticity, defined by equation (39)	[mN/m]
F%	=drop cumulative-volume density	[1/mm, -]
G	= shear rate	[s <sup>-1</sup> ]
H	= tank height	[mm]
ID	= internal diameter	[mm]
M	=molar (mole/litre)	[gr/lit]
m	= mili (10 <sup>-3</sup> )	
N	= impeller revolution, drop-number density	[min <sup>-1</sup> , 1/mm]
n	=refractive index	[-]
n <sub>i</sub>	=number of drops in an interval	[-]
O	= oil phase	[-]

<b>P</b>	= power input	[watt]
<b>s.d.</b>	=standard deviation of a sample	
<b>s.e.</b>	=standard error	
<b>S</b>	= distance between the object immersed in a liquid and imaging tube	[mm]
<b>S'</b>	=apparent distance between the object immersed in a liquid and imaging tube	[mm]
<b>T</b>	= vessel diameter	[mm]
<b>t<sub>d</sub></b>	= phase inversion delay time	[sec]
<b>V%</b>	=drop-volume density	[mm <sup>2</sup> ]
<b>W</b>	= width of the impeller blade	[mm]
<b>We</b>	= Weber number, ratio of the kinetic energy to surface energy, $(\rho_c \epsilon^{2/3} d^{5/3} / \sigma)$	[-]

### **Greek**

<b><math>\epsilon</math></b>	= Energy dissipation rate per unit mass	[J/kg]
<b><math>\phi</math></b>	= Holdup	[-]
<b><math>\phi_d</math></b>	= phase-inversion holdup	[-]
<b><math>\mu</math></b>	= viscosity; micro ( $10^{-6}$ )	[Pa.s]
<b><math>\nu</math></b>	= kinematic viscosity	[mN.m]
<b><math>\gamma</math></b>	= interfacial tension	[mN/m]
<b><math>\rho</math></b>	= density	[kg/m <sup>3</sup> ]

### **Subscripts**

<b>A</b>	=aqueous phase
<b>c</b>	= continuous phase

**d** = dispersed phase

**I** = impeller

**O** = oil phase

## **ACKNOWLEDGEMENTS**

I thank God for health and life he gave me to start, continue and finish this work. I would also like to thank my supervisor Dr. A.M. Al Taweel for his continuous guidance, support and patience throughout the course of this study. I thank Drs. M. Fels, F. Hamdullahpur, and P. Gregson for their help, and for their participating in the examining committee. Thanks also to Dr. R. Pal for agreeing to be my external examiner.

I am thankful to Mr. R. Dube for assistance in building the experimental setup.

I wish to thank the financial support of the Higher Education Ministry of I.R. of Iran, the Iranian Research Office for Science and Technology, the Environmental Science and Technology Alliance of Canada (ESTAC), and Dalhousie University.

My thanks also go to my mother and my family, whose encouragement assisted the progress of this work. Finally my special thanks to my wife and my children whose spiritual support and understanding made this work possible.

## ABSTRACT

This thesis is mainly concerned with phase inversion and coalescence processes in immiscible liquid systems and how they are affected by their interfacial characteristics. The phase inversion was investigated using several oil-in-aqueous (O/A) and aqueous-in-oil (A/O) systems in which the interfacial characteristics were changed by the controlled addition of different concentrations of the Triton X family of non-ionic surfactants. The coalescence characteristics of O/A dispersions were determined at low dispersed-phase holdups. Little is known about the role of the interfacial characteristics in multi-phase systems, though it is believed their role is significant.

This investigation was triggered by the difficulties encountered in the “Inverse Doctor Treatment” used to remove impurities from gasoline that has been transported by pipelines carrying multiple products in sequence. The phase inversion behavior of several industrial samples obtained from this process was therefore investigated.

All experiments were carried out in a mechanically-agitated, baffled tank equipped with a single Rushton impeller. To facilitate comparison with other investigations, the dimensions of this unit were selected to conform to the “standard” dimensions used in many mixing studies. An improved imaging technique was developed and used to measure drop-size distribution. The presence of a large density difference between the continuous and dispersed phases was found to strongly affect the spatial homogeneity of the dispersion. This difficulty was overcome by imaging the dispersion away from the wall well inside the impeller stream, and by eliminating the density difference between the continuous and dispersed phase. The onset of phase inversion was identified by monitoring the dispersion conductivity, whereas the coalescence rate was determined by monitoring the temporal variation in drop-size distribution. Attention was then focused on the initial stages following a step decrease in agitation intensity where coalescence dominates.

The dynamic interfacial characteristics of the systems investigated were determined using several drop-based techniques (drop-volume technique, maximum-drop-pressure technique, and expanding-drop technique) and the resulting parameters, and factors derived therefrom (effective diffusivity, Gibbs elasticity, Marangoni elasticity) were determined.

For all the conditions investigated, the drop-size distributions, obtained from coalescence experiments, were found to follow a log-normal distribution. Furthermore, the cumulative-volume density of these distributions was found to be similar when the drop size was normalized with respect to the Sauter mean diameter.

Following a step decrease in agitation intensity, the Sauter mean diameter was found to increase rapidly and keep on increasing until a new steady state was reached. The presence of surfactants was found to result in slowing the rate of change in Sauter mean diameter as well as reducing its equilibrium value. This effect is more pronounced in higher surfactant concentrations. Our results show that the static (equilibrium) interfacial properties cannot suitably explain this behavior. On the other hand, the diffusivity of the surfactant, was found, to correlate with all coalescence rate data (covering a wide range of surfactants concentration and type) as well as quasi-steady Sauter mean diameter reasonably well.

Phase inversion was successfully interpreted as a dynamic process, in which inclusion and escape of the continuous phase droplets compete constantly. It was found that the system's tendency to invert increases as the dispersed phase holdup and agitation intensity increase, and as the surfactant concentration decreases. Significant delay times were observed in conjunction with A/O dispersions, with the magnitude being a function of the deviation from the critical phase-inversion holdup.

Our results show that the static (equilibrium) interfacial properties can not adequately be correlated with phase-inversion holdup. On the other hand, reasonably good correlation was obtained using the elasticity due to the presence of surface-active agent. Better

correlation was obtained when the diffusivity was used instead of the maximum elasticity. This was found to apply to simple systems dominated by a single surfactant as well as in the case of complex industrial streams.

## 1 INTRODUCTION

When a small amount of an immiscible oil phase is added to an aqueous one and the system is agitated, the oil becomes dispersed as oil drops that form an oil-in-aqueous dispersion (O/A). Further addition of oil to give an ever-increasing proportion eventually leads to the system becoming unstable at a certain high concentration of oil. This instability gives rise to an aqueous-in-oil dispersion (A/O); that is to say, phase inversion occurs. Conversely, starting with a small amount of water in oil eventually leads to the opposite inversion.

In the extraction/reaction process, the decision as to which phase is to stay dispersed is clearly an important one. The most obvious approach is to disperse the phase having the lowest flow rate. Since it is impossible to ensure sufficient stirring inside drops, and considering the fact that in the presence of surface active agents, drops act as rigid bodies, Weiss (1992) suggested that the phase with the greater resistance to mass transfer become the continuous phase. However, consideration must be given to the effect of such a choice on the ease of separation in the settler. According to Stoke's Law, settling velocity is proportional to the square of the drop diameter and inversely proportional to the continuous phase viscosity (Moore 1995). Phase separation will thus be faster if the more viscous phase is dispersed. In many industrial processes, the aqueous phase is dispersed to minimize organic losses by entrainment in the raffinate (Bailes et al., 1993). In mixer/settler units, separation is generally very rapid for water-in-oil systems but is much slower for oil in water (Nienow et al., 1994; Kato et al., 1991, Leonard et al., 1981).

In large-scale mixer/settler industrial plants, the most common operating problems are phase instability (i.e., spontaneous phase inversion) and phase entrainment (i.e., overflow of one phase as an integral part of the other). Spontaneous inversion can thus be disastrous for the throughput of such equipment. Unfortunately, the factors controlling inversion are not well known, particularly in industrial situations where impure systems



exist. For example, a step change in impeller speed can deliberately trigger phase inversion in what is otherwise a stable operating condition. On the other hand, phase inversion can impart desired characteristics to certain products. For instance, the dispersed drops are often much smaller after phase inversion and, especially in the presence of surface-active agents, this inversion may give rise to a stable product emulsion. The manufacture of commercial oil-continuous emulsions can thus utilize a phase inversion step as part of the process. Such processes are employed either for reasons of necessity, in that the mixing vessels can handle only low-viscosity mixtures, or for product reasons since an inverted A/O emulsion often has significantly different properties from an emulsion with the same composition produced from a non-inversion process. Churning of cream to butter is a good example of such a process (Campbell et al., 1996).

Nadler and Mewes (1997) discussed another important application of phase inversion; namely, reducing the pressure drop required for pumping a mixture of two immiscible liquids. The turbulent mixing taking place in the pipeline can sometimes be sufficient to disperse the initially separated phases so that dispersions and emulsions are formed, resulting in higher pressure-drops being required. If oil-in-water dispersions are formed, low pressure-drops are encountered, while in the case of water-in-oil emulsions the pressure drop can be significantly higher (even higher than that needed for the pure oil alone). Lower pressure-drops can therefore be achieved by inverting a water-in-oil emulsion into an oil-in-water emulsion. Similar observations were reported by Busaiffi, (1989). Phase inversion has also been used to facilitate the separation of fine liquid-liquid dispersions (Hadjiev and Aurelle, 1995).

Phase inversion is an extremely complex phenomenon. Even though the phenomenon has been studied for about 35 years (Quinn and Sigloh, 1963), the understanding of phase inversion is still extremely poor, especially in stirred vessels (Pacek et al., 1994b; Davies, 1992). A major obstacle in studying phase inversion is the lack of appropriate measuring tools to investigate highly concentrated dispersions. Even simple breakage/coalescence

studies are rare in concentrations above 5% by volume of the dispersed phase (Bae and Tavlarides, 1989).

Many investigators have measured the phase-inversion holdup, correlated the data, and produced a mathematical model to interpret the data. Unfortunately virtually no progress has been made on producing a satisfactory physical model. There is considerable variation in the results reported in the literature and no convincing correlations exist on which to base the design (Davies, 1992). However, the phenomenological interpretation presented below (which considers the phase inversion phenomenon as being the result of two counteracting competitive processes) holds the promise of developing a better understanding of the phenomenon and reconciling what seem to be contradictory findings.

The objective of this thesis is to investigate the effect of interfacial characteristics on phase inversion in liquid dispersions produced in agitated tanks and to understand the relationship between drop coalescence and phase inversion.

To accomplish this objective, phase inversion was investigated using O/A and A/O systems in which the interfacial characteristics were changed by the controlled addition of different surfactant types and concentrations. Similarly, the coalescence characteristics of these systems were determined at low dispersed-phase volume fractions. The phase inversion characteristics of several industrial streams were also determined. Equilibrium interfacial tension was measured using the Du Noüy ring method. The dynamic interfacial characteristics of the systems investigated were determined using several drop-based techniques and the resulting parameters, and factors derived therefrom, were determined. Finally, the relationship between interfacial characteristics, coalescence rate, and phase inversion was determined.

## **2 LITERATURE REVIEW**

When two immiscible liquids are vigorously mixed, a dispersion of one in another is formed. The question as to which phase stays continuous and which becomes the dispersed phase is qualitatively answered by rules of thumb. According to these rules, the phase with less volume fraction tends to be the dispersed one. In addition, the phase that has already been the continuous phase tends to stay so. However, these rules of thumb give a very general idea about which will probably be continuous phase and have no further application.

There is evidence indicating the strong role that coalescence plays in the phase inversion of liquid dispersions. It is also believed that interfacial properties play a controlling role in both coalescence and phase inversion processes.

Much work has been conducted in trying to determine the phase boundaries at which phase inversion occurs. Holdup was found to depend on a number of features such as the physical properties of the dispersed and continuous phases, the fluid dynamic conditions in the mixing unit, the nature of the equipment surface and the presence of additives. Unfortunately, gaining a proper understanding the mechanism of phase inversion has been a challenging problem in the area of two-phase flow for the past few decades. A large part of the problem can be attributed to the lack of a consistent interpretation of the phenomenon of phase inversion. To help in presenting the previous work in a consistent manner, a phenomenological interpretation of phase inversion will be presented first. Previous work will then be presented and re-interpreted using this unified approach.

### **2.1 Phase Inversion of Liquid Dispersion**

#### **2.1.1 Phenomenological Interpretation of Phase Inversion**

This interpretation is based on the findings of many investigators and is presented here in order to achieve a clear and consistent understanding of the processes involved in phase inversion.

When drops collide, the film of the continuous phase may drain and rupture, resulting in drop coalescence. Upon coalescence, there is a chance that a portion of the draining film of the continuous phase is engulfed within the resulting larger drop. Inclusion rate increases with higher collision and coalescence rate, resulting in higher “effective” holdup. At low dispersed phase holdup, binary collision is the prevalent type of collision, and thus it is responsible for the inclusion of the continuous droplets in the dispersed drop. At high holdups, however, simultaneous collision of three or four drops is likely and thus multiple collisions may also contribute to inclusion in high holdup. The droplets of the continuous phase present in the dispersed drop may also escape to the continuous phase (Figure 1). Droplets may move inside the dispersed drop and approach the interface. If a continuous phase droplet stays close to the interface for sufficient time, the film of the dispersed phase may drain and rupture and thus droplets may coalesce with the continuous phase. Escape becomes more important when the volume of continuous droplets increases. Larger numbers of continuous droplets have less room to move inside the drop and thus have higher probability of coalescing with the interface and escaping to the continuous phase.

Phase inversion takes place when the effective holdup exceeds a certain level. Inclusion of continuous droplets in dispersed drops is opposed by their escape to the continuous phase, and thus the balance between the counteracting inclusion and escape processes will determine the effective holdup required for the phase inversion. At the beginning, the inclusion process of continuous droplets is fast, and is followed by escape as the volume of droplets of the continuous phase increases. Under certain conditions, it is possible that the escape of continuous droplets balances their inclusion, and thus leads to a constant enclosed volume. If escape balances inclusion, the effective volume of the dispersed phase may not increase and thus phase inversion will not occur. Phase inversion is a gradual process in which the volume of continuous-phase droplets in dispersed drops progressively increases until effective holdup reaches a certain level. Then, catastrophic phase inversion is triggered, in which within a short period of time, a number of extremely large drops are formed, and the system is inverted. The increase of drop size in

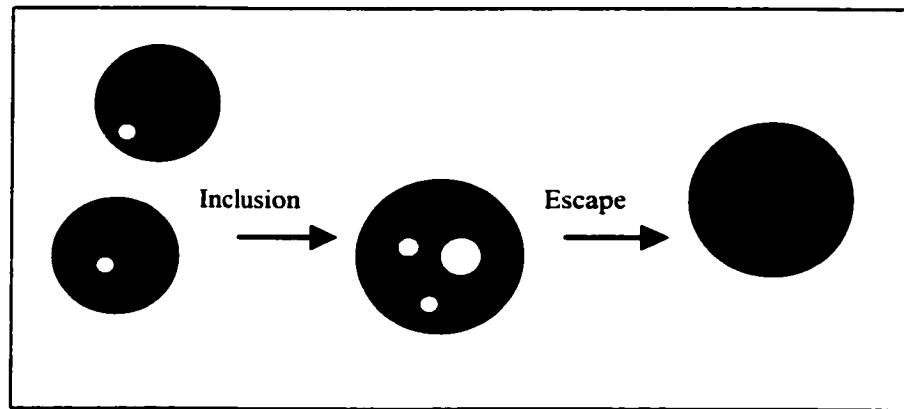


Figure 1. Schematic diagram of inclusion and escape processes

the last few seconds is so fast that it cannot be explained by simple film inclusion. An alternative explanation of this event could be that as large droplets deform easily, even a single droplet might surround and subsequently include a part of the continuous phase. Therefore, drops grow very quickly. As the duration of the final stage of phase inversion is of the same order as the time needed for dispersion preparation, a possible mechanism for catastrophic phase inversion could be that the impeller is engulfed and wetted by a very large globule drop. Such a globule drop creates a tiny inverted system around the impeller, and from that moment on the impeller recognizes the dispersed phase as continuous and breaks the former continuous phase into dispersed drops, within a few seconds. In this way, the continuous phase may be broken into dispersed drops very quickly, and phase inversion is completed rapidly.

Film drainage is an essential step in drop coalescence and thus in the inclusion process. As the viscosity of the dispersed phase decreases, draining of the continuous-phase film is shifted from a viscous- to inertia-dominated process; as a result, coalescence, and thus the inclusion of the continuous-phase droplets, decrease. Film drainage is retarded by the presence of the surface-active agent soluble in the continuous phase and therefore results in a lower coalescence and inclusion rate.

Also, as the density difference between the dispersed and continuous phases increases, the tendency of the dispersed phase to accumulate in higher or lower sections of the vessel increases and thus the chance of drop coalescence increases. However, at higher agitation intensity, gravitational effects will be lessened. Therefore, a density difference may increase the inclusion rate. In low agitation intensity, gravity effects would be pronounced.

Higher agitation intensity will increase collision frequency and therefore inclusion, but on the other hand it increases tendency to escape by deforming the dispersed-drop interface and by increasing droplets' movement. Most breakage is likely to occur in the impeller zone, where energy dissipation is very high, while coalescence has a better chance elsewhere. Inclusion of continuous-phase droplets in dispersed-phase drops takes some time before effective holdup reaches the critical value that is needed for starting catastrophic phase inversion. This period is called the phase-inversion delay time. The phase-inversion process should be considered as a time-dependent dynamic phenomenon, which takes place under conditions where the entrainment rate is higher than the escape rate. Increases in agitation intensity may increase inclusion rate as well as escape rate. Therefore, at higher impeller speed, effective holdup may reach critical holdup in a shorter delay time. However, critical holdup does not change significantly as both inclusion and escape processes may be affected by agitation intensity. As surface-active agents retard film drainage and consequently retard drop coalescence, they slow the inclusion of continuous droplets into dispersed drops. Thus, in higher concentrations of surface-active agent, critical holdup is reached after a longer delay time.

### **2.1.2 Phase Inversion Delay Time**

Phase inversion delay time is influenced by the factors that affect both the inclusion and escape processes. Using an A/O system, Gilchrist et al. (1989) were the first to study the factors affecting phase inversion delay time. They found it to be dependent on a variety of fluid-dynamic factors (impeller speed, baffling, pumping direction) and the physical properties of the system (e.g. viscosity and density ratios). Pacek et al. (1994b) reported

that phase-inversion delay time decreases with increasing dispersed phase. Recently, several investigators (Pacek et al., 1993; Nienow et al., 1994; and Groenweg et al., 1998) reported that the delay time is strongly influenced by the type and concentration of surface-active agents present in the system. For example, a ten-fold increase in phase inversion delay time was observed in the presence of trace quantities of sodium lauryl sulfate (Nienow et al., 1994).

Based on the phenomenological model proposed earlier, it is possible to make the conjecture that the phase inversion delay time depends on the net rate of the inclusion/escape processes, and the difference between the initial phase-inversion holdup and that at which the catastrophic inversion takes place. Film drainage, and thus inclusion of continuous droplets, is retarded by a SAA soluble in continuous phase or higher continuous phase viscosity. Also, as viscosity of the dispersed phase increases, delay time increases (Nienow et al., 1994), which may be attributed to a lower coalescence and inclusion rate. Gilchrist et al. (1989) postulated that the growth of the dispersed drops during the delay time is controlled by both rates of breakup and coalescence of the dispersed phase, and that inversion occurs once coalescence of the dispersed phase exceeds its breakup. Factors favoring droplet breakup of the dispersed phase retard phase inversion and therefore increase delay time whereas factors favoring coalescence of the dispersed phase accelerate phase inversion and thus shorten delay time. However, the Gilchrist et al. (1989) assumptions may not easily explain the effect of agitation intensity, which facilitates droplet breakup and at the same time reduces holdup and delay times of phase inversion. The increase of delay time has been ascribed by Pacek et al. (1994b) to either the fall in interfacial tension, the increase in viscosity of the dispersed phase or the decrease of the density difference between the phases. Pacek et al. (1994) reported that during the delay time, all mean drop sizes except  $d_{10}$  steadily grow, indicating that the total number of drops does not change significantly, while large drops are enlarged. Delay time reportedly varies between a few seconds and a few hours, and is then followed by a catastrophic phase inversion in which a dramatic increase in drop size, especially in the higher-moment diameters just before phase inversion, occurs. During

this period, a significant number of very large drops (up to 2 mm) are formed. After inversion, the drop size appears to become much smaller. Catastrophic phase inversion corresponds to a significant increase in conductivity fluctuations, as seen in Figure 2, and only takes a few seconds.

Most phase inversion studies were performed using conductivity measurements. The magnitude and fluctuation amplitude of conductivity may vary depending on the probe configuration. For example, using two plates on two sides of the vessel may not reveal conductivity fluctuations even when phase inversion is moments away. Two wires that are located close to each other may exhibit significant conductivity fluctuations as drops grow and reach a size equivalent to the wire spacing.

### **2.1.3 Effect of Hydrodynamic Factors on Phase Inversion**

Phase inversion has been investigated in different mixing devices such as mechanically agitated tanks (Pacek et al., 1994a; Norato et al., 1998; Weiss 1992; Arashmid and Jeffrey, 1980; Quin and Sigloh, 1963), static mixers (Tidhar et al., 1986), high shear rotating disks (Efthimiadu and Moore, 1994), and pipe flows (Nadler and Mewes, 1997; Pal, 1993). Since most mixing processes are presently performed in agitated tanks/columns, most investigations focused on this configuration. The effect of different geometries, impeller types and materials of construction on phase inversion was evaluated.

Several investigators (Selker and Sleicher, 1965; Nienow et al., 1994; Weiss 1992; Groeneweg et al, 1998; Norato et al., 1998) confirmed that initial conditions strongly influence the phase continuity in the ambivalence region. They showed that, within a limited range, both types of dispersion could be obtained if the impeller is located, prior to start-up, in the phase destined to be continuous. This can be explained if the inclusion process is balanced by the escape process and thus effective holdup in the ambivalent region may not be sufficient to trigger phase inversion. Some phase inversion investigation is shown in Table 1.



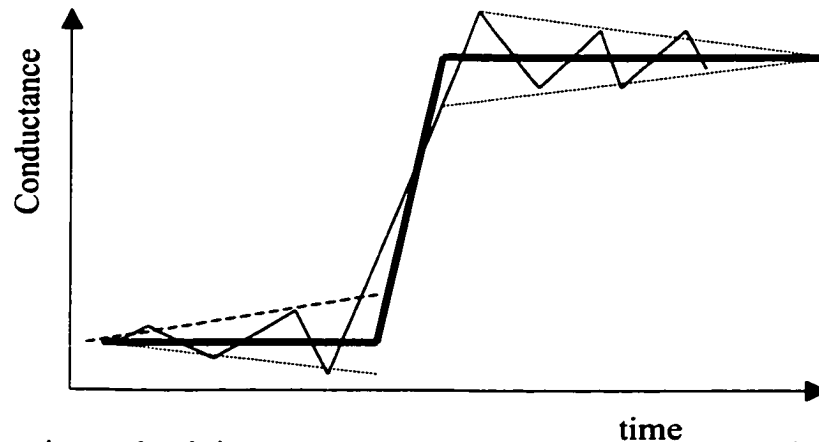


Figure 2. Dynamic conductivity trace as an aqueous phase dispersed in immiscible oil inverts to oil in water (Pacek et al., 1994)

Phase-inversion holdup of pure systems is usually higher for O/A (70-90%) than that for A/O systems (40-55%), as seen in Table 1. Based on the phenomenological model, phase inversion takes place when inclusion rate exceeds escape rate. Coalescence of the dispersed phase is lower in O/A than in A/O systems because of the charge effect of oil drops. Therefore, the inclusion rate of O/A system is lower than that of A/O system. In O/A system, the inclusion rate may increase and reach critical holdup if the initial holdup increases. Thus, phase-inversion critical holdup is higher for O/A than for A/O system.

The effect of agitation intensity on phase inversion is one of the most commonly investigated factors. The findings reported in the literature indicate that phase-inversion holdup for both O/A and A/O decreases slowly by increasing agitation intensity. Ninow et al. (1993) and Pacek et al. (1994b) found that phase-inversion holdup for both O/A and A/O systems is a weak function of impeller speed, while Groeneweg et al. (1998) reported no effect of impeller speed on phase-inversion holdup of both systems. Though a higher impeller speed increases the inclusion process by increasing collision frequency, it also increases the movement of droplets inside the drop and increases their chance of bouncing to the interface and coalescing with the continuous phase. Thus, inclusion and escape would be accelerated by increasing agitation intensity.

Table 1. Some phase inversion investigations in the literature.

Investigators	Operational Mode	Setup and conditions	Monitoring	Dispersed phase	Continuous phase	$\phi_d$ at Phase Inversion	Investigation objective(s) was to study
Groeneweg et al (1998)	Batch	Mixing tank with baffles	Conductivity, microscope	Sunflower seed oil Water	Water Sunflower seed oil	0.30-0.74	PI mechanism
Norato et al. (1998)	Batch	Mixing tank with baffles	Conductivity	Toluene+CCl <sub>4</sub> Water	Water Toluene+CCl <sub>4</sub>	0.65-0.75 0.40-0.50	Hydrodynamics of PI
Nadler and Mewes (1997)	Continuous	Long pipe	Conductivity	Mineral oil Water	Water Mineral oil	0.77 0.50	Hydrodynamics of PI
Campbell et al (1996)	Batch	Mixing tank	Conductivity	Sunflower oil	Water	N.A.	Effect of SAA, and fat crystal on PI
Efthimiadu and Moore (1994)	Continuous	Rotating plate with high shear stress	Visual	Paraffin	Water	0.10-0.45	Hydrodynamics of PI and effect of solid surface on PI
Brooks and Richmond (1994)	Batch	Mixing tank with baffles	Conductivity	Cyclohexane Water	Water Cyclohexane		Effect of SAA on PI
Nienow et al. (1993), Pacek et al (1993, 1994a, 1994b, 1995), Nienow et al (1994, 1995)	Batch	400<N<700 rpm	Video technique, Conductivity	Water 1cS silicon oil Water 20cS silicon oil Water 50cS silicon oil	1cS silicon oil Water 20cS silicon oil Water 50cS silicon oil	0.55-0.55 0.77-0.72 0.50-0.55 0.81-0.80 0.59-0.59 0.82-0.83	Hydrodynamics of PI
				Wash-out	Water	0.68	
				500 rpm	Chlorobenzene Water	0.545	

Kato et al (1991)	Batch	Mixing tank with baffles	Visual	Benzene	Water	0.717	Effect of impeller position, and SAA on PI.
				Water	Benzene	0.541	
				Toluene	Water	0.705	
				Water	Toluene	0.528	
				Cyclohexane	Water	0.843	
				Water	Cyclohexane	0.521	
				Hexane	Water	0.47-0.67	
Kumar et al., (1991)	Wash-out	T=0.105 m, Rushton turbine	Conductivity	Water	Benzene	0.41-0.51	Effect of solid interface
				Benzene	Water	0.67-0.66	
				Water	2-Methyl propanol	0.57-0.62	
				2-Methyl propanol	Water	0.85-0.80	
				Water	2-Methyl propanol	0.68-0.75	
				2-Methyl propanol	Water	0.85-0.80	
Gilchrist et al., (1989)	Batch	Mixing tank with baffles	Conductivity, video	water	Chlorobenzene	0.40-0.44	Dynamic of PI
				Chlorobenzene	Water		
Guilinger et al. (1988)	Wash-out	square vessels of side 0.10-0.27m, turbine impellers	Conductivity	KCl/H <sub>2</sub> O	Kerosene	0.41-0.51	Effect of viscosity on PI
				300<N<550 rpm			

						Kerosene	KCl/H <sub>2</sub> O	0.67-0.66	
Tidhar et al., (1986)	Continuous	Static mixer	Conductivity	Kerosene	Water			0.60-0.80	PI in static mixer
				Water	Kerosene			0.60-0.90	
Leonardo et al., (1981)	Continuous	Couette mixer	visual	Tri-n-Butyl phosphate(TBP) in n-Dodecane (nDD)	Nitric acid solution				Dispersion type in Couette flow
Arashmid and Jeffreys (1980)	Batch	T=0.102 m, four-bladed turbine	Conductivity						PI Boundary
		300<N<800 rpm		Water	Toluene			0.55-0.60	
		300<N<800 rpm		Toluene	Water			0.70-0.62	
		100<N<600 rpm		Water	CCl <sub>4</sub>			0.40-0.50	
				CCl <sub>4</sub>	Water			0.80-0.73	
				Water	Kerosene			0.45-0.52	
				Kerosene	Water			0.95-0.95	
McClarey and Mansoori (1978)	Batch	Tank T=0.127 m, up to 12 two-bladed impellers; 180<N<600 rpm	Conductivity	Sodium dichromite/H <sub>2</sub> O	Kerosene/CCl <sub>4</sub>			0.50-0.60	PI boundary
				Kerosene/CCl <sub>4</sub>	Sodium dichromite/H <sub>2</sub> O			0.73-0.77	
				Sodium dichromite/H <sub>2</sub> O	Benzene/CCl <sub>4</sub>			0.70-0.87	
				Benzene/CCl <sub>4</sub>	Sodium dichromite/H <sub>2</sub> O			0.85-0.88	
				Sodium dichromite/H <sub>2</sub> O	Benzene/CCl <sub>4</sub> /Silic one oil			0.90-0.90	

Selker and Steicher (1965)	Batch	four different tank vessels; T=0.12-0.32 m (polyethylene, glass, steel) paddle and propeller impellers 420<N< 2000 rpm	Visual, Conductivity	Benzene/CCl <sub>4</sub> - Silicone oil	Sodium dichromite/H <sub>2</sub> O	0.45-0.50	Hydrodynamic of PI
				6.5%NaCl/H <sub>2</sub> O	Isooctane/CCl <sub>4</sub>	0.54	
				Isooctane/CCl <sub>4</sub>	6.5%NaCl/H <sub>2</sub> O	0.60	
				3.4%NaCl/H <sub>2</sub> O	Isooctane/CCl <sub>4</sub>	0.43	
				Isooctane/CCL4	3.4%NaCl/H <sub>2</sub> O	0.68	
				2.9%NaCl/H <sub>2</sub> O	Isooctane	0.56	
				Isooctane	2.9%NaCl/H <sub>2</sub> O	0.72	
				2.9%NaCl/H <sub>2</sub> O	Calvous 17	0.56	
				Calvous 17	2.9%NaCl/H <sub>2</sub> O	0.86	
				2.9%NaCl/H <sub>2</sub> O	Mineral Oil	0.25	
				Mineral Oil	2.9%NaCl/H <sub>2</sub> O	0.76	
				2.9%NaCl/H <sub>2</sub> O	Nitrobenzene	0.71	
				Nitrobenzene	2.9%NaCl/H <sub>2</sub> O	0.50	
Quin and Sigloh (1963)	Batch	Mixing tank	Conductivity	Isobutanol	Water	0.60-0.63	PI Boundary
				CCl <sub>4</sub>	Water	0.4-0.47	
				Toluene	Water	0.50-0.59	
				Hexane	Water	0.45-0.57	
				Heptane	Water	0.52-0.57	

These effects counteract each other, and therefore the net balance may not effectively promote the system to phase inversion, and thus phase-inversion holdup might be only slightly affected by impeller speed variations. However, although agitation intensity has little effect on phase-inversion holdup, it significantly reduces phase inversion delay time.

Kato et al. (1991) reported that impeller position slightly affects phase-inversion holdup while Guilinger et al. (1988) found that location of the impeller within the tank does not affect phase inversion. Norato et al. (1998) found that the ratio of impeller to tank diameter has no significant effect on phase-inversion holdup. They also reported that density ratio has little effect on phase inversion boundary, whereas Kumar et al. (1991) found that systems with large density differences between the phases show a slightly greater tendency to invert. Part of the difference can be attributed to the fact that impeller speeds used by Norato et al. (1998) were higher than those used by Kumar et al., (800-1300 rpm in the former vs. 400-650 rpm for the latter) thereby counteracting the segregation tendencies. When a large difference exists between the density of the continuous and dispersed phases, drops tend to concentrate at either the top or bottom of the vessel depending on the density ratio. Such an effect will increase the chances of dispersed-phase coalescence. Higher coalescence may be interpreted as a larger chance of droplet inclusion, and thus lower initial holdup is needed for phase inversion. The density difference effect may decrease with agitation intensity, since smaller drops are less affected by the force of gravity.

Selker and Sleicher (1965) reported that both the minimum volume fraction of a hydrocarbon phase that can remain continuous, and the maximum volume fraction of a hydrocarbon phase that can be dispersed, were found to increase as the kinematic viscosity ratio, ( $\nu_O/\nu_A$ ), increases. This conclusion has been recently confirmed by Weiss (1992). These findings conform to the proposed phenomenological model since it is known that coalescence efficiency decreases as the viscosity of the dispersed phase

increases (Chesters, 1991). This leads to a reduced chance of droplet inclusion and the consequent need to go to higher holdups before phase inversion takes place.

Efthimiadu and Moore (1994) studied the phase inversion of liquid-liquid dispersions produced between shearing plates. Their setup consisted of two disks, one stationary, and the other rotating with a gap of less than 1mm between them through which the fluid mixture is passed. Liquids enter the gap through two holes at the center of the stationary plate and continuously exit via the disk circumference. Residence time and shear rate was about 3-30 sec and 2350-104,100  $\text{sec}^{-1}$  respectively. The tendency of the phase to stay continuous was found to increase with its viscosity and no ambivalent region was observed. They suggested that if parallel plates were preferentially wetted by the more viscous liquid, hydrodynamic instability could develop so that long fingers of the less viscous liquid would penetrate the more viscous one. These fingers would then break up into droplets because of the high shear-rate gradient between the plates. The parallel shearing plates may simulate the impeller zone in the agitated vessel due to high shear rate, small residence time, and low probability of drop collision. In simple shear flow, drop breakup is almost impossible if the viscosity ratio of the drop phase to the continuous phase exceeds 4.0, while for a viscosity ratio of 0.1-1.0, it is the easiest (Stone, 1994). Therefore, the tendency of a liquid to stay continuous increases with viscosity. Considering the fact that residence time is short and thus drops do not collide frequently, phase inversion in shearing plates may be controlled by a breakage rather than coalescence process. Tidhar et al. (1986) investigated phase inversion of liquid dispersions in a static mixer. Their setup consisted of a long thin stainless steel tube. They reported that the ambivalent region tends to shrink as flow velocity increases.

Very high shear rates and small residence time are shared by Efthimiadu and Moore (1994) and Tidhar et al. (1986) whose flow velocity was about 30-110 m/sec, which results in shear rate about 3000-11,000  $\text{sec}^{-1}$ , and residence time about 2.7-10 milliseconds. In both of these works, no ambivalent region was seen at high shear rates. Certainly the phenomenological model proposed earlier may not be applied to such a

condition, since phase inversion at the high shear-rate plate is fully controlled by the breakage process.

#### **2.1.4 Effect of Interfacial Factors on Phase Inversion**

Phase inversion takes place under conditions where the rate of inclusion of the continuous phase into the dispersed phase exceeds its escape rate. In general, the presence of SAA in the system was found to have a much more pronounced influence on the coalescence rate of either phase and can thus strongly influence phase inversion of either (Velve et al., 1997 and Lucasen-Reynder, 1996). For example, a large part of the confusion associated with the phase inversion literature may stem from the fact that most investigations have been conducted using essentially-pure mixtures. The phase inversion behavior of the resulting systems is thus extremely sensitive to the presence of contaminants. Yet, with the exception of very few experiments, no special precautions were undertaken to insure that the system were not contaminated by previous usage (e.g. ultrasonic cleaning).

In pure systems, drop breakup is facilitated by lower interfacial tension; the dispersion/coalescence equilibrium is shifted towards the formation of finer drops. Inclusion of continuous-phase droplets increases because coalescence rate increases with decreasing interfacial tension (Chester, 1991). However, since dispersed-phase drops are small, continuous-phase droplets can easily bounce to the interface and escape to the continuous phase. Thus, escape of the continuous-phase droplets increases rapidly with decrease in drop size. In low interfacial tension, drop size is small and the escape process rate is high; therefore, larger initial holdup is needed to reach the critical phase-inversion holdup. This conjecture explains the findings of Kumar et al. (1991) and Norato et al. (1998) that the ambivalence region widens as interfacial tension decreases.

Groenweg et al. (1998) investigated a phase-inversion system of triglyceride oil/water with surfactant tristearoyl crystals. They observed that the presence of 1% tristearoyl crystals in triglyceride oil decreased the phase-inversion holdup from 90% to 50%. This



difference is caused by the large increase in the coalescence frequency of the oil drops due to the presence of fat crystals. They explained that the fat crystals protrude into the film between the drops and enhance film rupture. This penetration into the film does not occur due to a single crystal, but by irregularities in the interfacial crystal layer. Nienow et al. (1994) investigated delay times of A/O systems and found that the presence of an oil-soluble surfactant increases phase-inversion delay time dramatically. Similarly, Kato et al., (1991) found that increasing the concentration of Tween 85 (soluble in the aqueous phase) favors the continuity of the aqueous phase of a hexane-water system in an agitated vessel, shifting the onset of phase inversion to higher holdups. A similar effect was reported by Efthimiadu and Moore (1994) who found that the presence of Tween 80 (a hydrophilic agent) in the aqueous phase favored the maintenance of aqueous-continuous dispersions. On the other hand, the presence of oleic acid (a lipophilic agent) favored the formation of the oil-continuous dispersion in rotating disks with shear flow.

Campbell et al. (1996) studied phase inversion of milk (O/A system) with different surfactants, by cooling the dispersion and monitoring the time at which phase inversion is reached. They found that formation of solid crystals is necessary for phase inversion of the system investigated and complete phase inversion of milk could be accomplished using a wide range of hydrophilic and lipophilic emulsifiers. Furthermore, they found that the type of emulsifier used did affect the inversion time with good stabilizers (skim milk powder, butter milk powder, gelatin and sodium caseinate) having long phase inversion time, and poor stabilizers (e.g. monoglycerides and lecithin) having the faster inversion times. However, they found that Tween 40, which is a good O/W stabilizer, also has a short inversion time. They suggested that emulsifier and fat crystals are both essential requirements for dispersion stabilization, and the emulsifier is responsible for positioning the fat crystals at the oil/water interface. Therefore, a poor emulsifier can not stabilize the system because fat crystals are in lower concentration at the interface.

The above findings can be systematically interpreted using the proposed phenomenological model in combination with some of the general information

concerning the effect of SAA on drop coalescence. For instance, it is well known that SAA, soluble in the continuous phase, retards film drainage and can, therefore, retard drop coalescence (Krawczyk et al., 1991 and Lucassen-Reynder, 1996). This is expected to slow down the rate of inclusion of continuous-phase droplets and shift the phase-inversion holdup to higher initial holdup values. Conversely, the presence of SAA, soluble in the dispersed phase, is known to destabilize emulsion droplets and enhance coalescence (Velve et al., 1997 and Krawczyk et al., 1991). This is expected to shift phase inversion towards lower holdups and stabilize the inverted system.

Dispersed phase coalescence, and subsequent inclusion, may be enhanced if the dispersed phase wets the solid interfaces. The coalescence of adjacent drops is promoted as they impact a wettable surface whereas coalescence of the droplets contained therein is not promoted by this action. Eftimiadu and Moore (1994) found that the liquid wetting the disks has a tendency to be continuous. Tidhar et al. (1986) found that the solid interface favors continuity of the wetting phase. Using a glass impeller instead of stainless steel, Kumar et al. (1991) could reverse the trend of the ambivalent curve of A/O, whereas for O/W dispersions the curve remains unaffected. Guilinger et al. (1988) studied the effect of tank material on phase inversion in continuous flow systems and found that the material from which the tank is built has a strong influence on the value of the phase-inversion holdup.

### **2.1.5 Phase Inversion Experiments**

#### *Phase inversion onset*

Quinn and Sigloh (1963) were the first to use a conductivity probe to monitor on line the onset of phase inversion, and since then, it has been widely used by other investigators. It is based on the observation that the conductance of most immiscible dispersions is much higher when the aqueous phase is continuous. Their conductivity probe was made of a small platinum plate mounted horizontally in the tip of a glass tube and soldered to a platinum wire. The other electrode consisted of 5 turns of platinum wire wound around

the outer tube, extending from the tip to a point 2 inches above the end of the probe. Quinn and Sigloh (1963) did not report violent fluctuations in conductance during phase inversion.

The conductivity probe used by Selker and Sleicher (1965), and then by Pacek et al. (1994a, b, 1995), and Nienow et al. (1994, 1995) simply consisted of two thin copper wires, 7 mm apart, that were placed in the upper section of the tank, close to the impeller, between the wall and the impeller shaft. Nienow and his co-workers reported large fluctuations during the period of inversion from A/O to O/A.

Campbell et al. (1996) used two parallel rectangular plates (25×4×0.5-mm thick) positioned on opposite sides of the vessel to measure the average conductance across the vessel's diameter. They subsequently observed a dramatic change in the system's conductivity with little fluctuation. Using a commercial conductivity probe, Norato et al. (1998) found little fluctuation in the transient conductance of dispersion during inversion.

The measured conductance represents the average over the whole length of the sensor and different parameters (varying from the local point value to the average at a certain radius) can be obtained by varying the geometry of the sensor. Because of its sensitivity to local conditions, a probe consisting of two wires with a small spacing arrangement will result in violent fluctuations in conductivity as the phase-inversion point is approached, due to an increase in dispersed-phase drop size. The commercial conductance meter has a probe that consists of a plastic rod with two copper rings of width about 1mm fixed to the rod with separation of about 10 mm. The drawback of such a configuration is that a drop hitting the top ring spreads, and, if large enough, it can cover both rings and therefore corrupt the measurement.

Several off-line methods can be used to determine the nature of the dispersion, with microscopy (with and without the use of UV light to identify the organic phase) being the most commonly used approach. A video camera equipped with a microscope reveals the size and structure of the dispersion. This can be used as a means for monitoring phase

inversion. This approach is very difficult and time consuming unless a fully-automated image analysis system is used.

An alternative method for determining the nature of the dispersion was proposed by Pal (1997). In it, one of the phases is added to the vessel containing the unknown dispersion; if the continuous phase is the same as the added phase then they mix easily; otherwise they will form two distinguishable layers. Leonard et al. (1981) studied a few types of dispersions and observed that the settling times of aqueous-continuous dispersions is longer than that for oil-continuous dispersions. Introducing a dimensionless number as the ratio of settling time to residence time, and plotting this ratio versus impeller speed, they found that the ratio was a function of dispersion type but independent of impeller speed.

The effective viscosity of the dispersion is a function of the viscosity of both phases, the dispersed phase holdup, the drop size and drop-size distribution, as well as the tendency towards structure formation within the system. At any particular speed, both the torque and power consumption could therefore change as phase inversion takes place. If the viscosity of two phases differ significantly, torque monitoring may be used as an online phase inversion detector. Campbell et al. (1996) investigated phase inversion of milk and found that the torque, and power consumption, varied by as much as 4-fold when the system inverted to A/O.

### *Operational Mode*

Batch mode is the most common approach used for studying phase inversion. These experiments are relatively easy to conduct and the results obtained are free from concerns such as accuracy in measuring delay time, noting that delay time is sensitive to holdup. Batch mode, therefore, has higher reproducibility than most other techniques. The drawback of this method is that it requires long experimentation times and the conduct of many runs. In the batch mode, a tank is filled with both phases and the impeller is placed in the phase to be continuous. If no phase inversion is observed after a reasonable

agitation period, the process is stopped and repeated using a different holdup and/or agitation intensity. This operational mode is very time-consuming and may not be suitable if it is necessary to investigate a large number of parameters.

In the wash-out mode used by Kumar et al. (1991) and Pacek et al. (1994a), mixing is initiated after the tank is filled with the continuous phase. The dispersed phase is then introduced in small quantities while the equivalent volume of the dispersion is simultaneously discharged. This process is continued until phase inversion is observed. At that point, the operation is stopped and the holdup measured.

As pointed out by Pacek et al. (1994a) and Gilchrist et al. (1989), the presence of air bubbles can influence the value of the delay time and, presumably, the inversion point conditions. It is therefore recommended to use closed mixers with tight openings and a lid to prevent a gas-liquid interface. Such units would more closely resemble the hydrodynamic conditions in industrial units where the presence of a central gas/liquid vortex plays a minimal role (e.g. multi-stage columns, multi-impeller mixers, and baffled tanks).

Tidhar et al. (1986) and Efthimiadu and Moor (1994) studied phase inversion in the continuous flow mode. A brief description of their experimental setup has already been supplied (section 2.1.3). Both of these investigations were completed at very high shear rate and in laminar flow with residence times of few seconds. Residence times of large-scale industrial vessels may be up to tens of minutes. In such a case, the batch or semi-batch flow vessel may better simulate large-scale vessels provided that the delay time of the experimental vessel and the residence time of the large-scale vessel are of the same order. It may be speculated that phase inversion in large-scale vessels may not happen if its residence time is smaller than the delay time of the system in the experimental vessel, even though conditions in both vessels are otherwise the same.

## **2.2 Effect of Interfacial Characteristics on Drop Coalescence**

### **2.2.1 Introduction**

For many chemical-process industry (CPI) operations, this topic is of significant importance and is covered by several reviews (Seidshazileh 1998, Chesters, 1991, and Davies, 1992). Therefore, it will be briefly discussed here with an emphasis on the issues of particular importance to phase inversion in industrially-significant systems. As pointed out by Leo et al. (1994), experimental investigation of coalescence in liquid dispersion so far has been mainly concentrated on the effects of holdup and agitation intensity.

The competing processes of drop breakage and coalescence control the drop size of the dispersed phase. In turbulent conditions, breakage is a result of the interaction between the Reynolds stresses applied on the drop by the continuous phase, and the forces resisting deformation, namely surface forces and viscous stresses in the dispersed phase. Drops moving in the continuous phase may collide with each other, and should they stay in touch a sufficiently long time, the film between them may rupture and the drops coalesce. The size of the dispersed drops is therefore controlled by two competing processes in such a way that if the breakage rate exceeds the coalescence rate, the size of the dispersed-phase drops become smaller, whereas it becomes bigger if the reverse is true. Many factors affect the rate of drop breakage and coalescence. Some factors may enhance one while retarding the other, whereas other factors may enhance/retard both phenomena by different amounts.

Hydrodynamic factors (such as energy dissipation rate, volume ratio of the dispersed to continuous phases, and the viscosity and density ratios) affect both the breakage and coalescence of drops. Mostly, drops break in the impeller region where shear rate is highest, and coalesce elsewhere. The region adjacent to the impeller zone is considered to have a large collision frequency due to the high rate of energy dissipation. In addition to the hydrodynamic factors, interfacial characteristics play an important role in determining drop size via their effect on breakage and coalescence rates. Assuming equilibrium

interfacial tension, Chatzi and Kiparissides (1994, 1995) studied the dispersion of highly concentrated *n*-butyl chloride in a water system in the presence of PVA (poly vinyl alcohol). They found that the Sauter mean diameter is not a simple function of impeller speed and goes through a minimum point as impeller speed increases. Sauter mean diameter ( $d_{32}$ ) is defined as following:

$$d_{32} = \frac{\sum_{i=1}^{all} n_i d_i^3}{\sum_{i=1}^{all} n_i d_i^2}$$

Where,

$d_i$  = drop diameter

$n_i$  = number of drops with diameter  $d_i$

They proposed that at high agitation intensity, high breakage frequency is responsible for low Sauter mean diameter. Therefore, as the interfacial area increases due to the presence of a larger number of small drops, the effectiveness of surfactant molecules on the interface begins to diminish, leading to a size increase in the droplets. Skelland and Jeffrey (1992) studied the effect of surfactant on droplet breakup in a chlorobenzene-water system. They found that as concentration of Triton X100 surfactant increases, transient Sauter mean diameter decreases.

All industrial streams contain surface active agents (e.g. alcohol, protein, organic acids, electrolytes, surfactants, finely divided catalysts, clays, and emulsions) which can significantly modify the interfacial properties of the system. Their presence is manifested in the development of viscoelastic forces at the interface and/or a reduction of the static interfacial tension. The former is created by drop-shape deformation and consequent enlargement of the interface, due to the shear stresses encountered in the mixer. Enlarged interfaces have lower surface-active concentrations and exhibit, therefore, higher interfacial tensions. Gradients of interfacial tension give rise to elastic forces (Marangoni effect) which oppose interface mobility and reduce it.

### 2.2.2 Effect of Mixing Time

Tobin and Ramkrishna (1992) found that the size of acetophenon drops dispersed in aqueous NaOH solutions reached steady state in 2 hours agitation at 600 rpm. Chatzi et al. (1991a) examined the effects of the initial state of the system on the steady state distribution by a step change in impeller speed for a system of 1% Styrene/ water/ 0.1 g/L PVA (a highly hydrolyzed SAA with very large molecular weight). Starting from zero, the steady state was reached in 1 hour for an impeller speed of 300 rpm, and in 3 hours for 200 rpm. They also found that steady state was reached in about 90 minutes for a step increase in impeller speed (200→300 rpm), while it was reached in 9 hours when the impeller speed was decreased from 300 to 200 rpm.

In system of 50% *n*-butyl chloride in water and 0.5-1.0 g/L PVA, Chatzi and Kiprassides (1995) found that steady state drop-size distribution was essentially achieved in less than 90 minutes for impeller speeds between 400-700 rpm. Calabrese et al. (1993) investigated the coalescence of silicon oil in distilled water and found that  $d_{32}$  reaches equilibrium in about one hour when the impeller speed is dropped from 330 rpm to 180 rpm.

### 2.2.3 Film Drainage

When two drops approach each other, the film between them starts draining. If the film thickness reduces to a certain critical value, about 500Å (Tsouris and Tavlarides, 1994), the film may rupture and the drops coalesce. Film draining is therefore an essential step in the coalescence process and is affected by interfacial characteristics as well as hydrodynamic factors. Complete film drainage between two drops with an immobile, deformable interface is theoretically impossible (Chesters, 1991; Tsouris and Tavlarides, 1994), while it is possible for drops with a mobile deformable interface. Drainage of a thin layer is a creeping flow (Das and Hartland, 1989). As it drains, the film pulls the interface along and stretches it.

Krawczyk et al. (1991) suggested that the solubility of the surfactant in the continuous phase is a crucial factor to emulsion stability. The dramatic difference between drop



coalescence of a system with surfactants soluble in the continuous phase, and those soluble in the dispersed phase, is due to the way the surfactant is transported from the bulk to the interface. Since the interfacial surfactant concentration increases in the direction of liquid flow, there is a region on the film interface in which the interfacial concentration is greater than its equilibrium value. Conversely, there is a region on the film interface in which the interfacial concentration is lower than its equilibrium value. In order to restore equilibrium, surfactant desorption occurs in the compressed region and surfactant adsorption occurs in the depleted region.

In systems with the surfactant in the continuous phase, the surfactant must travel from the bulk of the continuous phase to the interior of the film. However, in a system with surfactant in the drop phase, the surfactant must travel a much shorter distance. It is transported from the bulk of the droplet onto the interface across the diffusion boundary layer, whose thickness is much smaller than the film radius. Furthermore, the surfactant flux is driven by the normal gradient of concentration, so that it can completely counterbalance the perturbation of interfacial concentration caused by the interfacial convective flux. Petroleum emulsions that contain demulsifiers that are soluble only in the oil phase behave like a system with a surfactant soluble only in the continuous phase (Krawczyk et al., 1991). The advantage of demulsifier partitioning derives from the fact that petroleum emulsions containing these demulsifiers will behave more like a system with the surfactant in the drop phase, which is not stable because the interfacial-tension gradient and elasticity are suppressed.

Foam films behave like a system with surfactant in the continuous phase (Krawczyk et al., 1991). In these systems, the tension gradient has the ability to initially prevent rupture of the thin film. Since the surfactant flux in the bulk of the droplet is sufficient to suppress or eliminate tension gradients in systems with surfactant in the dispersed phase, these systems behave like oil-water systems in the absence of surfactant. The elasticity of an oil-water interface without surfactant is zero (no interfacial tension gradients). Reducing the elasticity increases the velocity of thinning, thus producing less stable

films. Krawczyk et al. (1991) concluded that for a demulsifying molecule to be sufficiently active it must be an amphiphile. Since an amphiphile is a molecule that possesses a hydrophobic part and a hydrophilic part, it is slightly soluble in the both oil and water phases. Due to this criterion and the fact that demulsifiers are initially added to the continuous (oil) phase, demulsifiers that are soluble only in water are not effective. Demulsifiers possessing a partition coefficient of unity were found to optimize performance.

Krawczyk et al. (1991) presented a conceptual model of the drop-drop coalescence process which indicates that the interfacial activity of the demulsifier must be high enough to suppress the interfacial tension gradient. This accelerates the rate of film drainage, thus promoting coalescence. The approach of two drops under capillary pressure acting normal to the interface causes liquid to be squeezed out of the film into the bulk. This liquid flow results in the convective flux of surfactant in the sublayer. Therefore, the surfactant concentration at the interface is increased in the direction of that flow. The other fluxes associated with the drainage process include:

- bulk flux in the droplet,
- bulk flux in the film phase, and
- interfacial diffusion flux caused by the concentration gradient at the interface.

The bulk fluxes can be conveniently divided into two subsequent steps:

- diffusional flux up to a layer adjacent to the film interface, and
- adsorption flux from this layer onto the interface.

Non-uniform surfactant distribution leads to interfacial flow, which in turn gives rise to interfacial stresses. The difference in concentration along the interface results in a difference in the local values of interfacial tension which, in turn, produce a force (equal per unit length to the gradient of interfacial tension) opposite to liquid flow. In addition, the surfactant monolayer may undergo dilating and shearing deformations, which also produce interfacial stresses. The sum of the above stresses and the tangential bulk stress

from the liquid in the droplet must counterbalance the tangential bulk stress from the film liquid that causes interfacial flow.

Velev et al. (1997) observed the thinning of aqueous films between xylene drops in the presence of Tween 20 and 80 (initially dissolved in water, but also soluble in oil). As soon as the film reaches a 100-nm thickness, a dimple (a lens-like formation that is thicker than the film) spontaneously forms and starts growing around its center. When the dimple becomes bigger and approaches the contact line, it forms a channel to the periphery and the water inside it flows out, leaving an almost plane-parallel film behind. Just afterwards, a new dimple starts to grow and the process repeats again and again. Velev et al. (1997) experimentally showed that dimple formation originates from the depletion of the surfactant in the film. This depletion is a result of its retarded diffusion from within the aqueous meniscus towards the film center. Following the depletion, tangential movement of the surface (connected with the Marangoni effect) appears. The movement is coupled with convective fluxes inside the film, feeding the dimple. The “diffusion dimple” appears to be a process leading to stabilizing of thin emulsion films due to the “sucking” of additional liquid between the droplets.

Velve et al. (1997) also studied film stability of a water-in-benzene system in the presence of surfactants. For a surfactant dissolved in the drop phase, they found the average lifetime of the film to be the same for all surfactant concentrations, whereas when the system is inverted (surfactant is soluble in the continuous phase) it was about 70 times higher. When the surfactant is soluble in the drop phase, the surfactant flux is carried out not only by diffusion but also by the convection of the liquid inside the drop. This results in the suppression of any interfacial tension gradients that oppose the film thinning. As a result, film thinning is rapid.

Peru and Lorenz (1989) used the spinning drop technique to study the effect of interfacial properties on the film-drainage time of crude-oil emulsions. They found that as temperature increases, coalescence time increases while film mobility decreases. Coalescence time was found to increase sharply at the beginning and then to increase gradually, upon addition of

surfactant. They also found that the area of drop contact decreases with increasing surfactant concentration. Low concentrations of Pfizer Flocon 4800Cx polymer, a biopolymer with molecular weight greater than one million daltons, did not appear to reduce coalescence rates; in fact, oil drops appeared to coalesce faster in the surfactant-enhanced bicarbonate brines with 220 ppm polymer, while, in high concentration, coalescence rate was distinctly reduced. Peru and Lorenz (1989) did not explain their results.

Kourio et al. (1994) studied the effect of drop size and equilibrium interfacial tension on the drainage of drop-interface films. In a tank filled with both phases, a drop is formed on the tip of a syringe inside the continuous phase. Fluid is then slowly drained and the interface moves toward the drop, and eventually the drop coalesces with the interface. The relative velocity of the interface to the drop and the drainage time were of the order of mm/s and seconds respectively. They found that drainage time increases with increasing drop size in the case of water-hexane system, while in hexane-water systems drainage time was not affected by drop size. Drainage time was also found to increase with decreasing equilibrium interfacial tension.

Nakache et al. (1995) found that the drainage time of the heptane drop-interface increases with increasing polymeric surfactant concentration. Bhardwaj and Hartland (1994) studied the kinetics of coalescence of water droplets in water-in-crude oil emulsions in the presence of demulsifier in an agitated tank. The coalescence rate of water drops was found to increase dramatically in the first few seconds, and to slow down in the next period. They found the coalescence rate to increase with temperature and demulsifier concentration.

#### **2.2.4 Equilibrium Interfacial Tension**

Groenweg et al. (1994) studied the breakup of water-in-oil emulsions in an agitated tank. In the presence of an emulsifier, a bimodal size distribution was observed with a very large number of very small droplets. The bimodality behavior was attributed to drop breakup by tip streaming in the impeller zone. In the case of surfactant-free systems, the Sauter mean diameter was satisfactorily correlated with impeller speed and equilibrium

interfacial tension. The correlation was, however, poor in the presence of surfactants but improved significantly when the Sauter mean diameter of only the large drops was considered. They proposed that the breakup of large drops is mainly viscosity-dominated whereas the finer drops are generated by tip-streaming breakup in the impeller zone.

Lucassen-Reynders and Kuijpers (1992) studied the steady-state drop size of sunflower-seed oil in water in the presence of triacylglycerol surfactant. They found no correlation between Sauter mean diameter and equilibrium interfacial tension. They concluded that equilibrium interfacial tension is not the only interfacial parameter determining the drop size of emulsions. They proposed that as surfactant concentration increases, the interfacial viscosity of the drop interface rises to such high levels that the viscosity ratio becomes unfavorable for breakup.

Stewart et al. (1996) studied the effect of demulsifiers and corrosion inhibitors on the stability of kerosene in water emulsions. They found that mixtures of these additives exhibited synergistic effects resulting in a decrease in interfacial tension greater than that observed in the presence of single additives. They also found that the presence of corrosion inhibitors decreases the effectiveness of the demulsifier markedly. They attributed this to the formation of stable interfacial films by the additive mixture, which could result in the overdosing of demulsifiers when used in combination with certain other additives. Lyford et al. (1998) found that equilibrium interfacial tension decreases with increase in concentration and molecular weight of aliphatic alcohols.

### **2.2.5 Equilibrium Interfacial Concentration**

The equilibrium interfacial concentration,  $\Gamma_{Eq} = -1/RT \cdot \partial\gamma / \partial(\ln c)$ , is commonly known as Gibbs surface excess, a parameter which has been extensively used to quantify the effect of SAA on bubble coalescence. Although it accounts for the variation of surface tension with concentration, it does not take into consideration the ability of the SAA to replenish the interface by diffusion (since it is based on static interfacial measurements).

Borwankar et al. (1986) studied the stability of very-low-holdup dispersions and found that above a certain interfacial concentration of hydroxypropyl methylcellulose, the dispersion is stabilized against coalescence. They proposed that the coalescence efficiency decreases when the stabilizer is adsorbed on the surface of the drops, and coalescence would be eliminated completely when the interfacial concentration of stabilizer reaches a certain level.

### **2.2.6 Viscoelasticity**

Cairns et al. (1976) investigated the rheological behavior of Zakum and Murban (Middle Eastern crude containing 0.08% w/w asphaltene) and Tia Juana (Venezuelan crude containing 3% w/w asphaltene) crudes over the pH range 2-11. As the pH was increased, the interfacial shear viscosity decreased. It also decreased with the addition of an electrolyte such as NaCl at the same pH. High values of interfacial shear viscosity were encountered with increased aging time. High asphaltene content did not necessitate high interfacial shear viscosity. For instance, Murban, which has the lowest asphaltene content, had the highest interfacial shear viscosity. They concluded from the correlation of interfacial shear viscosity with emulsion stability tests that the maximum emulsion stability for each crude occurs at the pH value at which interfacial shear viscosity is the greatest. Also, high NaCl concentration in the aqueous phase was found to lead to low interfacial shear viscosity and low emulsion stability. However, some of the anomalies led them to conclude that the stability of emulsions is increased when there is a rapid initial adsorption of natural surfactant (i.e., a rapid fall in the interfacial tension) followed by a rapid rise in interfacial viscosity.

Neustadter et al. (1979) used a biconical bob torsion pendulum to measure the interfacial shear viscosity of crudes and investigated the extent of film viscoelasticity as a function of both the pH and the salinity of the aqueous solution. They found that at pH 6, interfacial films exhibited maximum viscoelasticity and maximum emulsion stability. Despite this result, they concluded that one could not rely solely on interfacial shear viscosity measurements to predict emulsion behavior because specific effects such as

changes in the film compressibility and elasticity would not be reflected in the shear viscosity measurements.

Wasan et al. (1979) employed a deep-channel interfacial viscometer to study the effect of the interfacial shear viscosity on the stability of Salem crude oil-in-water emulsions containing different concentrations of petroleum sulfonates and salt. Their results showed a linear decrease in the coalescence rate of drop-interface as the interfacial viscosity increased. They also examined the effect of adding n-hexanol cosurfactant on the stability of the same emulsion systems containing Petrostep 420 and NaCl. These systems exhibited the least-stable emulsions and also had the lowest interfacial shear viscosity values. In contrast with the above system, Salem crude-oil water systems containing TRS 10-80 exhibited more stable emulsions and had higher values of interfacial shear viscosity.

Mohammed et al. (1993) investigated de-watering of crude oil emulsions and found that de-emulsification (coalescence) is hindered by the formation of solid interfacial films. They also found that film drainage rate increases as interfacial viscosity is decreased. Taylor (1988) reported some relative trends in interfacial shear viscosity for Ninian, Romashkino and Kuwait crudes upon aging the crude oil-water interface, in which the presence of specific surface-active chemicals retarded the increase of interfacial shear viscosity.

The composition of natural films encapsulating water drops in the crude oil of offshore emulsions is thought to be predominantly asphaltenes and resins (Mohammed et al., 1993). Asphaltenes form solid films which retard the rate of oil-film drainage during the coagulation of water drops. This greatly reduces the rate of emulsion breakdown. Also, it is believed that the stability of water-in-crude oil emulsions is due to rheological characteristics of the interface, which are controlled by the asphaltic constituents of the oil. These constituents form a "bag" encapsulating water drops dispersed in the oil. A very high interfacial shear viscosity is observed when asphalt is dispersed in a poor solvent and a low interfacial viscosity is observed when it is dispersed in a good solvent.

A possible explanation of the latter observation is that a poor solvent (e.g. alkanes) cannot bring about complete dissociation of the asphaltic material. Therefore, asphaltic fractions that do not dissolve tend to self-associate, reducing the free energy of the system.

Mohammed et al. (1993) studied rheological properties of Buchan crude oil-water interfaces using a biconical bob rheometer. They found that interfacial film at the crude oil-water interface initially exhibits low Newtonian viscosity due to the adsorption of low molecular-weight species. The build-up of interfacial films continues by the adsorption of higher-molecular-weight material over a period of hours. During this period, the interfacial tension attains a steady value. They suggested that during this time, the adsorbed asphaltene species rearrange to form a network structure. It is anticipated that weak structures would form which might or might not be destroyed by applying a stress. The development of stronger interfacial-film structures, through increased packing and rearrangement of asphaltenes, continues with time. They found that film viscoelasticity increases sharply with temperature. The effect of temperature on film viscoelasticity suggests that interfacial films become more liquid-like at high temperatures. The increase in interfacial shear viscosity with increasing temperature can be attributed to the loss of some light components of the crude through evaporation.

Campanelli and Cooper (1989) investigated the relationship between interfacial viscosity and emulsion stability for a few O/A systems. They found the conditions that maximize emulsion stability would also maximize interfacial viscosity. Goodrich and Goupil (1980) found that fatty acids tend to concentrate at the interface at a specific pH, forming an extremely rigid film. At higher pH, fatty acids become soluble in the water phase and leave the interface, thereby lowering its viscosity. At lower values of pH, they become soluble in the oil phase, resulting again in a decrease in the interfacial viscosity.

Graham et al. (1979) demonstrated that a reduction in the interfacial shear viscosity of Forties crude oil-water interfaces occurs upon the addition of a demulsifier dissolved in methanol, which may result in increasing coalescence rate. "Overdosing" the interface



with high concentrations of the demulsifier was found to result in an increased interfacial viscosity, with a concomitant increase in emulsion stability.

Janssen et al. (1994, 1997) studied droplet breakup in simple shear flow and hyperbolic flow in the presence of surfactants. They found that in both flows, drop size is not a simple function of equilibrium interfacial tension as it is thought to be. Droplet breakup implies a significant deformation of the droplet interface. This generally leads to an interfacial tension that will locally deviate from its value at adsorption equilibrium. The magnitude of this deviation depends on the competition between the interfacial deformation and the mechanisms that tend to restore the adsorption equilibrium: interface-bulk emulsifier exchange, and lateral emulsifier redistribution. Only when the latter mechanisms are so effective that they can keep the interfacial tension close to its value for the adsorption equilibrium throughout the deformation process, can the influence of the surfactant be accounted for by using equilibrium interfacial tension. This will be the case, for instance, at high surfactant concentration and/or low deformation rates. They also found that, for a wide range of surfactant concentration, the breakup process is affected significantly by the viscoelastic properties of the interface and particularly by the elasticity modulus. They introduced an apparent interfacial tension as the sum of the value for the adsorption equilibrium under quiescent conditions and a contribution proportional to the elasticity modulus.

Wasan et al. (1979) investigated the coalescence of crude oil drops at an oil-water interface containing surfactants and concluded that there is a qualitative correlation between the coalescence rate of oil drops and the interfacial viscosity. However, they did not find a correlation between coalescence rate of the oil drops and equilibrium interfacial tension. The coalescence time of oil drop interface was of the order of a few minutes, while it is of the order of parts of a second in turbulent liquid dispersion.

Dreher et al. (1999) investigated the coalescence time of water drop with the water-oil interface where the oil phase consisted of *n*-decane and Hyvis 3 Polybutene. They found that for Newtonian fluids, the coalescence time increases monotonically with continuous

phase viscosity and drop diameter. Elasticity of the continuous phase was modified by a small quantity of a heavy polymer (2,100,000 MW), and it was found that it caused a significant increase (up to three fold) in the coalescence times of drops of diameter less than 1 mm, but had no discernible effect on the coalescence of larger drops. Dreher et al. (1999) explained that shear rate at the interface of the smaller drops was high enough for the non-Newtonian fluids to exhibit some elastic characteristics. The maximum shear rate at the interface of the squeezing film increases rapidly with decreasing drop size and with increasing film thickness. They concluded that for two Newtonian and non-Newtonian fluids of the same viscosity, the effective viscosity in squeezing, or elongational flow, is greater for non-Newtonian fluids, providing the shear rate is high enough. However, the presence of the polymer may have produced interfacial elasticity and thus retarded the thinning of the drop-interface, while for the case of large drops, shear rate and thus interfacial elasticity could have been lower.

### **2.2.7 Elasticity**

Film elasticity is a crucial parameter in stabilizing thin films against rupture. The interfaces between two colliding drops may be flattened to two disks. Velocity of flow in the center of the continuous-phase film is the highest, and, moving out, velocity of flow decreases because of flow continuity. The continuous-phase film shows elasticity and retards interface stretching, and consequently retards film drainage. Interface stretching and consequently film elasticity is thus highest at the center of the continuous-phase film. The requirement for film stability is not so much that the elasticity be high, but that it be higher in the thinner parts of the film than in its thicker parts (Lucassen-Reynders, 1996). This requirement is fulfilled if the SAA is soluble mainly in the continuous phase. If soluble in the dispersed phase, SAA can diffuse to the interface freely and this condition no longer holds. Kim et al. (1996) found that the best demulsifier had the lowest film elasticity.

### **2.2.8 Diffusivity**

Most industrial systems contain many components with different polarities, which tend to concentrate at the interface. This higher interfacial concentration results in dispersion behavior that is analogous to that observed in the presence of surface-active agents. The aqueous phase may contain many soluble ionic and non-ionic compounds as well as finely-divided suspended matter that can straddle the interface (e.g. clay and catalyst particles). The interaction of these SAA, present at the interface between continuous and dispersed phases, is therefore very complicated. The dynamic and static interfacial characteristics measured in such systems are indeed average values that are determined by all species present at the interface at the moment of measurement. In dynamic processes, such as breakage and coalescence, interface stretching may be so fast that some SAA may not have the opportunity to reach the interface in sufficient quantities. Smaller SAA molecules can, therefore, diffuse to interfaces faster. In other words, under dynamic conditions, the relative interfacial concentration of smaller SAA molecules may be higher than it is under equilibrium conditions. Therefore, the diffusivity measured over a short period is higher than when measured over a long period.

Kim et al. (1996) investigated the demulsification of water in crude oil emulsions and found that a good demulsifier must create low interfacial tension, low elasticity, and high diffusivity. They also proposed that an efficient oil-soluble demulsifier usually reduce the interfacial tension and the interfacial viscosity, which causes an increase in the rate of film thinning and a decrease in the time it takes the film to reach a certain thickness. They suggested that surfactant diffusivity be inversely proportional to the square of the molecular weight.

Krawczyk et al. (1991) investigated the factors affecting the coalescence and interfacial behavior of water-in-crude oil emulsions in the presence of oil-soluble demulsifiers. They found that a high interfacial activity and a high rate of diffusion/adsorption are the most important parameters governing demulsifier performance.

### 2.2.9 Charge Effect

Kumar et al. (1996) proposed that oil drops take on a negative charge when contacting the aqueous phase. Similarly, Tobin and Ramkrishna (1992) suggested that the negative charge of organic drops in aqueous solutions is supplied by the preferential adsorption of the  $\text{OH}^-$  ions of the aqueous bulk onto the surface. Surface charges are accompanied by counter-ions in the surrounding liquid and create a double layer, which generates a difference in electrical potential between the dispersed particles and the medium (Stein, 1995). When two drops approach each other, there will be an excessive crowding of the counter-ions in the continuous film between the particles and a shortage of co-ions. This will cause an osmotic pressure between the particles and the medium far away from the particles. Practically, osmotic pressure will be a repulsive force over the double-layer length, and hence the repulsive energy is proportional to double layer length. Increasing the ionic strength in the continuous phase will result in a thinner double layer, and therefore smaller repulsive energy between the charged drops. The coalescence of the charged drops therefore decreases as the ionic strength increases (Stein, 1995). This interpretation may provide an explanation for the experimental observation that coalescence of oil drops is slower than that of water drops (Kato et al., 1991). Furthermore, it may justify the findings of Tobin and Ramkrishna (1992), who investigated the charge effect on the coalescence of acetophenon in water system, that an increase in pH strongly retards the coalescence of oil drops. It also explains the findings of Velve et al. (1997) who found that the stability of emulsion films is dramatically decreased with increasing electrolyte concentration.

Chen et al. (1998) investigated the effect of the electrolyte and polarity on the coalescence of drop-interface. They found that, in general, coalescence time increases with increasing drop size. The coalescence time of MIBK (methyl isobutyl ketone) drops in an aqueous solution was found to increase with increasing NaCl concentration, whereas it decreases in the case of aqueous drops dispersed in polar organic liquids (e.g., *n*-butyl acetate). The effect of higher electrolyte valency was found to be relatively less important. They proposed that in systems of polar organic liquids, an increase in the

concentration of the dissolved electrolytes has the effect of speeding up the coalescence of aqueous drops in organic media and of slowing the coalescence of organic drops in aqueous media. The higher the valency of the electrolytes, the stronger the effect on the coalescence rates of organic drops, but the weaker the effect on the coalescence rate of aqueous drops. In the cases of non-polar organic liquids (cyclohexane or n-heptane) the coalescence rate of aqueous drops is not affected by the type, valency or concentration of the added electrolytes. Acidic and basic electrolytes exhibit effects similar to salts. In systems of polar organic liquids, the addition of NaOH or HCl causes the coalescence rate of aqueous drops in polar organic media to increase and that of polar organic drops in aqueous NaOH solution to decrease.

Chen et al. (1998) proposed that the main difference between polar and non-polar organic liquids lies in their mutual solubility in water. When these polar organic liquids are in contact with water, both phases becomes binary solutions, and the salt effect due to the addition of electrolytes may change the intermolecular forces and consequently the composition of both phases through preferential association in liquid phases, causing the coalescence rate of liquid drops to be altered.

Gaonkar (1992) investigated interfacial behavior of soybean oil/water using a Wilhelmy plate tensiometer, and found that the interfacial tension between commercial soybean oil and water decreased with time in the presence of NaCl. This phenomenon was attributed to the increase in interfacial activity of polar impurities present in the soybean oil. In the presence of the salt, the impurities are salted out and concentrate at the oil/water interface, thereby lowering interfacial tension. The interfacial tension increases with increasing temperature when the aqueous phase was water, while in the presence of NaCl, interfacial tension was found to decrease with increase in temperature. In this case, although the solubility of impurities increases with temperature, they are salted out due to the presence of NaCl and concentrate at the oil/water interface and lead to a lowering in the interfacial tension. Interfacial tension did not change or increased slightly in the presence of salt on a purified soybean oil/water system containing surfactants, such as stearic acid, oleic acid and linoleic acid, whereas it lowered significantly with ricinoleic acid. This was attributed by Gaonkar (1992) to the presence of the

-OH group close to the double bond (between C-9 and C-10) in the case of ricinoleic acid.

Deshikan and Papadopoulos (1995) studied coalescence of *n*-hexadecane oil drops suspended in an aqueous medium of varying pH and ionic strength. They found that at high constant ionic strength, the coalescence time decreases by two orders of magnitude when the pH decreases from an intermediate to a low value. They suggested that pH is more effective than ionic strength in controlling the coalescence of oil drops. They attributed this to variation in interfacial characteristics of the thin liquid film owing to a change in pH and ionic strength, without further elaboration.

#### **2.2.10 Mass Transfer Effect**

Skelland and Jeffrey (1992) studied the effect of mass transfer on droplet breakup of chlorobenzene drops dispersed in water. They found that, in the presence of Triton X100 surfactant, the transient Sauter mean diameter was higher when mass diffusion was from drop to continuous phase. They attributed this to enhancement of the coalescence rate due to solute transferring from the droplet phase.

Kourio et al. (1994) investigated the effect of mass transfer on the drainage time of water-acetone/toluene. They found that drainage rate is rather low when mass transfer is from the continuous phase to the drop, while it is fast when mass transfer is from drop to continuous phase. Lyford et al. (1998) found that dynamic interfacial tension strongly depends on mass transfer and the phase to which it is directed. They found that dynamic interfacial tension changes are much higher when mass transfer is from oil drop to water or from oil to water drop.

### 3 EXPERIMENTAL

#### 3.1 Experimental Setup

A schematic diagram of the experimental apparatus is shown in Figure 3. The mixing tank is a glass cylinder 6 inches internal diameter and 6 inches high. The tank's top and bottom are flat and made of high-density-polyethylene (HPD). Four HPD baffles of 1-cm width and 2mm thickness are placed vertically on the tank wall at equal distances. Details of the mixing tank and impeller are shown in Figure 4.

A shaft with a six-blade Rushton impeller of 3 inches diameter goes through a hole in the center of the tank lid and extends to one third of the tank height from the bottom. The vessel is placed inside a square, water-filled jacket with optically-flat glass sides that serves as a temperature-controlling bath. After each run, the vessel is washed with detergent, and rinsed with tap water and then de-ionized water.

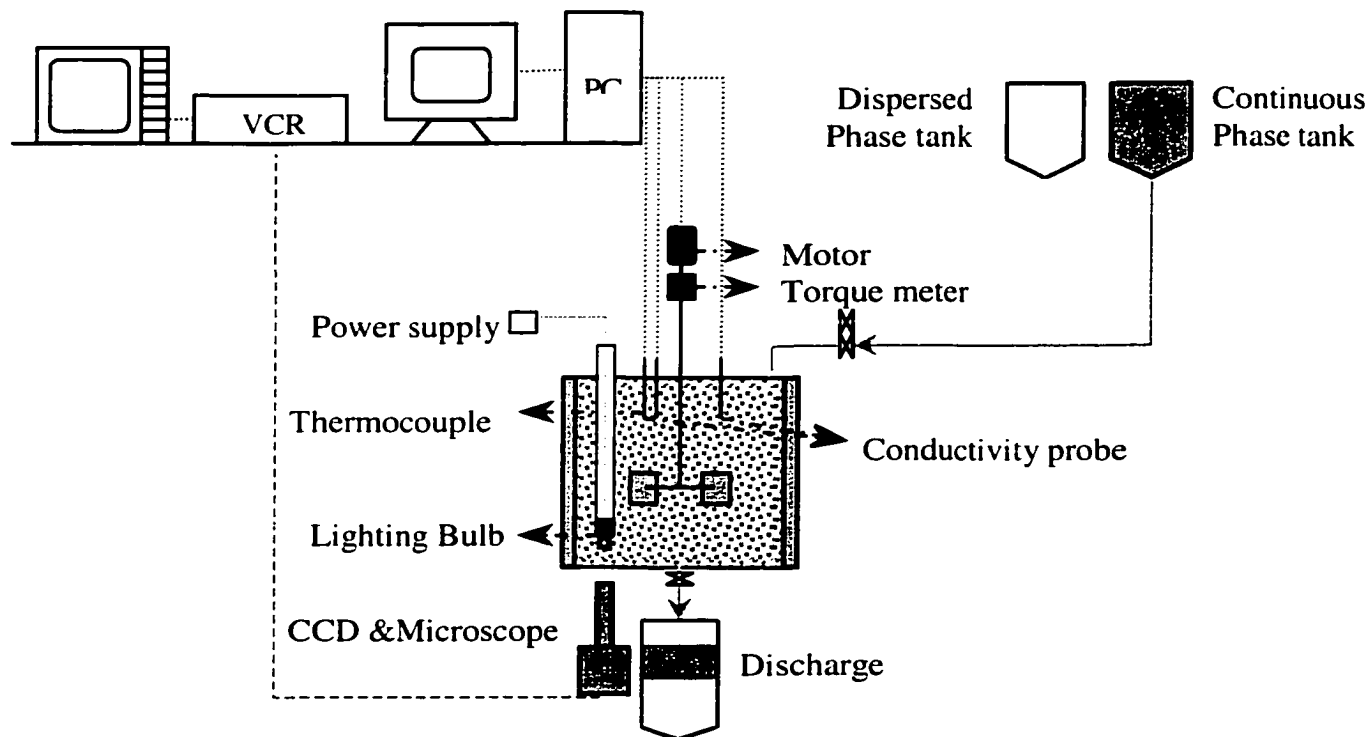


Figure 3. Schematic diagram of experimental setup

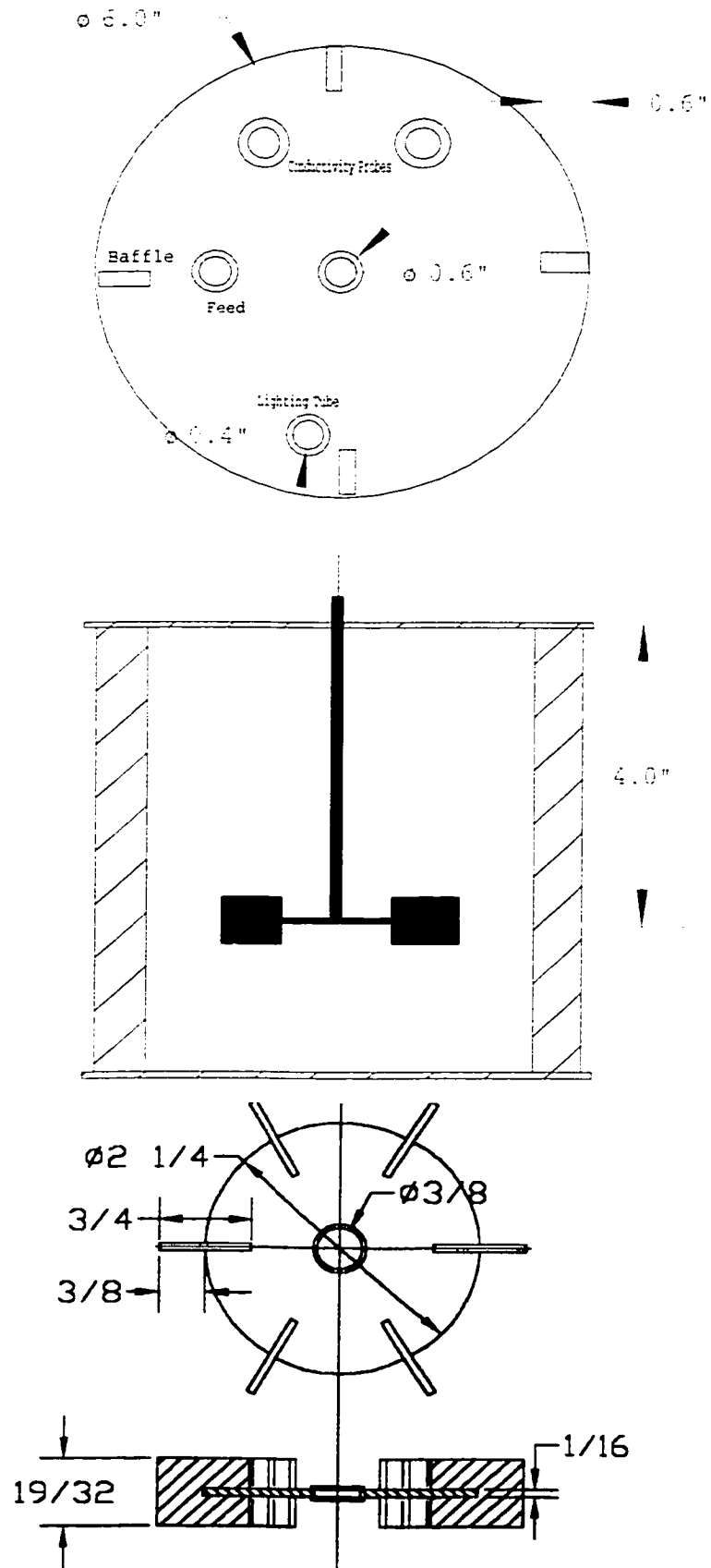


Figure 4. Mixing vessel and impeller design (dimensions in inches)



The motor shaft enters the tank through a central hole in the lid to which a 2-cm tube is attached. This tube helps free the tank of air entrained when filling. Tank is operated completely filled. The shaft is connected to a torque sensor (Lebow Assoc. Inc. Model 1602) and then to the driving motor (G.K.H. Heller Corp., Model HST20N) capable of running between 0 and 1800 rpm. The driving motor, torque meter and shaft are mounted on a stand above the tank. The stand can move vertically, allowing the impeller height to be changed when desired. Impeller speed is digitally monitored and controlled manually. The temperature was controlled by a temperature controlled bath; all the experiments were conducted at  $27 \pm 0.5$  °C.

A conductivity probe was used to monitor the onset of inversion. It consists of two 1-mm diameter and 40 mm long copper wires that were inserted through the top of the tank, 50 mm apart from each other, and from the center of the tank top. A digital conductivity meter (Yellow springs Instrument Co. Model 35) was used to monitor conductivity of the liquid. A two-pen plotter (Houston Instrument, Model B52175I) was used to record conductivity and torque signals. A sharp change in conductivity indicates phase inversion.

A 2/3" chip, 640×380-pixel resolution CCD video camera, capable of very short exposures (FlashCam by PCO Co.) equipped with a microscope (Edmund Scientific Co., VZM model 450) was used to image dispersion. The microscope allows varying magnification without refocusing, unlike conventional microscopes. It is mounted with its optical axis vertical to capture dispersion images 3-4 mm above the tank bottom. A polarizing filter was mounted on top of the microscope to minimize lighting from sources other than that of the dispersion. The microscope field of view is adjustable from 1.4-7.0 mm, allowing drops from 3  $\mu\text{m}$  to 1400  $\mu\text{m}$  diameter to be imaged.

A stainless steel tube of 8 mm OD, sealed with a flat glass, enters the tank through a tight fitting in the tank bottom, providing a viewing port for the camera to see inside the tank. From a point directly opposite this viewing port, at the tank top a 10 mm ID test tube

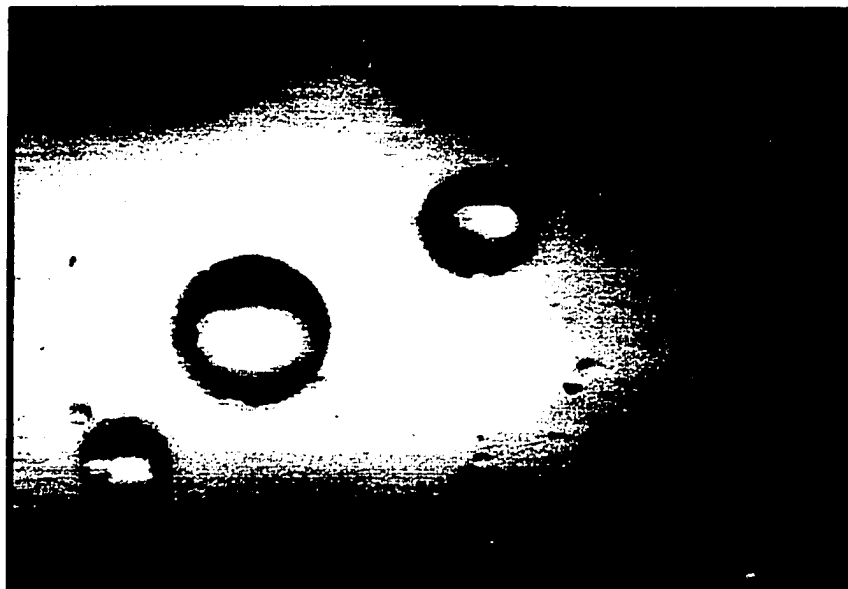
enters the tank through the top and is positioned 8 mm above the tank bottom so that it provides lighting for imaging dispersion. The lighting tube had a 12-volt, 100-watt photo lamp (VICO Co., FCR); its light intensity was adjusted using a variable auto transformer (Staco Energy products Co., type 3PN1010). The gap between the illumination tube and viewing port for the camera was 7 mm.

The exposure time of the camera could be adjusted from 10-1000 microseconds. A good compromise between image quality and light requirements was obtained using a 60 microseconds exposure time and a light power of 50 watts (Figure 5).

### **3.2 Experimental Procedure**

In the phase inversion experiments, the tank is filled with the appropriate holdup and continuous phase. The impeller is placed within the continuous phase. Conductivity, impeller speed, and torque measurement and plotting are begun. The impeller starts running at a relatively low speed (about 400 rpm) for 5 minutes. The systems studied in this research was O/A and A/O. Depending on the conditions, the conductivity of the O/A systems was typically about 40-60 millimho, while it was about 0.01 mho for A/O. The impeller speed is then increased stepwise (by 20 rpm increments) and is left for at least 4-5 minutes between speed changes. If any change in conductivity is observed, mixing is allowed to proceed until conductivity is stabilized before the next speed increment is applied. A sharp conductivity decrease or increase indicates phase inversion. Impeller speed is recorded and holdup is measured. At the end, lamp, impeller, and recordings are stopped.

In the coalescence experiments, the tank is fully filled with the continuous phase and appropriate holdup of the dispersed phase. The impeller is then run at the desired speed and the system is left for a period of 3 hours, to approach steady state. The steady state condition is discussed in the next chapter. The dispersion is then imaged for a period of 2 minutes to get the drop-size distribution. Impeller speed is reduced suddenly and at the same time imaging of dispersion is begun. The dispersion was imaged for 180 minutes.



a) 0.5% Bayol oil/ water, 250 rpm



b) 0.75% acetophenon/ 0.05 molar aq. NaCl /1.0 mmole Triton X100, 300 rpm

Figure 5. Samples of drops imaged.

Impeller speed was calibrated using a sensitive tachometer (Cole-Parmer, 8204-00) (Figure 6). Torque measurement was calibrated using a set of standard weights and disks that provided accurate static torque forces (Figure 7). Torque measurement was monitored during the phase inversion experiment with the objective of finding a technique for identifying phase-inversion onset.

### 3.3 Phase Inversion Measurement

Onset of phase inversion is identified by a sharp shift in conductivity of the dispersion. Typically, conductivity starts declining from  $60 \pm 1$  millimho to about  $40 \pm 5$  millimho when phase inversion is approached. When phase inversion takes place, conductivity drops to  $0.01 \pm 0.01$  millimho within few seconds. A typical conductivity graph is shown in Figure 19. In a few preliminary tests, torque measurement was not found to be a suitable indicator of the onset of phase inversion since torque variation was not significant. This could differ if the viscosity ratio between the dispersed and the continuous phase was large.

Holdup was measured after the phase inversion test was completed. Before stopping the impeller, a sample of about 250 mL of dispersion from tank bottom was withdrawn. Total volume and weight were measured. Using the following relation, the dispersed phase holdup was calculated as:

$$Holdup = \frac{\left( \frac{weight}{volume} \right)_{dispersion} - density_{Aqueous}}{density_{oil} - density_{Aqueous}} \quad (1)$$

The measuring cylinder of 250 ml was graduated to 100 units. Therefore, the reading resolution of total volume is 1.25 ml, or 0.5% error in volume reading. Scale resolution is 0.1 g, which represents a 0.04% error in weight reading. Thus the highest error in measuring holdup is about 0.8% for typical holdup (80%).

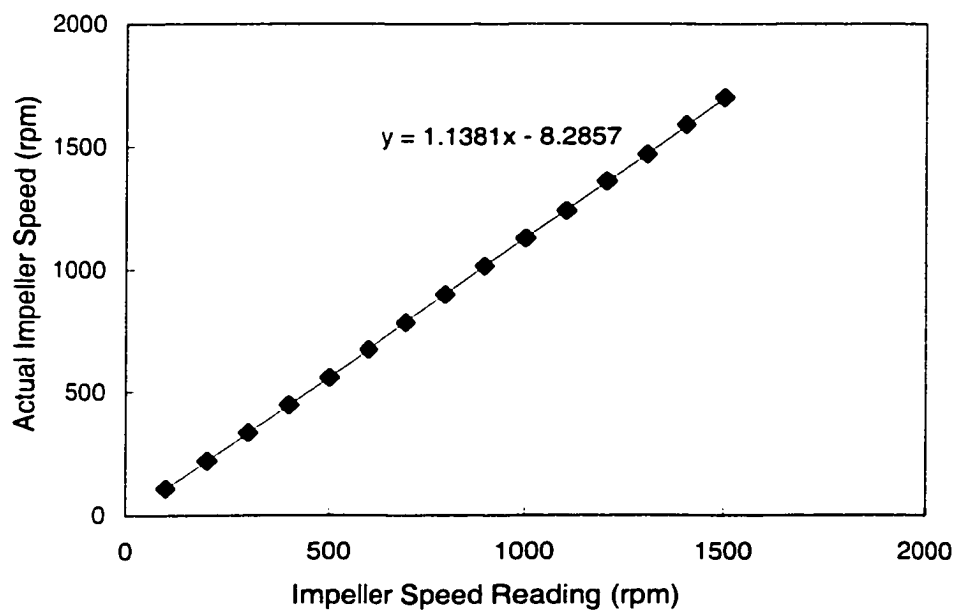


Figure 6. Impeller speed calibration curve

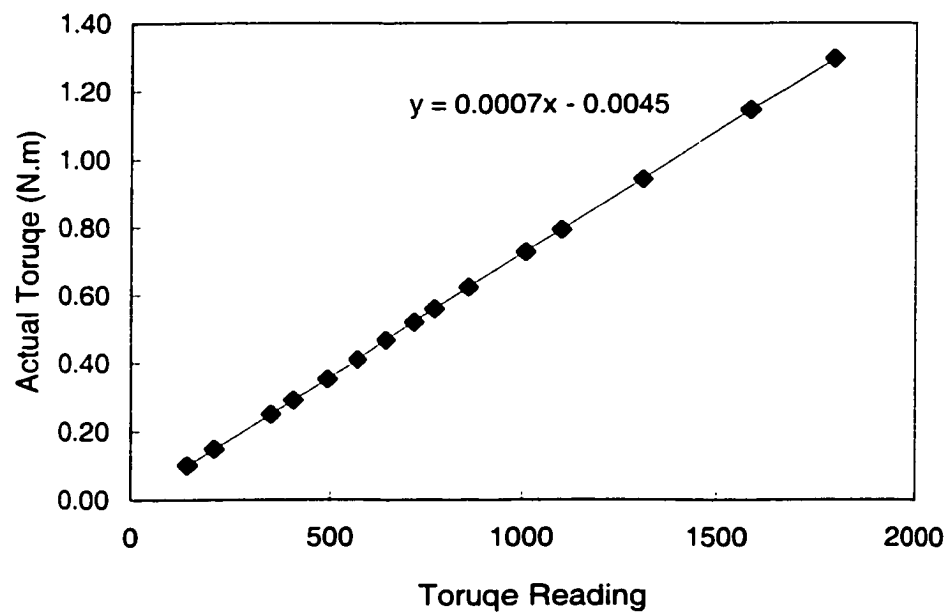


Figure 7. Torque calibration curve

### 3.4 Drop Size Measurement

In this study, image processing was used for drop-size measurement. This technique and its accuracy will be discussed in this section.

#### 3.4.1 Image Processing

In all the tests undertaken in this study, the objects were displayed on the 13" TV monitor (JVC model C-13910), while images were recorded and replayed from a VCR (JVC model HR-DD840U). The magnification of the overall imaging system was constantly 180X. A transparent grid was used to subdivide the screen into a set of 85 equally-spaced strips, which facilitated the manual measurement of drop sizes. This tedious process was facilitated by the fact that in coalescence experiments almost all drops were essentially spherical.

To minimize the time required for accurately determining the drop-size distribution, it is desirable to measure the minimum number of drops. On the other hand, large drop numbers are required to ensure that the sample analyses are representative. As seen in Table 2, most previous investigations were conducted using 300-1,000 drops. This may introduce some bias particularly when a manual drop-size analysis technique is used, as the operator generally tends to ignore small drops.

Table 2. Number of drops to make a sample used in literature

Investigator(s)	Number of drops
Brook and Richmond (1994)	300
Ni et al.(1998)	400
Pacek et al. (1998)	600
Pacek et al. (1994a)	800
Tobin et al. (1990)	1000

The diameter of 1319 drops of 0.75% acetophenon in a system of 0.05 aqueous NaCl with impeller speed of 300 rpm was measured. The number-length mean ( $d_{10}$ ) was identified as  $47.6 \pm 0.7 \mu\text{m}$ . The 95% confidence interval of the number-length mean of

600 drops was then calculated to be about 4  $\mu\text{m}$ . With the 95% confidence interval of 4  $\mu\text{m}$ , the sample size of 600 drops provides a good representation of the population. However, sample sizes used in this research were between 900-2500 drops. Depending on the conditions, each image includes about 10-20 drops. One-minute imaging therefore gives a sample size of about 20,000 drops.

### **3.4.2 Accuracy of drop size measurement**

The potential sources of error in measuring drop sizes in this research are:

1. Sizing drops that are out of focus
2. Round-off error
3. Assuming that drops are spherical
4. Inappropriate magnification
5. Systematic error
6. Refractive index

The microscope has a depth of field of 1 mm, while its field distance is 90 mm, and its length is 160 mm. Magnification errors of less than  $\pm 0.2\%$  are generated as a result of the 1 mm difference in the depth of field. The gap between the illumination tube and the imaging tube was about 7 mm; consequently, magnification error would, at worst, be less than 1.2%. The microscope was used at its highest magnification (180X).

The magnification of the imaging system, including the camera and microscope together, was tested using a precise Rounchi ruling (Edmund Scientific). The Rounchi ruling was mounted horizontally at the same field distance that was used for drop imaging. The magnification of the imaging system was found to follow closely the specification given by the manufacturer (Figure 8).

Supposing that the accuracy of the video camera, at worst, is  $\pm 0.5$  pixel, a drop of diameter 500  $\mu\text{m}$  is associated with a measurement error of  $\pm 0.3\%$  and drop diameter of 30  $\mu\text{m}$  with error of  $\pm 5\%$ . The most significant source of error in this investigation arises, therefore, from discretizing the field of view. The field of view was partitioned into horizontal strips

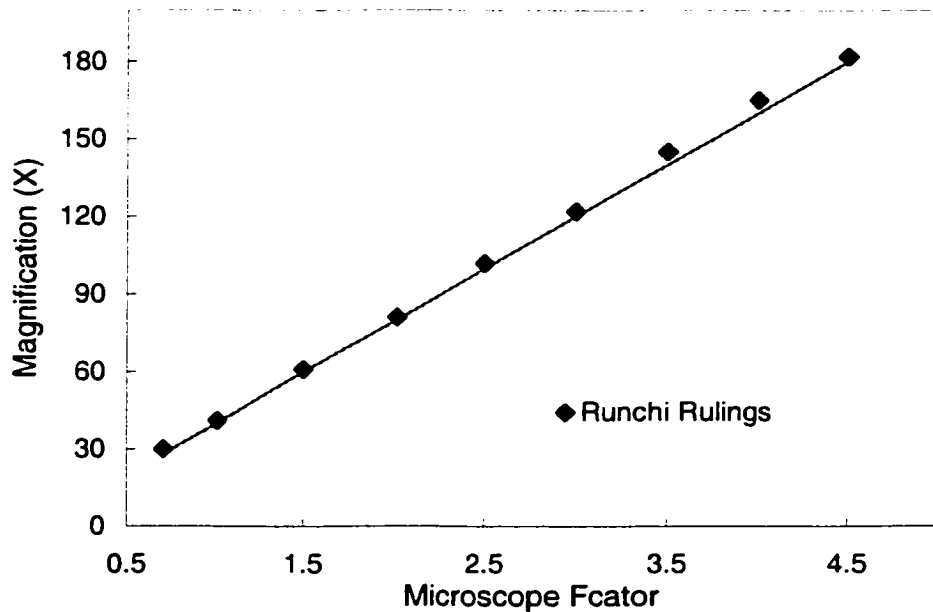


Figure 8. Microscope calibration curve

of 16.6  $\mu\text{m}$ . For a drop of 30  $\mu\text{m}$  diameter the error will be about 27 % and for the drops of 500  $\mu\text{m}$  the error will be down to 1.7%. A finer grid was found to markedly increase the amount of work needed, and was abandoned. It would be difficult to visually distinguish drop boundaries with accuracy better than 5 microns unless higher magnification was used.

Objects immersed in a liquid with refractive index  $n$ , appear closer. The apparent distance of an object is given by (Sears and Zemansky, 1960):

$$S = S'(n_{air} / n_{liquid}) \quad (2)$$

where,

$S'$  = actual distance

$S$  = apparent distance

On average, the distance between the imaging plane and the imaging tube is about 3-4 mm. Thus, considering that the refractive index of water is 1.33 and of air is 1.00, the



drops appear about 1 mm closer to the imaging system than their actual distance. The outcome error of drop size measurement will be less than 0.2%.

### 3.5 Reproducibility of drop size measurement

A system of 0.75% acetophenon in 0.05 mole aqueous NaCl in the presence of 0.1 mmole/m<sup>3</sup> Triton X100 was agitated constantly at 300 rpm and at room temperature for 180 minutes. This experiment was performed for different batches of the same system and conditions for three consecutive days, and results are shown in Table 3. The results show that measuring drop size has a good reproducibility.

Table 3. Reproducibility of drop size measurement (0.75% acetophenon/0.05M aq. NaCl/0.1 mmole/m<sup>3</sup> at 300 rpm)

	d <sub>10</sub> (mm)	s.e. (mm)	d <sub>30</sub> (mm)	s.e. (mm)	d <sub>32</sub> (mm)	s.e. (mm)	d <sub>43</sub> (mm)	s.e. (mm)
Day 1	0.0409	0.0009	0.0470	0.0009	0.0537	0.0036	0.0606	0.0066
Day 2	0.0362	0.0008	0.0438	0.0009	0.0528	0.0038	0.0632	0.0077
Day 3	0.0414	0.0010	0.0480	0.0012	0.0555	0.0045	0.0650	0.0102

### 3.6 Measurement of Interfacial Tension

Using the Du Nouÿ ring method (Kruss Interface tensiometer Model No. F8400e), the equilibrium interfacial tension was measured at least 5 times and the average is reported in this thesis. The dynamic interfacial tension was measured by Ms. Y. Xue using a recently-developed setup in Dalhousie's Mixing and Separation Lab (Xue, 1999). Three dynamic measurement techniques were used, namely: the drop-volume technique, the maximum-drop pressure technique, and the expanding-drop technique. Briefly, drops are formed at a specially-designed tip (254 µm in diameter) using a controlled flow rate that allows drop formation to take place over the desired time period. The pressure within the drop is continuously monitored via a sensitive transducer and translated to interfacial tension using the Laplace equation (Lucassen-Reynder, 1996):

$$\gamma = \Delta P / (r / 2) \quad (3)$$

where,

$r$  = drop diameter

$\Delta P$  = pressure difference between inside and outside of the drop

$\gamma$  = interfacial tension

The drops formed exhibit a pressure maximum when they are hemispherical and detach when their interfacial tension is balanced with the acting gravity forces. The drop-volume technique utilizes the interfacial tension value at the detachment point whereas the maximum pressure technique uses the interfacial tension value at the point where the drop is hemispherical in shape. In the expanding-drop technique, the interfacial tension is continuously monitored as the drop expands from the hemispherical point until its detachment. Details of these techniques and the apparatus used to measure dynamic interfacial tension in this research are found in Xue (1999).

### 3.7 Data Treatment

In this section, the procedures for calculating drop average diameter(s) and drop-size distribution(s) are discussed. Also the calculation of the secondary static and dynamic interfacial characteristics such as diffusivity and Marangoni elasticity is presented.

#### 3.7.1 Drop Size Calculation

Details of the drop size calculation is given by Orr, (1983). Drops with diameters within 16.6  $\mu\text{m}$  size intervals are measured and grouped in one class. Each class is arithmetically averaged and all drops within the class are given the average diameter of the class. A typical calculation is shown in Table 4.

Drop number density,  $N_i$  is calculated as follows (Orr, 1983):

$$N_i = \frac{n_i}{n_{\text{total}} \cdot \Delta d_i} \times 100 \quad (4)$$

Cumulative drop-volume density,  $F_i$  is calculated as follow:

Table 4. Example of drop size calculation

Drops within range (mm)	Average diameter of the interval (mm)	Number of Drops	N	F	d/d32
0.000-0.017	0.008	202	1200	0.1	0.1
0.017-0.033	0.025	290	1723	2	0.4
0.033-0.050	0.041	269	1598	13	0.7
0.050-0.066	0.058	168	998	36	1.0
0.066-0.83	0.075	57	339	61	1.2
0.083-0.100	0.091	15	89	77	1.5
0.100-0.116	0.108	8	48	86	1.8
0.116-0.133	0.124	4	24	94	2.0
0.133-0.149	0.141	1	6	99	2.3
Total(1014)					

$$F_i = \frac{\sum_{j=1}^{j=i-1} (n_j \cdot d_j^3) + 0.5(n_i \cdot d_i^3)}{\sum_{total} n_j \cdot d_j^3} \times 100 \quad (5)$$

The volume density is calculated by differentiating cumulative-volume density with respect to drop diameter,  $V\% = \partial F / \partial d$ , using the central difference approximation (Riggs 1994, page 123):

$$V_i\% = \left( \frac{F_{i+1} - F_{i-1}}{2\Delta d} \right) \times 100 \quad (6)$$

As an example, the number density and cumulative-volume density for drops with diameters in the range of 0.017-0.033 mm (row 2 of the Table 4) are:

$$N = \frac{290}{1041 \times (0.0166)} \times 100 = 1723$$

$$F = \frac{202 \times 0.008^3 + 0.5(290 \times 0.025^3)}{11.25} \times 100 = 2$$

Average drop sizes ( $d_{10}$ ,  $d_{32}$ , and  $d_{43}$ ) are calculated based on following equation:

$$d_{pq} = \left( \frac{\sum_{All} n_i \cdot d_i^p}{\sum_{All} n_i \cdot d_i^q} \right)^{\frac{1}{p-q}} \quad (7)$$

The value of the average size with lowest moment ( $d_{10}$ ) is strongly influenced by the fraction of small drops present in the distribution, and therefore its value will be the smallest. With increasing moment, average drop size will be increasingly influenced by larger drops ( $d_{43}$  is the highest value among average drop size). Likewise, drop-size distributions of lower moment such as number density emphasizes small drops while drop-size distribution of higher moment (volume density) emphasizes larger drops. Therefore, aspects of smaller drops are shown better by number density while aspects of larger drops will be more pronounced in volume density.

Attempts were successfully made to fit the experimentally-obtained cumulative-drop-number density and drop-volume density data with statistical distributions (normal, and log-normal). Normal and log-normal probability functions are the most common distribution used in the literature to model drop size distribution (Orr, 1983). Normal, and log-normal cumulative probability distributions are given by:

$$F_N(x) = 0.5 \left( 1 + \operatorname{erf} \left( \frac{x - \bar{x}}{\sigma_v \sqrt{2}} \right) \right) \quad (8)$$

$$F_{LogN}(x) = 0.5 \left( 1 + \operatorname{erf} \left( \frac{\ln(x) - \ln(\bar{x})}{\ln(\sigma_v \sqrt{2})} \right) \right) \quad (9)$$

Normally-distributed, cumulative data form a straight line on normal-probability graph paper. If a straight line is not obtained, the data are not normally distributed. The cumulative data following the log-probability function plot a straight line on log-probability graph paper. The diameter corresponding to 50% distribution density is the mean. The standard deviation is the width, centered on the mean, containing 62.3% of the data. The correlation coefficient of the straight line is then calculated. Using the standard

deviation and mean calculated by fitting the data to the cumulative density, the cumulative and distributive values corresponding to the drop size were calculated and plotted along with the experimentally obtained data. Then the calculated cumulative and distributive points were connected using a smoothing subroutine provided in the Excel 97 software.

The standard deviation of a sample is calculated as follows (Kennedy and Neville, 1986, p. 47):

$$s = \sqrt{\frac{\sum_{i=1}^n (d_i - \bar{d})^2}{n-1}} \quad (10)$$

To calculate the standard deviation of  $d_{32}$ , it is noted that  $d_{32}$  can be written as follow:

$$d_{32} = 6 \frac{\sum_{i=1} n_i v_i / \sum_{i=1} n_i}{\sum_{i=1} n_i s_i / \sum_{i=1} n_i} \quad (11)$$

$$d_{32} = 6 \frac{\bar{v}}{\bar{s}} \quad (12)$$

where,

$$\bar{v} = \frac{\sum_{i=1} n_i v_i}{\sum_{i=1} n_i} \quad (13)$$

$$\bar{s} = \frac{\sum_{i=1} n_i s_i}{\sum_{i=1} n_i} \quad (14)$$

The standard deviations of the drop-volume distribution and the drop-surface distribution are calculated. Considering that the number-volume mean and number-surface mean are independent of each other, the standard deviation of  $d_{32}$  is calculated as follows (Kennedy and Neville, 1986, p. 347):

$$s_{d_{32}} = 6 \left[ \left( \frac{\partial d_{32}}{\partial v} \right)^2 \cdot s_v^2 + \left( \frac{\partial d_{32}}{\partial s} \right)^2 \cdot s_s^2 \right] \quad (15)$$

Likewise, the standard deviation of  $d_{43}$  is calculated.

The standard error of the mean is calculated as follows (Chatfield, 1983, p. 112):

$$s.e. = \frac{s}{\sqrt{n}} \quad (16)$$

Statistical significance and the confidence interval were calculated using the  $t$ -test. The  $t$ -values were given by Hine and Wetherill, (1975, p. 51). The correlation coefficients were tested for significance against zero by comparing with the critical values, given by Kennedy and Neville, (1986, pp. 587-588). For sample sizes larger than 30, the correlation coefficients were also tested for significance, using the following relation for calculating the  $t$ -value and comparing with the tabulated value (Sachs, 1984, p. 400):

$$t = r \sqrt{\frac{n-2}{1-r^2}} \quad (17)$$

where,

$r$  = correlation coefficient

$n$  = sample size

The significance of the difference between a pair of correlation coefficients was tested by the method given by Sachs (1984, pp 429-430) in which correlation coefficients were first normalized as follows:

$$z = 1.1513 \cdot \log\left(\frac{1+r}{1-r}\right) \quad (18)$$

Then the z-value corresponding to the pair of correlation coefficients is calculated as follows and compared with the 5% level of the significance, 1.96:

$$z = |z_1 - z_2| \sqrt{n-3} \quad (19)$$

Details of this technique are given by Sachs (1984). To compare a pair of regression coefficients, the method proposed by Kennedy and Neville (1986, p. 311), was used. All mathematical calculations, including data fitting to statistical models, were carried out using Excel 97 software.

### 3.7.2 Calculation of the Equilibrium Interfacial Concentration

The equilibrium interfacial concentration of surfactant,  $\Gamma_{eq}$ , or the so-called Gibbs surface excess can be derived as follow (Campanelli and Wang, 1998):

$$\Gamma_{eq} = -1/RT (d\gamma_{Eq}/d\ln C_{Eq}) \quad (20)$$

where  $C_{Eq}$  is the equilibrium surfactant concentration in the aqueous phase. The equilibrium adsorption at the interface can be described by the so-called Langmuir isotherm, which relates the interfacial concentration  $\Gamma$  and the bulk concentration  $c$  as follows (Lucassen-Reynder, 1996):

$$\Gamma/\Gamma^\infty = c/(c+a_L) \quad (21)$$

where,  $\Gamma^\infty$  is the interfacial concentration value for a fully-saturated interface and  $a_L$  is the half-saturation concentration. Combining Eqs. (20) and (21) results in the following equation (Lucassen-Reynder, 1996):

$$\gamma = \gamma_0 - RT \Gamma^\infty \ln(1 + c/a_L) \quad (22)$$

Where  $\gamma_0$  is the equilibrium interfacial tension of a clean system.

### 3.7.3 Diffusivity Calculation

Diffusivity of surfactant is calculated from either of the following equations, depending on whether adsorption is in the early stage or near the equilibrium condition (Campbell and Wang, 1998; Miller et al., 1994):

For the short-time approximation, the equation is:

$$\gamma(t) = \gamma_0 - 2RTC_0 \left( \frac{3Dt}{7\pi} \right)^{1/2} \quad (23)$$

The long-time approximation is:

$$\gamma(t) = \gamma_{eq} + RT\Gamma_{eq}^2 \left( \frac{12Dt}{7\pi} \right)^{-1/2} / C_0 \quad (24)$$

To calculate diffusivity from the above equations, the interfacial concentration,  $\Gamma_{eq}$ , bulk concentration,  $C_0$ , and equilibrium interfacial tension,  $\gamma_{eq}$  are needed. In industrial systems, these values are not usually available, not to mention that in many cases even the nature of the surface-active species (and their synergies) is not known. To facilitate the comparative evaluation of the diffusivity of industrial streams, an apparent diffusivity was calculated on the basis that the total SAA concentration is 1 mole/m<sup>3</sup>. In this way, the diffusivity values estimated for different industrial systems may be compared with each other.

### 3.7.4 Elasticity Calculation

Marangoni elasticity is calculated using the equation:

$$E_M = \partial\gamma / \partial \ln A \quad (25)$$

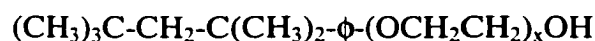
Dynamic interfacial tension and drop interface value are given as a function of the drop formation time. Marangoni elasticity is a dynamic interfacial characteristic that depends on both the hydrodynamic conditions (rate of stretching of the interface) and the temporal



rate of surface/interface tension change (controlled mainly by the diffusion/adsorption rate). It has the advantage of not requiring knowledge of the actual SAA concentration in the system but it requires knowledge of the surface-stretching rate. Unfortunately, the stretching rates encountered during drop breakage and coalescence are a complicated function of the system's physical characteristics as well as of the hydrodynamic conditions encountered in the mixer. They can therefore not be easily predicted and are expected to vary throughout the mixer. Furthermore, the very high interfacial stretching rates encountered in breakage and coalescence situations cannot be easily simulated in the most advanced devices for measuring interfacial characteristics. The Marangoni elasticity values measured at the highest stretching rate (flow rate 0.0316 ml/min, and a tip size of 250  $\mu\text{m}$ ) were therefore used to yield a basis for the comparative evaluation of the effect of interfacial characteristics at constant hydrodynamic conditions.

### 3.8 Systems Examined

Table 5 and Table 6 list the chemicals and surfactants used in this work along with their physical properties. Properties of pure components were obtained from the 71st edition of *The CRC Chemical and Physical Handbook (1991)*. Properties of the other components were obtained from the manufacturer/supplier. The Triton X- series of surfactants (supplied by the Sigma Co.) were selected because of their non-ionic nature, a factor that can strongly influence the formation of electric charges on the drops and the consequent influence on coalescence and phase inversion. They are generally described as alkylaryl polyether alcohols prepared by the reaction of octylphenol with ethylene oxide. The products are mixtures with respect to the length of the polyoxyethylene chain. The subscript "X" value represents the average number of ethylene oxide units. The general structure of these products is given by:



where,

$\phi$ =phenyl , and

x = number of ethylene oxide units in the surfactant.

Table 5. Physical properties of chemical investigated at 25°C.

Chemicals	Density (g/ml)	Viscosity (cP)
Water	0.997	1.0
0.05M aq. NaCl	1.000	1.0
20%wt. NaOH	1.221	2.1
Esso Caustic(capacity 1179)	1.148	0.98
Esso Caustic(capacity 1700)	1.159	1.54
Esso Caustic(capacity 1940)	1.170	1.13
Esso gasoline	0.730	0.68
Irving gasoline	0.731	0.75
Acetophenon	1.028	1.62
Bayol Oil	0.792	2.26
Chlorobenzene-Bayol Oil (65%v/v)	1.000	1.30

Table 6. Physical properties of surfactants at 25°C

Surfactants	Ethylene oxide #	Density (g/ml)	MW (g/mole)	HLB
Triton X45	5	1.040	426	10.4
Triton X100	9-10	1.065	625	13.5
Triton X165	16	1.080	910	15.8
Triton X305 (70%)	30	1.095	1525	17.3
Triton X405 (70%)	40	1.100	1966	17.9

The hydrophile-hypophile balance (HLB) is widely used as an index for surfactant solubility. Surfactants soluble in oil have HLB below 10; surfactants with HLB=10 are soluble in both phases, whereas surfactants with HLB above 10 are soluble in the aqueous phase. Water-soluble Triton surfactants were chosen to cover a wide range between 10.4 and 17.9 with molecular weights between 400-2000.

Table 7 shows the physical properties of synthetic systems studied in coalescence experiments. Coalescence tests were conducted using 0.05 Molar aqueous NaCl solutions

to suppress the thickness of the double layer and to eliminate the buoyancy effect on coalescence by equating its density to that of acetophenon. Unless otherwise stated, the gasoline used in this thesis was regular Irving gasoline.

The systems investigated in the phase inversion study can be broadly classified into two groups, namely aqueous in oil systems (A/O) and oil in aqueous systems (O/A). In the A/O system, distilled water was dispersed in Irving gasoline in order to provide a better understanding of what happens in the opposite (i.e. O/A) industrial systems.

As shown in Table 8 and Table 9, the O/A systems used in phase inversion experiments encompass both synthetic and industrial systems. The oil phase of the synthetic system was mineral oil (Bayol oil), donated by Imperial Oil Canada. Bayol oil typically consists of 13.7% naphthalenes, 86.3% paraffines, and less than 0.03% aromatics, by volume. It was chosen because of its lower vapor pressure, appropriate viscosity, relative purity and because it has been used in many other investigations, a situation that facilitates comparative evaluation of results.

In addition to the synthetic systems, the phase inversion behavior of a number of industrial O/A systems was investigated. This project was initiated because of interest in properly understanding the phase inversion behavior encountered during the “Inverse Doctor” treatment of gasoline pipelined from Edmonton, Alberta to Vancouver, British Columbia (US Patents 5,250,181, 5,160,045). Briefly, it is a process for removing elemental sulfur from the refined gasoline transported through pipelines, which have been previously used for the transportation of sour hydrocarbon streams. As shown in Figure 9, the gasoline is in contact with an aqueous solution containing 20% (w/w) caustic solution. This is accomplished using a semi-batch, 8-unit extraction column where caustic is circulated and gasoline is continuously fed and removed. Under these conditions, phase separation is easily accomplished unless the system inverts from O/A to A/O where a very stable emulsion is formed (which requires a long time to separate in the settler). The gasoline is contacted with an aqueous solution containing 20% (w/w)

Table 7. Systems and condition investigated in coalescence experiments

	Dispersed phase	Continuous phase	rpm	Triton	Conc. ( $\mu\text{M}$ )	$\gamma_{\text{Eq}}$ (mN/m)	$\Gamma_{\text{Eq}}$	D(m <sup>2</sup> /s) (DVT)	D(m <sup>2</sup> /s) (MDPT)	$E_{\text{M}})_{\text{max}}$ mN/m
1	0.50% CLB-Bayol oil (65%v/v)	Water	300→200	-	-	N/A	-	-	-	-
2	1.8% Bayol Oil	Tap water	500→250	-	-	N/A	-	-	-	-
3	0.5% Bayol Oil	Water	500→250	-	-	19	-	-	-	-
4	0.5% Bayol Oil	Water	500→250	X100	0.25	7.1	-	-	-	-
5	0.5% Bayol Oil	Water	500→250	X100	1.0	6.0	-	-	-	-
6	0.5% Bayol Oil	Water	500→250	X100	4.5	4.9	-	-	-	-
7	0.75% Acetophenon	0.05 M NaCl	300→200	-	-	6.7	-	-	-	5.15
8	0.75% Acetophenon	0.05 M NaCl	300→200	X100	0.1	4.1	2.1E-06	1.9E-04	2.9E-05	5.36
9	0.75% Acetophenon	0.05 M NaCl	300→200	X100	0.2	3.8	2.1E-06	2.2E-05	2.1E-06	-
10	0.75% Acetophenon	0.05 M NaCl	300→200	X100	1.0	2.6	2.1E-06	1.1E-06	8.5E-08	-
11	0.75% Acetophenon	0.05 M NaCl	300→200	X165	0.1	6.5	1.9E-06	4.1E-04	4.1E-04	-
12	0.75% Acetophenon	0.05 M NaCl	300→200	X165	0.2	6.2	2.0E-06	8.4E-05	6.4E-05	-
13	0.75% Acetophenon	0.05 M NaCl	300→200	X305	0.1	6.2	1.0E-06	1.6E-05	1.8E-05	4.42
14	0.75% Acetophenon	0.05 M NaCl	300→200	X305	0.2	5.9	1.0E-06	4.6E-06	2.8E-05	-
15	0.75% Acetophenon	0.05 M NaCl	300→200	X405	0.1	5.6	5.8E-07	2.2E-06	1.4E-05	-
16	0.75% Acetophenon	0.05 M NaCl	300→200	X405	0.2	4.8	5.8E-07	1.7E-07	1.1E-05	-

Table 8. Synthetic systems investigated in phase-inversion experiments

	System	Triton	Conc. (mole/m <sup>3</sup> )	$\gamma_{\text{Eq}}$ (mN/m)	$\Gamma_{\text{Eq}}$	D(m <sup>2</sup> /s) (DVT)	D(m <sup>2</sup> /s) (MDPT)	$E_{\text{M}})_{\text{max}}$
1	Bayol oil-water	-	-	19	-	-	-	-
2	Bayol oil-water/Triton	X45	0.1	11	1.2E-06	8.0E-11	2.3E-10	22.3
3	Bayol oil-water/Triton	X100	0.1	2.5	3.9E-06	4.2E-11	8.0E-10	11.3
4	Bayol oil-water/Triton	X100	0.2	2.0	3.9E-06	2.5E-11	3.2E-12	5.9
5	Bayol oil-water/Triton	X100	0.3	2.0	3.9E-06	1.5E-11	1.1E-12	4.8
6	Bayol oil-water/Triton	X165	0.1	4.1	1.3E-06	3.3E-11	7.4E-11	12.0
7	Bayol oil-water/Triton	X305	0.1	3.0	1.0E-06	2.1E-11	5.7E-11	9.3
8	Bayol oil-water/Triton	X405	0.1	3.5	9.0E-07	1.4E-12	9.1E-12	7.8

Table 9. Industrial streams investigated in phase inversion experiments

System	Type	$\gamma_{Eq}$ (mN/m)	$D(m^2/s)$ (DVT)	$D(m^2/s)$ (MDPT)	$E_M)_{max}$
1 Water/Irving gasoline	A/O	14	-	-	-
2 Irving gasoline/water	O/A	14	1.5E-13	1.9E-12	27.0
3 Esso gasoline-water	O/A	23	2.2E-13	4.1E-12	-
4 Irving gasoline-20%caustic	O/A	<1	2.0E-12	6.1E-13	3.6
5 Irving gasoline-"1179" caustic	O/A	<1	3.2E-15	1.2E-11	6.1
6 Irving gasoline-"1700" caustic	O/A	6	5.5E-15	4.0E-12	4.0
7 Irving gasoline-"1940" caustic	O/A	<1	4.8E-15	4.1E-13	2.7

caustic, an aliphatic mercaptan and optionally a sulfide to produce an aqueous phase containing metal polysulfides and a gasoline phase having reduced elemental sulfur. The concentration of the impurities accumulated in the recycled caustic will generally increase with increasing re-circulation ratio (usually referred to as capacity number), while the concentration of the caustic is reduced. The accumulation of these impurities was found to facilitate phase inversion from O/A to A/O.

To keep caustic concentration level constant, fresh caustic solution is often introduced when deemed necessary (after a number of circulations). The nature and concentration of the impurities present in the pipelined gasoline cannot be predicted and the addition of caustic is not performed on a scheduled basis. The characteristics of the system encountered during the treatment are therefore not necessarily a monotonic function of the recirculation capacity.

Aqueous phase samples of the process stream (representing capacity number of 1179, 1700, and 1940) were obtained courtesy of Imperial Oil in Sarnia, Ontario. Samples from Irving and Esso gasolines were used as the dispersed organic phase.

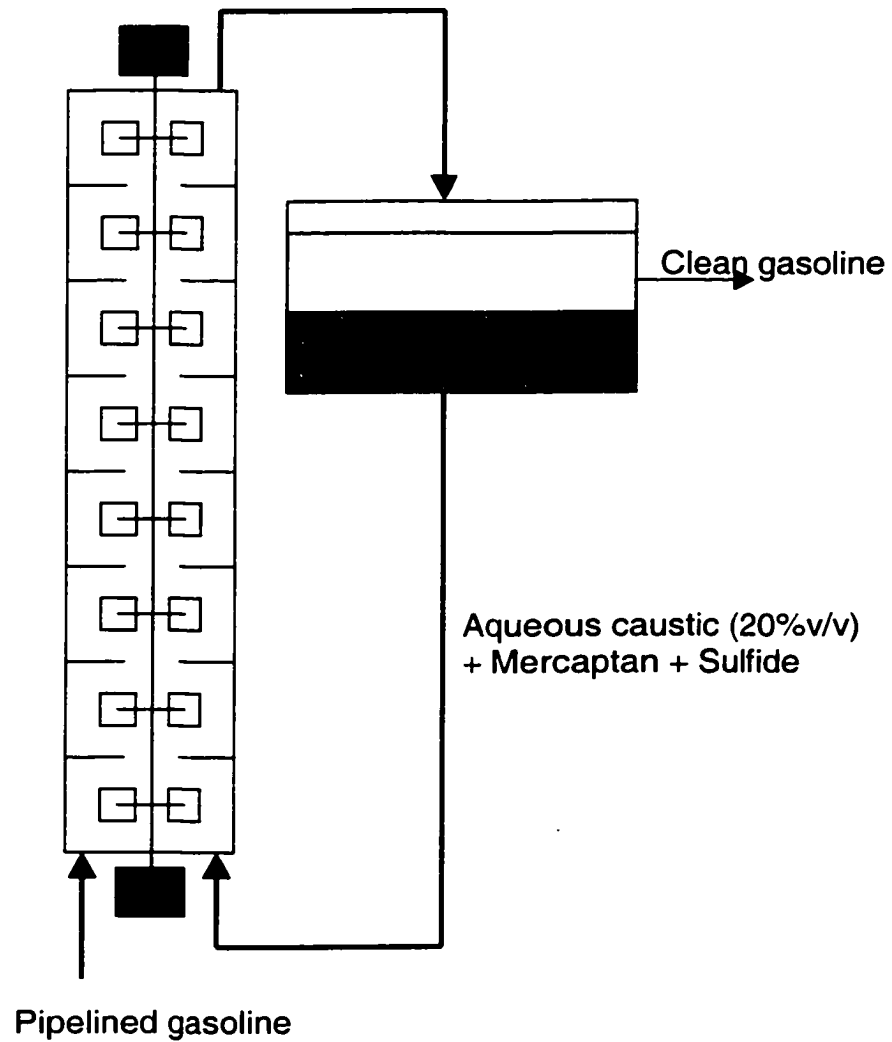


Figure 9. Schematic diagram of the "Inverse doctor treatment" for removing elemental sulfur from gasoline in Esso Canada unit, Vancouver, BC.

## 4 RESULTS AND DISCUSSIONS

### 4.1 Effect of Interfacial Characteristics on Coalescence

This investigation was undertaken with the objective of identifying the role of interfacial characteristics in phase inversion processes. As shown in the proposed phenomenological model, the inclusion rate is strongly related with the rate at which drops coalesce. It is, therefore, important that adequate attention be given to the role of interfacial characteristics in coalescence processes in order to develop a good understanding of the role it plays in phase inversion.

Coalescence and dispersion are counteracting and competing dynamic processes. Hence, difficulties in identifying coalescence frequency may arise if one relies solely on the steady-state size distribution. With the exception of Howarth (1967), most investigators of the 60's and 70's used a convenient approach in which steady-state drop-size distribution is fitted to the population balance equation assuming certain breakage and coalescence expressions. This resulted in reducing the ability to discriminate between the various models describing the many sub-processes involved. For example, Chatzi and Lee (1987) found that no combination of breakup and coalescence models is superior to another with regard to their ability to fit the steady-state drop-size-distributions of kerosene in water. On the other hand, a more rigorous test of the various proposed coalescence frequency expressions may be provided using transient data. This was confirmed by Tobin et al. (1990) who showed that predicted transient size distributions differ significantly depending on the coalescence expression used.

Assuming breakage to be negligible during the initial period following a sudden reduction in agitation intensity, Howarth (1967) developed an expression for the coalescence rate of a single drop. It is based on the initial Sauter mean diameter data and its rate of change with time.

A more robust approach addressing the transient aspect of the coalescence process is the so-called inverse population balance. This approach has been successfully applied to the aggregation process in the 60's (Swift and Friedlander, 1964) but was only recently applied to liquid dispersion and coalescence by Ramkrishna and his co-worker (1987, 1989, 1990, 1991, 1992, 1994, 1996). In this approach, the observed similarity in transient cumulative size distribution is used to extract a universal drop-size distribution. Using this universal drop-size distribution, the population balance equation may be analytically solved to obtain the dependence of coalescence frequency on drop size. Recently, Mishra et al. (1998), Vinckier et al. (1998) and Wynn and Hounslow (1997) applied the inverse population balance technique to extract the coalescence frequency in simple shear flow. However, they did not address the effect of interfacial properties on coalescence.

Although dispersion and coalescence processes are always present in any multi-phase system, the temporal evolution of drop size is predominantly controlled by coalescence in the initial stages following a sudden reduction in impeller speed or agitation intensity. To achieve a pure coalescence process, Wright and Ramkrishna (1994) suggested that the impeller speed be suddenly reduced to half of its initial value. Their argument is based on the assumption that the maximum drop size is twice that of the Sauter mean diameter; the initial impeller speed must therefore be reduced by a factor of at least 2 in order for the initial and final drop-size distributions not to overlap. In this way, the whole drop-size-distribution will be coalescence dominated at the initial stages following speed reduction.

When the impeller speed is suddenly reduced, the drop-size-distribution begins to change; this process continues until a new steady drop-size distribution is reached (Figure 10). The smaller the difference between initial and final impeller speed, the larger the size of the overlap section. The whole drop-size-distribution can therefore be considered coalescence-dominated, at the initial stages following impeller speed reduction, if the size of the overlap is kept small. In this work, the initial and final impeller speeds were 300 and 200 rpm respectively.



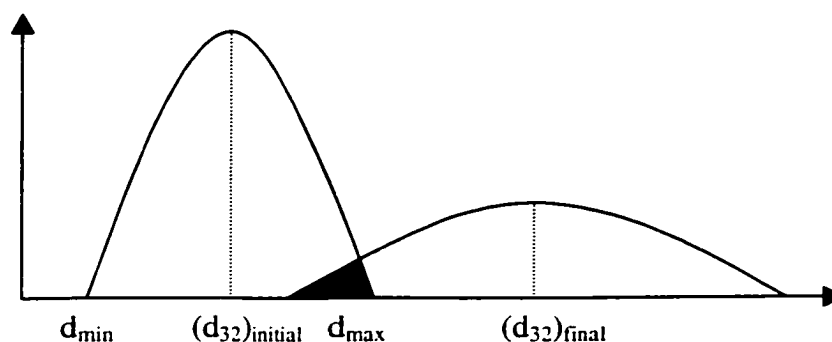


Figure 10. Schematic diagram of shifting drop-size distribution due to decrease in impeller speed

#### 4.1.1 Drop-Size Distribution

There is a large amount of literature on modeling drop-size distribution, yet there is no single model that is capable of successfully fitting most of the experimental data. Progress in developing such a model may have been limited by several difficulties. The drop-size distribution models, which appeared in the literature in the 60's and 70's, are based on very low holdup measurements (below 0.01%) and may not apply to moderate and high holdups. In such dispersions, breakage is the dominant process and coalescence does not gain importance in short mixing times. The second difficulty is related to drop size measurement in dispersions with high holdups. Most studies have been limited to small holdup (below 1%) and measurement of dispersions with higher holdup is rare (Bae and Tavlarides, 1989). Most drop size measurement techniques for high-holdup dispersions use some sort of sampling. In such techniques, a sample is withdrawn, to which surfactant is added, and thereafter dispersion is imaged under the microscope. Problems related to the acquisition of representative samples are often encountered, and the sample may lose its characteristics in the process of size determination.

The other obstacle is related to the time that is required for a dispersion to reach equilibrium. In most investigations reported in the literature, mixing was maintained for 2-3 hours before sampling was carried out to determine steady state drop-size distributions. Such information may not be representative of real equilibrium conditions since there are reports that the equilibrium condition is achieved after several days of continuous mixing (Lam et al., 1996).

#### 4.1.1.1 Effect of Mixing Time

In this investigation, a 65% (v/v) mixture of chlorobenzene-Bayol oil (with density 1.0 g/mL) was dispersed in water in quantities needed to form 0.5% holdup and used to study the time needed for a dispersion to reach equilibrium. The dispersion was mixed at 250 rpm for a period of 2.5 hours. Afterwards, a dose of aqueous Triton X100 solution was added via a syringe (sufficient to bring the SAA concentration in the dispersion up to 1.0 mmole/m<sup>3</sup>). The variation of drop-size distribution was monitored as a function of time. The temporal variation in the number and volume densities resulting from sudden change in the interfacial characteristics, is shown in Figure B56-Figure B58.

As time progresses, the drop size at which the peak number and volume density occurs was found to shift to a lower value while the magnitude of the peak increases. This is caused by the net disappearance of larger drops, and the increased formation of finer drops, as mixing continues. Consequently, the average drop size was found to decrease during this period (Figure B59). However, as seen in the Figure B56-Figure B58, the number, volume and cumulative-volume density of the dispersion drop-size-distribution at 2 hours and 48 hours do not differ significantly. It can therefore be concluded that quasi-steady state drop-size distribution can be considered to be approached after 48 hours of mixing in the case of the system of CLB-Bayol oil/ water/ 1.0 mmole/m<sup>3</sup> Triton X100 and a dispersed phase holdup of 0.5%.

The observation that quasi-steady drop-size distributions can be achieved within 3 hours was confirmed by tests conducted using 0.05 mole aqueous NaCl and 0.1 mmole/m<sup>3</sup> Triton X100 in which acetophenon was introduced (holdup of 0.75%). The results obtained at 300 rpm and room temperature (Table 10) show very little change as the agitation period is increased from 210 minutes to 300 minutes (the Sauter mean diameter decreased by about 5%). For all the coalescence experiments reported in this thesis, mixing was undertaken for 180 minutes at 300 rpm before a step decrease in impeller speed was applied.

Table 10. Effect of mixing time on average quasi-steady state drop size

Agitation period	d <sub>10</sub> ( $\mu\text{m}$ )	s.e. ( $\mu\text{m}$ )	d <sub>30</sub> ( $\mu\text{m}$ )	s.e. ( $\mu\text{m}$ )	d <sub>32</sub> ( $\mu\text{m}$ )	s.e. ( $\mu\text{m}$ )	d <sub>43</sub> ( $\mu\text{m}$ )	s.e. ( $\mu\text{m}$ )
210 min	43	1	49	1	56	3	62	5
300 min	39	0.8	46	0.7	53	3	60	6

#### 4.1.1.2 Effect of Gravity Forces

As the density difference between the dispersed and continuous phases increases, the buoyancy forces tend to segregate the phases; it, therefore, plays a more significant role in dispersion and coalescence processes. A lower density dispersed-phase tends to concentrate in the upper regions of the vessel with a consequent increase in the spatial inhomogeneity of the dispersion formed. Drag forces tend to counteract the buoyancy force and reduce the segregation tendency. Since the drag force is proportional to surface area of the drop, the ratio of buoyancy to drag force is proportional to drop diameter. Consequently, the relative importance of the buoyancy force increases under conditions promoting the formation of larger drops (such as lower impeller speed, absence of SAA). On the other hand, the interference of buoyancy is minimized near the impeller zone where the drops are smallest.

The dispersion/coalescence behavior of the Bayol oil/water system (relative density of 0.78) was investigated. The resulting evolution of the drop-size distribution is shown in Figure B60-Figure B75 in the Appendix B. When the impeller speed is suddenly reduced from 500 to 250 rpm, the measured drop-size distributions indicate a shift favoring the formation of smaller size distributions (Figure B60). This anomaly is most probably caused by the large deviation of the density ratio (0.78), defined as  $\rho_d/\rho_c$ , from unity, and the presence, near the sampling point, of relatively large drops, which tend to segregate within the mixing tank. The characteristics of the dispersion present at the measurement point may therefore not be truly representative of the average conditions prevailing throughout the tank. For  $\rho_d/\rho_c < 1$ , the system tends to emphasize the finer drop sizes particularly in the initial stages following the reduction of agitation intensity. That is to

say that larger drops will be under-represented in the zones close to bottom of the tank where imaging was conducted. The tendency for the apparent formation of a finer dispersion was not as strong in the presence of SAA (Figure B63, Figure B67, and Figure B71) with the changes being slower as the surfactant concentration increases. This observation can be attributed to the ability of SAA to retard drop coalescence and the consequent formation of larger drops that promote spatial segregation.

In order to investigate dispersion/coalescence processes accurately and isolate the spurious effect of gravity forces, it is desirable to minimize the density difference between the continuous and dispersed phases. To minimize the possible wall effects on drop-size-distribution measurements, imaging was conducted at a point 20 mm above the tank bottom and 50 mm from the tank center. To further minimize buoyancy effects, it was decided to conduct the rest of the coalescence experiments using acetophenone (density 1.028 g/mL) and 0.05 molar aqueous NaCl solution (density 0.999 g/mL).

#### **4.1.1.3 Number Density**

Zhou and Kresta (1998) measured the steady-state drop-size distribution in a very dilute liquid dispersion (0.03% by volume) using a phase Doppler particle analyzer. They found that four types of drop-size distributions evolve with increasing rotational speed: long tail, double peak (bimodal), skew and skew-normal distribution. They concluded that the shape of the drop-number density depends on impeller speed. Pacek et al. (1998) also reported the formation of a bimodal drop-number density in a system of 0.5-10% chlorobenzene/ water, agitated at 180 rpm. They found that higher speeds tend to produce uni-modal distributions, whilst low speed enhances a bimodality which decreases with increasing holdup. Similarly, Chen and Middleman (1967) reported bimodality in drop-number density of a dilute system in a static mixer.

Some of the statistical models presented in the literature, as successfully representing drop-volume density may not succeed in fitting the experimental data when converted to number density. For example, Nishikawa et al. (1991) found that the use of the number

distribution (estimated from the volumetric distribution) might not provide the best correlation. Instead, they proposed using two normal distributions, the characteristics of which are influenced by the energy dissipation rate and the dispersed-phase volume fraction. Pacek et al. (1998) also found that none of the analytical distributions successful in modeling cumulative-volume density gave a satisfactory fit to the number density data. The main reason for this difficulty could be that the model's statistical characteristics (mean, standard variation, and skewedness) were determined by fitting the model to the experimental measurements of drop size moments for which they were designed. The weighting functions given to the experimental points are therefore strongly influenced by whether number or volume densities are used. For example, if a distribution model successfully fits the volume density (drop size of moment 3), its number density form may not properly fit the number density data where the drop size moment is 0. That is to say, the significance of the drop-size-distribution fit is strongly influenced by the type of distribution fitted with the number density biasing smaller drop sizes while volume distributions favor a better fit of the larger drops.

Two systems were investigated in this work, namely: a 65% (v/v) mixture of CLB-Bayol oil dispersed in water, and acetophenon dispersed in 0.05 molar aqueous NaCl solution. To approach equilibrium conditions, all these systems were mixed for 3 hours before drop-size measurements were carried out. The quasi-equilibrium number density (distributive and cumulative) of these systems at 300 and 200 rpm are shown in Figure C76-Figure C97 (Appendix C), along with their log-normal fit.

As seen in Figure C76-Figure C97 the number density of the smaller drops is higher at higher agitation intensities. No bimodality was observed in the number density of the systems investigated in this work. Number density curves are generally skewed towards smaller drop sizes, a characteristic of log-normal distributions. This is in agreement with the findings of Zhou and Kresta (1998) who found that up to an impeller speed of 680 rpm, a uni-modal skewed distribution was observed. The results obtained are, however, contrary to the finding of Pacek et al. (1998) who observed that a bimodality in number

density develops when impeller speed shifts from 300 rpm to 180 rpm. It is also different from the findings of Nishikawa et al. (1991) where the cumulative number distribution of a honeybee wax/water system depicts a bimodality with the mean and standard deviation of number density being a function of dispersed-phase holdup and the average energy dissipation rate.

The number-density data obtained at quasi-steady state (at 300 and 200 rpm) were fitted to normal and log-normal distributions and the results obtained are shown in Table A19. All the correlation coefficients were found to be statistically significant at the 99% confidence level ( $p < 0.01$ ). Although both distributions fit the number density data well, the log-normal distribution generally provides a better fit. It provides a statistically better fit (at the 95% confidence level) for most cases run at 200 rpm, while, on the other hand, it does not provide a statistically better fit (at the 95% confidence level) for most runs at 300 rpm. Table A18 clearly shows that the average drop size and standard deviation both decrease with increasing agitation intensity and/or the molecular weight of the SAA. The effect of SAA concentration is most pronounced at lower values and tends to level off at higher concentrations

#### **4.1.1.4 Volume Density**

The volumetric distribution of the dispersed phase among the various drop sizes present in the dispersion plays an important role in inter-phase mass transfer, ease of separation, and the reaction rates taking place in a multi-phase system. Very few researchers represented their results in the form of drop volume-density. However, the volume-density distribution may have more practical application than other distribution types since larger drops contribute more significantly to the volume-density distribution than to number density.

The majority of work reported in the literature modeled drop-size distribution in its cumulative-volume density form. This may be due to fact that cumulative-volume density smoothes minor measurement errors (Pacek et al., 1998); however, it can also hide subtle variations. Sprow (1967) found that the Schwartz-Bezmer distribution fits his data well.

However, most other investigators found that log-normal distributions provides the best fit (Tavlarides and Stamatoudis, 1981; Pacek et al., 1998). On the other hand, Nishikawa et al. (1991) found that the cumulative-volume distribution is best represented by a combination of three normal distribution curves regardless of the controlling drop formation phenomenon. The first curve is for small size drops, which occupy almost half the drop number, though less than 1% of the volumetric fraction. The second one is for intermediate size drops, which account for 94% in volumetric fraction, and the third one is for larger drops, which occupy about 5% of the volumetric fraction though only 1% in number.

To provide a better understanding of the factors affecting the dispersion, the distributive- and cumulative-volume densities are shown in Figure D98-Figure D119 for the two systems investigated. As can be seen from these figures, the size at which the volume density peaks was found to shift to larger drop sizes as the agitation intensity decreases. In general, volume-number-distributions are slightly skewed to smaller drop sizes and occasionally show bi-modality particularly in the presence of high surfactant concentration (e.g. Figure D106 and Figure D116). In these cases, the persistence of a bi-modal distribution, a phenomenon usually encountered under transient conditions (Section 4.1.1.5) even after 170 minutes is probably attributable to the large coalescence retardation encountered at high SAA concentration (Figure D106) or when a highly effective SAA is used (Figure D116). Chen and Middleman (1967) reported a similar bi-modal volume distribution in the case of kerosene dispersed in water, while Chatzi et al. (1991a) observed a similar phenomenon in the case of surfactant-containing dispersions even after 9 hours.

To characterize a bimodal system accurately, it is necessary to identify the properties of the two constituent distributions. However, depending on the extent of bimodality, the system may be approximated using a single distribution. To test the accuracy of this simplification, the case showing the highest degree of bimodality was used (Figure 11). The cumulative-volume distribution associated with these results (Figure 12) was fitted using the log-normal distribution, yielding the following correlation coefficient values:

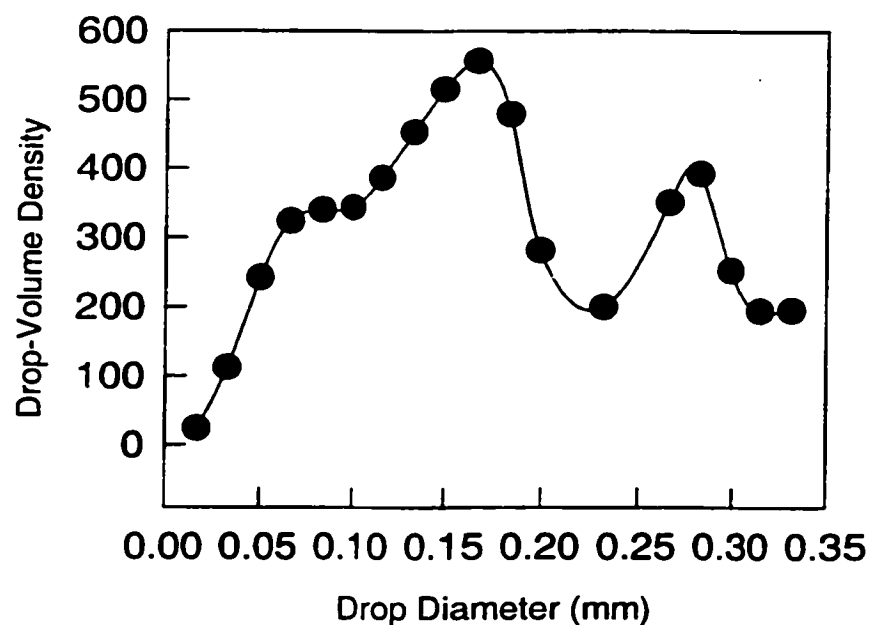


Figure 11. Bimodality in volume density (0.75% acetophenon/ 0.05 molar aq. NaCl, 300→200 rpm, after 120 minutes)

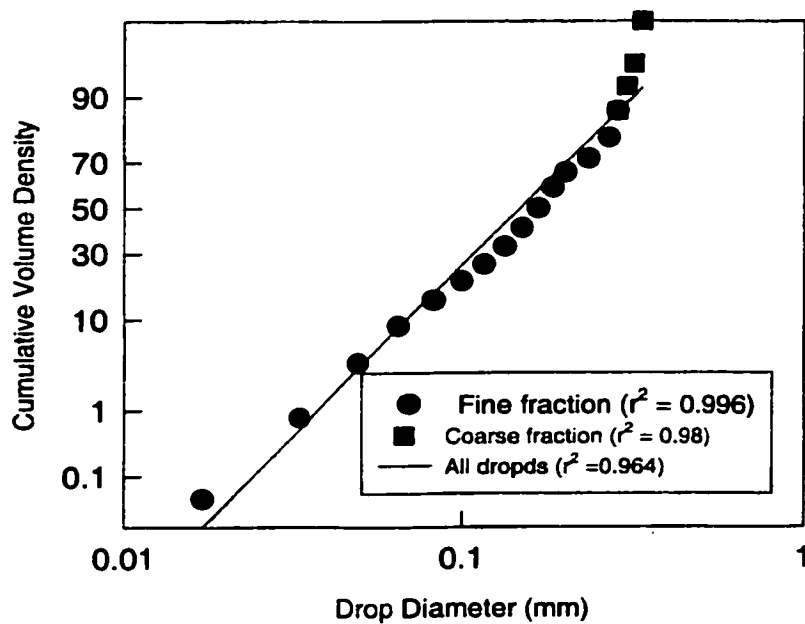


Figure 12. Bimodality in cumulative-volume density (0.75% acetophenon/ 0.05 molar aq. NaCl, 300→200 rpm, after 120 minutes)



a) using a single distribution

$$R=0.977$$

b) using two distributions

$$R=0.998 \text{ (for the finer drop size fraction, 14 points)}$$

$$R=0.990 \text{ (for the coarser drop size fraction, 5 points)}$$

The fit obtained using a single distribution was found to be not significantly different from that obtained using two distributions at the 95% confidence level (using the finer drop size fraction for testing purposes). Since this inability to distinguish between the two approaches was found in conjunction with the most-severe bimodal case, it was decided to describe all distributions using a single function.

The cumulative-volume densities of the systems studied in this research (Figure D99-Figure D119) clearly show that the contribution of small drops to the cumulative-volume density is more pronounced at higher agitation intensities. The quasi-steady cumulative-volume density data were fitted by normal and log-normal distributions and the results obtained are shown in Table A21. Although both distributions fit the volume density data well, the log-normal distribution generally provides a better fit. It provides a statistically better fit (at the 95% confidence level) for most cases run at 200 rpm, while, on the other hand, it does not provide a statistically better fit (at the 95% confidence level) for most runs at 300 rpm.

The correlation coefficient was found to decrease systematically with increasing surfactant concentration and with decreasing impeller speed, suggesting that a deviation from log-normal and normal distribution is being caused by those factors. This is probably caused by the incomplete disappearance of the bi-modal distribution encountered under transient conditions. And is particularly pronounced when coalescence rates are reduced by lower collision frequencies (rotational speed) and/or lower coalescence efficiencies (higher SAA concentrations). Figure D99-Figure D119 and Table A20 clearly show that the average drop size and standard deviation both decrease with increasing agitation intensity and/or the molecular weight of the SAA. The effect of

SAA concentration is most pronounced at lower values and tends to level off at higher concentrations.

#### **4.1.1.5 Transient Drop Size Distribution**

The temporal variation of the drop-size distributions (number, volume, and cumulative volume densities) following a sudden reduction in agitation speed (300→200 rpm) are shown in Figure E120-Figure E129, Figure E131-Figure E139, and Figure E140-Figure E149. Following a sudden decrease in impeller speed, the peak in the number-, and volume-density was found to shift towards the formation of larger drop sizes. The drop growth is caused by the coalescence rate being larger than the breakage rate during the initial stages. This difference progressively decreases until coalescence is balanced by breakage where steady state is reached.

Transient number densities were found to follow a uni-modal distribution, which is best fitted by a log-normal model (Figure E120-Figure E129). As time progresses, the size at which the peak of the number-density is located slightly shifts towards larger drop size and at the same time a number of large drops appear. The formation of these large drops is due to coalescence of small drops, which is caused by the lower breakage and higher coalescence rate following a step decrease in impeller speed. This finding is in line with that of Tobin et al. (1990) who investigated the dispersion of benzene-CCl<sub>4</sub> in water, whereas it is in contradiction with the findings of Laso et al. (1987) who observed bimodality in the number density of CCl<sub>4</sub>-*n*-heptane dispersion in water, following a step decrease in impeller speed. This is also in contradiction with findings of Hong and Lee (1983) who observed bimodality in ethyl acetate dispersed in water as agitation starts.

As can be seen from Figure E131-Figure E139, the temporal evolution of the drop-volume density is associated with a broadening of the distribution and a significant decrease in the size of the distribution peak. As seen from the drop-number-distributions (Figure E120-Figure E129), this results from the formation of only few large drops combined with minor variations in the drop-number distribution at smaller drop sizes.

Only after very long coalescence times are perceptible changes seen in the small drop size fractions.

Though not seen in the transient number densities, bimodality was observed to occur in transient volume density. When the coalescence rate is high, bi-modal distributions can appear as soon as 5 minutes and vanish as the steady state is approached after 170 minutes (Figure E130). On the other hand, bi-modality first appears at a later time when coalescence rate is slow (as late as 100 minutes in the case of 1.0 mmole/m<sup>3</sup> Triton X100) and continues to persist even after 180 minutes (Figure E133). The time at which bimodality in drop-volume density first appears was found to depend on the type of SAA used and its concentration (Figure E136) (Figure E138). Bimodality is therefore associated with the presence of a transient condition (due to changes in hydrodynamic and/or interfacial conditions) and the rate at which drop-size distributions evolve from initial to final steady state conditions. This observation is similar to those reported by Chatzi et al. (1991a, b) who observed bi-modality in drop-volume density for wide range of PVA concentrations. It is also in line with findings of Laso et al. (1987) who observed bimodality in drop-volume density of CCL<sub>4</sub>-*n*-heptane dispersion in water, following a step decrease in impeller speed.

The transient cumulative drop number-, and the volume-density data were fitted by normal and log-normal distributions and the results obtained are shown in Table A23-Table A41. All the correlation coefficients were found to be statistically significant at the 99% confidence level. Although both distributions fit the number and volume density data well, the log-normal distribution generally provides a better fit. It provides a statistically better fit (at the 95% confidence level) for systems of acetophenon/ 0.05 molar aq. NaCl and in the presence of Triton at concentrations up to 1.0 mmole/m<sup>3</sup>, while, on the other hand, it does not provide a statistically better fit (at the 95% confidence level) for acetophenon/ 0.05 molar aq. NaCl and in the presence of 0.1 mmole/m<sup>3</sup> Triton X100, X305, or X405. Deviations from these analytical models was found to increase with increasing surfactant concentration and with an increase in

molecular weight, and the progression of time. This may be attributed to the bi-modality that is developed in the temporal drop-volume density following a step decrease in impeller speed.

The formation of bi-modal distributions in SAA-containing systems undergoing net breakage was attributed to the prevalence of the erosive breakage mechanism which involves the removal of a number of small drops from a larger one (Chatzi et al., 1991b). This gives rise to two superimposed distributions with the mode of the smaller one corresponding to the size of the daughter or satellite drops. This explanation does not apply to the situation at hand since no bimodality was observed under steady state conditions (at 200 and 300 rpm) in SAA-containing systems. Furthermore, bi-modality was observed to occur in the absence of SAA (where erosive breakage is unlikely to happen) under unsteady conditions following sudden reductions in speed from 300 to 200 rpm.

The formation of bi-modal drop distributions could be caused by the large spatial variation in local energy dissipation rate ( $\epsilon$ ) in mechanically-agitated tanks ( $\epsilon$  in the impeller zone is at least an order of magnitude higher than that in the rest of the vessel) and the continuous recirculation of the dispersion between regions of high and low  $\epsilon$ . Different shear-rate zones are expected to contribute differently to the dispersion/coalescence processes, particularly since the residence time in the impeller region and the rest of the vessel are significantly different. Coalescence may thus take place in the zone beside the impeller zone (very high collision rate) as well as in the rest of the tank (very low energy dissipation rate). These two different zones provide different coalescence efficiencies, and consequently drops may grow differently in these regions. Two distinct drop-size distributions may thus appear as the droplets undergo net growth.

#### **4.1.1.6 Self-Similarity**

Several investigators (Pacek et al., 1998; Sprow, 1967; Chen and Middleman, 1967; Tobin et al., 1990; Wright and Ramkrishna, 1994) found that the cumulative-volume densities as a function of normalized drop diameter can be fitted by a single correlation.

A dispersed system is thus considered to have self-similarity behavior when its cumulative-volume density as a function of normalized drop diameter fits a certain function.

The cumulative-drop-volume densities at the quasi-steady state (i.e. after 3 hours of mixing at 300 rpm) were normalized using their corresponding Sauter mean diameter and fitted to normal and log-normal distributions. The cumulative-volume density of all systems is shown in Figure F154. The results of the regression analysis (of the data obtained using the acetophenon/ 0.05 molar aq. NaCl/ Triton systems) are listed in Table 11 which also includes the results reported by other investigators. The correlation coefficients were found to be statistically significant at the 99% confidence level. The correlation coefficient obtained using the log-normal distribution was found to be significantly better (99% confidence level) than that obtained using the normal distribution. This is in agreement with the results obtained by Pacek et al. (1998) for silicone oil in water, as well as Wright and Ramkrishna (1994) who investigated benzene  $\text{CCl}_4$ /water dispersions.

The value of the normalized mean and standard deviation of the cumulative-volume distributions obtained in this investigation were found to be higher than those reported by the investigators listed in Table 11. This is particularly true at 200 rpm and can possibly be attributed to the fact that steady state has not been sufficiently approached after 3 hours agitation at 200 rpm. However, as can be seen from Figure F152-Figure F153 the fit is very good. A possible explanation for the large average  $(\overline{d/d_{32}})$  and standard deviation could be the fact that steady state was not sufficiently approached in our case due to the presence of surfactants in the system. The small drops that may have not yet coalesced will strongly influence the value of  $d_{32}$  (i.e. reduce it because of their relatively large specific surfaces) resulting in the value of the normalized mean being higher than that achieved as steady state is approached.

Table 11. Regression analysis of the normalized cumulative-volume density for (0.75% acetophenon/ 0.05 molar aq. NaCl/ Triton)

a) Normal distribution

	This work (300 rpm)	This work (200 rpm)	Pacek et al. (1998)	Berkman and Calabrese (1988)	Wang and Calabrese (1986)	Chen and Middleman (1967)	Brown and Pitt (1972)
R	0.967	0.945	0.995	N/A	N/A	N/A	N/A
$\overline{d/d_{32}}$	1.275	1.322	0.98	1.12	1.07	1.06	1.07
s.d.	0.434	0.472	0.26	0.31	0.24	0.23	0.20

b) LogNormal distribution

	This work (300 rpm)	This work (200 rpm)	Pacek et al., (1998)
R	0.996	0.998	0.995
$\overline{d/d_{32}}$	1.06	1.09	0.97
s.d.	1.51	1.62	1.318

Similar observations were obtained in the case of CLB-Bayol oil dispersions  $\rho_d/\rho_c=0.99$  under quasi-steady state (Figure F150), whereas a significant deviation from a log-normal distribution was observed in the case of Bayol oil dispersions,  $\rho_d/\rho_c=0.79$  (Figure F151).

In a fashion similar to that of Sprow (1967b), attempts were made to fit the cumulative drop volume data by the Schwartz-Bezmer distribution:

$$\ln(F) = a / d_{\max} - a / d \quad (26)$$

where,

F = cumulative volume density

d = drop diameter

a = constant

$d_{\max}$  = maximum drop diameter

However, as seen in Table 12, the fit is not as good as that obtained using either the normal or log-normal distributions. Since the Schwartz-Bezmer distribution was unable to fit the cumulative-volume density adequately, it was decided not to use this distribution furthermore.

To examine the existence of self-similarity under transient conditions, the cumulative volume densities obtained using different systems, and monitored at different times, were normalized using their corresponding Sauter mean diameter and fitted to normal and log-normal distributions. The results obtained are given in Table 13, Table A42 and shown in Figure F155-Figure F169.

The correlation coefficients were significant (at the 95% confidence level). Although both distributions fit the volume density data well, the log-normal distribution generally provides a better fit. It provides a statistically better fit (at 99% confidence level).

In the absence of surfactants (Figure F156 and Figure F160), the deviation from self-similarity behavior is larger in the Bayol oil/water (density ratio of 0.79) than that in the 0.75% acetophenon/ 0.05 molar aq. NaCl (density ratio of 0.99), suggesting that deviation from self-similarity increases as the density difference between two phases increases. This is particularly true at the larger time following the impeller speed reduction. This is probably caused by the greater segregation tendencies (which result in an inhomogeneous spatial distribution of the drop concentration) in the former system. In such a case, the measured drop-size distribution will be biased against larger drop sizes (which tend to concentrate at the top of the mixing tank and are therefore not recorded by the imaging probe) the fraction of which increases with time following the sudden reduction in mixing speed. The presence of surfactants was found to suppress the deviation from self-similarity behavior in the case of systems with large density differences such as Bayol oil/water (Figure F156 and Figure F158). This may be due to fact that the drop size decreases in presence of surfactants, and therefore the negative effect of density differences on the self-similarity behavior is reduced.

Table 12. Regression analysis of fitting normalized cumulative-volume density to Schwartz-Bezmer distribution

a	a/d <sub>max</sub>	R
1.749	5.27	0.955

Table 13. Regression analysis of normalized cumulative-volume-densities obtained under transient condition (300→200 rpm)

System	Normal distribution			Log-normal distribution		
	$\frac{\bar{d}}{d_{32}}$	s.e.	s.d.	$\frac{\bar{d}}{d_{32}}$	s.e.	s.d.
0.75% acetophenon / 0.05 M aq. NaCl	1.334	0.036	0.457	1.099	0.046	1.681
0.75% acetophenon / 0.05 M aq. NaCl / 0.1 μM X100	1.269	0.045	0.382	1.044	0.049	1.498
0.75% acetophenon / 0.05 M aq. NaCl / 0.2 μM X100	1.447	0.110	0.574	1.162	0.115	1.672
0.75% acetophenon / 0.05 M aq. NaCl / 1.0 μM X100	1.420	0.090	0.596	1.141	0.091	1.691
0.75% acetophenon / 0.05 M aq. NaCl / 0.1 μM X165	1.387	0.067	0.478	1.124	0.072	1.583
0.75% acetophenon / 0.05 M aq. NaCl / 0.2 μM X165	1.334	0.074	0.476	1.101	0.077	1.571
0.75% acetophenon / 0.05 M aq. NaCl / 0.1 μM X305	1.241	0.042	0.359	1.037	0.049	1.500
0.75% acetophenon / 0.05 M aq. NaCl / 0.2 μM X305	1.356	0.076	0.457	1.114	0.077	1.513
0.75% acetophenon / 0.05 M aq. NaCl / 0.1 μM X405	1.317	0.053	0.473	1.068	0.054	1.566
0.75% acetophenon / 0.05 M aq. NaCl / 0.2 μM X405	1.346	0.095	0.556	1.094	0.084	1.567
0.5% CLB-Bayol oil / water	1.399	0.083	0.493	1.172	0.072	1.667
0.5% Bayol oil / water	1.488	0.076	0.646	1.167	0.079	1.776
0.5% Bayol oil / water / 0.25 μM X100	1.624	0.165	0.887	1.231	0.142	1.861
0.5% Bayol oil / water / 1.0 μM X100	1.432	0.091	0.659	1.151	0.083	1.683
0.5% Bayol oil / water / 4.5 μM X100	1.302	0.135	0.558	1.079	0.111	1.530

As can be seen from Figure F156-Figure F158 the deviation of the cumulative-volume density data from a log-normal distribution increases with the time elapsed following the sudden change in agitation intensity. This is particularly true at higher surfactant concentrations and is slightly affected by the molecular weight of the SAA. (Figure F161-Figure F163). This deviation from self-similarity is caused by the development of bi-



modal distributions which, as discussed in section 4.1.1.5, is affected by the surfactant concentration and surfactant molecular weight.

#### 4.1.2 Average Drop Size

When a dispersion of immiscible liquids undergoes a step reduction in agitation intensity, the equilibrium between dispersion and coalescence processes is disturbed and coalescence rate prevails. Consequently, the drop sizes start to increase until a new steady state is reached at which coalescence is balanced by breakage. The variation of the drop number-volume mean, Sauter-mean, and volume-moment mean ( $d_{30}$ ,  $d_{32}$ , and  $d_{43}$ ) with time are shown in Figure G170-Figure G179 for the system acetophenon/ 0.05 M aqueous NaCl solution/ Triton. In general, all average drop sizes were found to increase with time. This is caused by the shift in equilibrium conditions following a step decrease in agitation intensity, resulting in higher coalescence and lower breakage rates. These findings are in agreement with those of Bhardwaj and Hartland (1994) who found that in the case of water/ crude oil emulsions (to which demulsifiers are added), the drop size increases dramatically in the first few seconds following a step reduction in agitation intensity, but the rate of change slows down considerably as time progresses. These findings are also in line with Calabrese et al. (1993) where  $d_{32}$  was found to increase sharply in the first 10 minutes following a reduction in agitation intensity. As can be seen from Figure G170-Figure G179, average drop sizes with higher moments (e.g.  $d_{43}$ ) change faster than those with lower moments (e.g.  $d_{30}$ ). Similarly, the maximum average diameter value reached after 3 hours is higher for the larger moments. For any particular system, average drop sizes with higher moment show a larger rate of change with respect to time while those with smaller moments show a smaller rate of change. This is caused by the fact that average drop sizes with higher moments are more sensitive to the number of large drops, whereas those with smaller moments are more sensitive to the number of smaller drop.

The rate of change of the Sauter mean diameter was found to decrease as the surfactant concentration increased (Figure 13). This is attributed to the surfactant's ability to decrease coalescence rate by retarding the drainage of the continuous-phase film present between dispersed-phase drops, and by increasing the elasticity of the interface. Hence, the rate of drop growth is slowed at higher surfactant concentrations. Also, Figure 14 and Figure 15 show that in the presence of heavier or longer surfactants, drop growth is slower, suggesting that heavier/longer surfactants are more effective in retarding drop coalescence.

No correlation/theory is available to describe the temporal variation in drop diameter under coalescence-dominated conditions. However, few investigations addressed breakage-dominated situations. Using a light transmission technique, Hong and Lee (1985) measured the variation in Sauter mean diameter of liquid dispersions starting immediately after the agitation was initiated and continued until equilibrium was reached.

They noted that  $d_{32}$  decreases exponentially during the initial period of mixing and asymptotically approaches the equilibrium value,  $d_{32\infty}$ . They found that their data near equilibrium fitted the power law given by:

$$\frac{d_{32}}{d_{32\infty}} = 1 + \alpha t^\beta \quad (27)$$

where  $\beta$  is approximately -0.7. Skelland and Kanel (1992) found that in the case of chlorobenzene drops in aqueous Triton X100 solutions, the temporal variation of  $d_{32}$  follows Eq. (27). To account for the effect of surfactants on the evolution of drop size, they proposed that  $\beta$  be calculated as follows:

$$\beta = -0.28 \frac{\gamma - \gamma_{Eq}}{\gamma - \gamma_{0SAA}} - 0.66 \quad (28)$$

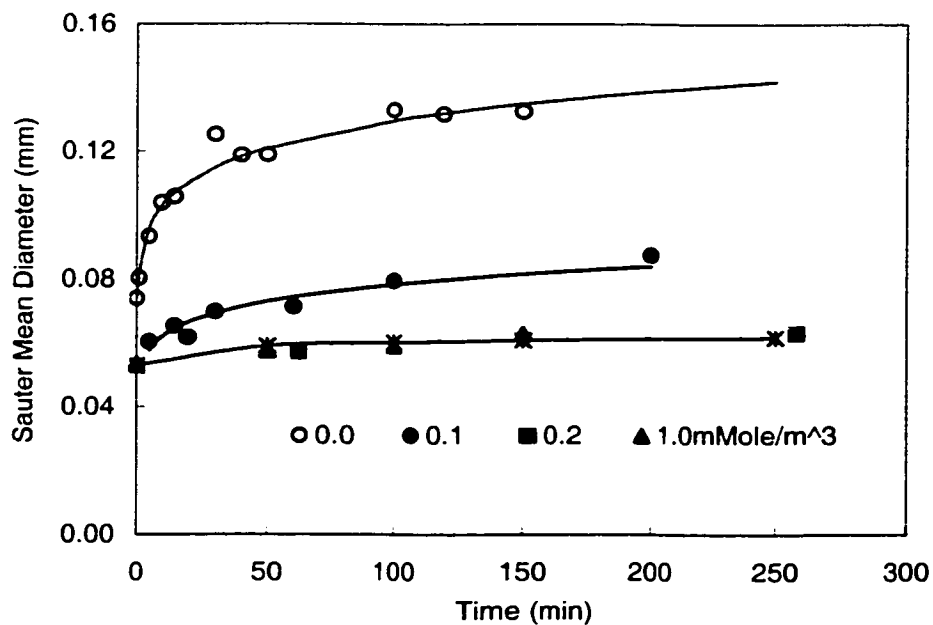


Figure 13. Effect of surfactant concentration on Sauter mean diameter of (0.75% acetophenon/ 0.05 molar aq. NaCl / Triton X100)

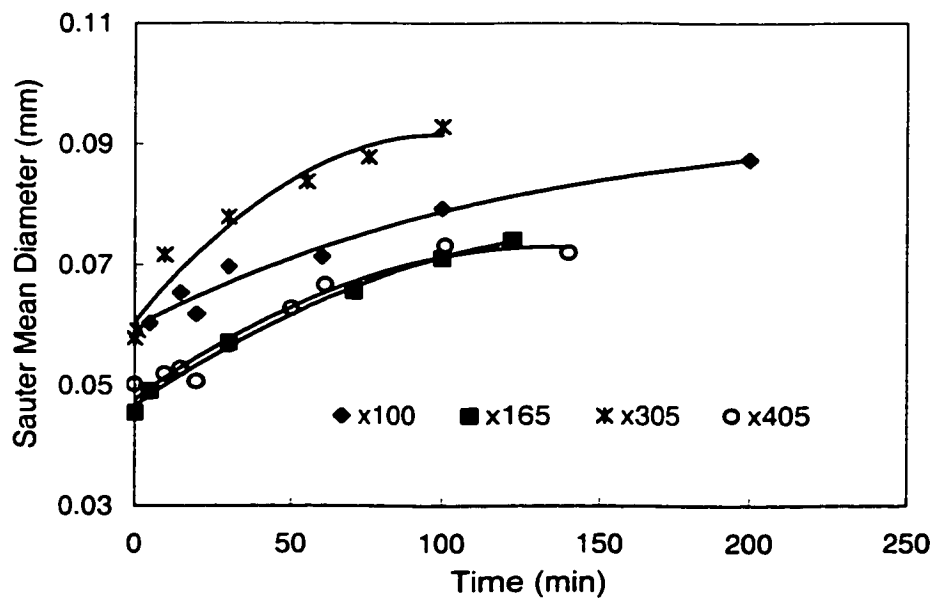


Figure 14. Effect of surfactant molecular weight/length on Sauter mean diameter of (0.75% acetophenon / 0.05 molar aq. NaCl/ 0.1 mmole/m<sup>3</sup> Triton)

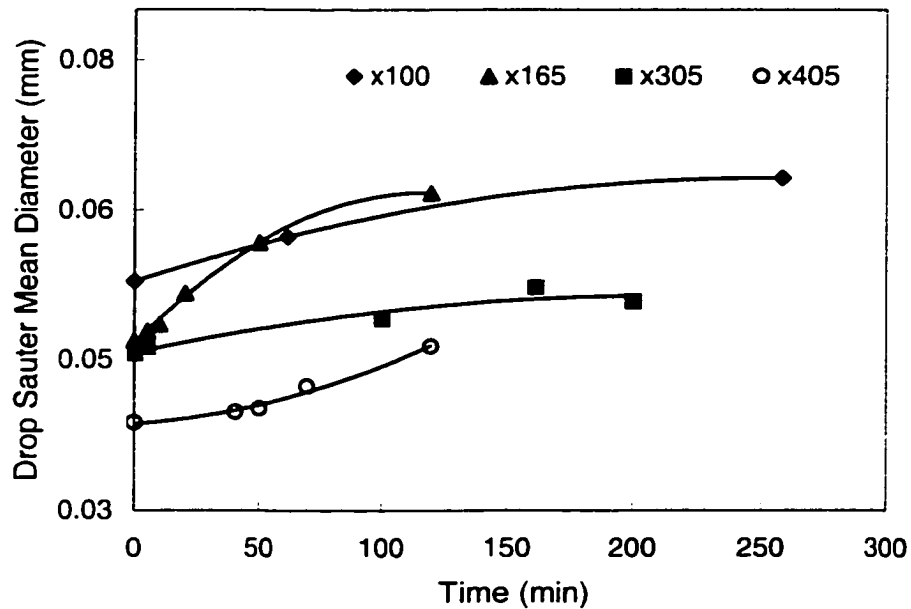


Figure 15. Effect of surfactant molecular weight/lenght on Sauter mean diameter of (0.75% acetophenon/0.05 molar aq. NaCl/ 0.2 mmole/m<sup>3</sup> Triton)

Skelland and Kanel (1992) found  $\beta$  to vary between  $-0.6$  and  $-1.0$ . It must be noted that these results are valid for breakage-dominated conditions (which are encountered immediately after a sudden increase in agitation intensity) and are therefore not directly relevant to the coalescence-dominated situation here. Konno et al. (1993) investigated breakup of toluene drops in water in the early period of agitation, in 0.01% holdup and in the presence of surfactant Tween 20. They proposed a value of  $-0.25$  for  $\beta$  in Eq. (27).

The development of a model that describes the evolution of  $d_{32}$  in the early stages following a step reduction in impeller speed is of special interest to coalescence studies. Such a model can then be differentiated to calculate the coalescence rate of the dispersed phase at time zero (where the rate of coalescence is much higher than that of breakage) yielding accurate measures of coalescence rates. Consequently, the power function form proposed by Hong and Lee (1985) and revised by Skelland and Kanel (1992) may not be suitable for the case of coalescence since its differential value at time zero is infinite. Attempts to use an exponential function of the form:

$$d_{32} = a + b \text{Exp}(ct) \quad (29)$$

to fit the data was found to be inadequate because it failed to provide good fit in the initial, as well as the latter, stages of drop growth. Use of a limited number of experimental points focused on the early stages was deemed to be statistically incorrect because of the large number of adjustable parameters (three) present in this expression, Eq. (29).

Wright and Ramkrishna (1994) proposed that following a step decrease in impeller speed, the evolution of the average drop volume (defined as  $\sum n_i v^2 / \sum n_i v$ ) may be expressed as follows:

$$v_{av} \propto t^{0.5} \quad (30)$$

in the case of benzene-carbon tetrachloride drops dispersed in water. Translated to  $d_{63}$ , the above equation can be rewritten as:

$$d_{63} \propto t^{0.17} \quad (31)$$

In our attempt to identify a suitable expression for the evolution of the Sauter mean diameter as a function of time, it was deemed preferable to have a form that incorporates the initial value of  $d_{32}$ . This value is obtained at higher impeller speeds and can thus have a better chance of being at equilibrium. A modified form of Equation (27) was therefore used:

$$d_{32} = a (t+1)^b \quad (32)$$

where  $a$  is the value of  $d_{32}$  at time zero (i.e. the equilibrium value at the higher impeller speed), and  $b$  is an exponent the value of which depends on the hydrodynamic and interfacial conditions encountered in the system. The experimental data were fitted to Eq. (32) and the value of the regression parameters obtained ( $a$  and  $b$ ) are listed in Table 14.

Table 14. Regression analysis of transient Sauter mean diameter (Eq. 28)

System	Quasi-equilibrium $d_{32}$ at 300 rpm (mm)	a	b	R
0.75% acetophenon/ 0.05 M aq. NaCl	0.074	0.075	0.148	0.979
0.75% acetophenon/ 0.05 M aq. NaCl / 0.1 mmole/m <sup>3</sup> X100	0.053	0.053	0.072	0.962
0.75% acetophenon/ 0.05 M aq. NaCl / 0.2 mmole/m <sup>3</sup> X100	0.053	0.052	0.029	0.944
0.75% acetophenon/ 0.05 M aq. NaCl / 1.0 mmole/m <sup>3</sup> X100	0.053	0.053	0.027	0.938
0.75% acetophenon/ 0.05 M aq. NaCl / 0.1 mmole/m <sup>3</sup> X165	0.046	0.043	0.102	0.966
0.75% acetophenon/ 0.05 M aq. NaCl / 0.2 mmole/m <sup>3</sup> X165	0.047	0.044	0.059	0.971
0.75% acetophenon/ 0.05 M aq. NaCl / 0.1 mmole/m <sup>3</sup> X305	0.058	0.057	0.095	0.916
0.75% acetophenon/ 0.05 M aq. NaCl / 0.2 mmole/m <sup>3</sup> X305	0.046	0.045	0.023	0.933
0.75% acetophenon/ 0.05 M aq. NaCl / 0.1 mmole/m <sup>3</sup> X405	0.050	0.048	0.043	0.810
0.75% acetophenon/ 0.05 M aq. NaCl / 0.2 mmole/m <sup>3</sup> X405	0.039	0.038	0.026	0.681

The correlation coefficients of the resulting expressions were found to be significant at the 99% confidence level. However, in the case of the slowest coalescing system (0.75%acetophenon/ 0.05 molar aq. NaCl / 0.2 mmole/m<sup>3</sup> Triton X405) the correlation coefficient was significant only at the 80% confidence level.

As noticed from Table 14, the value of the exponent b is affected by the surfactant type and concentration. It decreases as the surfactant concentration increases, indicating a slower rate of drop coalescence. The value of the exponent b for the pure system (b = 0.148) is very close to that predicted by Eq. (31) for the system of benzene-carbon tetrachloride/ water. However, considering that the rate of change of  $d_{63}$  is higher than that of  $d_{32}$ , due to the higher moment, the exponent value obtained in this study is in very good agreement with that proposed by Wright and Ramkrishna (1994).

Under steady state conditions, Wright and Ramkrishna (1994) found that, in the case of benzene-carbon tetrachloride drops dispersed in water, the dependence of  $d_{32}$  on the impeller speed can be expressed as follows:

$$d_{32} \propto N^{-6/5} \quad (33)$$

where  $N$  is the impeller speed. According to this equation, the equilibrium average drop diameter increases by a factor of 1.4 as the impeller speed is reduced from 300 to 200 rpm. The values predicted using this approach are generally larger than those experimentally observed with the deviation being larger at higher surfactant concentration. This systematic deviation is therefore probably caused by the fact that steady-state conditions have not been adequately approached even after three hours of mixing at 200 rpm. The quasi-equilibrium values of the Sauter mean diameter for the systems studied in this thesis are shown in Table 15.

Table 15. Quasi-equilibrium Sauter mean diameter (0.75% acetophenon / 0.05 M aq. NaCl / Triton systems)

Triton	Conc. (mmole/m <sup>3</sup> )	d <sub>32</sub>		
		300 rpm	200 rpm	Predicted @ 200 rpm*
No SAA	0.0	0.074	0.132	0.120
X100	0.1	0.053	0.087	0.086
X100	0.2	0.053	0.063	0.086
X100	1.0	0.053	0.072	0.086
X165	0.1	0.046	0.074	0.075
X165	0.2	0.047	0.062	0.076
X305	0.1	0.058	0.093	0.094
X305	0.2	0.046	0.051	0.075
X405	0.1	0.050	0.072	0.081
X405	0.2	0.039	0.046	0.063

\*Predicted using equation (33)

#### 4.1.3 Coalescence Rate

One of the main objectives of this thesis was to study the effect of interfacial characteristics on coalescence rate. The inverse population balance approach was successfully used to study the effect of hydrodynamic factors on coalescence frequency

(Wright and Ramkrishna, 1994). Inverse population balance is based on the assumption of ignoring the breakage process under coalescence-dominated conditions, a situation that is prevalent at the early stages following a sudden reduction in agitation intensity. In certain systems, normalizing the drop diameter unifies all the transient size distributions in a unique form. Thus, the time domain is concealed and an analytical solution to the population balance equation is made possible at the coalescence-dominated condition. So far, inverse population balance has not been applied to identify the dependence of coalescence frequency on interfacial factors.

Assuming a homogeneous mono-dispersed system, Howarth (1967) derived the following equation for the coalescence frequency of a single droplet per unit time:

$$\text{Coalescence frequency} = \left. \frac{\partial d_{32}}{\partial t} \right|_{t=0} \frac{1}{d_{320}} \frac{1}{2 - 2^{2/3}} \quad (34)$$

This expression is based on the rate of change of  $d_{32}$  with time normalized by the initial value of  $d_{32}$  at the higher impeller speed. Taken at an early stage of the drop size evolution, this parameter yields a good indication of the coalescence rate without interference of breakage. This expression was used by Campbell et al. (1996) and by Bhardwaj and Hartland (1994) as a measure of the coalescence rate of a single droplet with an average drop diameter ( $d_{32}$ ). A similar approach was adopted in this work.

Substituting Eq. (32) into Eq. (30) results in:

$$\text{Coalescence rate} = b/(2-2^{2/3}) \quad (35)$$

Estimates of the coalescence rates, their standard deviation, and the corresponding correlation coefficient of the various systems investigated are shown in Table 16. The correlation coefficients were found to be significant at the 99% confidence level. However, in the case of the slowest coalescing system (0.75% acetophenon/ 0.05 molar aq. NaCl / 0.2 mmole/m<sup>3</sup> Triton X405) the correlation coefficient was significant only at the 80% confidence level.



Table 16. Effect of concentration and molecular weight of surfactants on coalescence rate of the systems studied

System	Coalescence rate (min <sup>-1</sup> )	s.e.	R
0.75% acetophenon/ 0.05 M aq. NaCl	0.140	0.010	0.979
0.75% acetophenon/ 0.05 M aq. NaCl / 0.1 mmole/m <sup>3</sup> X100	0.071	0.015	0.962
0.75% acetophenon/ 0.05 M aq. NaCl / 0.2 mmole/m <sup>3</sup> X100	0.029	0.010	0.944
0.75% acetophenon/ 0.05 M aq. NaCl / 1.0 mmole/m <sup>3</sup> X100	0.025	0.005	0.938
0.75% acetophenon/ 0.05 M aq. NaCl / 0.1 mmole/m <sup>3</sup> X165	0.102	0.014	0.966
0.75% acetophenon/ 0.05 M aq. NaCl / 0.2 mmole/m <sup>3</sup> X165	0.046	0.015	0.920
0.75% acetophenon/ 0.05 M aq. NaCl / 0.1 mmole/m <sup>3</sup> X305	0.031	0.005	0.916
0.75% acetophenon/ 0.05 M aq. NaCl / 0.2 mmole/m <sup>3</sup> X305	0.024	0.007	0.933
0.75% acetophenon/ 0.05 M aq. NaCl / 0.1 mmole/m <sup>3</sup> X405	0.023	0.002	0.810
0.75% acetophenon/ 0.05 M aq. NaCl / 0.2 mmole/m <sup>3</sup> X405	0.026	0.003	0.681

The effect of surfactant concentration on coalescence rate is shown in Figure 16. For any particular surfactant, the coalescence rate was found to decrease as the concentration of the surfactant increases. This is in agreement with the findings of Peru and Lorenz (1989) that upon the addition of a small amount of surfactant, coalescence time increases markedly, and a further increase in concentration reduces the coalescence time more gradually. Our findings are also in agreement with those of Nakache et al. (1995) where the interface-drainage time of a heptane drop approaching a water surface was found to increase with increasing polymeric surfactant concentration. However, there is no systematic variation with molecular weight of SAA.

On the other hand, at any particular molecular concentration of the Triton -X series, the coalescence rate was found to be a non-monotonic function of the molecular weight of the SAA. As can be seen from Figure 17-Figure 18, the coalescence rate first increases with increasing molecular weight/size of the surfactant, reaches a maximum at X165 (molecular weight 916) beyond which the coalescence rate was found to decrease as the molecular weight/size of surfactant increases. This phenomenon is somewhat similar to

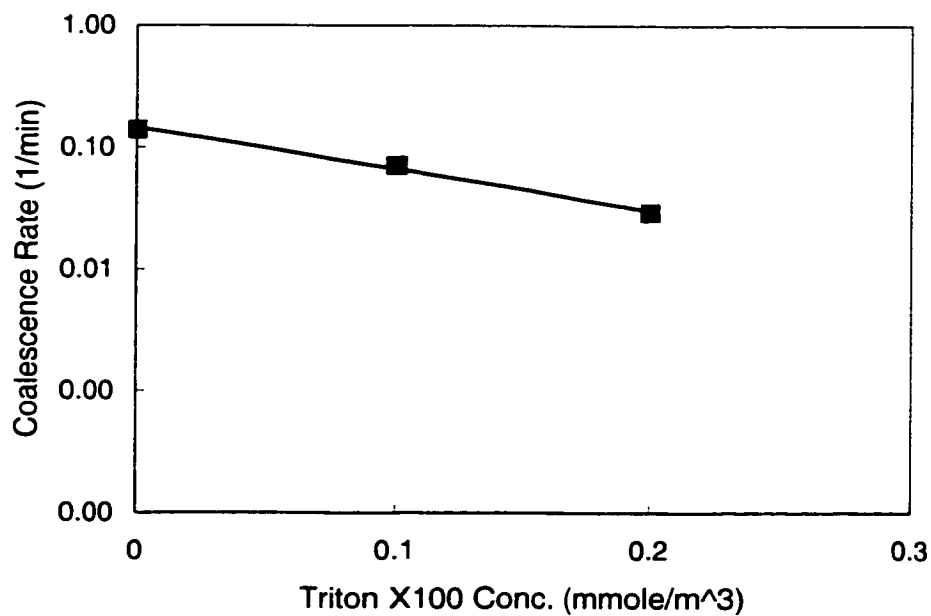


Figure 16. Effect of surfactant concentration on the coalescence rate of (0.75% acetophenon/ 0.05 molar aq. NaCl / Triton X100, 200 rpm)

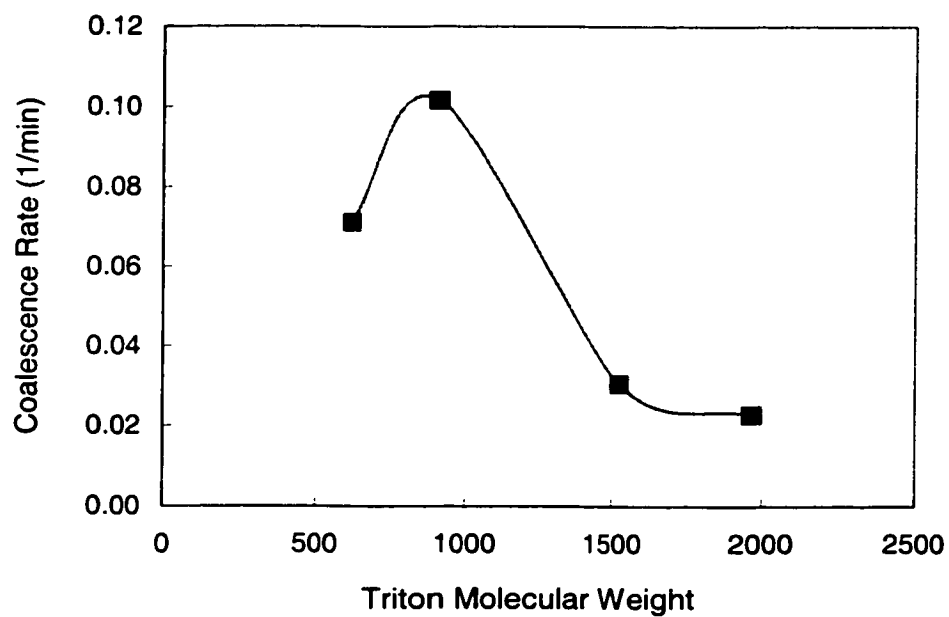


Figure 17. Effect of surfactant molecular weight/length on the coalescence rate of (0.75% acetophenon/ 0.05 molar aq. NaCl / 0.1 mmole/m<sup>3</sup> Triton, 200 rpm)

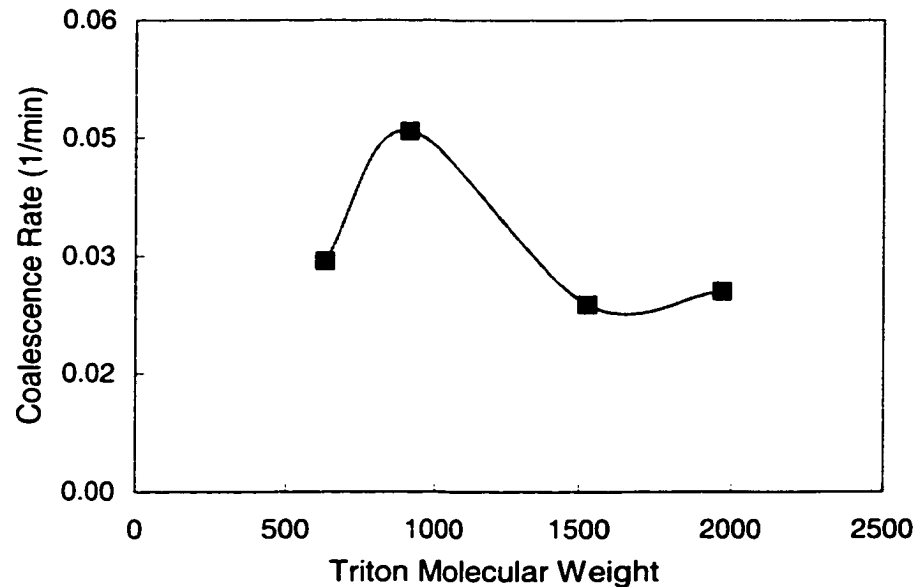


Figure 18. Effect of surfactant molecular weight/length on the coalescence rate of (0.75% acetophenon/ 0.05 molar aq. NaCl / 0.2 mmole/m<sup>3</sup> Triton, 200 rpm)

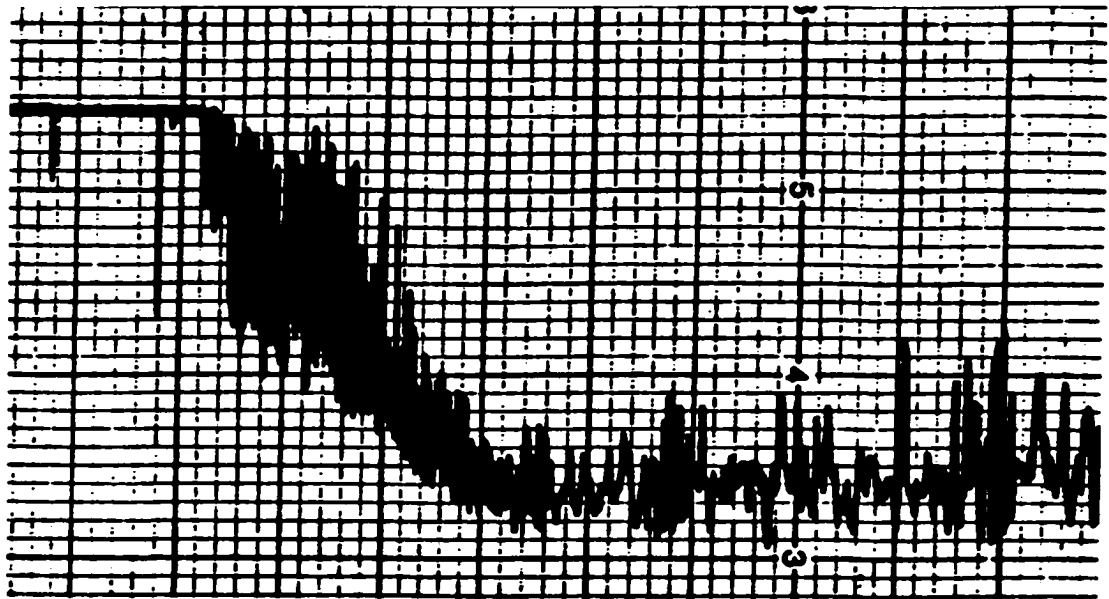
the results reported by Wasan et al. (1979) who observed a maximum in the effect of salt concentration on the coalescence time of the crude oil-water interface.

#### 4.2 Phase Inversion

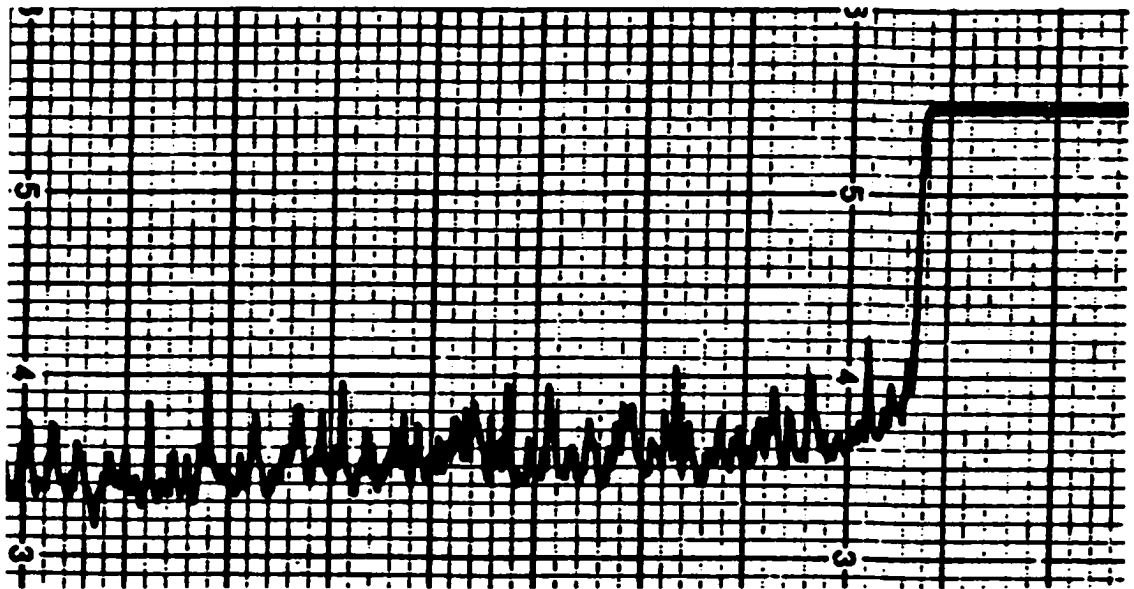
It is therefore desirable to have a parameter that can be related directly to coalescence rates. An attempt to use various dynamic interfacial characteristics for that purpose is given in Section 4.4.

In this section, phase inversion observations obtained in O/A and A/O systems are considered. This is followed by a discussion of the experimental findings of the measured phase-inversion delay time. Finally, the effect of hydrodynamic and interfacial characteristics on phase inversion is discussed.

Phase inversion was primarily monitored using changes in the conductivity of the dispersion. A typical example of the conductivity signal obtained is shown in Figure 19.



a) Bayol oil/water→ water/ Bayol oil, 700 rpm



b) water/gasoline→gasoline / water, 700 rpm

Figure 19. A typical example of conductivity signal during phase inversion

This signal is similar to those reported by most investigators who used closely-spaced conductivity probes. However, it differs from that reported by Campbell et al. (1996) who used a conductivity technique that measured the average conductivity of the vessel's contents.

The dynamics of the phase inversion of water/Irving kerosene system was experimentally studied by increasing the dispersed-phase holdup gradually until phase inversion was observed. Video recordings revealed the presence of continuous-phase droplets within the dispersed-phase drops once the water holdup reaches 10% for the kerosene/water system (Figure 20). The size and number of droplets enclosed within the dispersed phase were found to be small at the 10% holdup. This is in agreement with the finding of Pacek et al. (1995) and Neinow et al. (1994). As the holdup increased to 30%, the number and size of droplets included in the dispersed phase drops were found to increase significantly (Figure 21). Although phase inversion does not take place at these holdups, the equilibrium between the droplets' inclusion and escape results in an effective dispersed phase holdup which is higher than the initial one due to the increased volume of the dispersed phase (resulting from the inclusion of continuous-phase droplets), and the reduction of the freely available continuous phase volume. At critical holdup (45% for the water/Irving kerosene system), a number of very large globular drops, that include many droplets of the continuous-phase, were observed to appear (Figure 22). Those observations are in agreement to those reported by Pacek et al. (1994a, 1994b, 1995) and Nienow et al. (1993, 1995) but differ in the shape of the large globules encountered. They observed essentially spherical globules in the case of the water/CLB system, while elongated globules were encountered in case of water/kerosene. This is probably because of lower interfacial tension in the latter system (14 vs. 33.4 mN/m). In the present study, the critical holdup is defined as the holdup at which the system ultimately inverts, whereas the holdup at which phase inversion happens instantaneously (i.e. zero delay time) is referred to as the catastrophic holdup.

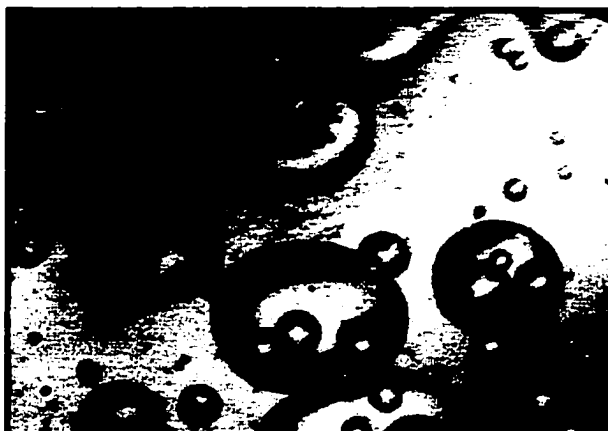


Figure 20. Inclusion of continuous droplets in dispersed drops (10% water/ Irving kerosene)



Figure 21. High packing of droplets in drop (30% water / Irving kerosene)



Figure 22. Long dispersed drops (45% water / Irving kerosene)

Images of kerosene dispersed in water show no water droplets to be present in kerosene drops, even at holdups close to the critical holdup of 52% (Figure 23). Similar observations have been reported by Pacek et al. (1994). With the presently available state of knowledge, it is difficult to conclude whether this is caused by very low inclusion rates or by very high escape rates. A more detailed investigation of this issue, particularly at conditions close to the phase inversion point, could shed light on this issue (Pacek et al. (1994a).

As mentioned in the phenomenological interpretation of phase inversion (discussed in Section 2.1.1), the phase-inversion delay time is generated by the net overall kinetics of the competing processes of droplet inclusion and escape. Shorter phase inversion times are thus obtained if the droplet inclusion rate is high and much larger than the droplet escape rate. Conversely, long phase inversion times are encountered if the droplet inclusion rate is small or if the difference between the droplet inclusion and escape rates is small. The phase inversion delay times measured in this investigation (for the case of water dispersed in gasoline) were found to vary between 10-700 seconds depending on how close the initial dispersed phase holdup is to the catastrophic value. The closer the initial holdup to the catastrophic value, the shorter the delay time.

The effect of initial water holdup on the phase inversion delay time is shown in Figure 24. The delay time was found to approach zero as the dispersed phase holdup exceeded 87.5%; this value may thus be considered as the catastrophic phase-inversion holdup for this system at 700 rpm. On the other hand, the delay times were found to grow exponentially for values smaller than 85%. This is in agreement with the findings of Nienow et al. (1994) where the delay time increased from 50→600 seconds as the initial holdup was reduced from 50%→40%.

It can be assumed that infinite mixing time is needed for phase inversion to take place at the critical phase-inversion holdup. To accommodate this and the observation that zero delay time is encountered at the catastrophic phase-inversion holdup, the following simple relationship was found to fit the data well (Figure 24).

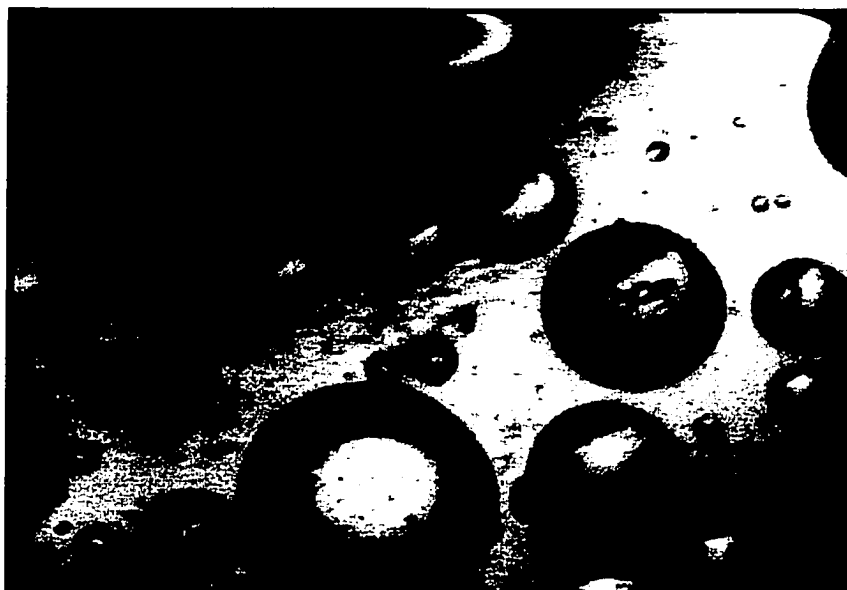


Figure 23. Dispersed drops of Irving kerosene in water (45% holdup)

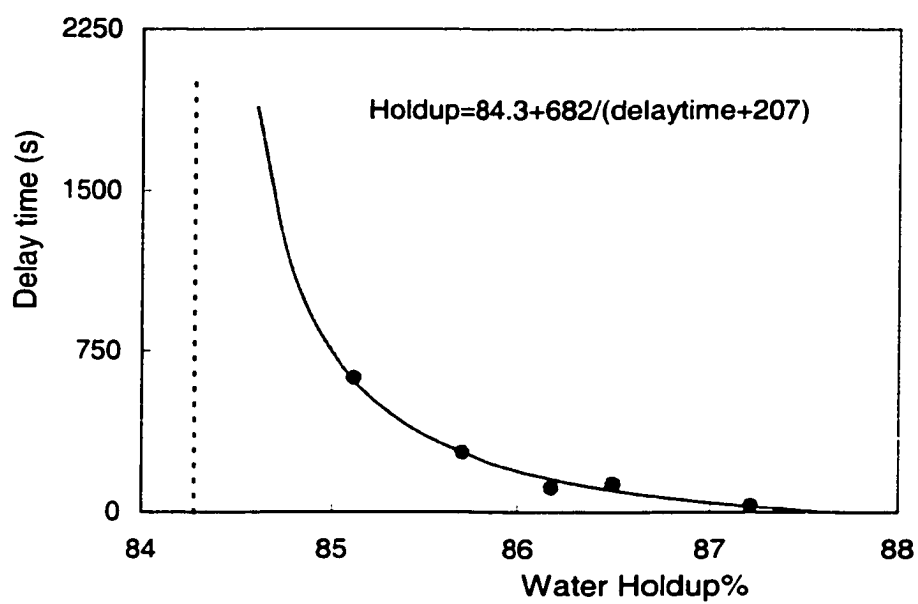


Figure 24. Effect of dispersed phase holdup on phase inversion delay time of (water/ Irving gasoline system, 700 rpm)



$$t_d = a' / (\Phi_{\text{initial}} - \Phi_{\text{Critical}}) + b' \quad (36)$$

where,

$\Phi_{\text{Initial}}$  = phase-inversion holdup at the beginning of the mixing process

$\Phi_{\text{Critical}}$  = holdup at which phase inversion begins to happen

For the system water/Irving gasoline, the values of  $a'$ ,  $b'$  and the critical phase holdup, obtained by regression analysis, are 682,  $-207$  and  $84.3$  respectively. The predicted catastrophic water holdup is thus estimated to be  $\Phi_{\text{Catastrophic}} = 87.6$ .

The effect of  $(\Phi_{\text{Catastrophic}} - \Phi_{\text{initial}})$  on delay time predicted by Eq. (36), is shown in Figure 25 which clearly shows that as the initial holdup approaches the catastrophic value the delay time decreases. In the phenomenological interpretation of phase inversion, it was suggested that the effective holdup increase due to the entrainment of continuous-phase droplets (and the consequent reduction of continuous-phase volume). Below the critical initial holdup, this process reaches equilibrium without phase inversion taking place. On the other hand, when the initial holdup is at, or exceeds the critical value, a net accumulation of droplets takes place until a critical value is reached at which catastrophic phase inversion takes place. It is suggested that this critical effective holdup value is close to the catastrophic holdup shown in Figure 24, since the physical properties (density and viscosity) of the kerosene and water are similar and coalescence rates of the dispersed phase drop are controlled mainly by their effective holdup.

The non-linear nature of the relationship between the phase inversion delay time and  $(\Phi_{\text{Catastrophic}} - \Phi_{\text{Initial}})$  suggests that the net rate of entrapment of the continuous-phase droplets into the dispersed phase is inversely proportional to  $(\Phi_{\text{Catastrophic}} - \Phi_{\text{Effective}})$ . However, further investigation is needed to elucidate phase-inversion kinetics.

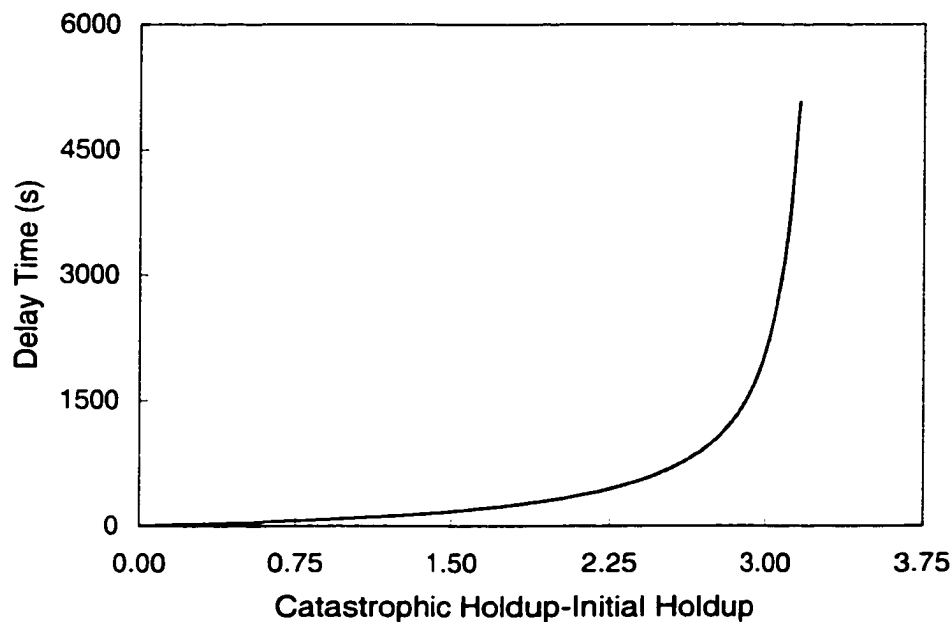


Figure 25. Effect of  $(\Phi_{\text{Catastrophic}} - \Phi_{\text{initial}})$  on phase inversion of (water / Irving gasoline system, 700 rpm)

In the case of the gasoline/water system, no phase-inversion delay time could be measured. This suggests that droplet inclusion within the dispersed-phase drops is practically non-existent until the catastrophic phase-inversion holdup is reached, or that the droplet escape rate is very high relative to the inclusion rate; beyond this point, the droplet inclusion rate is so large and much bigger than the droplet escape rate that phase inversion is essentially instantaneous.

#### 4.2.1 Effect of Hydrodynamics on Phase Inversion

The effect of agitation intensity on the critical phase-inversion holdup was investigated for the systems Bayol oil/water/Triton and gasoline/water, and the results obtained are shown in Figure 26 and in next Section (Figure 27-Figure 30). Phase inversion holdup was found to decrease as agitation intensity increases for systems having no surfactants as well as those containing surfactants. This is in line with the finding of almost all the literature including recent works by Norato et al. (1998), Pacek et al. (1994a, 1994b), Kumar et al. (1996), and Brooks and Richmond (1994). On the other hand, it differs from

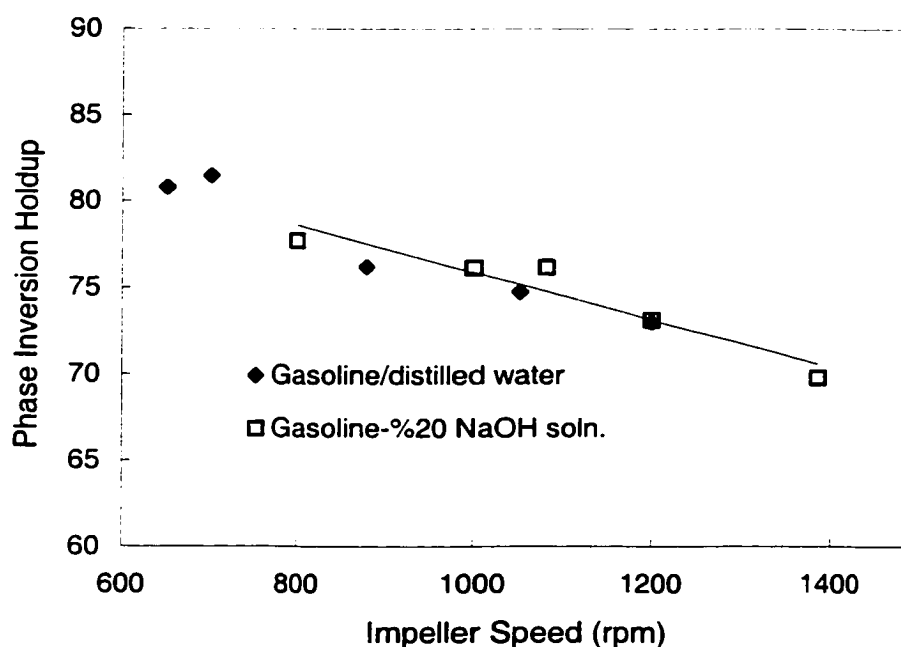


Figure 26. Effect of agitation intensity on phase-inversion holdup of gasoline/water and gasoline/20%(w/w) Caustic solution

the findings of Groeneweg et al. (1998) who reported that agitation has no effect on the phase-inversion holdup in the case of a “food grade” seed oil/water system. This is most probably due to the presence of surfactant in the “food grade” seed oil since in our case, the effect of agitation intensity on phase-inversion holdup was found to decrease at higher surfactant concentrations. Efthimiadu and Moore (1994) reported similar trends for the paraffin/ water/Tween 80 system (in which the effect of rotational speed decreased with increasing concentration of Tween 80). Higher impeller speed increases collision frequency and, consequently, increases the coalescence frequency; the resulting inclusion rate is therefore expected to increase with increasing agitation. A higher inclusion rate of the continuous phase droplets increases the effective holdup of the dispersed phase until it reaches the critical level necessary for triggering phase inversion. Phase inversion may, therefore, take place at lower initial holdups when higher impeller speeds are used.

As seen from Figure 26, no statistically-significant difference between the phase inversion behavior of gasoline/water and gasoline/aqueous caustic solution 20%(w/w) could be detected at the 5% significance level. This suggests that the presence of caustic has no significant role in the phase inversion of gasoline in water although its presence (as 20%w/w aqueous solution) raises the density ratio from 1.28 up to 1.9. This observation is in agreement with the findings of Norato et al. (1998) where density ratio appears to have little effect on the phase-inversion boundary. However, it contradicts the findings of Kumar et al. (1991) who reportedly found that systems with large density differences between the phases show a slightly greater tendency to invert.

#### **4.2.2 Effect of Surface Active Agents on Phase Inversion**

The effect of Triton X100 concentration on the phase-inversion holdup was studied using the system Bayol oil/water, and the results obtained are shown in Figure 27. Generally speaking, phase-inversion holdup was found to decrease with increasing agitation intensity, with the trend being slightly less pronounced at higher surfactant concentrations. On the other hand, the phase-inversion holdup was found to increase with increasing Triton X100 concentration. This result is in agreement with the findings of Kato et al. (1991), Efthimiadu and Moore (1994), and Groeneweg et al. (1998). Surfactants soluble in the continuous-phase retard film drainage by creating high film elasticity, and therefore reduce drop coalescence (Lucassen-Reynder, 1996). Consequently, the higher the concentration of these surfactants in the continuous-phase, the lower will be the coalescence frequency. Since inclusion takes place during the coalescence processes, inclusion is expected to be slowed down by the presence of surfactants soluble in the continuous phase and larger initial holdups are needed to achieve phase inversion. For example, in the case of the Bayol oil/ water system it was necessary to increase the initial holdup by 7% to reach phase inversion when 0.3 molar/m<sup>3</sup> Triton X100 was present. This is comparable to the findings of Efthimiadu and Moore (1994) where it was necessary to increase the phase-inversion holdup of system paraffin/water by 10% in the presence of 200 ppm Tween 80. On the other hand,

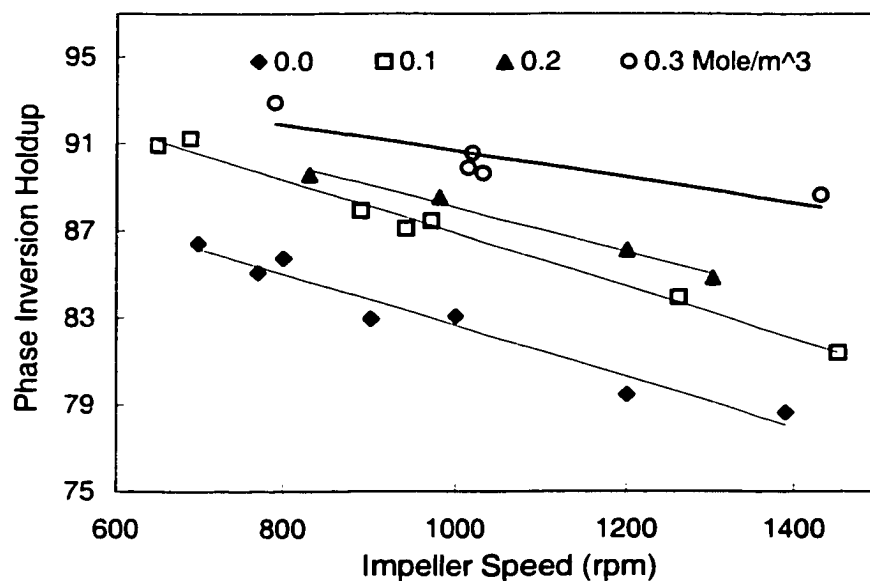


Figure 27. Effect of surfactant concentration on phase-inversion holdup of (Bayol oil/ water/ Triton X100)

Groeneweg et al. (1998) reported much larger differences (up to 45%) in the presence of very high emulsifier concentration (about 5000 ppm). These observations are in agreement with Bancroft's rule (Becher, 1965) that the phase dissolving the surfactant is liable to become the continuous phase. Solubility of surfactant is commonly expressed by its hydrophile-lipophile balance (HLB). For a homologous series of non-ionic surfactants, the HLB value increases as the hydrophilic portion of the molecule increases. Values in the range 4-10 indicate that water-in-oil dispersions should be stabilized while values from 10-18 indicate that oil-in-water dispersions are stabilized. The HLB for the Triton surfactants used in this work were in the range of 10.4-17.9 (Section 3.8, Table 6). The Triton surfactants used in this research are therefore considered to be water soluble and the solubility in the aqueous phase increases with increasing molecular weight. As seen in Figure 28, the phase-inversion holdup was found to increase as the molecular weight/length/HLB of the Triton surfactant increased.

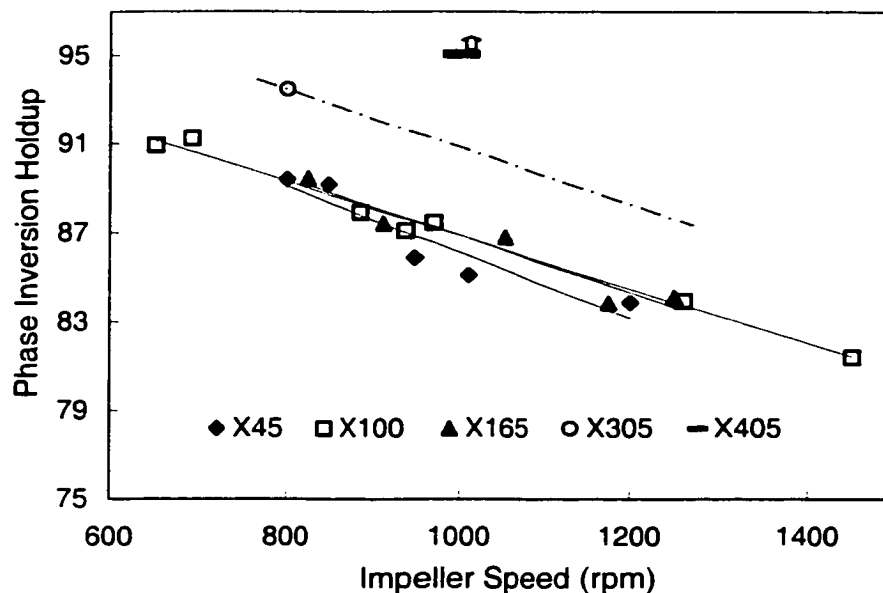


Figure 28. Effect of surfactant molecular weight/length on phase-inversion holdup of (Bayol oil/ water/ Triton)

Film drainage is very much controlled by whether the surfactant is soluble in the continuous-, or dispersed-phase. Velve et al. (1997) found that for water dispersed in benzene, the film lifetime is essentially the same for all concentrations of surfactant dissolved in the dispersed phase (water), while for the opposite system the film lifetime increased by two orders of magnitude. When the surfactant is soluble in the dispersed phase, the surfactant flux is carried out not only by diffusion, but also by the convection of the liquid inside the drop. This results in the suppression of the interfacial-tension gradients that generate elasticity and oppose film thinning; consequently, film thinning occurs very fast (Velve et al., 1997, Krawczyk et al., 1991).

As the molecular weight of the surfactants soluble in the continuous-phase increases, their ability to diffuse to the interface decreases; which in turn results in a higher film elasticity and low coalescence rate (Kim et al., 1996). However, larger surfactants are more surface-active since a larger number of the molecule segments are simultaneously adsorbed by the interface (Walstra, 1996). Larger surface activity results in decreased elasticity, which enhances coalescence rate. The effect of molecular weight on coalescence rate is thus governed by the combined effect of these two opposing factors.

As shown in section 4.1.3, the coalescence rate of the dispersed phase was found to decrease as the molecular weight of Triton surfactant increases (Figure 17). This is probably due to the lower diffusivity and higher continuous-phase solubility, associated with an increase in the molecular weight of the Triton surfactants. This reduction in coalescence rate results in lowering the rate of entrainment of the continuous-phase droplets (i.e. the inclusion mechanism). On the other hand, an increase in the molecular weight of the Triton will not significantly affect the coalescence rate of the aqueous droplets entrained in the dispersed phase (i.e. the escape mechanism) since the Triton molecules will, in this case, be soluble in the dispersed-phase. The net inclusion/escape rate will therefore be reduced, necessitating that the initial holdup of the system be increased in order for the critical phase-inversion holdup to be reached.

The effect of re-circulation (capacity number) on the phase inversion behavior of the system encountered during the “Inverse Doctor Treatment” of pipelined gasoline is shown in Figure 29. It clearly shows that the system’s tendency to invert is a non-monotonic function of the capacity number. As shown in section 3.8, this anomaly could be attributed to nonsystematic variation in the concentration of the surface-active ingredients and/or the uncontrolled addition of salt, caustic, glycol, alcohol, mercaptanes etc. As shown in the next section, this appears to be the case since the interfacial characteristics were found to vary in a non-monotonic fashion with the capacity number.

Since gasoline is a mixture of compounds the properties of which depend on the composition of the crude oil from which it was produced as well as the treatment processes used in the refinery, it is very difficult to control its interfacial characteristics. This is clearly evident from the phase-inversion behavior of the two gasoline samples (Irving refineries in St. John NB, and Imperial oil refinery in Dartmouth NS) used in this investigation (Figure 30). These results clearly show that the Irving gasoline has a higher tendency to invert. This could possibly be caused by the presence of a higher concentration of polar groups and/or surfactants in the Irving gasoline. Similar trends were reported by Chen (1996) who investigated the dispersion/coalescence behavior of kerosene in static mixers.

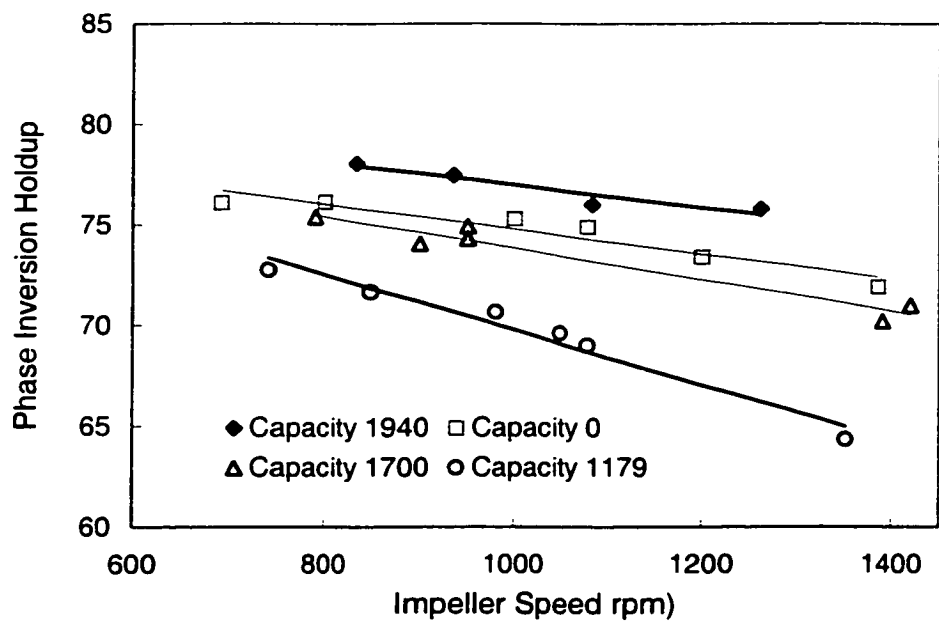


Figure 29. Effect of capacity number on phase-inversion holdup of industrial systems

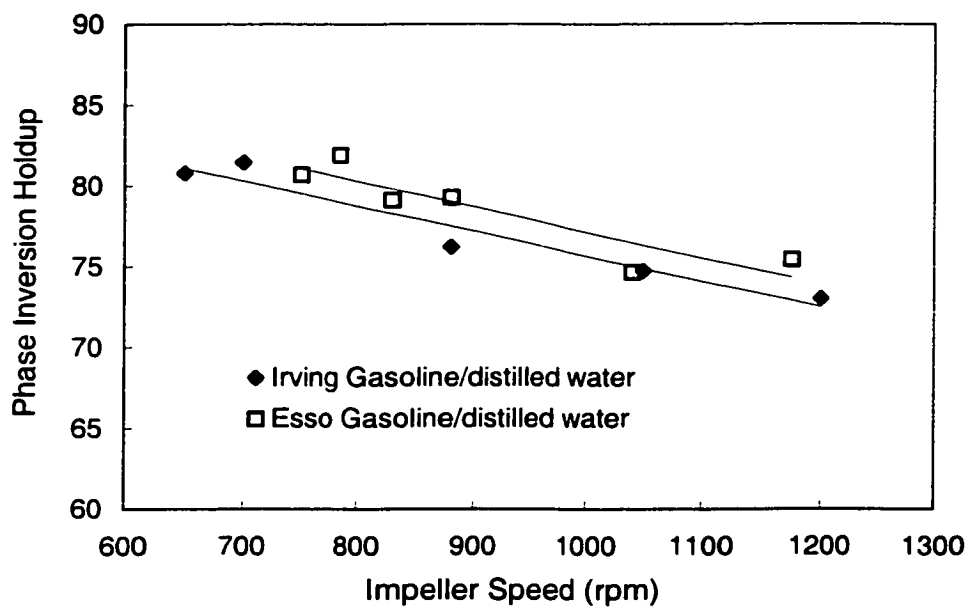


Figure 30. Effect of gasoline type on phase inversion of gasoline/water



### **4.3 Interfacial Characteristics**

In this section, the equilibrium (static) interfacial characteristics of the various systems investigated will be presented and discussed. Static interfacial characteristics derived from this information (equilibrium interfacial concentration) will then be discussed followed by several dynamic interfacial characteristics such as diffusivity, Gibbs elasticity and Marangoni elasticity.

#### **4.3.1 Equilibrium Interfacial Tension**

The effect of surfactant concentration on the equilibrium interfacial tension of several O/A systems is shown in Figure 31 and Figure H180-Figure H181. The equilibrium interfacial tension was found to decrease with increasing surfactant concentration. This is in agreement with the finding of Campanelli and Wang (1998), and Chatzi et al. (1993). Surfactant molecules, depending on their type and concentration, adsorb on the interface and thus, reduce the interfacial tension. The equilibrium interfacial tension decreases with increasing surfactant concentration due to the enhanced adsorption of the surfactant molecules on the interface. Increase in the surfactant concentration beyond the critical micelle concentration (cmc) will be less effective in decreasing interfacial tension.

Generally speaking, the equilibrium interfacial tension was found to decrease as Triton molecular weight/length increases (Figure H180-Figure H181). This may be explained by the fact that larger surfactant molecules have more segments that can be adsorbed by the interface and thus become highly surface-active, lowering the interfacial tension (Walstra, 1996). Surfactants commonly are long molecules whose head has an affinity for the aqueous phase while the tail has an affinity for the oil phase. Surfactant is adsorbed and paddled in the interface where its hydrophilic segment is in the aqueous and hydrophobic part is in the oil phase.

Attempts to measure the equilibrium interfacial tensions of the gasoline/ “inverse Doctor treatment caustic solutions” did not succeed since most of them fell within the accuracy

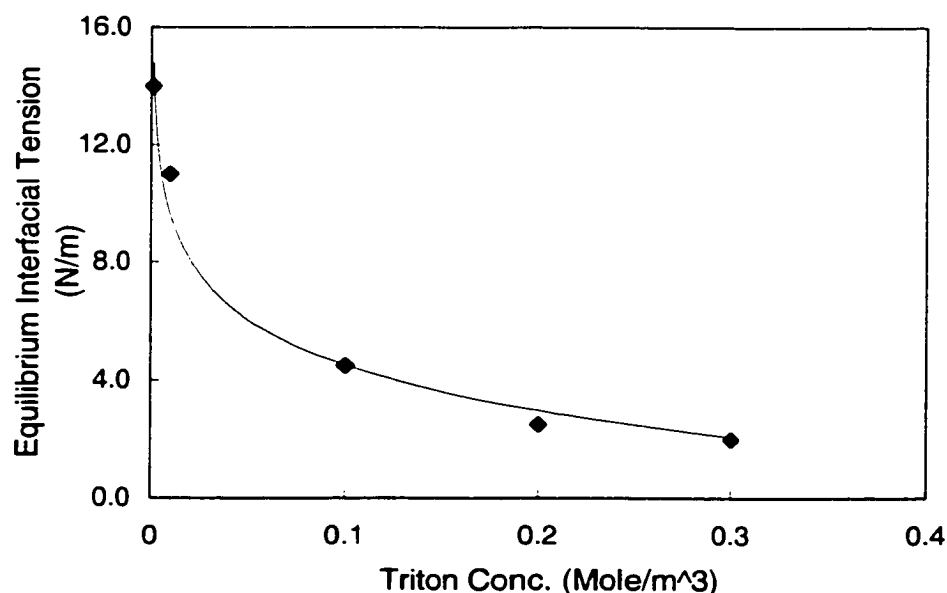


Figure 31. Effect of surfactant concentration on equilibrium interfacial tension of (Bayol oil/ water/ Triton X100)

range of the tensiometer ( $\pm 0.2$  mN/m). It was therefore necessary to dilute the caustic samples by a factor of 10 in order to develop comparative equilibrium-interfacial tension measures. The results obtained are shown in Figure H182.

#### 4.3.2 Equilibrium Interfacial Concentration

The equilibrium interfacial concentration ( $\Gamma$ ) was assumed to fit the Langmuir adsorption isotherm (21). The values of  $\Gamma^\infty$  and  $a_L$  were obtained by fitting the equilibrium interfacial tension data obtained at several (4-6) concentrations to Eq. (22) and the results obtained are given in Table 17. Figure 31 shows the goodness of data fitting to Eq. (22). Very good agreement was obtained in the case of Bayol oil/water/Triton X100 (Figure 31) where six experimental measurements were available. These results are in good agreement with those of Campanelli and Wang (1998) who reported similar values ( $\Gamma^\infty = 2.43 \times 10^{-6}$  and  $a_L = 2.38 \times 10^{-3}$ ) for the mineral oil/water/Triton X100 system.

Table 17. Parameters of Langmuir isotherm Equation for systems investigated

Triton	$\Gamma^\infty$	$a_L$
Bayol oil/water/Triton X45	1.9E-06	4.8E-05
Bayol oil/water/Triton X100	3.9E-06	1.9E-04
Bayol oil/water/Triton X165	3.4E-06	7.9E-05
Bayol oil/water/Triton X305	3.0E-06	1.6E-05
Bayol oil/water/Triton X405	2.6E-06	7.9E-06
Acetophenon/water/Triton X100	1.7E-06	7.0E-06
Acetophenon/water/Triton X165	1.2E-06	2.0E-06
Acetophenon/water/Triton X305	9.2E-07	5.0E-08
Acetophenon/water/Triton X405	9.0E-07	1.0E-07

Using the same approach, the fit obtained was not as good as with other surfactants and/or in the case of acetophenon/water/Triton (Figure H180-Figure H181). Other adsorption isotherm expressions may be more suitable in those cases. Unfortunately, the number of experimental points does not enable a systematic evaluation of this issue.

The values of  $\Gamma$  for the various systems investigated were then estimated using Eq. (21) and the corresponding values of  $\Gamma^\infty$ ,  $a_L$  and  $c$ . The results obtained and the physical properties are listed in Tables 7-8.

The effect of surfactant concentration on the equilibrium interfacial concentration is shown in Figure 32. As seen, the equilibrium interfacial concentration does not change significantly with surfactant concentration for of the concentration range investigated.

This is in agreement with the findings of Campanelli and Wang (1998), who reported that interfacial concentration was almost independent of bulk concentration of the surfactant for the system mineral oil/water with Triton X100 and concentrations varying between 0.0107-0.165 mole/m<sup>3</sup>, or with Span 80 and concentration between 0.12-1.2 mole/m<sup>3</sup>.

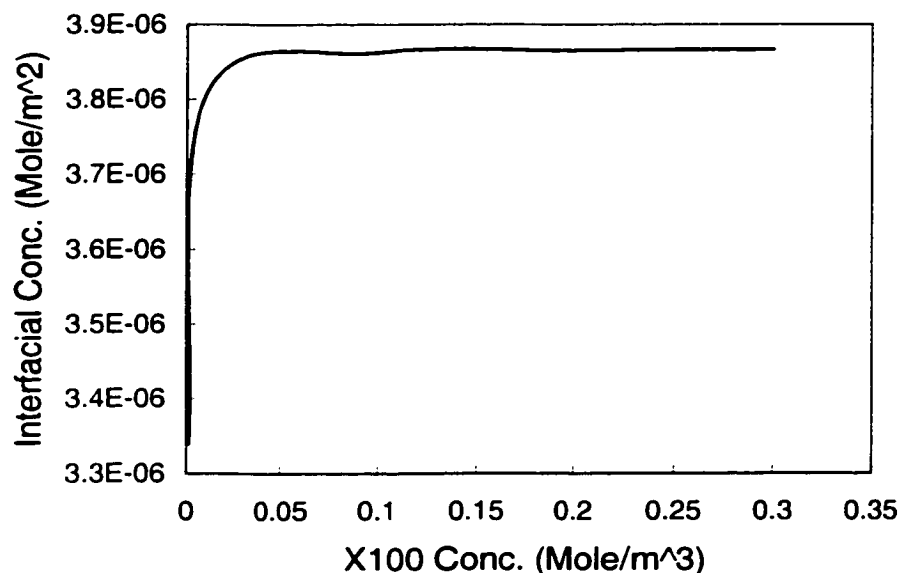


Figure 32. Effect of surfactant concentration on equilibrium interfacial concentration of (Bayol oil/ water/ Triton X100).

The effect of surfactant molecular weight/length on the equilibrium interfacial concentration is shown in Figure H183-Figure H184. In the case of the acetophenon system (Figure H183), it is seen that with increasing molecular weight/length, the equilibrium interfacial concentration decreases. This is explained by the fact that larger surfactants have more segments to be adsorbed by the interface (Walstra, 1996). A similar trend was observed to take place in the case of the Bayol oil system (Figure H184) (with the exception of Triton X165 in the Bayol oil/ water system where some unexplainable deviation was observed to take place at 0.1 mole/m<sup>3</sup>). The difference in behavior in the two systems can possibly be attributed to the fact that the Bayol oil system contains surfactant concentration that can exceed the cmc value.

### 4.3.3 Dynamic Interfacial Tension

The effect of surface age on the dynamic interfacial tension (obtained using both the drop volume and maximum-drop-pressure techniques) is shown in Figure H185-Figure H194

for the acetophenon/water/Triton system while Figure H195-Figure H196 depict the same effects in the case of Bayol oil/water. The dynamic interfacial tension of gasoline/industrial caustic was found to be below the accuracy limits of the device and techniques recently developed at Dalhousie (Xue, 1999). It was, therefore, necessary to dilute the aqueous stream by a factor of 10 using de-ionized water to maintain high accuracy in measuring dynamic interfacial tension. The dynamic interfacial tensions of the resulting systems are shown in Figure H205-Figure H208. Finally, the dynamic interfacial tension of acetophenon/water/Triton, Bayol oil/water/Triton, and industrial systems obtained using the expanding-drop technique (as drop expands from hemispherical shape until detachment) is shown in Figure H209-Figure H212.

As shown in Figure 33-Figure 34, the dynamic interfacial tension obtained using the maximum-drop-pressure and drop-volume techniques was found to decrease and tends to approach the equilibrium interfacial tension as the drop formation-time increases. On the other hand, the dynamic interfacial tension tends to approach the static interfacial tension of the pure system at very short surface ages. This is due to the fact that diffusion may not fully restore the equilibrium of surfactant interfacial adsorption at the rapidly-stretched interface; thus interfacial tension increases. If the interfacial concentration of surfactant decreases dramatically due to fast stretching, interfacial tension may approach that of a clean surface.

The dynamic interfacial tension obtained by the expanding-drop technique (Figure H209-Figure H212) was found to increase to a maximum (typically reached within 0.5 second after the hemispherical point) then decrease with time. This is caused by the very-high rates of interface expansion encountered in the initial stages following the hemispherical point and the resulting lowering of interfacial concentration. As time progresses, the surfactants are given the opportunity to diffuse to the interface and lower the interfacial tension, approaching the value of the equilibrium interfacial tension at large surface ages.

The Gibbs elasticity of the liquid-liquid system is defined as follows (Xue, 1999):

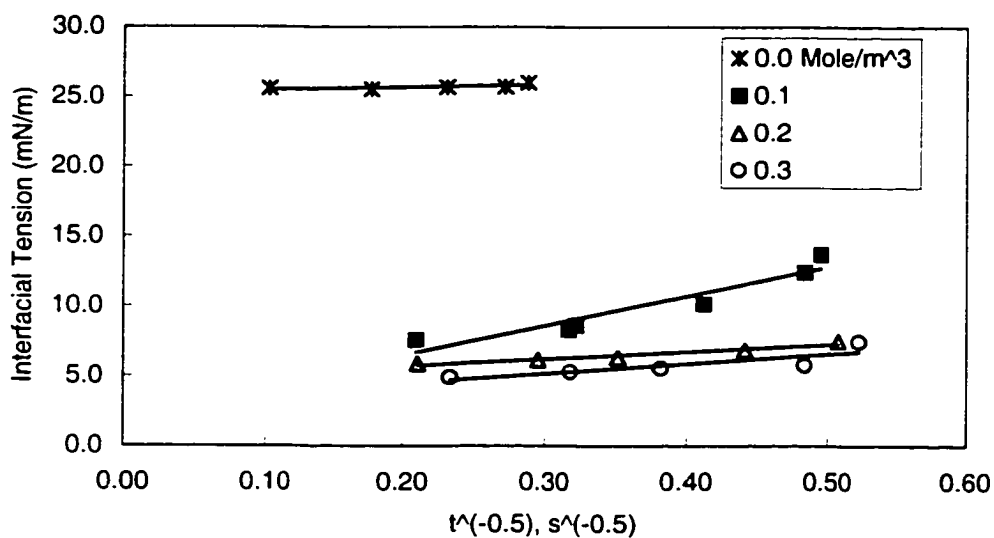


Figure 33. Effect of surfactant concentration on the dynamic interfacial tension of (acetophenon / water / Triton X100, drop-volume technique)

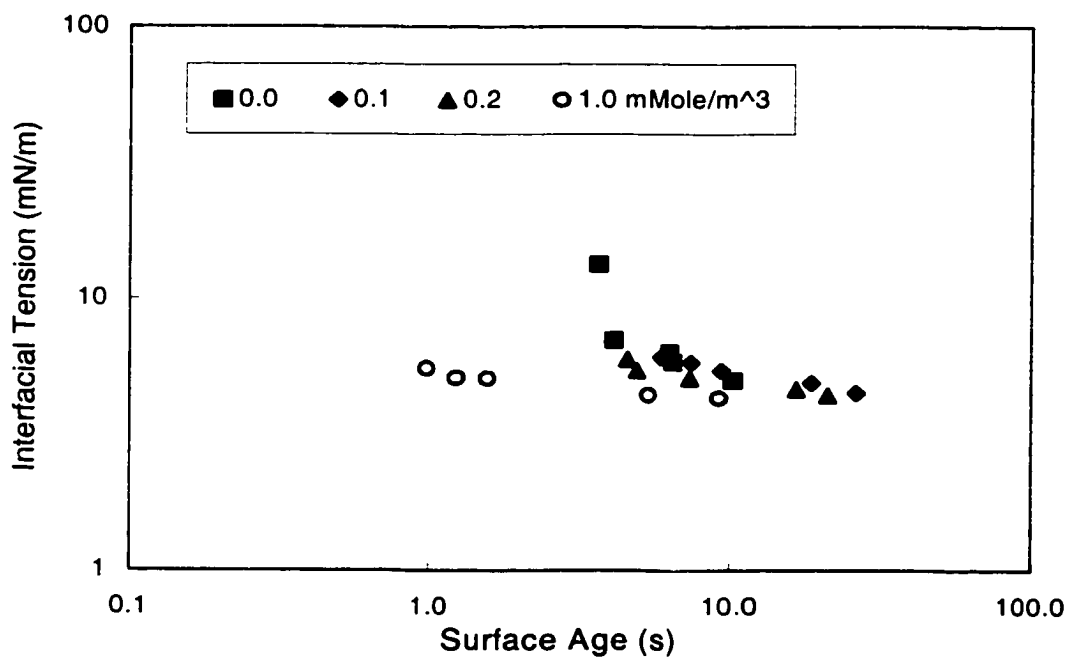


Figure 34. Effect of surfactant concentration on the dynamic interfacial tension of (acetophenon/ water / Triton X100, maximum-drop-pressure technique)

$$E_G = \partial\gamma/\partial t \quad (37)$$

To calculate the Gibbs elasticity, the interface is rapidly produced and its interfacial tension versus time is monitored. Surfactants diffuse to the newly developed surface and reduce the interfacial tension. In a similar fashion, the slope of the dynamic interfacial tension versus time as the drop starts growing beyond the hemispheric point may be an important interfacial characteristic. A combination of the high diffusivity and large dynamic interfacial activity decreases the initial slope of the stress-relaxation curve. The effect of surfactant concentration and structure on the value of this parameter is shown in Figure H213-Figure H215. It was calculated by fitting a straight line through interfacial tension data from the hemispherical point until the maximum point. Generally speaking, the slope of dynamic interfacial tension versus time was found to decrease as the molecular weight/length of the Triton surfactant increases. This is due to fact that smaller molecules diffuse faster and can, therefore, reduce the interfacial tension earlier. Similarly, Kim et al. (1996) found that the best de-mulsifier for breaking a water/oil emulsion had the largest value of Gibbs elasticity. They attributed this to higher diffusivity and higher interfacial activity of the de-mulsifier.

To identify which technique(s) (drop-volume technique, maximum-drop-pressure technique, and expanding-drop technique) is suitable for measuring the interfacial characteristics of coalescence and/or phase inversion processes, the secondary parameters obtained from all the above techniques (diffusivity and elasticity) will be presented, discussed and compared with each other.

#### 4.3.4 Diffusivity

Adsorption of surfactant at the interface at an early stage or near equilibrium is best described by the following equations (Campanelli and Wang, 1998; Miller et al., 1994; Xue, 1999):

$$\gamma(t) = \gamma_0 - 2RTC_0 (3Dt/7\pi)^{1/2} \quad (38)$$

for the short-time approximation, and:

$$\gamma(t) = \gamma_{eq} + RT\Gamma_{cq}^2(7\pi/12Dt)^{1/2} / C_0 \quad (39)$$

for the long-time approximation.

The diffusivity values of Triton surfactant in acetophenon/water and Bayol oil/water systems were calculated by fitting the dynamic interfacial tension data (obtained by the drop-volume technique, and maximum-drop-pressure technique) to the adsorption equations obtained using the short-time approximation (38) and long-time approximation Eq. (39). As can be seen from Figure 33, the data were well fitted by the long time approximation. To increase the accuracy of the diffusivity values, the experimentally-measured values for  $\gamma_{eq}$  were used as an input parameter (rather than as an output parameter) in the fit to Eq. (38). This was necessitated by the fact that the data collected emphasized small surface ages (where diffusivity is of paramount importance) rather than the collection of large surface ages that are needed to obtain accurate  $\gamma_{eq}$  values.

The correlation coefficients obtained by fitting the dynamic interfacial tension to the two surfactant-adsorption approximation models are shown in Table A43. Almost all the correlation coefficients of systems containing Triton were significant at 95% confidence level (Table A44 a, b, c). In general, for the systems containing Triton surfactants (Table A43 a, b, c), the dynamic interfacial tension data acquired by the drop-volume technique provides a better fit to the long-time approximation equation whereas the data obtained by the maximum-drop-pressure technique fits the short-time approximation equation better. In the industrial system gasoline/caustic, the results obtained using the drop-volume technique do not fit into the short-time approximation model since the majority of the correlation coefficients were not significant even at 90% confidence limit (Table A44d). Thus, discarding the diffusivity calculated by the drop-volume technique for the system gasoline/ "inverse Doctor treatment caustic solutions" is justified. In this



investigation, only the diffusivity values obtained with a high degree of confidence (larger than 95%) were used. The maximum normalized standard error was less than 12% in all values reported here.

The effect of concentration on the diffusivity of Triton X100 in the acetophenon/ water and Bayol oil/water systems is shown in Figure 35 and Figure H216. It is clear that diffusivity decreases as the surfactant concentration increases in the drop-volume and maximum-drop-pressure techniques. This observation is in agreement with the findings of Campbanelli and Wang (1998) and can be attributed to the partitioning of surfactant monomers between the interface and a growing number of micelles in the bulk solution as the surfactant concentration increases. This results in reducing the effective concentration of SAA molecules present in solution (Campbanelli and Wang, 1998).

As a rule, commercial surfactants are a mixture of molecules with different structures and weights. The dynamic interfacial characteristics (such as interfacial tension, diffusivity, and elasticity) of systems containing such compounds therefore depend on the contributions of the species present. Smaller and lighter molecules diffuse and are adsorbed faster; their contribution to the reduction of the interfacial tension is therefore more pronounced in short surface ages, whereas the contribution of larger and heavier molecules is more pronounced at longer surface ages. Therefore, the diffusivity value that is calculated from the dynamic interfacial tensions measured at short surface ages could be higher than those measured in long surface age measurements (Figure 35 and Figure H216). Although in general this conclusion is true, the diffusivity calculated from both techniques similar because the time scale of drop formation of both techniques is of same order of magnitude for both techniques.

As molecular weight/length increases, the diffusivity is expected to decrease, due to the decrease in surfactant mobility. The effect of molecular weight on the diffusivity of Triton, calculated from the drop-volume, and maximumd-drop-pressure techniques data

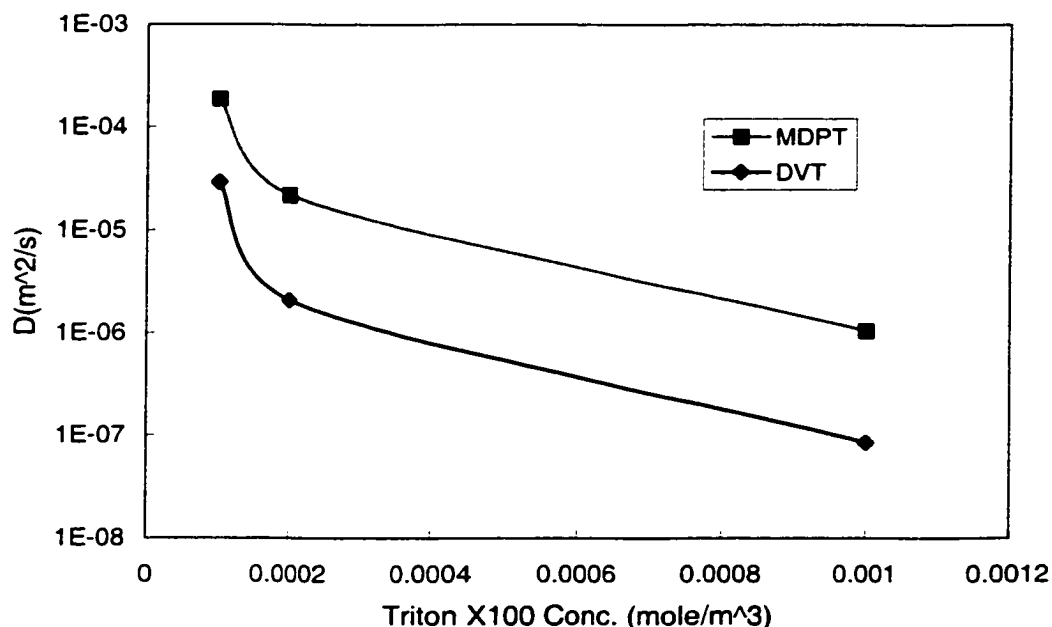


Figure 35. Effect of surfactant concentration on the Triton diffusivity in (acetophenon / water/ Triton X100)

(acetophenon/water/0.1 mmole/m<sup>3</sup> Triton systems) is shown in Figure H217-Figure H218. The diffusivity measured by both techniques exhibited a maximum at Triton X165 (molecular weight 910). The effect of molecular weight on the diffusivity of Triton in the Bayol oil/ water/ 0.1 mole/m<sup>3</sup> Triton system is shown in Figure H219-Figure H220. As seen, the Triton diffusivity, measured by the drop-volume technique was found to decrease monotonically with molecular weight, whereas the diffusivity of Triton measured by maximum-drop-pressure technique was found to exhibit a maximum at Triton X165. This may be attributed to the short surface ages encountered in the case of the maximum-drop-pressure technique (Bayol oil/water system containing Triton of concentration 0.1 mole/m<sup>3</sup>) resulting in only light surfactants being able to diffuse to the interface and contribute to the measured diffusivity. It was also found that in the case of the Bayol oil/ water/ 0.1 mole/m<sup>3</sup> Triton system, the diffusivity of Triton molecules in water, measured by the drop-volume technique, correlates well ( $R=0.97$ , 95% confidence level) with the inverse of the square of its molecular weight (Figure 36). This is in line with the findings

of Kim et al. (1996). No similar observation was found in the case of acetophenon/ 0.05 molar aq. NaCl/ Triton in which the Triton concentrations are three orders of magnitude lower.

The industrial caustic samples obtained from the “inverse Doctor treatment” contained a wide range of sodium hydroxide, mercaptans,  $\text{Na}_2\text{S}$ , sodium polysulfide, colloidal sulfur, glycols, alcohols, aliphatic/aromatic hydrocarbons, and a number of other additives that may have been incorporated during pipelining. No information is available concerning the nature and concentration of the surface-active species present in this stream. It is, therefore, impossible to calculate a meaningful diffusivity value. Furthermore, the long-term approximation equation cannot be used to calculate the diffusivity since the equilibrium interfacial concentration was not available. The short-time approximation equation was therefore used by employing a hypothetical unit concentration ( $1 \text{ mole/m}^3$ ) for all the gasoline/industrial caustic systems investigated. This provided diffusivity values that are not true in the absolute sense, but give a basis for the comparative evaluation of the various systems. The diffusivity of the surface-active species present in gasoline/industrial caustic systems was calculated from the measurements obtained using the drop-volume and maximum-drop-pressure techniques and the results are shown in Figure H221-Figure H222. The irregular behavior of the diffusivity calculated from drop-volume technique data (Figure H221-Figure H222), may be because this technique is not very suitable for investigating the diffusivity in systems where behavior is modeled by the short-time approximation. This model requires data obtained at short surface ages (corresponding to an early stage of adsorption), a situation that can be better achieved using the maximum-drop-pressure technique. Consequently, the data obtained using the drop-volume technique were not used further.

Diffusivity values were also calculated from expanding-drop measurements. The dynamic interfacial tension obtained using the expanding-drop technique was found to

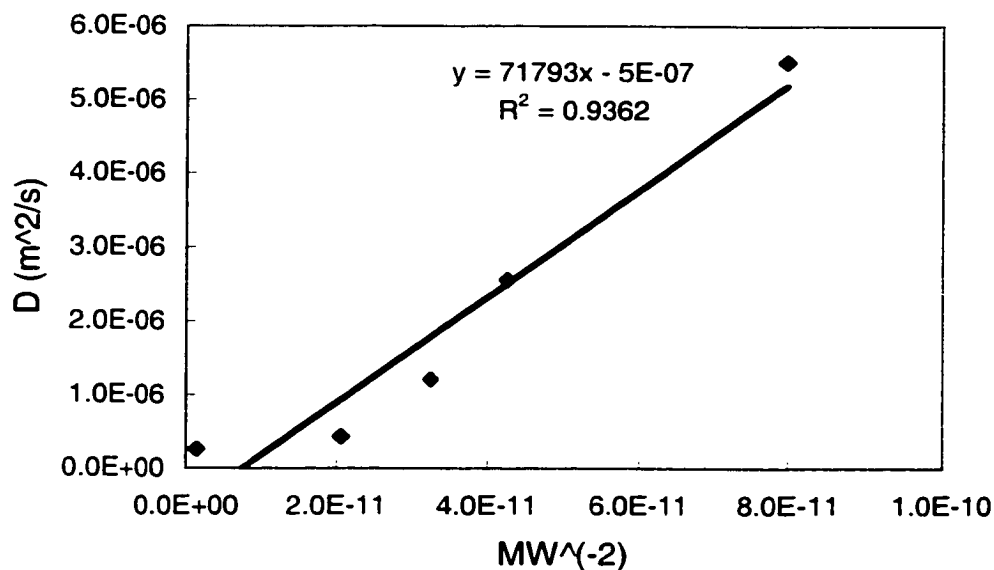


Figure 36. Effect of surfactant molecular weight/length on the Triton diffusivity in (Bayol oil/ water/ 0.1 mole/m<sup>3</sup> Triton, drop-volume technique)

increase with time initially and reach a maximum and then drop. It approaches the equilibrium interfacial tension at large surface ages. The short-time approximation Eq. (38), could be used to fit the interfacial tension of the expanding-drop data with the exception of the first part of the interfacial tension data (where interfacial contamination with SAA molecules stripped from the previous drop could have influenced the measurement). The regression analysis resulting from fitting the data to the short-time adsorption equation is shown in Table A45, and the resulting surfactant diffusivity is shown in Figure H223-Figure H225 for a number of the systems investigated. It is clear from Figure H223 that diffusivity decreases as the surfactant concentration increases. This is in agreement with results obtained from drop-volume and maximum-drop-pressure techniques, as well as with the findings of Campbanelli and Wang (1998) and Van Hunsel et al. (1986). Figure H225 also clearly shows that, in agreement with the results obtained from the drop-volume and the maximum-drop-pressure techniques, the

diffusivity of surfactant decreases as molecular weight increases; however, it was not inversely proportional to the square of molecular weight.

Figure 37 shows the effect of the capacity number of industrial caustic on the SAA diffusivity calculated from the interfacial tension data obtained by the expanding-drop technique. The variation of the diffusivity with capacity number generally follows trends similar to those obtained from drop-volume and maximum-drop-pressure techniques. It must be emphasized that the general trend of diffusivity with capacity is a non-monotonic one. As the time scale of the expanding drop in the early stages is short, calculated diffusivity is expected, and observed to be higher than that determined by drop-volume technique, but the calculated diffusivity is smaller than that of maximum-drop-pressure technique.

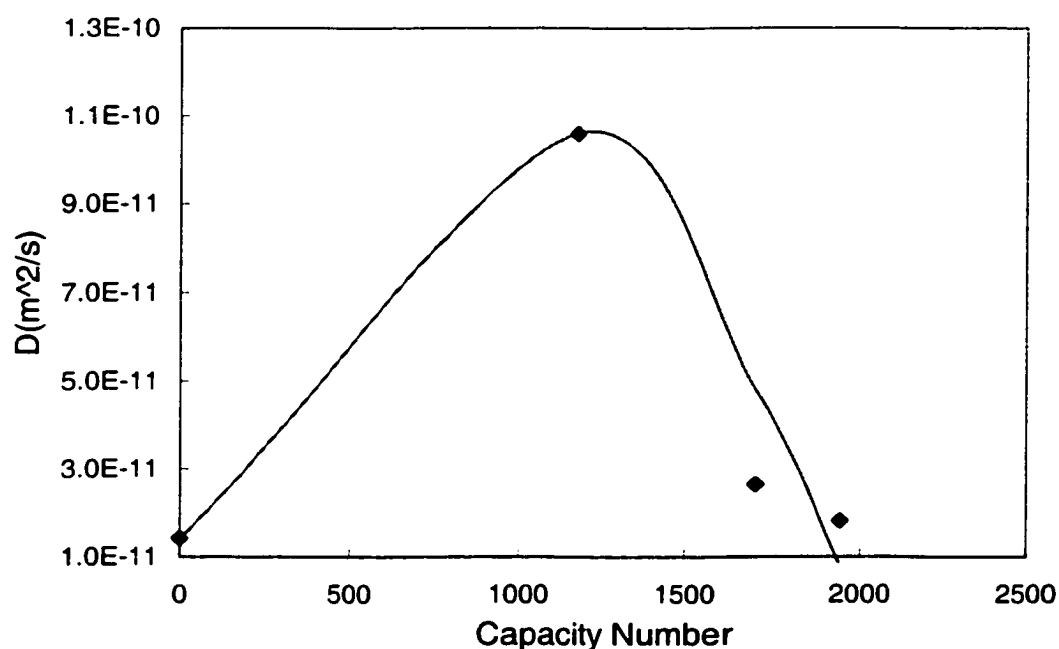


Figure 37. Effect of capacity number of the industrial caustic on the apparent diffusivity of the SAA on (gasoline/ industrial caustic, expanding-drop technique)

### 4.3.5 Marangoni Elasticity

The Marangoni elasticity of the interface,  $E_M$ , was computed using the following equation (Lucassen-Reynder, 1996):

$$E_M = \frac{d\gamma}{d \ln A} \quad (40)$$

where  $A$  is the drop interface. The results obtained for the various systems investigated are presented in Figure 38-Figure 39 and Figure H226-Figure H228, which clearly show that the elasticity of the interface decreases as the bulk surfactant concentration increases (Figure 38). At high concentrations, surfactants can more readily diffuse to the newly formed interface where they adsorb and quickly bring down the interfacial tension and the associated Marangoni elasticity (which is based on the difference in SAA concentration between different regions at the interface). Figure 39 and Figure H227 similarly show that Marangoni elasticity decreases with an increase in molecular weight/length. This could be due to the fact that larger molecules have higher surface activity and thus can decrease the interfacial tension (and consequently the Marangoni elasticity) faster. The interfacial elasticity of the gasoline/industrial caustic system is shown in Figure H228. It is clear from this graph that the Marangoni elasticity of the interface is not a monotonic function of the capacity number of the industrial caustic (i.e., the number of times it had been re-circulated). Similar trends are seen in the SAA diffusivity of those systems (Figure 37).

### 4.4 Effect of Interfacial Characteristics on Coalescence and Phase Inversion

In fast dynamic processes such as coalescence and phase inversion, interfacial tension deviates from its equilibrium value due to insufficient diffusion times. Attempts to correlate experimental data on the basis of static characteristics may therefore be of questionable value. Dynamic characteristics, such as elasticity and diffusivity may, therefore, be more suited for these purposes since they take into account the counteracting processes of surfactant diffusion and interfacial stretching. Some indication supporting this suggestion was obtained from previous investigations dealing with the

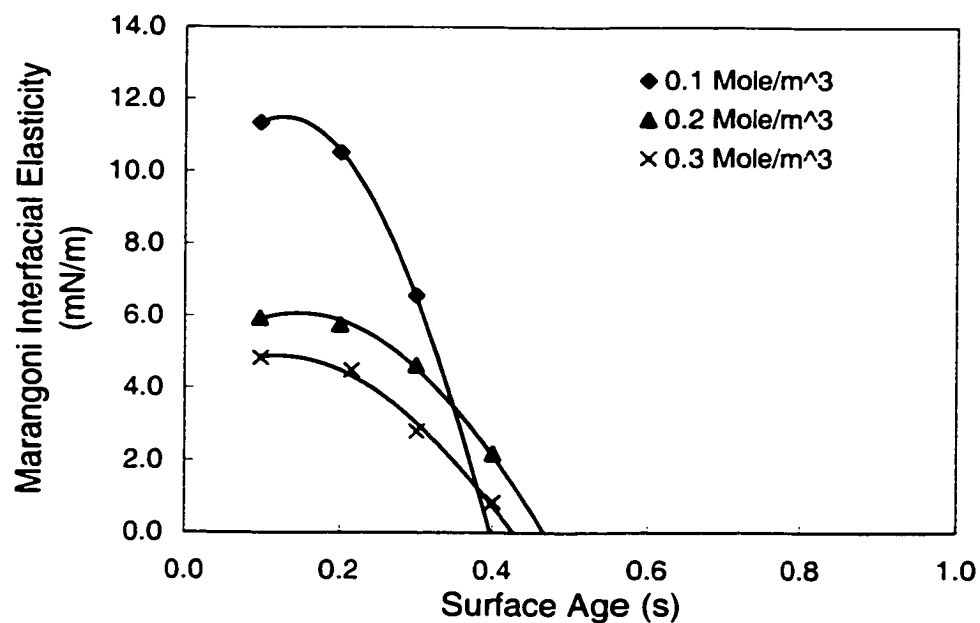


Figure 38. Effect of surfactant concentration on Marangoni interfacial elasticity of (Bayol oil/ water/ Triton X100, dispersed phase flow rate = 0.0316 mL, expanding-drop technique)

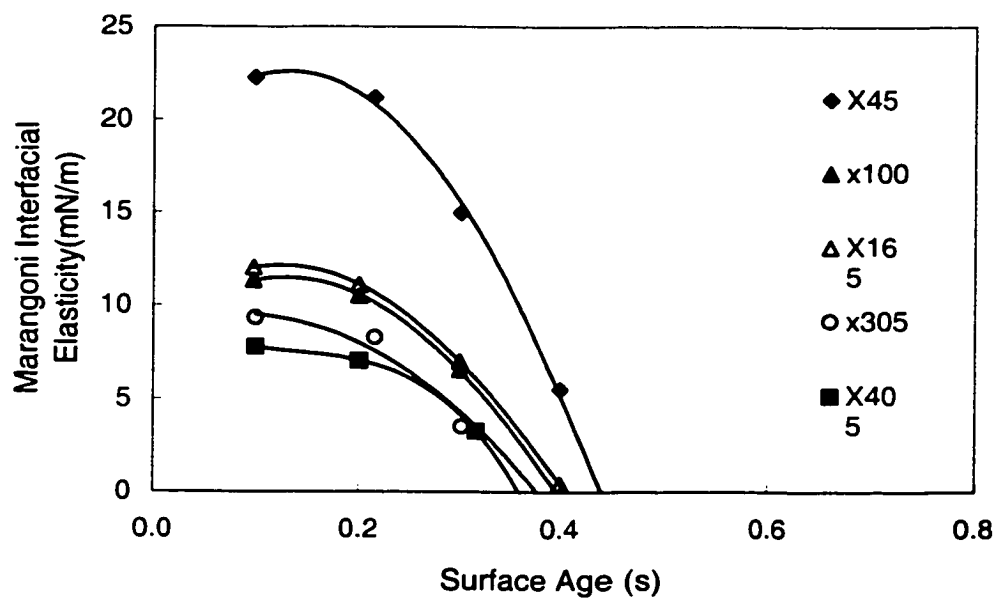


Figure 39. Effect of molecular weight/length on Marangoni interfacial elasticity of (Bayol oil/ water/ 0.1 mole/m<sup>3</sup> Triton, dispersed phase flow rate = 0.0316 mL, expanding-drop technique)

stability of petroleum emulsion; however, similar conclusions may not be suitable in the much-faster processes of coalescence and phase inversion. In this section, the correlation between coalescence and interfacial characteristics is discussed, and is followed by a discussion of correlation between interfacial characteristics and phase inversion.

#### 4.4.1 Effect of Equilibrium Interfacial Tension on Quasi-equilibrium Drop Size

The Sauter mean diameter is commonly assumed to be a function of equilibrium interfacial tension, given by (Godfrey et al., 1989):

$$d_{32} \propto \gamma_{eq}^{0.6} \quad (41)$$

Attempts were therefore made to correlate the quasi-steady Sauter mean diameter (obtained for the 0.75% acetophenon / 0.05 molar aq. NaCl/Triton systems) with the equilibrium interfacial tension,  $\gamma_{Eq}$  and the results obtained using a linear fit are given in Figure 40-Figure 41. It was found that the Sauter mean diameter correlates with the equilibrium interfacial tension at 300 and 200 rpm ( $R=0.91, 0.95$  respectively). A fair fit was obtained when the exponent of the equilibrium interfacial tension was allowed to vary ( $R = 0.84$  and  $0.92$ ) yielding best fit exponents of  $0.47$  and  $0.93$  for 300 rpm and 200 rpm respectively. No statistically significant differences between the correlations could be identified. It can thus be concluded that Eq. (41) predicts the quasi-steady Sauter mean diameter reasonably well (at 300 rpm) for the systems investigated. On the other hand, the quasi-steady Sauter mean diameter is linearly dependent on the equilibrium interfacial tension at 200 rpm. The difference between the exponents obtained at the two speeds is most probably caused by the fact that equilibrium between breakage and coalescence processes was not fully achieved in the case of 200 rpm, hence the contribution of breakage to the Sauter mean diameter was not fully developed.

The strong dependence on the equilibrium interfacial tension is in contradiction with the findings of Lucassen-Reynders and Kuijpers (1992), Groeneweg et al. (1994) and Janssen et al. (1994, 1997) who investigated systems with much higher SAA concentrations.



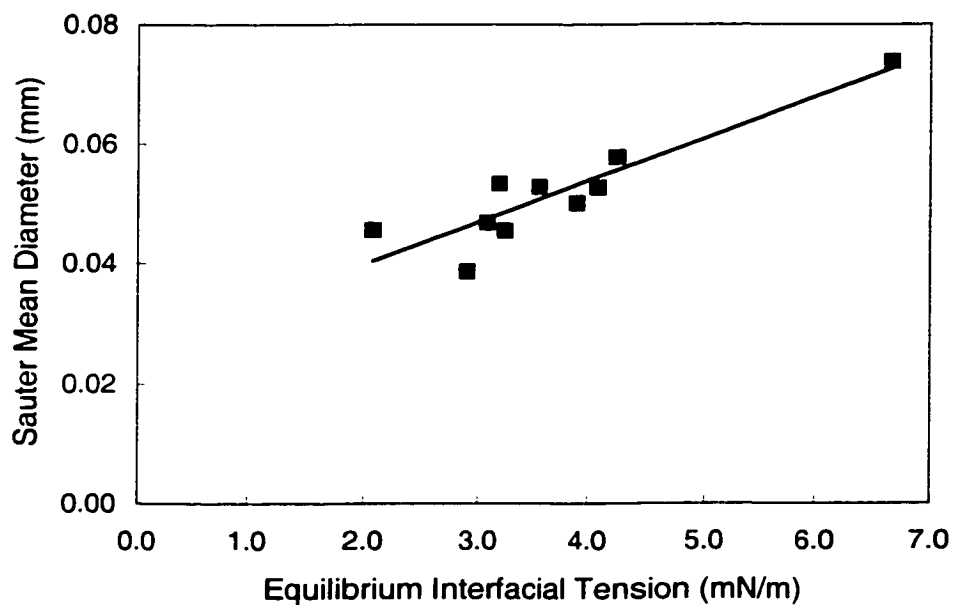


Figure 40. Effect of equilibrium interfacial tension on quasi-equilibrium Sauter mean diameter of (0.75% acetophenon / water / Triton systems, 300 rpm)

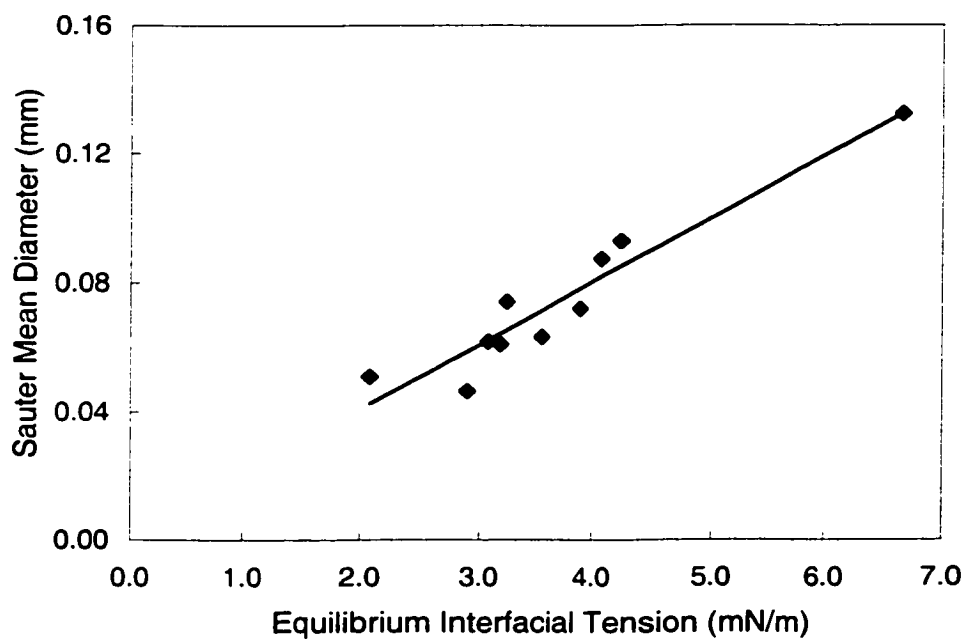


Figure 41. Effect of equilibrium interfacial tension on quasi-equilibrium Sauter mean diameter for (0.75% acetophenon / water / Triton systems, 200 rpm)

The equilibrium interfacial concentration did not provide a significant correlation with the quasi-equilibrium Sauter mean diameter. Attempts to correlate the Sauter mean diameter with the dynamic interfacial characteristics were not successful, as the correlation coefficients were small and not significant at the 95% confidence level.

#### 4.4.2 Effect of Interfacial Characteristics on Coalescence Rate

Attempts were made to correlate the coalescence rate of acetophenon drops dispersed in aqueous Triton solutions using the equilibrium interfacial tension as an indicator of the pertinent interfacial characteristic controlling this process. The results obtained are shown in Figure 42. It is clear that although there is a general tendency for the coalescence rate to increase with increasing equilibrium interfacial tension (correlation coefficient of  $R=0.71$  was significant at 95% confidence level), the correlation between those two parameters is rather poor. This is in line with the findings of Kourio et al. (1994), who reported that the drainage time of drop-interface films generally decreases with an increase in equilibrium interfacial tension.

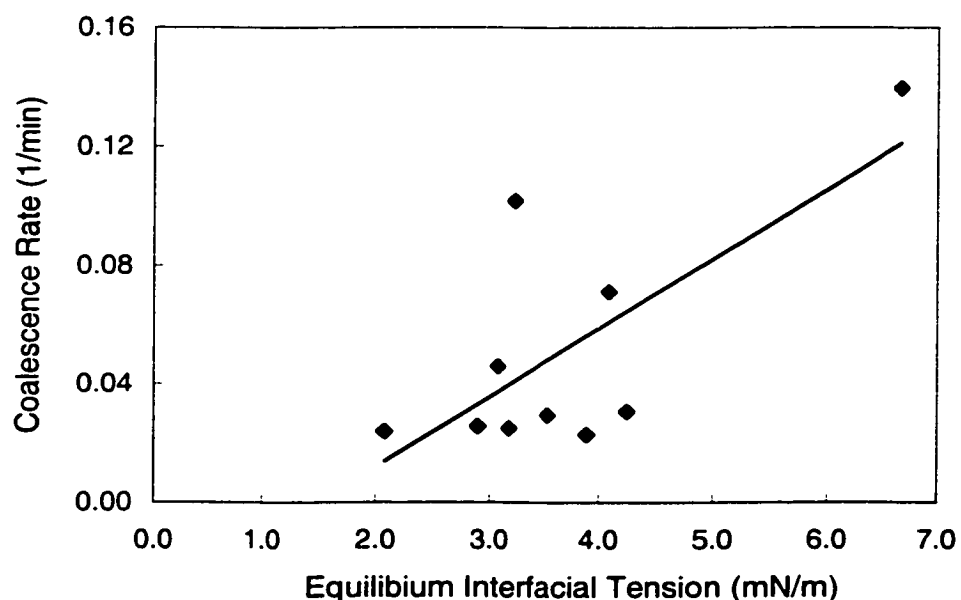


Figure 42. Effect of equilibrium interfacial tension on coalescence rate (0.75% acetophenon / 0.05 molar aq. NaCl / Triton, 200 rpm)

The correlation was found to be even worse when the equilibrium interfacial concentration,  $\Gamma_{eq}$ , was used as an indicator of the interfacial characteristics controlling coalescence (Figure 43). The correlation coefficient ( $R = -0.234$ ) was not significant even at the 70% level. Thus, no statistical evidence exists to assume that a correlation between coalescence rate and the interfacial concentration exists. On the other hand, an excellent correlation ( $R = 0.989$ ) was found between coalescence rate and surfactant diffusivity calculated from the data obtained using the drop-volume technique (Figure 44), suggesting that the coalescence process is highly controlled by surfactant diffusion. The correlation coefficient was significant at the 99% confidence level. The correlation parameters are given in Table A46. This correlation is significantly better (at the 99% confidence level) than that obtained using the equilibrium interfacial tension.

The coalescence rate of acetophenon drops in aqueous Triton solutions can generally be given as function of SAA diffusivity ( $D$ ) as follows:

$$\text{Coalescence rate} = (0.022 \pm 0.030) + (169.6 \pm 222.5) D \quad (42)$$

Although this correlation is based on a wide range of concentrations and molecular weights, further investigations (using other systems and agitation intensity) are needed in order to develop a more general relationship.

No significant correlation was found to exist between coalescence rate and the surfactant diffusivity calculated using the maximum-drop-pressure technique (Figure 45). This may be because the surface aging of maximum-drop pressure technique is shorter than the time scale of diffusion in acetophenon/water/Triton systems. Furthermore, Xue (1999) reported that this technique is prone to errors resulting from residual surfactants remaining from the previous drop.

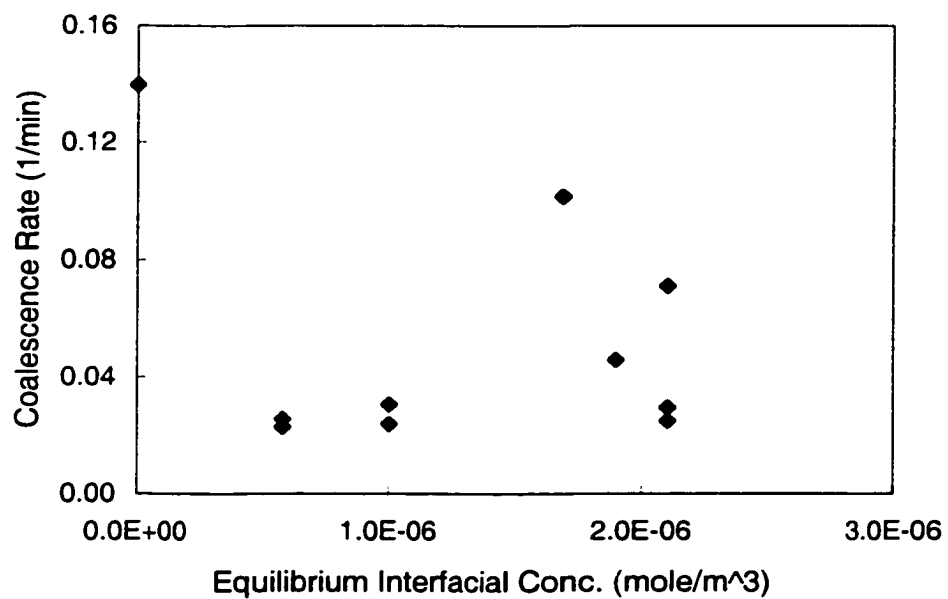


Figure 43. Effect of equilibrium interfacial concentration on coalescence rate (0.75% acetophenon / 0.05 molar aq. NaCl / Triton, 200 rpm)

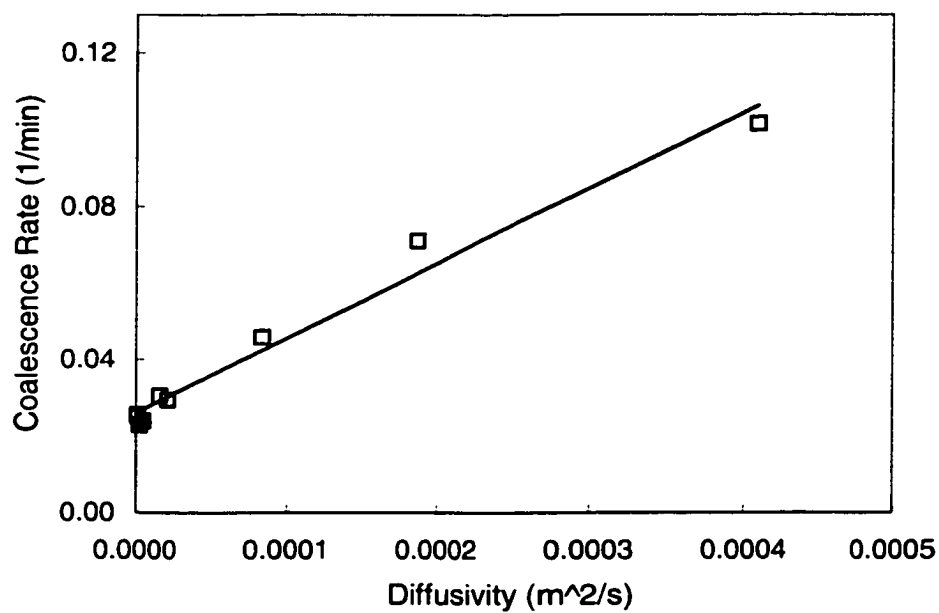


Figure 44. Effect of surfactant diffusivity on coalescence rate (0.75% acetophenon / 0.05 molar aq. NaCl / Triton, 200 rpm, drop-volume technique)

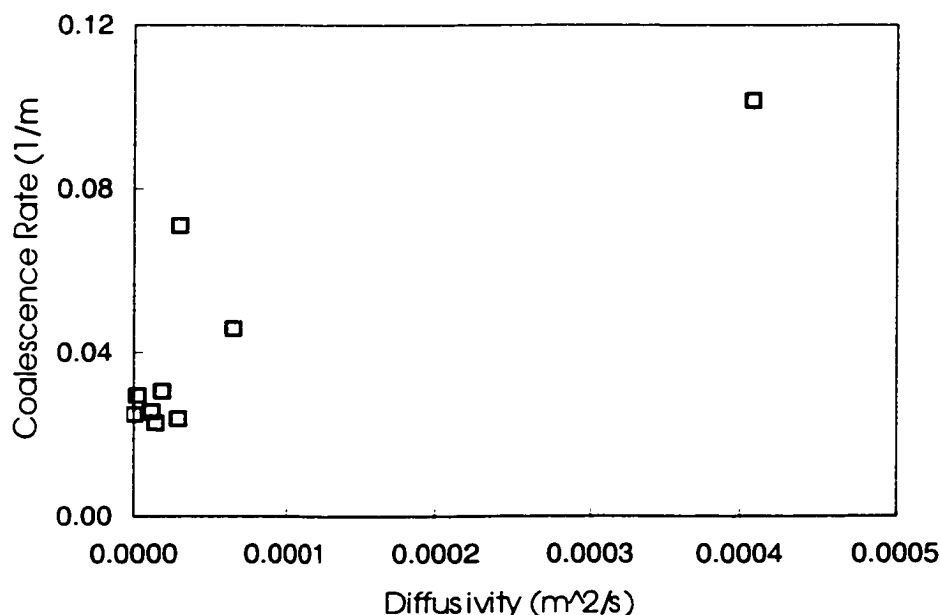


Figure 45. Effect of surfactant diffusivity on coalescence rate (0.75% acetophenon / 0.05 molar aq. NaCl / Triton, 200 rpm, maximum-drop-pressure technique)

As mentioned in the literature review section, spatial variations in the interfacial concentration of the surfactants are generated during the film drainage process. This phenomenon augments interfacial forces that retard film drainage, and hence drop coalescence. These forces are reduced by increasing surfactant diffusivity (Section 2.2); hence film drainage and drop coalescence are facilitated by increased surfactant diffusivity. This is in agreement with the finding of Kim et al. (1996) that a good demulsifier (which is based on achieving high coalescence) must create low interfacial tension, low elasticity, and high diffusivity. Also, it is in line with findings of Krawczyk et al. (1991), who reported that high interfacial activity and a high rate of diffusion /adsorption are the most important parameters governing demulsifier performance. Furthermore, the diffusivity of the surface-active species plays an important role in controlling the magnitude of the Marangoni elasticity forces, which could be important in controlling drop-coalescence processes at the time scales encountered in the present investigation (a few milliseconds). The value of the diffusivity therefore provides a good indication of both the elasticity and film drainage factors.

The coalescence rate was correlated with the maximum Marangoni elasticity and the results obtained are shown in Figure 46. No significant correlation was observed between the Marangoni elasticity of a drop's interface and the coalescence rate. This can be explained by the film thinning process that is opposed by the film Marangoni elasticity. The latter is a product of the interaction between the film stretching rate and surfactant diffusion. The film between coalescing drops drains to a thickness of about 500 Å before rupturing, while its diameter remains relatively large (Tsouris and Tavlarides, 1994). Therefore, as seen in Figure 47, only surfactants available in the film can diffuse to the interface, while surfactants in the bulk of the continuous phase may not, as they have to travel the film radius. In the absence of surfactant diffusion from the drop phase, film Marangoni elasticity is more likely controlled by the film surfactant concentration rather than by the surfactant concentration of the continuous bulk (Lucassen-Reynders, 1996). This renders the film Marangoni elasticity value to be different from that of the drop interface (which is measured by the expanding-drop technique). In the expanding-drop technique, surfactants diffuse to the interface freely from the continuous-phase bulk and, consequently, the elasticity decreases with increase of concentration of the surfactant present in the continuous bulk (Figure H226 and Figure 38). This is a characteristic of interface elasticity and not necessarily of the film. In contrast, the film elasticity was suggested to increase with increasing surfactant concentration in the film, thus with surfactant concentration of the continuous phase (Lucassen-Reynder, 1996; Kim et al., 1996).

It can, therefore, be concluded that the Marangoni elasticity of the drop's interface does not accurately represent the film Marangoni elasticity. This is the reason why Marangoni interfacial elasticity does not adequately correlate with coalescence rates in the case of organic drops dispersed in aqueous Triton solutions. However, if the surfactant is mainly soluble in the dispersed phase, it diffuses to the interface freely and in a similar fashion as it does in the expanding drop technique. Under such conditions, the film elasticity may be adequately represented by the interfacial elasticity and, consequently, coalescence data may be well correlated with the interfacial Marangoni elasticity.

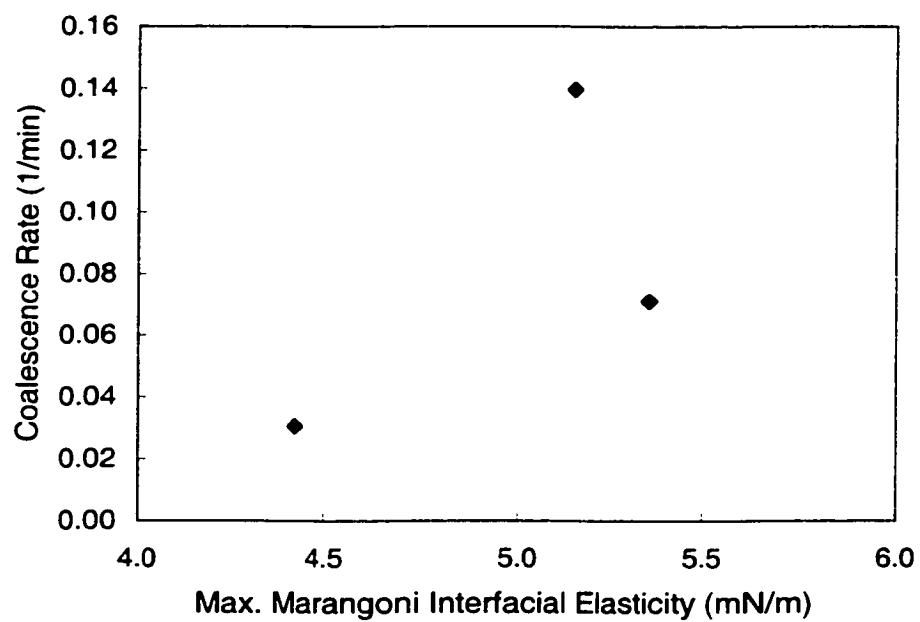


Figure 46. Effect of Marangoni interfacial elasticity on coalescence rate (0.75% acetophenon/ 0.05 molar aq. NaCl / Triton, 200 rpm)

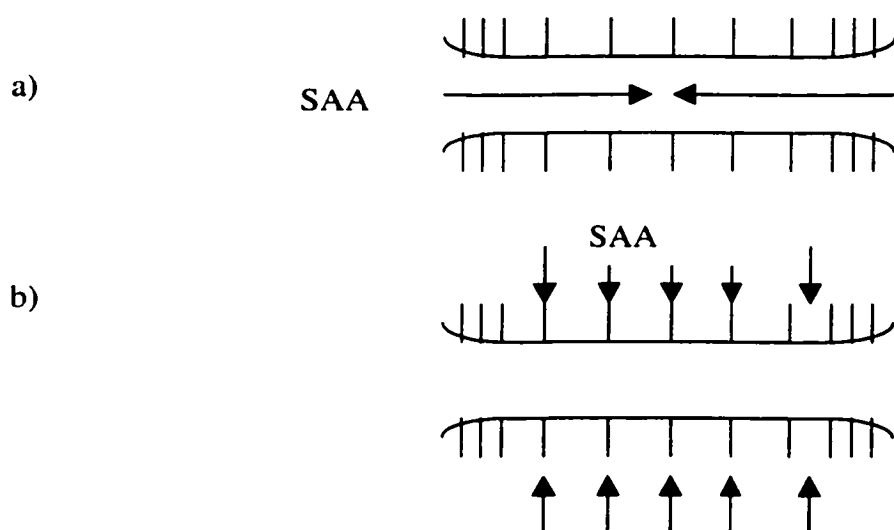


Figure 47. Diagram of film thinning. a) surfactant soluble in the continuous phase; b) surfactant soluble in the dispersed phase (Krawczyk, et al., 1991).

#### **4.4.3 Effect of Interfacial Characteristics on Phase Inversion of Systems Containing Surfactant**

Attempts were undertaken to correlate phase-inversion holdup for the system Bayol oil/aqueous Triton solutions using the equilibrium interfacial tension as an indicator of the interfacial characteristics relevant to this phenomenon (Figure 48). Although there are indications of a general trend (phase-inversion holdup decreases with equilibrium interfacial tension,  $R$  was significant at a 95% confidence level), a rather poor correlation exists between the two parameters ( $R = -0.73$ ). This suggests that the net inclusion/escape processes (and hence phase-inversion holdup) are somewhat affected by equilibrium interfacial tension. This is in line with Norato et al. (1998) and Kumar et al. (1991) who found that a pure system tends to invert more easily with increasing interfacial tension. This may be attributed to the factors controlling escape process of continuous-phase droplets being different from those controlling the inclusion process. As discussed previously (Section 4.3.5), the rate of drop coalescence is dependent on whether the surfactant is soluble in the dispersed- or continuous-phase.

When the surfactant is soluble in the continuous phase, its diffusion to the film interface is limited; the dynamic-interfacial tension of the film differs significantly from its equilibrium value and thus, coalescence is most likely controlled by the dynamic interfacial characteristics. On the other hand, when the surfactant is soluble in the dispersed-phase, it diffuses the interface easily; the dynamic interfacial tension of the film is close to its equilibrium value, and thus drop coalescence correlates well with the equilibrium interfacial tension.

As proposed earlier in the phenomenological interpretation of phase inversion (Section 2.1.1) the continuous-phase droplets are included into the dispersed-phase drops as the latter coalesce, whereas they escape from the dispersed-phase drop when they coalesce with the external interface. For the systems investigated in this study, the Triton surfactant was mainly soluble in the aqueous phase; consequently, the coalescence rate of



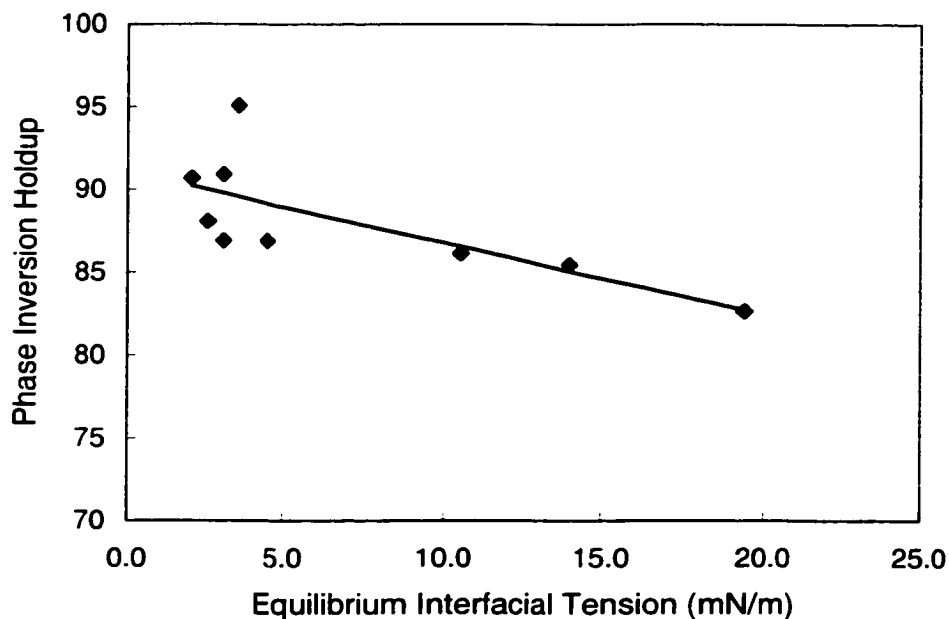


Figure 48. Effect of equilibrium interfacial tension on the phase inversion of (Bayol oil / water / Triton systems)

the oil drops is controlled by the dynamic interfacial characteristics; whereas the coalescence of the continuous-phase droplets is strongly related to the equilibrium interfacial tension.

An attempt to use the equilibrium interfacial concentration (a parameter that does not take into account the dynamic conditions at the interface) was not successful in correlating the phase-inversion holdup (Figure 49,  $R = 0.45$  not significant at the 95% confidence level). As proposed in section 2.1.1, phase inversion takes place when the rate of inclusion of the continuous-phase droplets into the dispersed-phase drops exceeds their rate of escape. Inclusion may take place when the film between approaching drops is swallowed by the dispersed phase. Droplets of the continuous phase present inside the drops may bounce to the interface and could coalesce with the surrounding continuous-phase. The inclusion process is, thus, expected to be controlled by factors affecting the thinning of the continuous film, whereas the escape process is expected to be controlled by factors controlling the thinning of the dispersed-phase film.

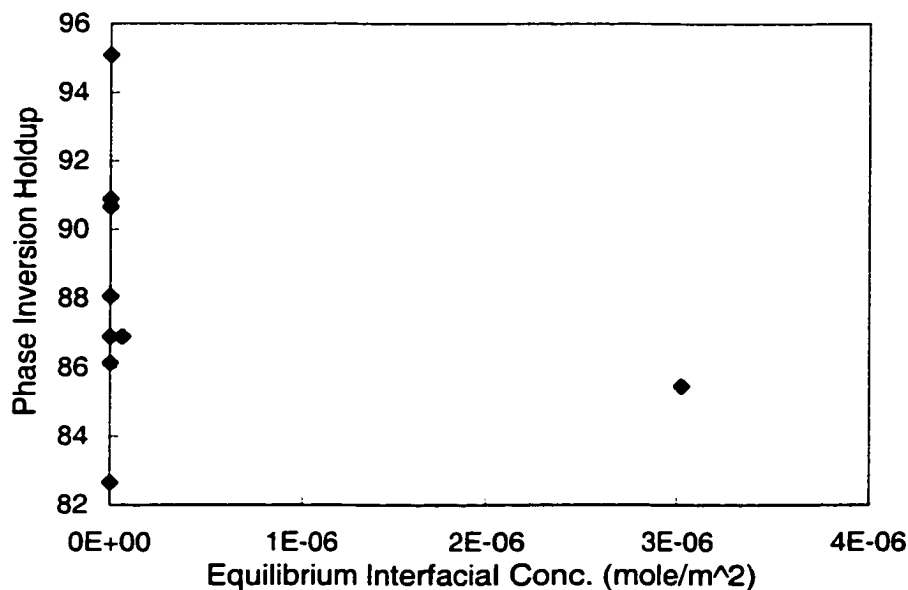


Figure 49. Effect of equilibrium interfacial concentration on the phase inversion of (Bayol oil / water / Triton systems)

Factors controlling the thinning of continuous-phase films may not be the same as those controlling the thinning of dispersed-phase films. For instance, Velve et al. (1997) found that film thinning was controlled by surfactant concentration only if it is soluble in the film phase. Therefore, the thinning of the dispersed-phase film formed during the droplet escape process could be independent of the concentration of the surfactants soluble in the continuous phase and with the associated properties (Krawczyk et al., 1991). Since Triton surfactants are soluble in the aqueous phase, they can retard the coalescence of oil drops, and consequently hinder the inclusion of water droplets into the oil phase. On the other hand, Triton does not retard film thinning and consequently does not affect the process of water droplets escaping from the oil drops. This argument suggests that while equilibrium interfacial tension and equilibrium interfacial concentration do not affect the thinning of the continuous phase (directly related to the inclusion rate), they are likely to affect the escape process which influences the value of the phase-inversion holdup. This justifies the findings reported above, namely, that the equilibrium interfacial tension is somewhat successful in correlating the phase-inversion holdup of acetophenon/water/ Triton (Figure 48). As seen in previously in Figure 44, the coalescence rate observed in the case of

acetophenon / an aqueous Triton solution is well correlated with the diffusivity of the SAA (calculated from the drop-volume technique data). An attempt was therefore made to correlate the phase-inversion holdup with the diffusivity of Triton surfactants in the aqueous phase of Bayol oil/water system. The diffusivity (calculated using the drop-volume technique) was found to correlate with the phase-inversion holdup data very well ( $R = -0.95$ ), whereas the diffusivity calculated using the other techniques did not (not significant at the 95% confidence level). The correlation parameters are given in Table A47. The correlation coefficient of the diffusivity (calculated using the drop-volume technique) was higher than that of the equilibrium interfacial tension at the 95% confidence level. Figure 50 shows the correlation between the phase-inversion holdup and surfactant diffusivity calculated from the drop-volume technique data. The excellent correlation between surfactant diffusivity and phase-inversion holdup suggests a strong role for diffusivity on both the inclusion and escape processes. No significant correlation was found between SAA diffusivity (calculated from data measured by expanding-drop technique) and the phase-inversion holdup. A similar attempt to correlate the phase-inversion holdup with the diffusivity calculated from the maximum-drop-pressure technique also failed.

As discussed in Section (2.2.2), the Marangoni film elasticity opposes film thinning and drop coalescence. It therefore retards the inclusion of the continuous phase droplets into the dispersed-phase drops, as well as the escape of the droplets back into the continuous phase. Surfactants soluble in the continuous phase slowly diffuse to the film interface, thus generating high Marangoni elasticity, which, in turn, retards drop coalescence. When the surfactant is soluble in the dispersed phase, its diffusion from the bulk to the film interface is fast and is enhanced by convective flow inside the drop. Lower Marangoni film elasticity is thus encountered, resulting in faster drop coalescence rates.

If the surfactant is soluble in the dispersed phase, the value of the Marangoni film elasticity is expected to be close to the Marangoni interfacial elasticity, (measured in this

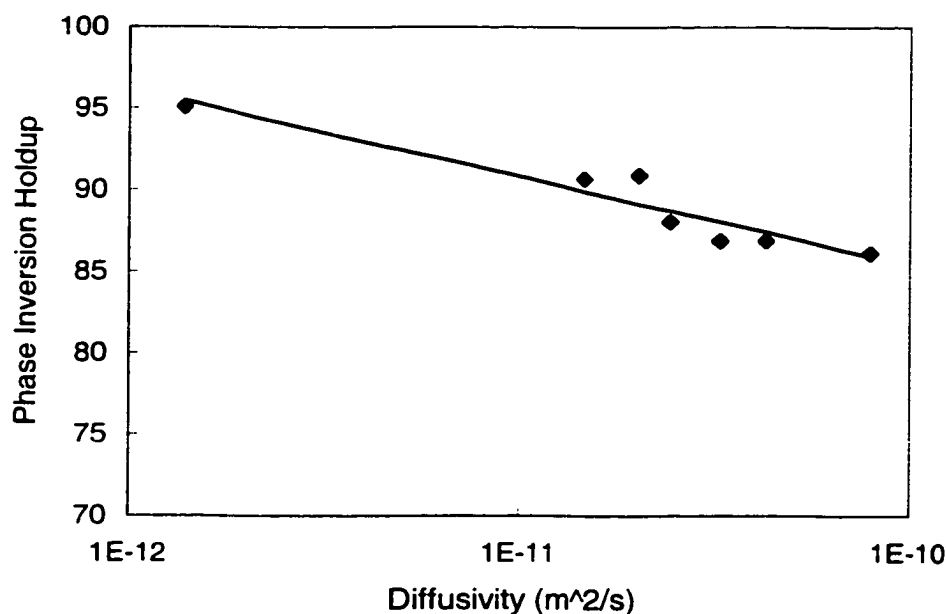


Figure 50. Effect of surfactant diffusivity on the phase inversion of (Bayol oil / water / Triton systems)

study) since in both cases, surfactant molecules can freely diffuse to the interface from the bulk of the drop. Significant differences between the two may, however, exist when the SAA is soluble in the continuous phase. Consequently, in the case of water-soluble Triton SAA, the Marangoni interfacial elasticity is expected to correlate well with the droplet-escape process which is controlled by the film thinning of the oil phase. The higher the Marangoni interfacial elasticity, the slower the escape process and thus the easier it is to reach phase-inversion holdup. The Marangoni interfacial elasticity may, however, not correlate with the droplet inclusion process that is controlled by the film thinning of the aqueous-phase.

The phase-inversion holdup was correlated using the maximum Marangoni elasticity of the interface and the results obtained are shown in Figure 51-Figure 52. They clearly show that the phase-inversion holdup generally decreases as the maximum Marangoni interfacial elasticity increases. This is probably due to the decreased escape rate encountered in higher Marangoni interfacial elasticity. However, the correlation obtained

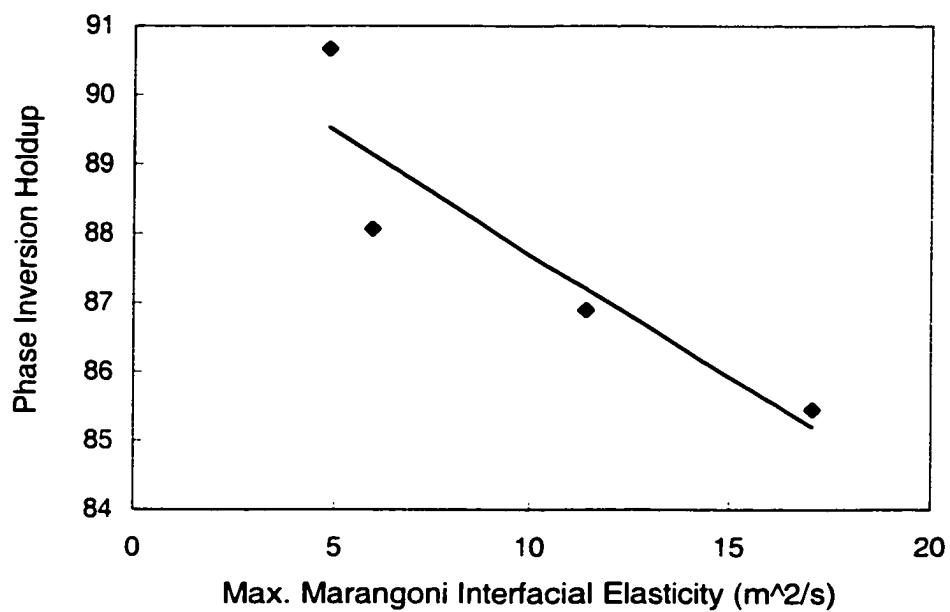


Figure 51. Effect of Marangoni interfacial elasticity on the phase inversion of (Bayol oil / water / Triton X100)

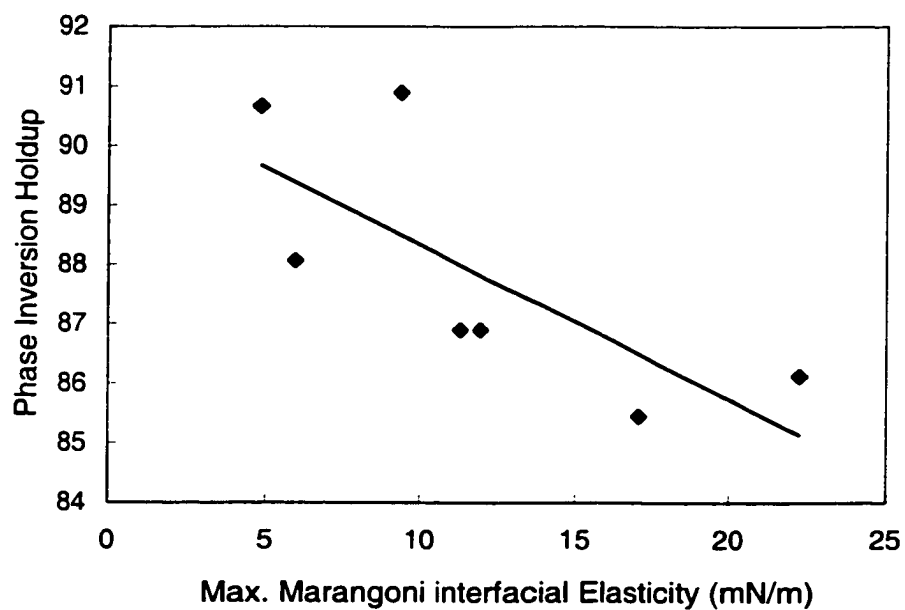


Figure 52. Effect of Marangoni interfacial elasticity on the phase inversion of (Bayol oil / water / Triton)

was found to be rather poor ( $R = -0.74$ , not significant even at 95% confidence level). This suggests that other interfacial factors such as the Marangoni film elasticity (which relates to the droplet inclusion process) plays an important role in the phase inversion process.

#### **4.4.4 Effect of Interfacial Characteristics on Phase Inversion of Industrial Systems**

The phase-inversion holdup obtained at 1000 rpm was correlated with several static and dynamic interfacial characteristics. When the equilibrium interfacial tension measurements were used, the resulting correlation was found to be not significant even at the 70% confidence level (Figure 53). It was not possible to correlate the phase-inversion holdup with the equilibrium interfacial concentration of the surface-active species because of the inability to calculate this parameter for the industrial systems. However, the diffusivity (determined using the maximum-drop-pressure technique with diluted samples) was found to fit the phase-inversion holdup data well ( $R = -0.84$ , Figure 54).

Use of the maximum Marangoni elasticity was found to yield a high correlation coefficient ( $R = 0.99$ ) which is significantly better than that obtained using SAA diffusivity (at the 99% confidence level) (Figure 55). The correlation parameters are given in Table A48.

From the above, it is possible to say that the maximum Marangoni interfacial elasticity correlates with phase-inversion holdup of the "Inverse Doctor Treatment" streams better than any other interfacial characteristic. It is expected that other industrial streams will behave in a similar fashion, but further investigation is needed before such a conclusion can be generalized.

Attempts to correlate the phase-inversion holdup of the synthetic and industrial systems with the initial slope of the dynamic interfacial tension vs. time (at the hemispheric point of the expanding-drop technique) defined by Eq. (37), were not successful. A similar attempt to correlate the coalescence rate of the 0.75% acetophenon/ 0.05 molar aq. NaCl/ Triton systems with the initial slope of their dynamic interfacial tension vs. time also failed to provide a significant correlation. This may be attributed to the difference

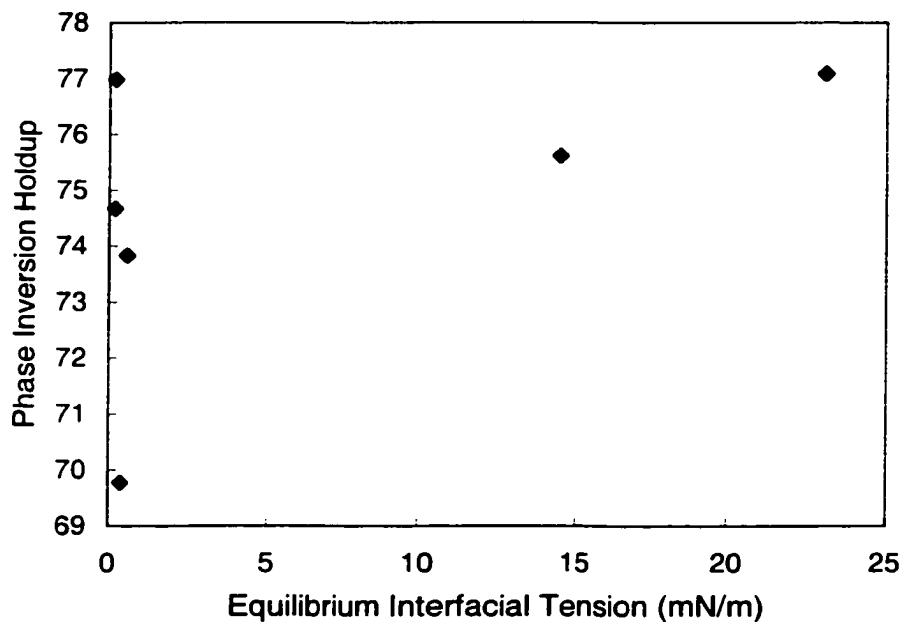


Figure 53. Effect of equilibrium interfacial tension on phase-inversion holdup (gasoline / industrial caustic, 1000 rpm)

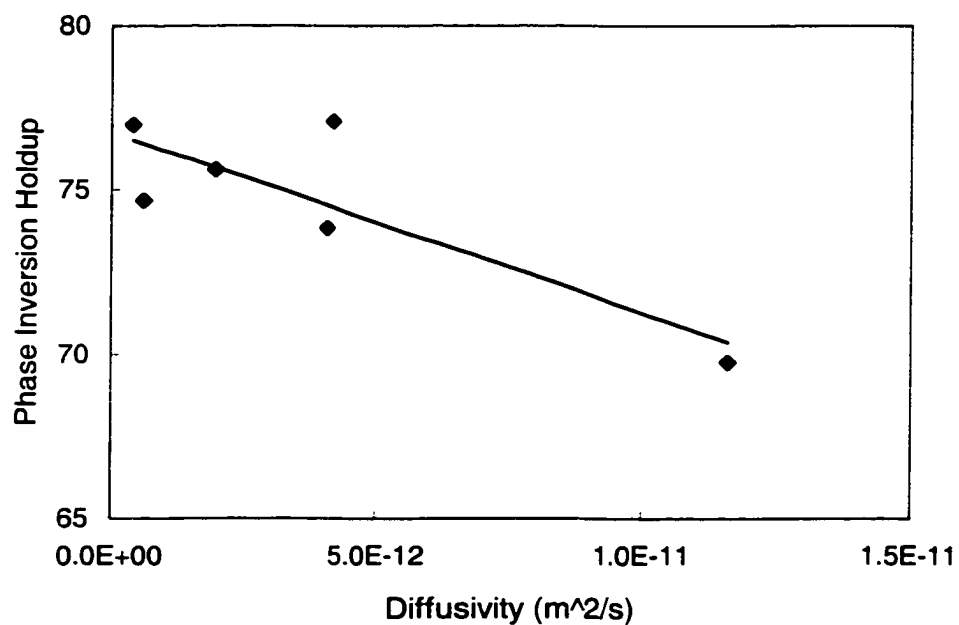


Figure 54. Effect of SAA diffusivity on the phase inversion of (industrial systems, maximum-drop-pressure technique).

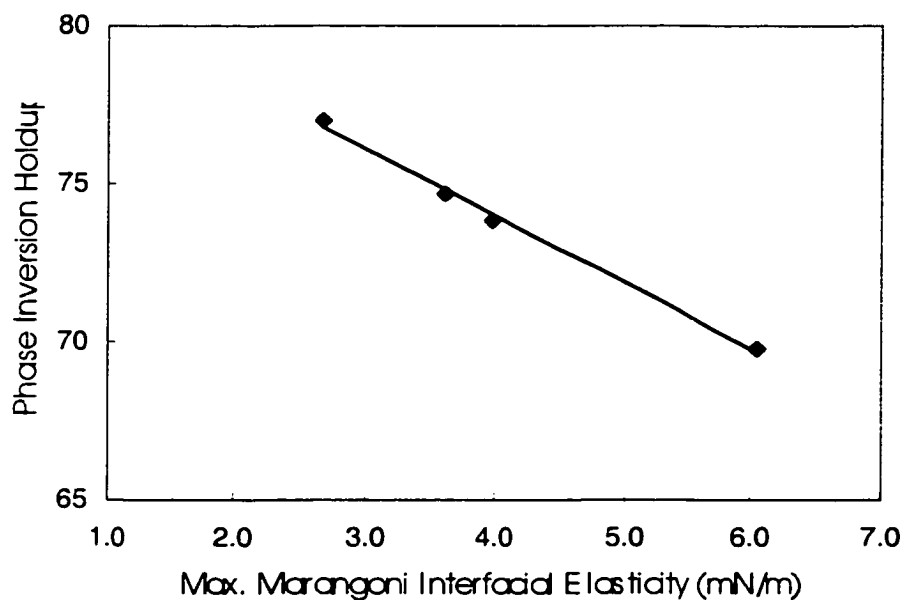


Figure 55. Effect of Marangoni interfacial elasticity on the phase inversion of (industrial systems, maximum-drop-pressure technique)

between the Gibbs elasticity of the film and that of the interface. In coalescence and phase inversion processes, film thinning is most likely controlled by the interfacial characteristics of the film rather than that of the interface. As seen in Sections 4.4.2, 4.4.3, and in this section, the diffusivity of the surface-active species correlates very well with: coalescence rate ( $R=0.989$ ), phase-inversion holdup of surfactant containing systems ( $R=-0.95$ ), and the phase-inversion holdup of industrial systems ( $R=-0.84$ ). This suggests that diffusivity is an interfacial characteristic that can be used in correlating both phase-inversion and drop-coalescence processes. It can be easily determined using many dynamic interfacial measurement techniques..



## 5 CONCLUSIONS AND RECOMMENDATIONS

The results of this study show that:

### Conclusions

1. Systems that their density differs significantly from each other (Bayol oil in water where  $\rho_d/\rho_c < 0.78$ ) showed a strong tendency towards spatial segregation following a sudden reduction in impeller speed (500→250 rpm). It is therefore advisable to use systems with density ratios close to one (e.g. acetophenon/ 0.05 molar aq. NaCl, where  $\rho_d/\rho_c < 0.99$  or CLB-Bayol mixture (65% v/v) where  $\rho_d/\rho_c < 0.99$ ) to overcome the effect introduced by this factor. The tendency towards segregation was found to decrease at higher impeller speeds and in the presence of SAA. This observation can be attributed to the formation of smaller drops that discourage spatial segregation.
2. Quasi-steady drop-size distributions can be considered to have been achieved within 3 hours of agitation (holdup of 0.75%, 300 rpm) in the case of CLB-Bayol oil drops dispersed in water containing 1.0 mmole/m<sup>3</sup> Triton X100 in which acetophenon was introduced. Under those conditions,  $d_{32}$  reached 95% of its value after 48 hours. However, quasi-steady state was only approached after 3 hours of agitation at 200 rpm for all the systems investigated with the deviation being greater the higher the SAA concentration and/or its activity.
3. No bimodality was observed in the number density for all the systems investigated (in the presence, or absence, of SAA). The number-density curves are generally skewed towards smaller drop sizes, and the number density of small drops was found to increase with agitation intensity.
4. The number-density data obtained at quasi-steady state (at 300 and 200 rpm) can be fitted by the normal and log-normal distributions at or better than the 95% confidence

level. Although both distributions fit the number density data well, the log-normal distribution generally provides a better fit. It provides a statistically better fit (at the 95% confidence level) for most cases run at 200 rpm, while, on the other hand, it does not provide a statistically better fit for most runs at 300 rpm.

5. The volume-density data obtained at quasi steady state (at 300 rpm) was found to be uni-modal for all the systems investigated and can be fitted by the normal and log-normal distributions. Although both distributions fit the quasi steady volume density data well, the log-normal distribution generally provides a better fit. On the other hand, the modality of the volume-density data obtained after 3 hours of agitation at 200 rpm was found to be dependent on the characteristics investigated. Systems possessing high coalescence rate almost reached equilibrium conditions and exhibited a uni-modal distribution. However, slightly bi-modal distributions were observed in systems having relatively-low coalescence rates due to the retention of some of the transient bi-modal characteristics. The log-normal distribution provides a statistically better fit (at the 95% confidence level) for most cases run at 200 rpm.
6. Following a sudden decrease in impeller speed (from 300→200 rpm), the peaks in the number-density distributions were found to shift towards the formation of larger drop sizes. Transient number densities were found to follow a uni-modal distribution, which can be fitted by normal and log-normal distributions with the latter providing a better fit. As time progresses, the size at which the peak of the number-density is located shifts slightly towards larger drop sizes while, at the same time, a number of large drops appear.
7. Bimodality was observed to occur in the transient volume-number distributions. When the coalescence rate is high, bi-modal distributions can appear as early as 5 minutes and vanish as the quasi steady state is approached (after 3 hours). On the other hand, bi-modality first appears at a later time when coalescence rate is and continues to persist even after 3 hours of agitation at 200 rpm. The time at which bi-modality in drop-volume density first appears was found to depend on the type of

- SAA used and its concentration. Bi-modality is therefore associated with the presence of a transient condition related to the rate at which drop-size distributions evolve from the initial to the final steady-state conditions.
8. The transient cumulative drop-volume density data were fitted by normal and log-normal distributions with the latter generally providing a better fit. All the correlation coefficients were found to be statistically significant at the 99% confidence level. Deviation from the analytical distributions was found to increase with increasing surfactant concentration and its molecular weight. This is caused by the development of a transient bi-modal distribution as the coalescence process progresses.
  9. At quasi steady state (i.e., after 3 hours of mixing), the cumulative drop-volume densities depict self-similarity when the drop diameters were normalized using the Sauter mean diameter. This applies to relatively pure systems as well as ones in the presence of SAA (up to 1.0 mmole/m<sup>3</sup>). As seen by other investigators, the self-similar distributions were best fitted using log-normal distributions. However, their characteristics (mean and standard deviation) were found to depend on the agitation intensity. The values of the normalized mean and standard deviation were found to be larger than those reported by other investigators, a factor which is most probably caused by the persistence of transient conditions (bi-modality) for longer times in the presence of SAA.
  10. Similar conclusions apply to the case of transient distributions (pure system and in the presence of SAA) obtained following a sudden reduction in agitation intensity. The mean and the standard deviation slightly decrease with increasing surfactant concentration.
  11. The rate of change of the Sauter mean diameter following a step reduction in agitation intensity can be expressed by  $d_{32} = d_{320} \cdot (t+1)^b$  where the value of the exponent  $b$  was found to depend on the molecular weight of SAA (a non-monotonic function) and decreases with increasing surfactant concentration. This is attributed to the surfactant's ability to decrease coalescence rate by retarding the drainage of the

continuous film present between dispersed-phase drops, and by increasing the elasticity of the interface

12. Based on the approach suggested by Howarth (1967) and using the above-mentioned expression for the rate of change of the Sauter mean diameter, the drop coalescence rate can be expressed as:

$$\text{Coalescence rate} = \frac{\partial n}{\partial t} = b/(2-2^{2/3})$$

For any particular surfactant, the coalescence rate was found to decrease as the concentration of the surfactant increases. On the other hand, at any particular molecular concentration of the Triton X series, the coalescence rate was found to be a non-monotonic function of the molecular weight of the SAA.

13. A consistent phenomenological interpretation of the phase-inversion phenomenon was developed. It is based on the assumption that phase inversion is a dynamic process that takes place when the rate of inclusion of the continuous-phase droplets within the dispersed-phase drops exceeds their rate of escape by coalescence with the external continuous-phase. This interpretation is capable of reconciling many apparently-contradictory results reported in the literature and consistently explains the findings observed in this work.
14. In the case of water dispersed in kerosene, the presence of droplets included within the dispersed-phase drops was observed at holdups as low as 10%. The number and size of these droplets was found to increase as the holdup was increased. Although phase inversion does not take place at these holdups, the equilibrium between the droplets' inclusion and escape results in an effective dispersed phase holdup. This is higher than the initial one due to the increased volume of the dispersed phase (resulting from the inclusion of continuous-phase droplets), and the reduction of the freely available continuous-phase volume. Near the critical holdup, a number of very large globular drops, that included many droplets of the continuous-phase, were observed to appear.

15. The phase inversion delay times measured in this investigation (for the case of water dispersed in gasoline) were found to vary between 10-700 seconds depending on how close the initial dispersed phase holdup is to the catastrophic value. The closer the initial holdup is to the catastrophic value, the shorter the delay time is. This is caused by the net overall kinetics of the competing processes of droplet inclusion and escape. Shorter phase-inversion times are thus obtained if the droplet inclusion rate is high and much larger than the droplet escape rate. Conversely, long phase-inversion times are encountered if the droplet inclusion rate is small or if the difference between the droplet inclusion and escape rates is small.
16. In the case of the gasoline/water system, no phase inversion delay time could be measured. This suggests that droplet inclusion within the dispersed phase drops is practically non-existent until the catastrophic phase-inversion holdup is reached, or that droplet escape rate is very high relative to the inclusion rate; beyond this point, the droplet inclusion rate is so large and so much bigger than the droplet escape rate that phase inversion is essentially instantaneous
17. Phase inversion holdup was found to decrease as the agitation intensity increased for systems having no surfactants as well as those containing surfactants. The phase-inversion holdup was found to increase with increasing Triton X100 concentration. However, the phase inversion behavior of the pipelined gasoline is a non-monotonic function of the re-circulation ratio (capacity number).
18. Generally speaking, the equilibrium interfacial tension was found to decrease as the Triton molecular weight/length increases. This may be because larger surfactant molecules have more segments that can be adsorbed by the interface and thus become highly surface-active, bringing down the interfacial tension. With increasing molecular weight/length, the equilibrium interfacial concentration was found to decrease.
19. The dynamic interfacial tensions obtained using the maximum-drop-pressure and drop-volume techniques were found to decrease and tended to approach an

equilibrium interfacial tension as the drop formation time increases. On the other hand, the dynamic interfacial tension tends to approach the static interfacial tension of the pure system at very short surface ages. This is attributed to the inability of diffusion to fully restore the interfacial surfactant concentration to its equilibrium value at the rapidly-stretched interface.

20. In general, for systems containing Triton surfactants, the dynamic interfacial tension data provided by the drop-volume technique provide a better fit to the long-time approximation equation, whereas the data obtained by the maximum-drop- pressure technique fit the short-time approximation equation better. Hence, the latter technique was used to determine the dynamic interfacial tension encountered in the “inverse Doctor treatment” of pipelined gasoline. This was necessary because the equilibrium interfacial concentration could not be determined for these industrial streams.
21. The diffusivity of the SAA was found to decrease with higher concentration of SAA, which was attributed to the partitioning of surfactant monomer between the interface and a growing number of micelles in the bulk as the surfactant concentration of the bulk increases.
22. The diffusivity of Triton in the acetophenon/ water/  $0.1 \text{ mmole/m}^3$  Triton systems (as measured by the drop-volume technique) exhibited a maximum at Triton X165 (molecular weight 910) whereas it was found to decrease monotonically (inversely proportional to the square of its molecular weight) in the case of the Bayol oil/ water/  $0.1 \text{ mole/m}^3$  Triton systems.
23. The apparent diffusivity of the surface-active species in the “inverse Doctor treatment” systems was found to be a non-monotonic function of the capacity number. This is most probably caused by the uncontrolled addition of one or more of the reagents involved in the reaction.
24. For the two systems investigated, the Marangoni interfacial elasticity was found to decrease as the concentration of SAA increased. This can be attributed to the higher

diffusion rate of the surfactants to the newly formed interface where they adsorb and quickly bring down the interfacial tension. Also, the Marangoni elasticity of the interface was found to decrease with increasing SAA molecular weight due to the higher surface activity of the larger SAA molecule. In the case of the industrial systems, the Marangoni interfacial elasticity was found to be a non-monotonic function of the capacity number of the caustic.

25. The quasi-equilibrium Sauter mean diameter at 300 and 200 rpm was found to correlate reasonably well with the equilibrium interfacial tension for the range of SAA concentrations investigated (0-1.0 mmole/m<sup>3</sup>). The value of the exponent obtained varied between 0.47 to 0.93 (as opposed to the theoretical value of 0.6) depending on how closely the equilibrium conditions were approached.
26. Although there is a general tendency for the coalescence rate to increase with increasing equilibrium interfacial tension, the correlation between these two parameters was found to be rather poor. An excellent correlation was, however, found between coalescence rate and surfactant diffusivity calculated from the data obtained using the drop-volume technique. This suggests that the coalescence process is largely controlled by surfactant diffusion of the surface-active species.
27. In the Bayol oil / water / Triton systems, a rather poor correlation was found to exist between the phase-inversion holdup and the equilibrium interfacial tension. However, a very good correlation was obtained with the diffusivity (calculated using the drop-volume technique). This may be attributed to the ability of the Triton molecules to retard film thinning, and the coalescence of the organic-phase drops, and the consequent reduction of the droplet-inclusion process. Similar trends were observed in the case of the industrial gasoline/caustic systems. However, a better correlation was obtained using the maximum Marangoni elasticity.
28. SAA diffusivity was found to correlate with phase-inversion holdup of both synthetic and industrial systems. It was also found to correlate well with the coalescence rate of

dispersed drops in system containing surfactants with a wide range of molecular weight (426-1966), and concentrations (up to 1.0 mmole/m<sup>3</sup>). Thus, the diffusivity is proposed as a universal interfacial characteristic correlating both the coalescence and phase-inversion processes. However, further investigation is needed in order to confirm this suggestion.



### **Recommendations for further work**

It is recommended that:

1. Pure surfactants with defined molecular weight and structure should be used in future coalescence/phase inversion studies rather than commercial surfactants that are mixtures of a number of different size molecules. The dynamic interfacial characteristic of a commercial surfactant is an “effective” value to which all species contribute. At the beginning of the adsorption, the light molecules adsorb faster and thus contribute larger to the overall diffusivity than the heavier molecules. Thus, the diffusivity value of the commercial surfactant will be dependent on the stretching rate of the interface. Therefore, a comparison between the diffusivity values obtained by different techniques for a certain surfactant will be limited.
2. In future phase inversion studies, the film Marangoni elasticity should be investigated in addition to the Marangoni interfacial elasticity. This is due to the fact that each of those characteristics will have a different effect on the two phases inversion sub-processes (inclusion and escape). For example, in the case of a surfactant soluble in continuous phase, the film Marangoni elasticity is expected to strongly influence the inclusion process whereas the Marangoni interfacial elasticity will affect the escape process. The situation will be reversed when the surfactants are soluble in the dispersed phase.
3. Phase inversion of a W/O system should be investigated and the drop size of the dispersed phase near the phase inversion should be monitored and correlated.
4. An automatic technique for evaluating drop-size distribution should be used in order to reduce the labour requirement for image analysis. The use of on-line sampling and analysis would facilitate data acquisition of temporal drop size variation in the presence of high SAA concentration.

5. The effect of the conductivity probe design (sensor size, geometry and spacing) on the signal obtained in liquid-liquid dispersion (particularly near the phase inversion point) should be investigated. This could lead to the development of an instrument that could provide warning prior to the onset of phase inversion. Such a tool would be important from a practical point of view.

## 6 REFERENCES

1. Arashmid, M., and Jeffreys, G. V., (1980), "Analysis of the Phase Inversion Characteristics of Liquid-Liquid Dispersions", *AIChE J.*, **26**, pp. 51-55.
2. Bae, J. H., and Tavlarides, L.L., (1989), "Laser Capillary Spectrophotometry for Drop-Size Concentration Measurements," *AIChE J.*, **35**, pp. 037-1084.
3. Bailes, P. J., Hanson, C., Hughes, M. A., and Pratt, M. W., (1993), "Liquid-Liquid Extraction", in Unit Operation Handbook, J. Mcketta., **1**, pp. 687-728. CRC Press, New York
4. Becher, P. (1965) Emulsions: Theory and Practice, 2nd Edition, Reinhold Publishing Co., New York.
5. Berkman, P. D., and Calabrese, R. V., (1988)," Dispersion of Viscous Liquids By Turbulent Flow in A Static Mixer", *AIChE J.*, **34**, pp. 602-609
6. Bhardwaj, A., and Hartland, S., (1994), "Kinetics of Coalescence of Water Droplets in Water-in-Crude Oil Emulsions", *J. Dispersion and Technology*, **15**, pp. 133-146.
7. Borwankar, R. P., Chung, S.I. and Wasan, D. T. (1986). "Drop Sizes in Turbulent Liquid-Liquid Dispersions Containing Polymeric Suspension Stabilizers. I. The Breakage Mechanism" *J. Applied Polymer Sci.*, **32**, pp. 5749-5762
8. Brooks, B. W., and Richmond, H. N., (1994), "Phase Inversion in Non-Ionic Surfactant-Oil-Water Systems-II. Drop Size Studies in Catastrophic Inversion with Turbulent Mixing", *Chem. Eng. Sci.*, **49**, pp. 1065-1075.
9. Brown, D. E., and Pitt, K., (1972),"Drop Size Distribution of Stirred Non-Coalescing Liquid-Liquid System", *Chem. Eng. Sci.*, **27**, pp. 577-583
10. Busaiffi, M. A., (1989). Pipeline Transportation of Petroleum Emulsions: Pressure Drop in Sudden Expansion and Sudden Contraction, M.Sc. Thesis, Technical University of Nova Scotia, Halifax, NS CANADA
11. Cairns, R. J. R., Grist, J.M., and Neustadter, E. L. (1976), "The Effect of Crude Oil-Water Interfacial Properties on Water-Crude Oil Emulsion Stability", in: Theory and Practice of Emulsion Technology. A. L. Smith Ed., Synthetic Press, New York, pp. 135-151.
12. Calabrese, R. V., Pacek, A. W., and Nienow, A. W., (1993) "Coalescence of Viscous Drops in a Stirred Dispersion", The ICHME Research Event ,Birmingham, U.K.,

published by ICE, Rugby, U.K., pp. 642-645

13. Campanelli, R. C., and Cooper, D. G., (1989), "Interfacial Viscosity and the Stability of Emulsions" *Can. J. Chem. Eng.*, **67**, pp. 851-855
14. Campanelli, J. R., and Wang, X., (1998), "Comments on Modeling the Diffusion-Controlled Adsorption of Surfactants", *Can. J. Chem. Eng.*, **76**, pp. 51-57
15. Campbell, L., Norton, I., and Morley, W., (1996), "Factors Controlling the Phase Inversion of Oil-in-Water Emulsions", *Netherlands Milk & Dairy Journal*, **50**, pp. 167-182.
16. Castleman, K. R., (1996), Digital Image Processing, Chapter 18, Prentice Hall Inc., New York.
17. Chatzi, E. G., and Kiparissides, C., (1994), "Drop Size Distributions in High Holdup Fraction Dispersion Systems: Effect of the Degree of Hydrolysis of PVA Stabilizer", *Chem. Eng. Sci.*, **49**, pp. 5039-5052
18. Chatzi, E. G., and Kiparissides, C., (1995), "Steady State Drop Size Distributions in High Holdup Fraction Dispersion Systems", *AIChE J.*, **41**, pp. 1540-1652
19. Chatzi, E. G., Boutris, C. J., and Kiparissides, C., (1991a), "On-Line Monitoring of Drop Size Distributions in Agitated Vessels 1. Effect of Temperature and Impeller Speed", *Ind. Eng. Chem. Res.*, **30**, pp. 536-543
20. Chatzi, E. G., Boutris, C. J., and Kiparissides, C., (1991b), "On-Line Monitoring of Drop Size Distributions in Agitated Vessels 2. Effect of Stabilizer Concentration", *Ind. Eng. Chem. Res.*, **30**, pp. 1307-1313
21. Chen, C. T., Maa, J. R., Yang, Y. M., and Chang, C. H., (1998), "Effects of Electrolytes and Polarity of Organic Liquids on the Coalescence of Droplets at Aqueous-Organic Interfaces", *Surface Science*, **406**, pp. 167-177.
22. Chen, H. T., and Middleman, S., (1967), "Drop Size Distribution in Agitated Liquid-Liquid Systems", *AIChE J.*, **13**, pp. 989-995.
23. Chen, Y., (1996), Dispersion and Coalescence in Static Mixers, Ph.D. Thesis, Technical University of Nova Scotia, Halifax, NS CANADA
24. Chesters, A.K. (1991), "The Modeling of Coalescence Processes in Fluid-Liquid Dispersions: A Review of Current Understanding", *Trans IChEM.*, **69(A)**, pp. 259-270

25. Das, P. K., Ramkrishna, D., and Narsimhan, G., (1987), "Effect of Mass Transfer On Droplet Breakup in Stirred Liquid-Liquid Dispersions", *AIChE J.*, **33**, pp. 1899-1902
26. Das, P., and Hartland, S., (1989), "A Simple Correlation for Coalescence Rate Constant in Batch Turbulent Liquid-Liquid Dispersions", *Chem. Eng. Comm.*, **84**, pp. 33-41
27. Davies, G. A., (1992), "Mixing and Coalescence Phenomena in Liquid-Liquid Systems," in Science and Practice of Liquid-Liquid Extraction, J. D. Thornton, Ed., Volume 1, Clarendon Press, Oxford Press, Oxford, pp. 245- 342.
28. Deshikan, S. R., and Papadopoulos, K. D., (1995), "London-Van Der Waals and EDL Effects in the Coalescence of Oil Drops. II. Ionic Strength and pH Effects", *J. Colloid and Interface Sci.*, **174**, pp. 313-318
29. Dreher, T. M., Glass, J., O'Connor, A. J., and Stevens, G. W., (1999) "Effect of Rheology on Coalescence Rates and Emulsion Stability", *AIChE J.*, **45**, pp. 1182-1190
30. Efthimiadu, I., and Moore, I. P. T., (1994), "Phase Inversion of Liquid-Liquid Dispersions Produced Between Parallel Shearing Plates", *Chem. Eng. Sci.*, **49**, pp. 1439-1449.
31. Falkiner, R. J., Peirier, M. A., and Cambell, I. D., (1992), "Process for Removing Elemental Sulfur From Fluids", US Patent 5,160,045
32. Falkiner, R. J., Peirier, M. A., and Cambell, I. D., (1993), "Process for Removing Elemental Sulfur from Fluids", US Patent 5,250,181
33. Gaonkar, A. G., (1992), " Effects of Salt, Temperature, and Surfactant on the Interfacial Tension Behavior of a Vegetable Oil/Water System", *J. Colloid and Interface Science*, **149**, pp. 256-260
34. Gilchrist, A., Dyster, K. N., Moor, I. P. T., Nienow, A. W., and Carpenter, K. J., (1989), "Delay Phase Inversion in Stirred Liquid-Liquid Dispersions." *Chem. Eng. Sci.*, **44**, pp. 2381-2384.
35. Godfrey, J. C., Obi, I. N., and Reeve, N., (1989), "Measuring Drop Size in Continuous Liquid-Liquid Mixers", *Chem. Eng. Progress*, Dec, pp. 61-69
36. Goodrich, F. C. and Goupil, D. W. (1980), "A New Surface Viscometer of High Sensitivity", *J. Colloid. Int. Sci.*, **75**, pp. 590-600
37. Graham, D. E., Neustadter, E. L., Stockwell, A., Whittingham, K. P., and Cairns, R. J.

- R., (1979), "????", Symp. Surface Active Agents, Soc. Chem. Ind., Colloid Surf. Chem. Group, London. pp. 127-?
38. Groeneweg, F., Van Dieren. F., and Agterof. W. G. M., (1994), "Droplet Breakup in a Stirred Water-in-Oil Emulsion in the Presence of Emulsifiers", *Colloids and Surfaces A: Physicochemical and Engineering Aspects*, **91**, pp. 207-214
  39. Groeneweg, F., Agterof, W. G. M., Jaeger, P., Janssen, J. J. M., Wieringa, J. A., and Klahn, J. K., (1998), "On the Mechanism of the Phase Inversion of Emulsions", *Trans. I. Chem. E., Part A*, **76**, pp. 55-63.
  40. Guilinger, T. R., Grislingas. A. K. and Erga. O., (1988), "Phase Inversion of Water-Kerosene Dispersions", *Ind. Eng. Chem. Res.*, **27**, pp. 978-982.
  41. Hadjiev, D. and Aurelle, Y., (1995), "Phase Inversion : A Method for Separation of Fine Liquid-Liquid Dispersions", *Chem. Eng. J.*, **58**, pp. 45-51
  42. Hazlett, R., Schechter, R., and Aggarwal, J. K., (1985), "Image Processing for the Estimation of Drop Size Distributions", *Ind. Eng. Chem. Fundam.*, **24**, pp. 101-105
  43. Hine, J., and Wetherill, G. B., (1975) A programmed text in Statistics, Book Three, The *t*-test and  $\chi^2$  Goodness of fit, Chapman and Hall Ltd., London, UK.
  44. Hocq, S., and Milot, J. F., (1994), "Electrical Conductivity Capillary Technique: a New Method for Bivariate Drop-Size-Concentration Distribution Measurements", *Chem. Eng. Sci.*, **49**, pp. 481- 489.
  45. Hong, P.O. and Lee, J.M., (1983), "Unsteady-State Liquid-Liquid Dispersions in Agitated Vessels", *Ind. Eng. Chem. Process Des. Dev.*, **22**, pp. 130-135.
  46. Hong, P.O. and Lee, J.M., (1985), "Changes of the Average Drop Sizes During the Initial Period of Liquid-Liquid Dispersions in Agitated Vessels", *Ind. Eng. Chem. Process Des. Dev.*, **24**, pp. 868-872
  47. Janssen, J. J., Boon, A, and Agterof, W. G. M. (1994), "Influence of Dynamic Interfacial Properties on Droplet Breakup in Simple Shear Flow", *AIChE J.*, **40**, pp. 1929-1939
  48. Janssen, J. J., Boon, A, and Agterof, W. G. M. (1997), "Influence of Dynamic Interfacial Properties on Droplet Breakup in Plane Hyperbolic Flow", *AIChE J.*, **43**, pp. 1436-1447
  49. Kato, S., Nakayama, E. and Kawasaki, J., (1991), "Types of Dispersion in Agitated Liquid-Liquid Systems.", *Can. J. Chem. Eng.*, **69**, pp. 222-227

50. Kennedy, J. B., and Neville A. M., (1986), Basic Statistical Methods for Engineers and Scientists , Third Ed., Harper & Row, Publishers, New York
51. Kim, Y., Nikolov, A.D., Wasan, D.T., Diaz-Arauzo, H., and Shetty, C.S., (1996), "Demulsification of Water-in-Crude Oil Emulsions: Effects of Film Tension, Elasticity, Diffusivity, and Interfacial Activity of Demulsifier Individual Components and Their Blends", *J. Dispersion Science and Technology*, **17**, pp. 33-53
52. Konno, M., Kosaka, N., and Saito, S., (1993), "Correlation of Transient Drop Size in Breakup Process in Liquid-Liquid Agitation", *J. Chem. Eng. Japan*, **26**, pp. 37-40
53. Kourio, M. J., Gourdon, C., and Casamatta, G., (1994), "Study of Drop-Interface Coalescence: Drainage Time Measurement", *Chem. Eng. Tech.*, **17**, pp. 240-254
54. Krawczyk, M. A., Wasan, D. T., and Shetty, C. S., (1991), "Chemical Demulsification of Petroleum Emulsions Using Oil-Soluble Demulsifiers", *Ind. Eng. Chem. Res.*, **30**, pp. 367-375
55. Kumar, R. and Kannan, S., (1994), "Drop Size Measurement in a Two-Phase Swirling Flow Using Image Processing Technique", *Int. J. Heat Mass Transfer*, **37**, pp. 559-570.
56. Kumar, S., (1996), "On Phase Inversion Characteristics of Stirred Dispersions", *Chem. Eng. Sci.*, **51**, pp. 831-834
57. Kumar, S., Kumar, R., and Gandhi, K. S., (1991), " Influence of the Wetting Characteristics of the Impeller on Phase Inversion.", *Chem. Eng. Sci.*, **46**, pp. 2365-2367
58. Lam, A., Sathyagal, A. N., Kumar, S., and Ramkrishna, D., (1996) "Maximum Stable Drop Diameter in Stirred Dispersions", *AIChE J.*, **42**, pp. 1547-1552.
59. Laso, M., L. Steiner, and S. Hartland (1987), "Dynamic Simulation of Liquid-Liquid Dispersions-II. Experimental Determination of Breakage and Coalescence Rates in a Stirred Tank", *Chem. Eng. Sci.*, **42**, pp. 2437-2445.
60. Leavers, R. H., and Thomas, T. R., (1974), Analysis and Presentation of Experimental Results, Macmillan Press Ltd. London
61. Leo, W., Moore, S. R., Campbell, I., Morley, W., and Ayazi Shamlou, P (1994), "Modeling of Drop Coalescence in Food Emulsions", *Trans IChEM* **72**, Part C, pp. 24-26

62. Leonard, R. A., Bernstein, G. J., Pelto, R. H., and Ziegler, A. A., (1981), "Liquid-Liquid Dispersion in Turbulent Couette Flow", *AIChE*, **27**, pp. 495-503
63. Lide, R. D., (1990-1991), Handbook of Chemistry and Physics, 71st Edition. CRC Press.
64. Lucassen-Reynders, and Kuijpers, K. A., (1992), "The Role of Interfacial Properties in Emulsification", *Colloids and Surfaces*, **65**, pp. 175-184
65. Lucassen-Reynders, E. H., (1996), "Dynamics Interfacial Properties in Emulsification" in Encyclopedia of Emulsion Technology, **4**, pp. 63-91
66. Luhnig, R. W., Sawistowski, H., (1971), "Phase Inversion in Stirred Liquid-Liquid Systems", in *Proceeding of the International Solvent Extraction Conference*, 2, The Hague, Holland, pp. 873-887, SCI Publisher, London.
67. Lyford, P.A., Shallcross, D. C., Grieser, F., and Pratt, R. C., (1998), "The Marangoni Effect and Enhanced Oil Recovery Part2. Interfacial Tension and Drop Instability", *Can. J. Chem. Eng.*, **76**, pp. 175-180
68. Miller, R., Joos, P., and Fainerman, V. B., (1994), "Dynamic Surface and Interfacial Tensions of Surfactant and Polymer Solutions", *Advances in Colloid and Interface Sci.*, **49**, pp. 249-302
69. Mishra, V., Kresta, S., and Masliyah, J., (1998), " Self-Preservation of the Drop Size Distribution Function and Variation in the Stability Ratio for Rapid Coalescence of a Polydisperse Emulsion in a Simple Shear Field", *J. Colloid and Interface Sci.*, **197**, pp. 57-67
70. Mohammed, R.A., Bailey, A. L., Luckhama, P. F., and Taylor, S. E. (1993), "Dewatering of Crude Oil Emulsions I. Rheological Behaviour of the Crude Oil-Water Interface", *Colloids and Surf. Sci.*, **80**, pp. 223-235.
71. Moore, I. P. T., (1995), "Phase Inversion of Liquid-Liquid Dispersions Produced Between Parallel Shearing Plates", *Advances in Engineering Fluid Mechanics*, pp. 165-183
72. Nadler, M. and Mewes, D., (1997), "Flow Induced Emulsification in the Flow of two Immiscible Liquids in Horizontal Pipes", *Int. J. Multiphase Flow*, **23**, pp. 55-68.
73. Nakache, E., Longaive, P., and Aiello, S., (1995), "Determination of a Coalescence Parameter Related to the Stability of Emulsions with Polymeric Surfactants", *Colloids and Surfaces*, **96**, pp. 69-76.



74. Neustadter, E. L., Whittingham, K. P. and Graham, D. E., (1979), in Surface Phenomena in Enhanced Oil Recovery, Plenum Press, New York, pp. 304-?
75. Ni, X., Zhang, Y., and Mustafa, I., (1998), " An Investigation of Droplet Size and Size Distribution in Methylmethacrylate Suspensions in a Batch Oscillatory-Baffled Reactor", *Chem. Eng. Sci.*, **53**, pp. 2903-2919
76. Nienow, A. W., Pacek, A. W., (1995), "A Problem for the Description of the Turbulent Dispersed Liquid-Liquid Systems", *Int. J. Multiphase Flow*, **21**, pp. 323-328.
77. Nienow, A. W., Pacek, A. W., Moore, I. P. T., and Homer, J., (1994), "Fundamental Studies of Phase Inversion in a Stirred Vessel." *ICHEM Symposium Series 136*, pp. 171-178.
78. Nishikawa, M., Mori, F., and Fujieda, S. (1987), "Average Drop Size in a Liquid-Liquid Phase Mixing Vessel", *J. Chem. Eng. Japan* **20**, pp. 82-88.
79. Nishikawa, M., Mori, F., Kayama, T., and Nishioka, S., (1991), "Drop Size Distribution in a Liquid-Liquid Phase Mixing Vessel", *J. Chem. Eng. Japan*, **24**, pp. 88-94
80. Nishikawa, M., Mori, F., Kayama, T., Nishioka, S., and Nishikawa, S., (1991), "Drop Size Distribution in a Mixing Vessel with Aeration", *J. Chem. Eng. Japan*, **49**, pp.2379-2384
81. Norato, M., Tsouris, C., and Tavlarides, L. L., (1998), " Phase Inversion Studies in Liquid-Liquid Dispersions", *Can. J. Chem. Eng.* **26**, pp. 486-494
82. Orr, C., (1983), "Emulsion Droplet Size Data" in Encyclopedia of Emulsion Technology, edited by P. Becher, **1**, pp. 369-404
83. Pacek, A. W., and Nienow, A. W., (1995), "Measurement of Drop Size Distribution in Concentrated Liquid-Liquid Dispersions: Video and Capillary Techniques," *Trans. I. Chem. E.*, **73** Part A, pp. 512-518.
84. Pacek, A. W., Moore, I. P. T., and Nienow, A. W., (1994b), "Video Technique for Measuring Dynamics of Liquid-Liquid Dispersions During Phase Inversion," *AIChE J.*, **40**, pp. 1940-1949
85. Pacek, A. W., Moore, I. P. T., Calabrese, R.V., and Nienow, A. W., (1993), "Evolution of Drop Size Distributions and Average Drop Diameter in Liquid-Liquid Dispersions Before and after Phase Inversion", *Trans. I. Chem. E., Part A*, **71**, pp. 340-341

86. Pacek, A. W., Nienow, A. W., and Moore, I. P. T., (1994a), "On the Structure of Turbulent Liquid-Liquid Dispersed Flows in an Agitated Vessel", *Chem. Eng. Sci.*, **49**, pp. 3485-3498.
87. Pacek, Man, and Nienow (1998), "On the Sauter Mean Diameter and Size Distributions in Turbulent Liquid/Liquid Dispersions in A Stirred Vessel", *Chem. Eng. Sci.*, **53**, pp. 2005-2011
88. Page, G. W., and Patton, C. V., (1991) Quick Answers to Qualitative Problems, Academic Press, Inc. New York
89. Pal. R., (1993), "Pipeline Flow of Unstable and Surfactant-Stabilized Emulsions", *AIChE J.*, **39**, pp. 1754-1764.
90. Pal. R., (1996), "Effect of Droplet Size on the Rheology of Emulsions", *AIChE*, **42**, pp. 3181-3190.
91. Peru, D. A., and Lorenz, P. B., (1989), " The Effect of Equilibration Time and Temperature on Drop-Drop Coalescence of Wilmington Crude Oil in a Weakly Alkaline Brine", *Chem. Eng. Comm.*, **77**, pp. 91-114.
92. Quinn. J. A., and Sigloh. D. B., (1963), "Phase Inversion in the Mixing of Immiscible Liquids." *Can. J. Chem. Eng.*, **41**, pp. 15-18
93. Riggs, J. B., (1994), An Introduction to Numerical Methods for Chemical Engineers, 2<sup>nd</sup> Ed., Texas Tech University Press
94. Sachs, L., (1984), Applied Statistics, 2<sup>nd</sup> Ed., Springer-Verlag, New York. USA
95. Sathyagal, A.N., Ramkrishna, D. and Narsimhan, G., (1994), "Solution of Inverse Problems in Population Balance II: Particle Breakup" *Computer. Chem. Engng.* **19**, pp. 435-451
96. Sathyagal, A.N., Ramkrishna, D., and Narsimhan, G., (1996), "Droplet Breakage in Stirred Dispersions. Breakage Functions from Experimental Drop-Size Distributions" *Chem. Eng. Sci.* **51**, pp. 1377-1391
97. Sears, F. W., and Zemansky, M. W. (1960) College Physics, Addison-Wisley Publishing Co., Massachusetts, USA
98. Seidshazileh, K., (1998), "Drop Breakage and Coalescence in Turbulent Flow", Technical report, Dalhousie University, Halifax, NS.
99. Selker, A. H., and Sleicher, C. A., (1965), "Factors Affecting Which Phase Will Disperse when Immiscible Liquids Are Stirred Together." *Can. J. Chem. Eng.*, **43**, pp. 298-301.

100. Skelland, A. H. P. and Kanel, J. S., (1992), "Transient Drop Size in Agitated Liquid-Liquid Systems, as Influenced by the Direction of Mass Transfer and Surfactant Concentration", *Ind. Eng. Chem. Res.* **31**, pp. 2556-2563
101. Sprow, F. B. (1967a), "Drop Size Distribution in Strongly Coalescing Agitated Liquid-Liquid Systems", *AIChE J.*, **13**, pp. 995-998
102. Sprow, F. B. (1967b), "Distribution of Drop Sizes Produced in Turbulent Liquid-Liquid Dispersion", *Chem. Eng. Sci.* **22**, pp. 435-442
103. Stein, H. N., (1995), The Preparation of Dispersions in Liquids, Chapter 1, pp. 19-26, Marcel Dekker, Inc. New York.
104. Stewart, A. C., El-Hamouz, A. M., and Davies, G. A., (1996), "Effect of Chemical Additives on the Stability of Kerosene-Water Dispersions", *J. Dispersion and Tech.*, **17**, pp. 675-696.
105. Stone, H (1994), "Dynamics of Drop Deformation and Breakup in Viscous Fluids" *Annual Rev. Fluid Mech.*, **26**, pp. 65-102
106. Swift, D. L., Friedlander, S. K., (1964), "The Coagulation of Hydrosols by Brownian Motion and Laminar Shear Flow", *J. Colloid Science*, **19**, pp. 621-647.
107. Tavlarides, L. L., and M. Stamatoudis (1981), "The Analysis of Interphase Reactors and mass Transfer in Liquid-Liquid Dispersions", in *Adv. Chem. Eng.*, **11**, pp. 199-273.
108. Taylor, S. E., (1988), "???", *Colloids Surfaces*, **29**, pp. 29-
109. Tidhar, M., Merchuk, J. C., Sembira, A. N., and Wolf, D., (1986), "Characteristics of a Motionless Mixer for Dispersion of Immiscible Fluids-II. Phase Inversion of Liquid-Liquid Systems", *Chem. Eng. Sci.*, **41**, pp. 457-462.
110. Tobin, T., (1989), Experimental Measurement of Drop Coalescence Frequencies in Turbulent Liquid-Liquid Dispersions, M. Sc. Thesis, Purdue University, Lafayette, Indiana, USA.
111. Tobin, T., Muralidhar, R., Wright, H., and Ramkrishna, D., (1990), "Determination of Coalescence Frequencies in Liquid-Liquid Dispersions: Effect of Drop Size Dependence", *Chem. Eng. Sci.*, **45**, pp. 3491-3504.
112. Tobin, T., and Ramkrishna, D. (1992), "Coalescence of Charged Droplets in Agitated Liquid-Liquid Dispersions", *AIChE J.*, **38**, pp. 1199-1205.

113. Tsouris, C., and Tavlarides, L. L., (1994) "Breakage and Coalescence Models for Drops in Turbulent Dispersions", *AIChE J.*, **40**, pp. 395-406
114. Van Husel, J., Bleys, G., and Joos, P., (1986), "Adsorption Kinetics at the Oil/Water Interface", *J. Colloid Interface Sci.*, **114**, pp. 432-441
115. Velev, O. D., Danov, K. D., and Ivanov, I. B., (1997), "Stability of Emulsions Under Static and Dynamic Conditions", *J. Dispersion Sci. and Tech.*, **18**, pp. 625-645.
116. Vinckier, I., Moldenaers, P., Terracciano, A. M., and Grizzuti, N., (1998), "Droplet Size Evolution During Coalescence in Semi-concentrated Model Blends", *AIChE J.*, **44**, pp. 951-958
117. Walstra, P., (1996), "Emulsion stability", in Encyclopedia of Emulsion Technology, **4**, pp. 1-62.
118. Wasan, D. T., Shah, S. M., Aderanji, N., Chan, M. S., and McNamara, J. J., (1978), "Observations on the Coalescence Behavior of Oil Droplets and Emulsion Stability in Enhanced Oil Recovery", *Society of Petroleum Engineer J.*, pp. 409-417
119. Wasan, D. T., Shah, S. M., Sampath, K., and Aderanji, N., (1979), "The Role of Coalescence Phenomena and Interfacial Rheological Properties in Enhanced Oil Recovery: an Overview", *J. Soc. Rheol.*, **23**, pp. 181-207
120. Weiss, J., (1992), "Phase Inversion in Two-Phase Liquid Systems", *Collect. Czech. Chem. Commun.*, **57**, pp. 1419-1423
121. Wright, H., (1991), Inverse problem in agglomeration, Ph.D. Thesis, Purdue University, Lafayette, Indiana, USA.
122. Wright, H., and Ramkrishna, D., (1994), "Factors Affecting Coalescence Frequency of Droplets on a Stirred Liquid-Liquid Dispersion", *AIChE J.*, **40**, pp. 767-776
123. Wynn, E. J. W., and Hounslow, M. J., (1997), "Integral Population Balance Equations for Growth", *Chem. Eng. Sci.*, **52**, pp. 733-746
124. Xue, Y., (1999), Measuring Dynamic Interfacial Characteristics of Industrial Streams, M.Sc. Thesis, Dalhousie University, DalTech, Halifax, Canada.
125. Yeh, G. C., Haynie, F. H., and Moses, R.A. (1964), "Phase Volume Relationship at the Point of Phase Inversion in Liquid Dispersion", *AIChE J.*, **10**, pp. 260-265

126. Zhao, W. Q., Pu, B. Y., and Hartland, S., (1993), "Measurement of Drop Size Distribution in Liquid-Liquid Dispersion by Encapsulation", *Chem. Eng. Sci.*, **48**, pp. 219-277
127. Zhou, G., and Kresta, S., (1998a), "Evolution of Drop Size Distribution in Liquid-Liquid Dispersions for Various Impellers", *Chem. Eng. Sci.*, **53**, pp. 2099-2113.
128. Zhou, G., and Kresta, S., (1998b), "Correlation of Mean Drop Size and Minimum Drop Size with the Turbulence Energy Dissipation and the Flow in an Agitated Tank", *Chem. Eng. Sci.*, **53**, pp. 2063-2079

## APPENDIX A

Table A18. The mean and the standard deviations of the quasi-steady drop-number-density.

System	300 rpm				200 rpm			
	Normal distribution		Lognormal distribution		Normal distribution		Lognormal distribution	
	Mean	s.d.	Mean	s.d.	Mean	s.d.	Mean	s.d.
0.75% acetophenon / 0.05 M aq. NaCl	0.047	0.037	0.040	0.025	0.059	0.070	0.051	0.045
0.75% acetophenon / 0.05 M aq. NaCl / 0.1 mM/m <sup>3</sup> X100	0.039	0.024	0.034	0.018	0.064	0.033	0.051	0.030
0.75% acetophenon / 0.05 M aq. NaCl / 0.2 mM/m <sup>3</sup> X100	0.036	0.026	0.032	0.018	0.028	0.040	0.029	0.023
0.75% acetophenon / 0.05 M aq. NaCl / 1.0 mM/m <sup>3</sup> X100	0.035	0.025	0.031	0.019	0.011	0.047	0.023	0.021
0.75% acetophenon / 0.05 M aq. NaCl / 0.1 mM/m <sup>3</sup> X165	0.037	0.020	0.031	0.016	0.054	0.033	0.043	0.026
0.75% acetophenon / 0.05 M aq. NaCl / 0.2 mM/m <sup>3</sup> X165	0.033	0.023	0.029	0.017	0.037	0.032	0.032	0.022
0.75% acetophenon / 0.05 M aq. NaCl / 0.1 mM/m <sup>3</sup> X305	0.046	0.024	0.038	0.019	0.068	0.037	0.053	0.034
0.75% acetophenon / 0.05 M aq. NaCl / 0.2 mM/m <sup>3</sup> X305	0.032	0.023	0.028	0.016	0.031	0.029	0.029	0.019
0.75% acetophenon / 0.05 M aq. NaCl / 0.1 mM/m <sup>3</sup> X405	0.032	0.024	0.029	0.017	0.024	0.045	0.029	0.024
0.75% acetophenon / 0.05 M aq. NaCl / 0.2 mM/m <sup>3</sup> X405	0.028	0.017	0.026	0.013	0.022	0.030	0.024	0.017
0.5% (65%v/v) CLB-Bayol oil/ water	0.079	0.092	0.064	0.060	0.061	0.059	0.049	0.038

Table A19. The correlation coefficients of the quasi-steady number density.

System	300 rpm			200 rpm		
	Normal	Log-normal	At 5% significance level, are the correlation coefficients different?	Normal	Log-normal	At 5% significance level, are the correlation coefficients different?
0.75% acetophenon / 0.05 M aq. NaCl	0.973	0.991	No	0.947	0.995	Yes
0.75% acetophenon / 0.05 M aq. NaCl / 0.1 mM/m <sup>3</sup> X100	0.977	0.991	No	0.994	0.977	No
0.75% acetophenon / 0.05 M aq. NaCl / 0.2 mM/m <sup>3</sup> X100	0.977	0.996	Yes	0.885	0.993	Yes
0.75% acetophenon / 0.05 M aq. NaCl / 1.0 mM/m <sup>3</sup> X100	0.986	0.994	No	0.883	0.988	Yes
0.75% acetophenon / 0.05 M aq. NaCl / 0.1 mM/m <sup>3</sup> X165	0.961	0.992	No	0.961	0.998	Yes
0.75% acetophenon / 0.05 M aq. NaCl / 0.2 mM/m <sup>3</sup> X165	0.970	0.994	No	0.974	0.996	Yes
0.75% acetophenon / 0.05 M aq. NaCl / 0.1 mM/m <sup>3</sup> X305	0.982	0.993	No	0.971	0.994	Yes
0.75% acetophenon / 0.05 M aq. NaCl / 0.2 mM/m <sup>3</sup> X305	0.964	0.996	Yes	0.952	0.998	Yes
0.75% acetophenon / 0.05 M aq. NaCl / 0.1 mM/m <sup>3</sup> X405	0.988	0.990	No	0.954	0.998	Yes
0.75% acetophenon / 0.05 M aq. NaCl / 0.2 mM/m <sup>3</sup> X405	0.993	0.992	No	0.951	0.997	Yes
0.5% CLB-Bayol oil (65%v/v) / water	0.881	0.995	Yes	0.915	0.997	Yes

Table A20. The mean and the standard deviations of the quasi-steady drop-volume density.

System	300 rpm		200 rpm	
	Normal distribution	Lognormal distribution	Normal distribution	Lognormal distribution
	Mean s.d.	Mean s.d.	Mean s.d.	Mean s.d.
0.75% acetophenon / 0.05 M aq. NaCl	0.095 0.034	0.076 0.044	0.176 0.064	0.147 0.113
0.75% acetophenon / 0.05 M aq. NaCl / 0.1 mM/m <sup>3</sup> X100	0.066 0.023	0.054 0.027	0.101 0.029	0.086 0.044
0.75% acetophenon / 0.05 M aq. NaCl / 0.2 mM/m <sup>3</sup> X100	0.068 0.026	0.056 0.032	0.097 0.047	0.078 0.073
0.75% acetophenon / 0.05 M aq. NaCl / 1.0 mM/m <sup>3</sup> X100	0.066 0.024	0.055 0.032	0.107 0.060	0.087 0.107
0.75% acetophenon / 0.05 M aq. NaCl / 0.1 mM/m <sup>3</sup> X165	0.057 0.020	0.047 0.023	0.096 0.033	0.080 0.048
0.75% acetophenon / 0.05 M aq. NaCl / 0.2 mM/m <sup>3</sup> X165	0.061 0.024	0.050 0.029	0.080 0.031	0.066 0.042
0.75% acetophenon / 0.05 M aq. NaCl / 0.1 mM/m <sup>3</sup> X305	0.071 0.023	0.059 0.029	0.114 0.035	0.098 0.058
0.75% acetophenon / 0.05 M aq. NaCl / 0.2 mM/m <sup>3</sup> X305	0.060 0.024	0.049 0.030	0.070 0.030	0.056 0.038
0.75% acetophenon / 0.05 M aq. NaCl / 0.1 mM/m <sup>3</sup> X405	0.062 0.023	0.051 0.028	0.102 0.045	0.082 0.064
0.75% acetophenon / 0.05 M aq. NaCl / 0.2 mM/m <sup>3</sup> X405	0.046 0.016	0.039 0.019	0.066 0.032	0.053 0.041
0.5% (65%v/v) CLB-Bayol oil/ water	0.248 0.088	0.213 0.183	0.159 0.061	0.128 0.105

Table A21. The correlation coefficients of the quasi-steady state volume density

System	300 rpm			200 rpm		
	Normal	Log-normal	At 5% significance level, are the correlation coefficients different?	Normal	Log-normal	At 5% significance level, are the correlation coefficients different?
0.75% acetophenon / 0.05 M aq. NaCl	0.973	0.991	No	0.961	0.989	Yes
0.75% acetophenon / 0.05 M aq. NaCl / 0.1 mM/m <sup>3</sup> X100	0.970	0.996	Yes	0.993	0.977	No
0.75% acetophenon / 0.05 M aq. NaCl / 0.2 mM/m <sup>3</sup> X100	0.980	0.995	No	0.901	0.997	Yes
0.75% acetophenon / 0.05 M aq. NaCl / 1.0 mM/m <sup>3</sup> X100	0.988	0.993	No	0.939	0.989	Yes
0.75% acetophenon / 0.05 M aq. NaCl / 0.1 mM/m <sup>3</sup> X165	0.949	0.997	Yes	0.964	0.998	Yes
0.75% acetophenon / 0.05 M aq. NaCl / 0.2 mM/m <sup>3</sup> X165	0.972	0.990	No	0.981	0.991	No
0.75% acetophenon / 0.05 M aq. NaCl / 0.1 mM/m <sup>3</sup> X305	0.979	0.996	No	0.972	0.994	Yes
0.75% acetophenon / 0.05 M aq. NaCl / 0.2 mM/m <sup>3</sup> X305	0.960	0.998	Yes	0.959	0.998	Yes
0.75% acetophenon / 0.05 M aq. NaCl / 0.1 mM/m <sup>3</sup> X405	0.989	0.989	No	0.978	0.988	No
0.75% acetophenon / 0.05 M aq. NaCl / 0.2 mM/m <sup>3</sup> X405	0.989	0.989	No	0.978	0.988	No
CLB-Bayol oil/water	0.991	0.995	Yes	0.969	0.992	Yes

Table A22. The transient mean and the standard deviations of (0.75% acetophenon/ 0.05 molar aq. NaCl)

Time (min)	Volume density				Number density			
	Normal distribution		Lognormal distribution		Normal distribution		Lognormal distribution	
	Mean	s.d.	Mean	s.d.	Mean	s.d.	Mean	s.d.
0	0.095	0.034	0.076	0.044	0.047	0.037	0.040	0.025
1	0.109	0.041	0.089	0.062	0.047	0.042	0.040	0.029
5	0.129	0.049	0.104	0.074	0.048	0.051	0.042	0.032
10	0.142	0.054	0.117	0.088	0.048	0.056	0.042	0.035
15	0.143	0.053	0.124	0.105	0.051	0.053	0.043	0.037
30	0.166	0.060	0.138	0.104	0.054	0.066	0.047	0.042
40	0.160	0.060	0.137	0.115	0.046	0.064	0.041	0.040
50	0.161	0.061	0.134	0.106	0.049	0.065	0.044	0.040
100	0.173	0.061	0.149	0.117	0.059	0.067	0.050	0.045
120	0.182	0.068	0.146	0.111	0.056	0.072	0.049	0.043
150	0.176	0.064	0.147	0.113	0.059	0.070	0.051	0.045

Table A23. The correlation coefficients of (0.75% acetophenon/ 0.05 molar aq. NaCl)

Time (min)	Volume density			Number density		
	Normal	Log-normal	At 5% significance level, are the correlation coefficients different?	Normal	Log-normal	At 5% significance level, are the correlation coefficients different?
0	0.973	0.991	No	0.973	0.991	No
1	0.950	0.996	Yes	0.950	0.995	Yes
5	0.967	0.986	No	0.955	0.994	Yes
10	0.974	0.986	No	0.955	0.996	Yes
15	0.946	0.998	Yes	0.934	0.999	Yes
30	0.973	0.984	No	0.958	0.994	Yes
40	0.969	0.987	No	0.949	0.997	Yes
50	0.969	0.988	No	0.950	0.996	Yes
100	0.973	0.987	No	0.955	0.996	Yes
120	0.969	0.982	No	0.944	0.995	Yes
150	0.961	0.989	Yes	0.947	0.995	Yes



Table A24. The transient mean and the standard deviations of (0.75% acetophenon / 0.05 molar aq. NaCl / 0.1 mmole/m<sup>3</sup> Triton X100)

Time (min)	Volume density				Number density			
	Normal distribution		Lognormal distribution		Normal distribution		Lognormal distribution	
	Mean	s.d.	Mean	s.d.	Mean	s.d.	Mean	s.d.
0	0.066	0.023	0.054	0.027	0.039	0.024	0.034	0.018
5	0.074	0.024	0.062	0.031	0.046	0.025	0.038	0.021
15	0.086	0.029	0.069	0.039	0.050	0.030	0.040	0.023
20	0.077	0.025	0.063	0.031	0.048	0.027	0.039	0.021
30	0.094	0.033	0.076	0.046	0.052	0.034	0.042	0.025
60	0.084	0.025	0.070	0.034	0.053	0.028	0.043	0.024
100	0.097	0.029	0.082	0.044	0.062	0.031	0.049	0.028
200	0.101	0.029	0.086	0.044	0.064	0.033	0.051	0.030

Table A25. The correlation coefficients of (0.75% acetophenon/ 0.05 molar aq. NaCl/ 0.1 mmole/m<sup>3</sup> Triton X100)

Time (min)	Volume density			Number density		
	Normal	Log-normal	At 5% level, are the correlation coefficients significantly different?	Normal	Log-normal	At 5% level, are the correlation coefficients significantly different?
0	0.970	0.996	Yes	0.977	0.991	No
5	0.982	0.993	No	0.985	0.990	No
15	0.960	0.995	Yes	0.966	0.992	Yes
20	0.977	0.994	No	0.982	0.989	No
30	0.891	0.990	Yes	0.912	0.986	Yes
60	0.990	0.986	No	0.993	0.981	No
100	0.961	0.993	Yes	0.967	0.988	No
200	0.993	0.977	No	0.994	0.977	No

Table A26. The transient mean and the standard deviations of (0.75% acetophenon/ 0.05 molar aq. NaCl/ 0.2 mmole/m<sup>3</sup> Triton X100)

Time (min)	Volume density				Number density			
	Normal distribution		Lognormal distribution		Normal distribution		Lognormal distribution	
	Mean	s.d.	Mean	s.d.	Mean	s.d.	Mean	s.d.
0	0.068	0.026	0.056	0.032	0.036	0.026	0.032	0.018
62	0.086	0.040	0.068	0.057	0.031	0.036	0.030	0.021
258	0.097	0.047	0.078	0.073	0.028	0.040	0.029	0.023

Table A27. The correlation coefficients of fitting transient drop size to normal and log-normal distribution (0.75% acetophenon/ 0.05 molar aq. NaCl/ 0.2 mmole/m<sup>3</sup> Triton X100)

Time (min)	Volume density			Number density		
	Normal	Log-normal	At 5% level, are the correlation coefficients significantly different?	Normal	Log-normal	At 5% level, are the correlation coefficients significantly different?
0	0.980	0.995	No	0.977	0.996	Yes
62	0.891	0.994	Yes	0.891	0.992	Yes
258	0.901	0.997	Yes	0.885	0.993	Yes

Table A28. The transient mean and the standard deviations of (0.75% acetophenon / 0.05 molar aq. NaCl / 1.0 mmole/m<sup>3</sup> Triton X100)

Time (min)	Volume density				Number density			
	Normal distribution		Lognormal distribution		Normal distribution		Lognormal distribution	
	Mean	s.d.	Mean	s.d.	Mean	s.d.	Mean	s.d.
0	0.066	0.024	0.055	0.032	0.035	0.025	0.031	0.019
1	0.062	0.021	0.052	0.025	0.035	0.023	0.031	0.017
50	0.086	0.042	0.068	0.058	0.026	0.037	0.028	0.021
100	0.093	0.048	0.075	0.074	0.023	0.040	0.026	0.021
150	0.107	0.060	0.087	0.107	0.011	0.047	0.023	0.021

Table A29. The correlation coefficients of (0.75% acetophenon / 0.05 molar aq. NaCl / 1.0 mmole/m<sup>3</sup> Triton X100)

Time (min)	Volume density			Number density		
	Normal	Log-normal	At 5% level, are the correlation coefficients significantly different?	Normal	Log-normal	At 5% level, are the correlation coefficients significantly different?
0	0.988	0.993	No	0.986	0.994	No
1	0.996	0.980	No	0.995	0.983	No
50	0.909	0.998	Yes	0.902	0.995	Yes
100	0.932	0.994	Yes	0.901	0.993	Yes
150	0.939	0.989	Yes	0.883	0.988	Yes

Table A30. The transient mean and the standard deviations of (0.75% acetophenon / 0.05 molar aq. NaCl / 0.1 mmole/m<sup>3</sup> Triton X165)

Time (min)	Volume density				Number density			
	Normal distribution		Lognormal distribution		Normal distribution		Lognormal distribution	
	Mean	s.d.	Mean	s.d.	Mean	s.d.	Mean	s.d.
0	0.057	0.020	0.047	0.023	0.037	0.020	0.031	0.016
5	0.071	0.032	0.056	0.038	0.033	0.029	0.030	0.018
30	0.084	0.036	0.067	0.049	0.038	0.033	0.033	0.021
70	0.087	0.032	0.071	0.043	0.044	0.032	0.037	0.023
100	0.095	0.035	0.079	0.053	0.048	0.034	0.039	0.026
122	0.096	0.033	0.080	0.048	0.054	0.033	0.043	0.026

Table A31. The correlation coefficients of (0.75% acetophenon/ 0.05 molar aq. NaCl / 0.1 mmole/m<sup>3</sup> Triton X165)

Time (min)	Volume density			Number density		
	Normal	Log-normal	At 5% level, are the correlation coefficients significantly different?	Normal	Log-normal	At 5% level, are the correlation coefficients significantly different?
0	0.949	0.997	Yes	0.961	0.992	No
5	0.843	0.981	Yes	0.868	0.984	Yes
30	0.902	0.993	Yes	0.909	0.992	Yes
70	0.976	0.992	No	0.967	0.997	Yes
100	0.952	0.999	Yes	0.945	0.999	Yes
122	0.964	0.998	Yes	0.961	0.998	Yes

Table A32. The transient mean and the standard deviations of (0.75% acetophenon / 0.05 molar aq. NaCl / 0.2 mmole/m<sup>3</sup> Triton X165)

Time (min)	Volume density				Number density			
	Normal distribution		Lognormal distribution		Normal distribution		Lognormal distribution	
	Mean	s.d.	Mean	s.d.	Mean	s.d.	Mean	s.d.
0	0.061	0.024	0.050	0.029	0.033	0.023	0.029	0.017
5	0.060	0.022	0.052	0.032	0.034	0.022	0.029	0.018
10	0.068	0.030	0.054	0.036	0.033	0.028	0.029	0.018
20	0.069	0.027	0.056	0.036	0.035	0.027	0.031	0.019
50	0.074	0.029	0.062	0.041	0.035	0.029	0.031	0.021
120	0.080	0.031	0.066	0.042	0.037	0.032	0.032	0.022

Table A33. The correlation coefficients of (0.75% acetophenon / 0.05 molar aq. NaCl / 0.2 mmole/m<sup>3</sup> Triton X165)

Time (min)	Volume density			Number density		
	Normal	Log-normal	At 5% level, are the correlation coefficients significantly different?	Normal	Log-normal	At 5% level, are the correlation coefficients significantly different?
0	0.972	0.990	No	0.970	0.994	No
5	0.961	0.999	Yes	0.963	0.995	No
10	0.937	0.998	Yes	0.938	0.996	Yes
20	0.955	0.996	Yes	0.955	0.996	Yes
50	0.977	0.994	No	0.970	0.998	Yes
120	0.981	0.991	No	0.974	0.996	Yes

Table A34. The transient mean and the standard deviations of (0.75% acetophenon / 0.05 molar aq. NaCl / 0.1 mmole/m<sup>3</sup> Triton X305)

Time (min)	Volume density				Number density			
	Normal distribution		Lognormal distribution		Normal distribution		Lognormal distribution	
	Mean	s.d.	Mean	s.d.	Mean	s.d.	Mean	s.d.
0	0.071	0.023	0.059	0.029	0.046	0.024	0.038	0.019
1	0.072	0.022	0.060	0.028	0.048	0.023	0.039	0.020
5	0.081	0.025	0.068	0.035	0.053	0.026	0.043	0.023
10	0.090	0.030	0.074	0.041	0.052	0.032	0.043	0.025
30	0.098	0.031	0.081	0.045	0.059	0.032	0.046	0.027
55	0.103	0.032	0.088	0.052	0.060	0.035	0.047	0.030
75	0.107	0.033	0.090	0.050	0.063	0.035	0.050	0.031
100	0.114	0.035	0.098	0.058	0.068	0.037	0.053	0.034

Table A35. The correlation coefficients of (0.75% acetophenon / 0.05 molar aq. NaCl / 0.1 mmole/m<sup>3</sup> Triton X305)

Time (min)	Volume density			Number density		
	Normal	Log-normal	At 5% level, are the correlation coefficients significantly different?	Normal	Log-normal	At 5% level, are the correlation coefficients significantly different?
0	0.979	0.996	No	0.982	0.993	No
1	0.980	0.996	No	0.984	0.991	No
5	0.966	0.997	Yes	0.971	0.994	No
10	0.963	0.995	Yes	0.967	0.992	No
30	0.967	0.996	Yes	0.970	0.994	Yes
55	0.975	0.994	No	0.975	0.993	No
75	0.983	0.989	No	0.982	0.991	No
100	0.972	0.994	Yes	0.971	0.994	Yes

Table A36. The transient mean and the standard deviations of (0.75% acetophenon / 0.05 molar aq. NaCl / 0.2 mmole/m<sup>3</sup> Triton X305)

Time (min)	Volume density				Number density			
	Normal distribution		Lognormal distribution		Normal distribution		Lognormal distribution	
	Mean	s.d.	Mean	s.d.	Mean	s.d.	Mean	s.d.
0	0.060	0.024	0.049	0.030	0.032	0.023	0.028	0.016
5	0.063	0.025	0.050	0.029	0.036	0.024	0.031	0.017
100	0.061	0.020	0.051	0.026	0.040	0.020	0.034	0.017
161	0.065	0.022	0.055	0.030	0.039	0.023	0.033	0.018
200	0.070	0.030	0.056	0.038	0.031	0.029	0.029	0.019

Table A37. The correlation coefficients of (0.75% acetophenon / 0.05 molar aq. NaCl / 0.2 mmole/m<sup>3</sup> Triton X305)

Time (min)	Volume density			Number density		
	Normal	Log-normal	At 5% level, are the correlation coefficients significantly different?	Normal	Log-normal	At 5% level, are the correlation coefficients significantly different?
0	0.960	0.998	Yes	0.964	0.996	Yes
5	0.941	0.994	Yes	0.950	0.993	Yes
100	0.957	0.998	Yes	0.966	0.995	No
161	0.978	0.996	No	0.978	0.996	No
200	0.959	0.998	Yes	0.952	0.998	Yes

Table A38. The transient mean and the standard deviations of (0.75% acetophenon / 0.05 molar aq. NaCl / 0.1 mmole/m<sup>3</sup> Triton X405)

Time (min)	Volume density				Number density			
	Normal distribution		Lognormal distribution		Normal distribution		Lognormal distribution	
	Mean	s.d.	Mean	s.d.	Mean	s.d.	Mean	s.d.
0	0.062	0.023	0.051	0.028	0.032	0.024	0.029	0.017
10	0.063	0.023	0.053	0.029	0.034	0.024	0.030	0.018
15	0.066	0.025	0.054	0.029	0.034	0.026	0.031	0.018
20	0.066	0.027	0.053	0.030	0.033	0.027	0.030	0.017
30	0.074	0.029	0.059	0.035	0.034	0.030	0.031	0.020
50	0.083	0.034	0.068	0.046	0.034	0.034	0.031	0.022
61	0.089	0.036	0.073	0.051	0.034	0.037	0.032	0.024
101	0.105	0.045	0.086	0.073	0.031	0.043	0.031	0.026
140	0.102	0.045	0.082	0.064	0.024	0.045	0.029	0.024

Table A39. The correlation coefficients of (0.75% acetophenon / 0.05 molar aq. NaCl / 0.1 mmole/m<sup>3</sup> Triton X405)

Time (min)	Volume density			Number density		
	Normal	Log-normal	At 5% level, are the correlation coefficients significantly different?	Normal	Log-normal	At 5% level, are the correlation coefficients significantly different?
0	0.989	0.989	No	0.988	0.990	No
10	0.991	0.988	No	0.989	0.990	No
15	0.986	0.991	No	0.985	0.991	No
20	0.960	0.997	Yes	0.964	0.995	Yes
30	0.981	0.992	No	0.978	0.994	No
50	0.977	0.993	No	0.965	0.997	Yes
61	0.979	0.993	No	0.968	0.998	Yes
101	0.962	0.995	Yes	0.942	0.999	Yes
140	0.978	0.988	No	0.954	0.998	Yes



Table A40. The transient mean and the standard deviations of (0.75% acetophenon / 0.05 molar aq. NaCl / 0.2 mmole/m<sup>3</sup> Triton X405)

Time (min)	Volume density				Number density			
	Normal distribution		Lognormal distribution		Normal distribution		Lognormal distribution	
	Mean	s.d.	Mean	s.d.	Mean	s.d.	Mean	s.d.
0	0.046	0.016	0.039	0.019	0.028	0.017	0.026	0.013
40	0.049	0.019	0.041	0.021	0.030	0.019	0.027	0.014
50	0.053	0.026	0.043	0.027	0.024	0.024	0.025	0.014
70	0.060	0.028	0.047	0.033	0.027	0.026	0.026	0.016
120	0.066	0.032	0.053	0.041	0.022	0.030	0.024	0.017

Table A41. The correlation coefficients of (0.75% acetophenon / 0.05 molar aq. NaCl / 0.2 mmole/m<sup>3</sup> Triton X405)

Time (min)	Volume density			Number density		
	Normal	Log-normal	At 5% level, are the correlation coefficients significantly different?	Normal	Log-normal	At 5% level, are the correlation coefficients significantly different?
0	0.991	0.995	No	0.993	0.992	No
40	0.969	0.999	Yes	0.976	0.995	No
50	0.943	0.998	Yes	0.946	0.996	Yes
70	0.933	0.994	Yes	0.939	0.994	Yes
120	0.969	0.992	No	0.951	0.997	Yes

Table A42. The correlation coefficients of normalized cumulative volume at transient condition (300→200 rpm) shown in Table 13

System	Normal	Log-normal	At 1% level, are the correlation coefficients significantly different?
0.75% acetophenon / 0.05 M aq. NaCl	0.963	0.988	Yes
0.75% acetophenon / 0.05 M aq. NaCl / 0.1 mmole/m <sup>3</sup> X100	0.955	0.995	Yes
0.75% acetophenon / 0.05 M aq. NaCl / 0.2 mmole/m <sup>3</sup> X100	0.905	0.993	Yes
0.75% acetophenon / 0.05 M aq. NaCl / 1.0 mmole/m <sup>3</sup> X100	0.932	0.995	Yes
0.75% acetophenon / 0.05 M aq. NaCl / 0.1 mmole/m <sup>3</sup> X165	0.909	0.996	Yes
0.75% acetophenon / 0.05 M aq. NaCl / 0.2 mmole/m <sup>3</sup> X165	0.952	0.991	Yes
0.75% acetophenon / 0.05 M aq. NaCl / 0.1 mmole/m <sup>3</sup> X305	0.972	0.994	Yes
0.75% acetophenon / 0.05 M aq. NaCl / 0.2 mmole/m <sup>3</sup> X305	0.945	0.989	Yes
0.75% acetophenon / 0.05 M aq. NaCl / 0.1 mmole/m <sup>3</sup> X405	0.982	0.997	Yes
0.75% acetophenon / 0.05 M aq. NaCl / 0.2 mmole/m <sup>3</sup> X405	0.962	0.992	Yes
0.5% CLB-Bayol oil / water	0.893	0.996	Yes
0.5% Bayol oil / water	0.933	0.998	Yes
0.5% Bayol oil / water / 0.25 mmole/m <sup>3</sup> X100	0.874	0.979	Yes
0.5% Bayol oil / water / 1.0 mmole/m <sup>3</sup> X100	0.937	0.990	Yes
0.5% Bayol oil / water / 4.5 mmole/m <sup>3</sup> X100	0.942	0.988	Yes

Table A43. The correlation coefficients (R) of adsorption model approximation.

## a) Bayol oil / water / Triton X100

Mole/m <sup>3</sup>	Drop volume technique		Maximum drop pressure technique	
	Long approx.(t <sup>-0.5</sup> )	Short approx.(t <sup>0.5</sup> )	Long approx.(t <sup>-0.5</sup> )	Short approx.(t <sup>0.5</sup> )
X100(0.001)	0.926	0.981	0.931	0.965
X100(0.01)	0.938	0.994	0.927	0.895
X100(0.1)	0.954	0.840	0.929	0.958
X100(0.2)	0.981	0.876	0.945	0.983
X100(0.3)	0.984	0.768	0.781	0.919

## b) Bayol oil / water / Triton

Mole/m <sup>3</sup>	Drop volume technique		Maximum drop pressure technique	
	Long approx.(t <sup>-0.5</sup> )	Short approx.(t <sup>0.5</sup> )	Long approx.(t <sup>-0.5</sup> )	Short approx.(t <sup>0.5</sup> )
X45(0.1)	0.949	0.992	0.975	0.962
X100(0.1)	0.954	0.840	0.929	0.958
X165(0.1)	0.967	0.942	0.968	0.983
X305(0.1)	0.951	0.964	0.921	0.916
X405(0.1)	0.976	0.777	0.985	0.939

## c) Acetophenon / water / Triton

Mole/m <sup>3</sup>	Drop volume technique		Maximum drop pressure technique	
	Long approx (t <sup>-0.5</sup> )	Short approx (t <sup>0.5</sup> )	Long approx (t <sup>-0.5</sup> )	Short approx (t <sup>0.5</sup> )
X45(0.0001)	0.974	0.976	0.847	0.883
X100(0.0001)	0.988	0.940	0.996	0.988
X100(0.0002)	0.990	0.941	0.964	0.940
X100(0.001)	0.975	0.891	0.986	0.943
X165(0.0002)	0.974	0.967	0.961	0.826
X305(0.0001)	0.966	0.968	0.845	0.881
X305(0.0002)	0.962	0.966	0.841	0.877
X405(0.0001)	0.975	0.978	0.850	0.886
X405(0.0002)	0.952	0.893	0.969	0.980

## d) Gasoline/industrial caustic

System	Drop volume	Maximum drop
	technique	pressure technique
	Short approx. ( $t^{0.5}$ )	
Gasoline/distilled water	0.897	0.967
Esso gasoline/distilled water	0.897	0.962
Irving gasoline/(20%wt%) NaOH aq. Solution	0.808	0.998
Irving gasoline /(90-10%v/v) distilled water-caustic 1179	0.836	0.931
Irving gasoline /(90-10%v/v) distilled water-caustic 1940	0.942	0.981
Irving gasoline /(90-10%v/v) distilled water-caustic 1700	0.916	0.974

Table A44. Is the R-value reported in Table A43, significant, at 95% confidence level?

a) Bayol oil / water / Triton X100

Mole/m <sup>3</sup>	Drop volume technique		Maximum drop pressure technique	
	Long approx.(t <sup>-0.5</sup> )	Short approx.(t <sup>0.5</sup> )	Long approx.(t <sup>-0.5</sup> )	Short approx.(t <sup>0.5</sup> )
X100(0.001)	Yes	Yes	Yes	Yes
X100(0.01)	Yes	Yes	Yes	Yes
X100(0.1)	Yes	No	Yes	Yes
X100(0.2)	Yes	No	Yes	Yes
X100(0.3)	Yes	No	No	Yes

b) Bayol oil / water / Triton

Mole/m <sup>3</sup>	Drop volume technique		Maximum drop pressure technique	
	Long approx (t <sup>-0.5</sup> )	Short approx (t <sup>0.5</sup> )	Long approx (t <sup>-0.5</sup> )	Short approx (t <sup>0.5</sup> )
X45(0.1)	Yes	Yes	Yes	Yes
X100(0.1)	Yes	No	Yes	Yes
X165(0.1)	Yes	Yes	Yes	Yes
X305(0.1)	Yes	Yes	Yes	Yes
X405(0.1)	Yes	No	Yes	Yes

c) Acetophenon / water / Triton

Mole/m <sup>3</sup>	Drop volume technique		Maximum drop pressure technique	
	Long approx.(t <sup>-0.5</sup> )	Short approx.(t <sup>0.5</sup> )	Long approx.(t <sup>-0.5</sup> )	Short approx.(t <sup>0.5</sup> )
x45(0.0001)	Yes	Yes	No	Yes
X100(0.0001)	Yes	Yes	Yes	Yes
X100(0.0002)	Yes	Yes	Yes	Yes
X100(0.001)	Yes	Yes	Yes	Yes
X165(0.0002)	Yes	Yes	Yes	No
X305(0.0001)	Yes	Yes	No	Yes
X305(0.0002)	Yes	Yes	No	No
X405(0.0001)	Yes	Yes	No	Yes
X405(0.0002)	Yes	Yes	Yes	Yes

## d) Gasoline/industrial caustic

System	Drop volume	Maximum drop
	technique	pressure technique
Short approx.(t <sup>0.5</sup> )		
Gasoline/distilled water	Yes	Yes
Esso gasoline/distilled water	Yes	Yes
Irving gasoline/(20%wt%) NaOH aq. Solution	No	Yes
Irving gasoline /(90-10%v/v) distilled water-caustic 1179	No	Yes
Irving gasoline /(90-10%v/v) distilled water-caustic 1940	Yes	Yes
Irving gasoline /(90-10%v/v) distilled water-caustic 1700	No	Yes

Table A45. Regression analysis of fitting data (expanding-drop technique) into approximation model of surfactant adsorption equation.

a) Acetophenon/ water/ Triton (the correlation coefficients are significant against zero at 5% level)

Triton	$E_{m_{max}}$	Slope @ t=0 (mN/m/s)	R (slope)	D(m <sup>2</sup> /s)	R (D)
0 SAA	5.153	35.016	0.971	1.60E-11	-0.991
X100(0.1)	5.360	26.056	0.989	1.19E-11	-0.984
X305(0.1)	4.3967	24.3124	0.990	3.40E-12	-0.9997

b) Bayol oil / water/ Triton X100 (the correlation coefficients of the slope are not significant against zero at 5% level)

Triton X100 (mole/m <sup>3</sup> )	$E_{m_{max}}$	slope at t=0 (mN/m/s)	R(slope)	D(m <sup>2</sup> /s)	R(D)
0.001	17.3	60.2	0.991	6.4E-08	-0.995
0.1	11.3	36.6	0.979	3.0E-08	-0.973
0.2	5.9	20.1	0.986	1.3E-09	-0.982
0.3	4.8	15.7	0.980	2.9E-10	-0.961

c) Bayol oil / water/ Triton (the correlation coefficients are significant against zero at 5% level)

Triton (0.1 mole/m <sup>3</sup> )	$E_{m_{max}}$	slope at t=0, (mN/m/s)	R(slope)	D(m <sup>2</sup> /s)	R(D)
X45	22.28	74.42	0.98	6.4E-08	-0.953
x100	11.34	36.63	0.98	1.2E-07	-0.993
X165	12.02	38.64	0.98	7.4E-08	-1.000
X305	9.33	28.59	0.97	7.4E-08	-0.997
X405	7.80	23.42	0.97	1.4E-08	-0.965

d) d) Gasoline / industrial caustic (the correlation coefficients of the slope are not significant against zero at 5% level)

System	$E_{m_{max}}$	slope at t=0, R(slope) (mN/m)/s	D	R(D)
Irving gasoline/water	-	95.94	-0.97	3.6E-09
Irving gasoline / caustic 1179 _ water (10%v/v)	6.05	20.09	-0.92	1.1E-10
Irving gasoline / caustic 1700 _ water (10%v/v)	3.98	12.96	-0.97	2.6E-11
Irving gasoline/ NaOH _ water (20%w/w)	3.60	12.10	-0.93	1.4E-11
Irving gasoline / caustic 1940 _ water (10%v/v)	2.67	8.39	-0.91	1.8E-11

Table A46. Linear correlation of the interfacial characteristic (x) in form of  $y = a + b \cdot x$  for (acetophenon/ 0.05 molar aq. NaCl/ 0.0-1.0 mmole/m<sup>3</sup> Triton)

y	x	a (confidence limit 95%)	b (confidence limit 95%)	Impeller speed (rpm)
d <sub>32</sub> (quasi-steady)	$\gamma_{Eq}$	0.016-0.036	0.040-.010	300
d <sub>32</sub> (quasi-steady)	$\gamma_{Eq}$	-0.017-0.021	0.015-0.025	200
Coalescence rate	$\gamma_{Eq}$	-0.108-0.038	0.005-0.042	200
Coalescence rate	D (DVT)	0.022-0.030	169.6-222.5	200

Table A47. Linear correlation of the interfacial characteristic (x) in form of  $y = a + b \cdot x$  for (Bayol oil/ water/ 0.0-300 mole/m<sup>3</sup> Triton, 600-1300 rpm)

y	x	a (confidence limit 95%)	b (confidence limit 95%)
Phase inversion holdup	$\gamma_{Eq}$	87.8-94.3	-0.79-(-0.07)
Phase inversion holdup	ln(D)	9.44-53.15	-3.24-(-1.47)

Table A48. Linear correlation of the interfacial characteristic (x) in form of  $y = a + b \cdot x$  for (gasoline/ industrial caustic, 600-1300 rpm). Dispersed flow rate of drop formation was 0.0316 mL/min)

y	x	a (confidence limit 95%)	b (confidence limit 95%)
Phase inversion holdup	D	74.1-79.4	$-1.0 \times 10^{12}$ - $(-5.3 \times 10^{10})$
Phase inversion holdup	$E_M$	80.6-84.1	-2.51-(-1.69)



## APPENDIX B

This appendix contains graphs showing the effect of mixing time and gravity on drop size

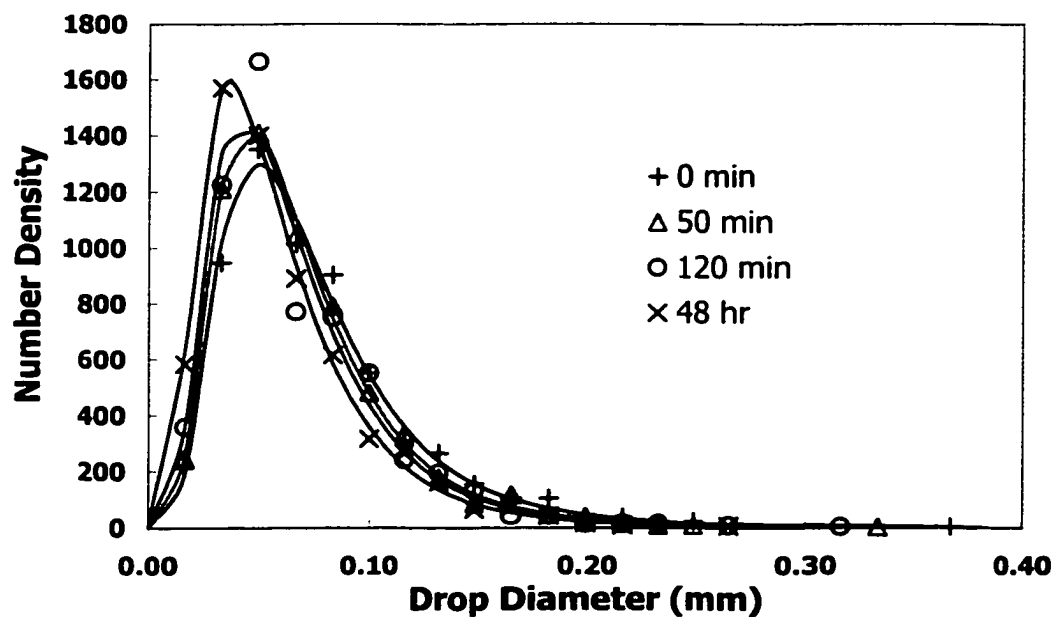


Figure B56. Effect of mixing time on drop-number-density of (0.5% CLB-Bayol oil / water / 1.0 mmole/m<sup>3</sup> Triton X100, 250 rpm)

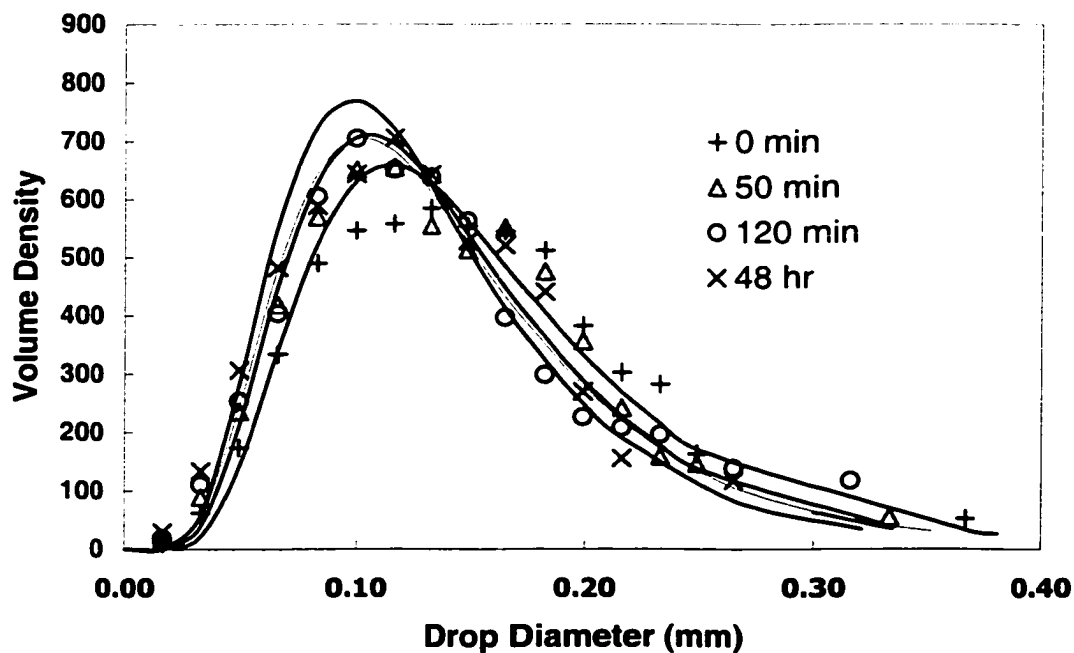


Figure B57. Effect of mixing time on drop-volume-density of (0.5% CLB-Bayol oil / water / 1.0 mmole/m<sup>3</sup>, Triton x100, 250 rpm)

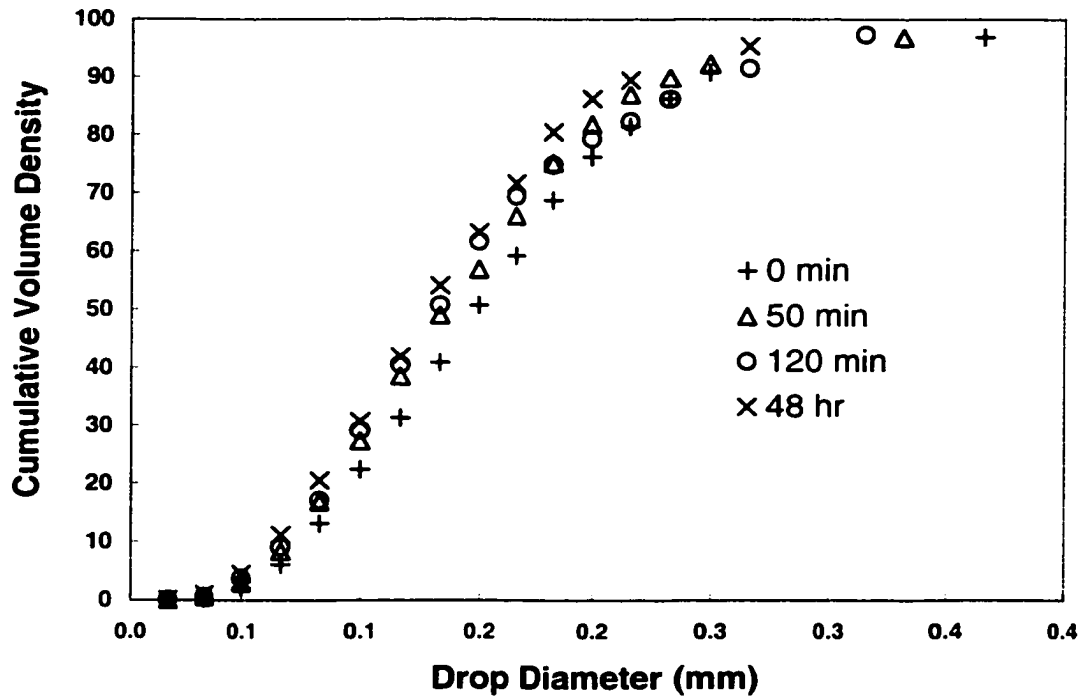


Figure B58. Effect of mixing time on drop-cumulativ-volume-density of (0.5% CLB-Bayol oil / water / 1.0 mmole/m<sup>3</sup>, Triton X100, 250 rpm)

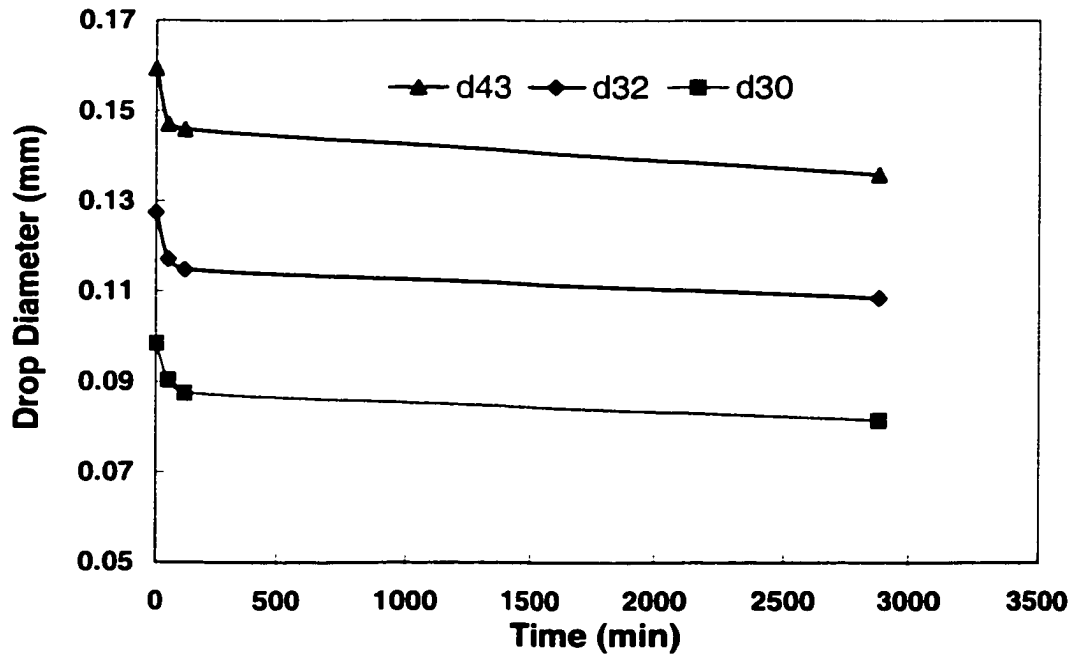


Figure B59. Effect of mixing time on average drop size of (0.5% CLB-Bayol oil / water / 1.0 mmole/m<sup>3</sup>, Triton X100, 250 rpm)

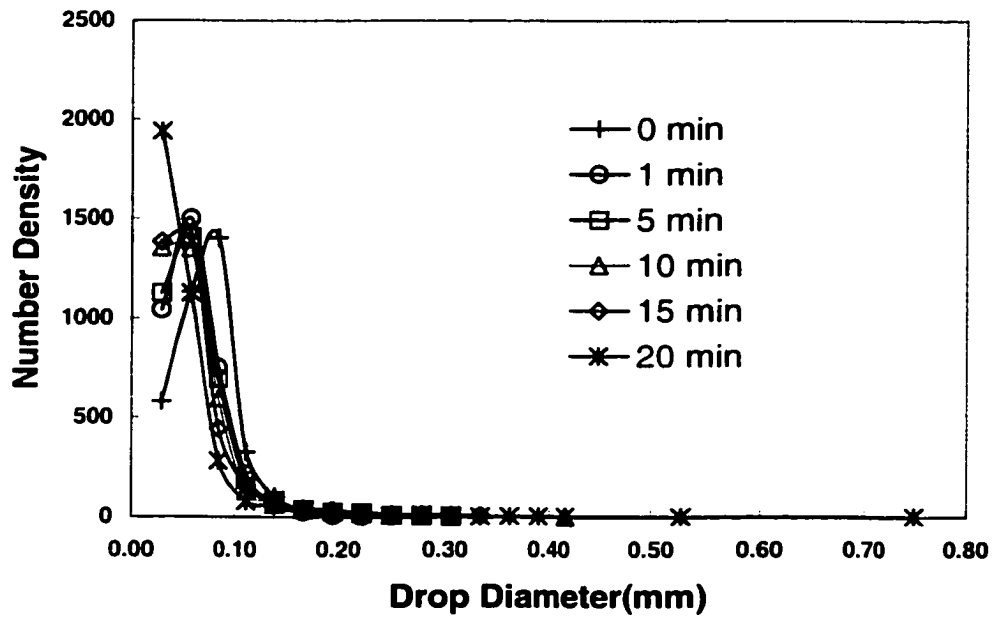


Figure B60. Effect of gravity on evolution of number density of (0.5% Bayol oil/ water, 500->250 rpm)

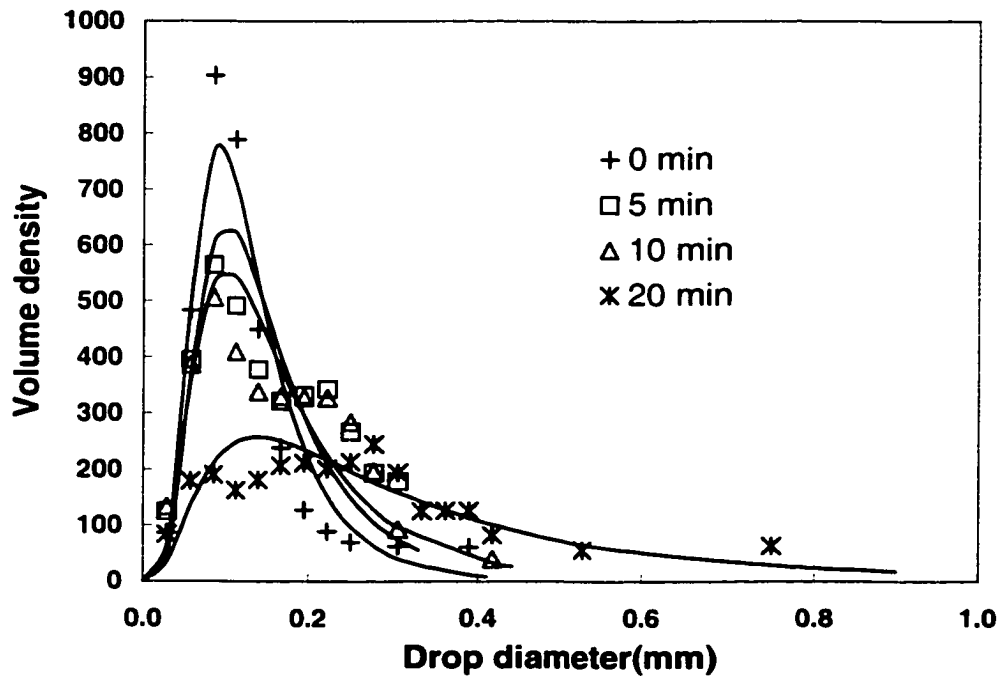


Figure B61. Effect of gravity on evolution of volume density of (0.5% Bayol oil/water, 500->250 rpm)

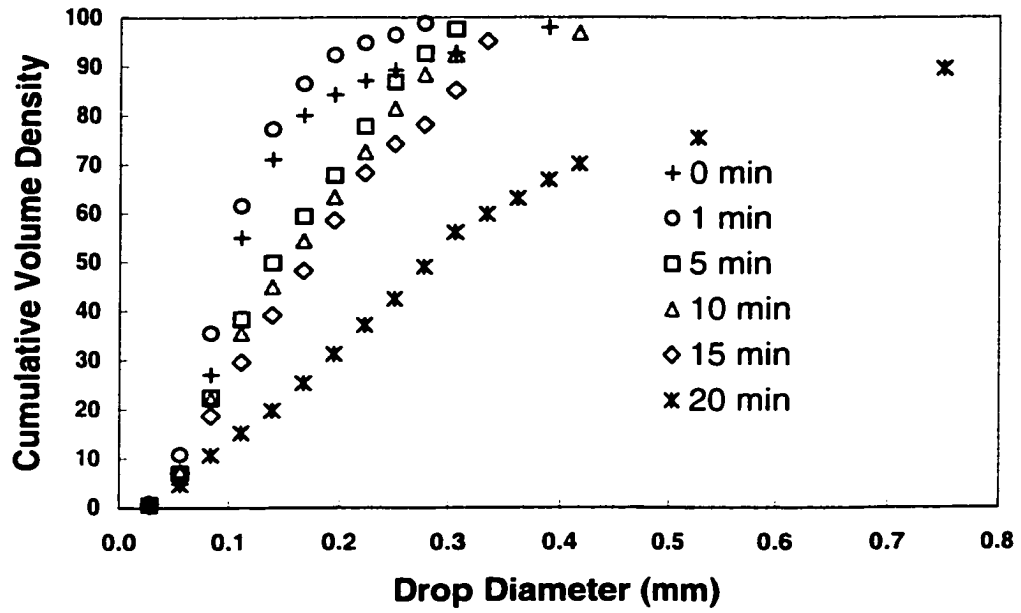


Figure B62. Effect of gravity on evolution of cumulative volume density of (0.5% Bayol oil/ water, 500->250 rpm)

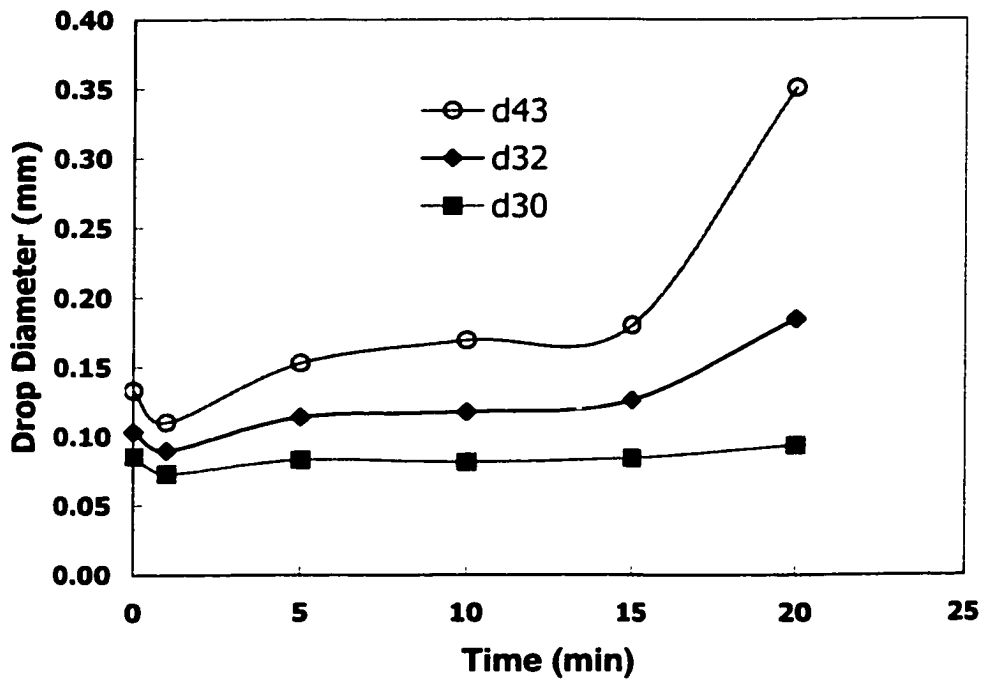


Figure 63. Effect of gravity on evolution of drop mean diameter of (0.5% Bayol oil/ water, 500->250 rpm)

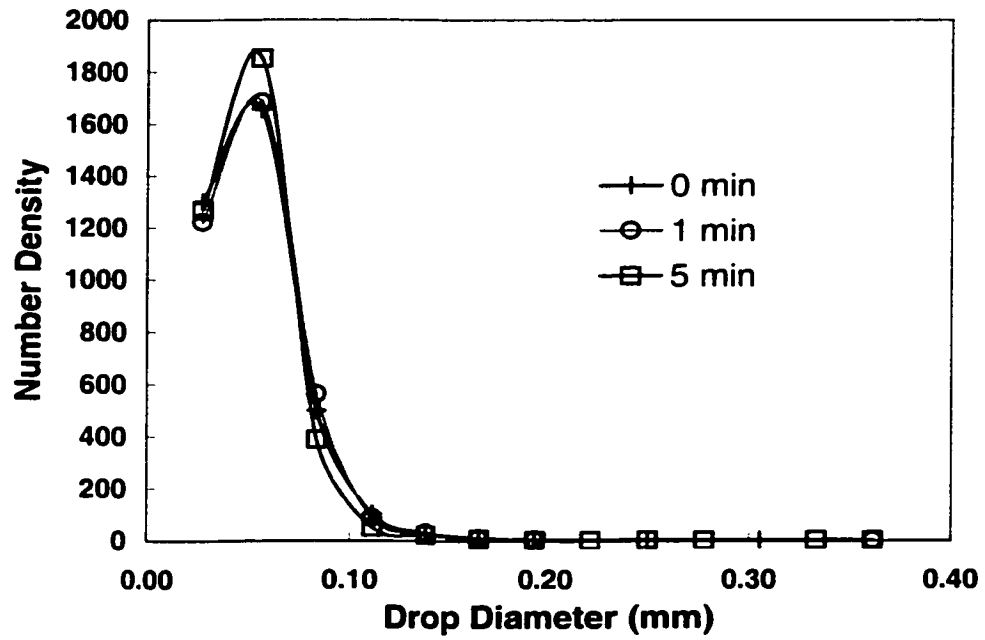


Figure B64. Effect of gravity on evolution of number density of (0.5% Bayol oil/ water/ 0.25 mmole/m<sup>3</sup>, Triton X100, 500->250 rpm)

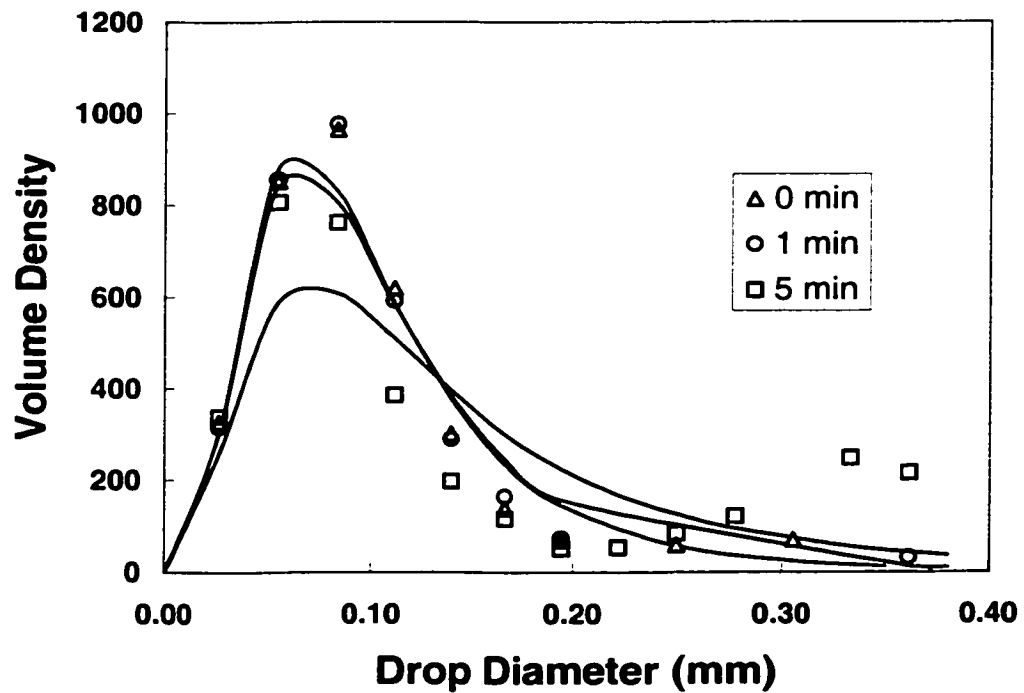


Figure B65. Effect of gravity on evolution of volume density of (0.5% Bayol oil/ water/ 0.25 mmole/m<sup>3</sup> Triton X100, 500->250 rpm)

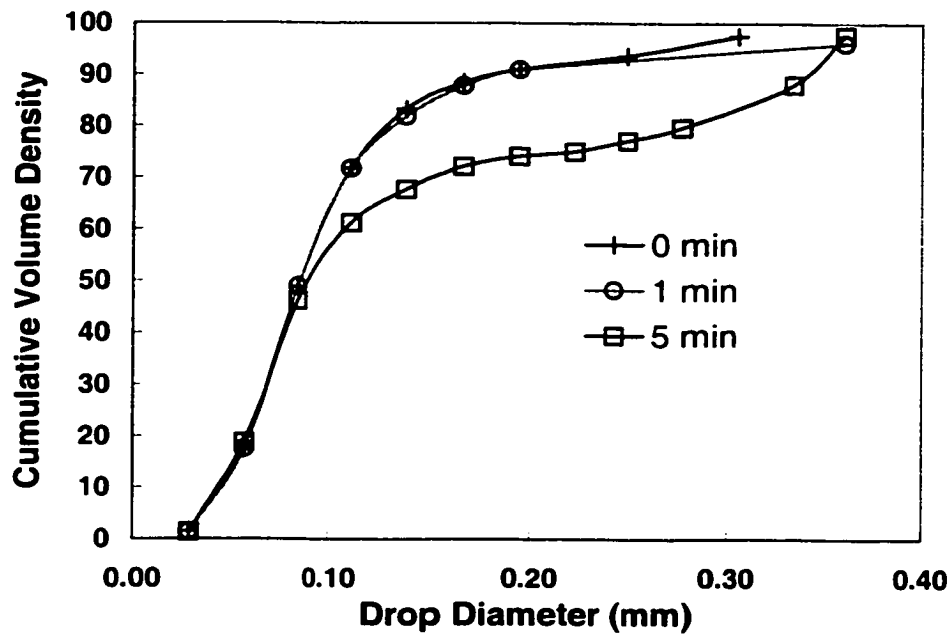


Figure B66. Effect of gravity on evolution of cumulative volume density of (0.5% Bayol oil/ water / 0.25 mmole/m<sup>3</sup>, Triton X100, 500->250 rpm)

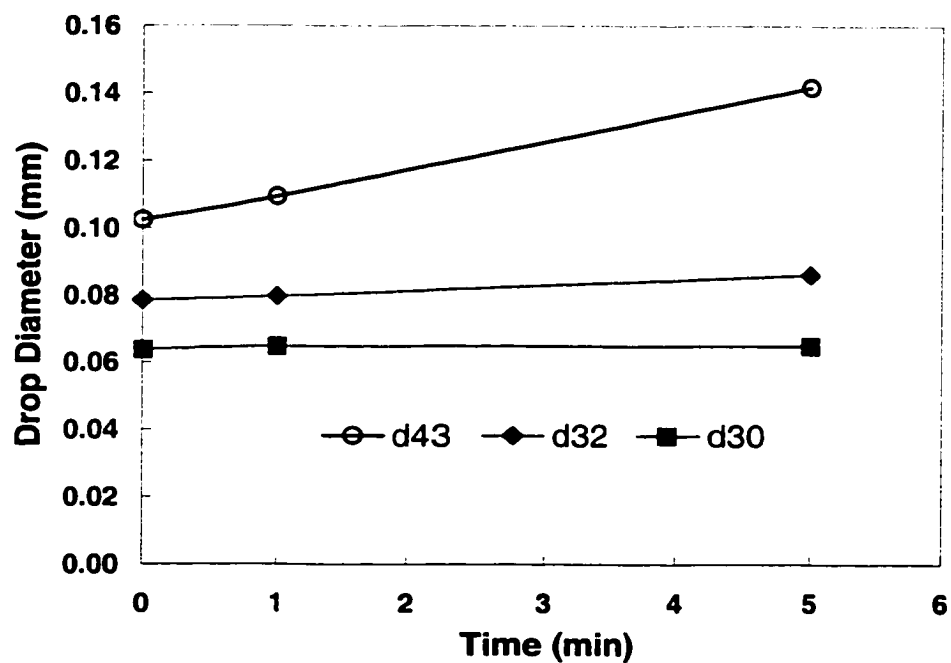


Figure B67. Effect of gravity on evolution of mean drop diameter of (0.5% Bayol oil/ water/ 0.25 mmole/m<sup>3</sup>, Triton X100, 500->250 rpm)

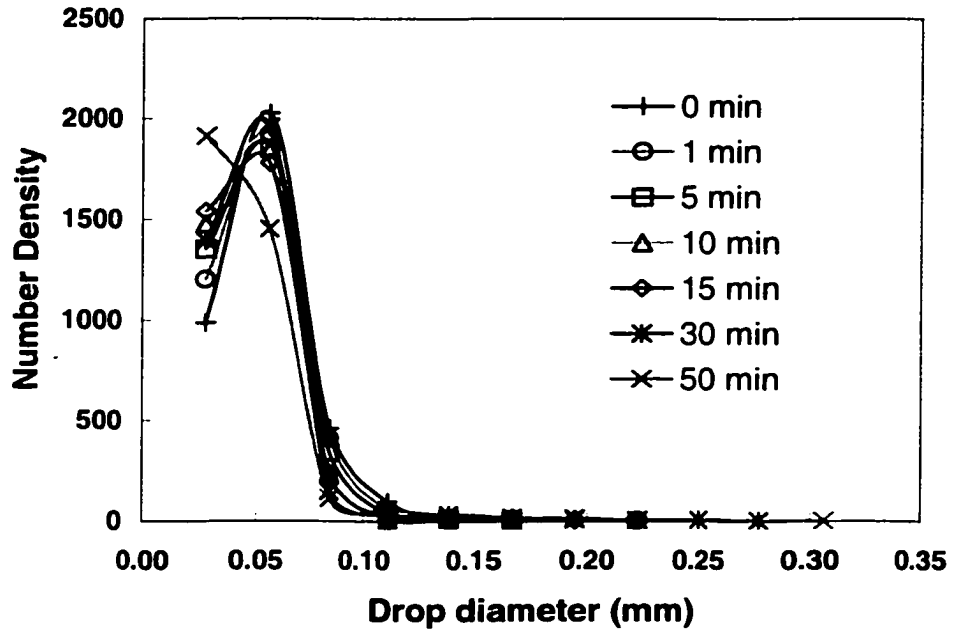


Figure B68. Effect of gravity on evolution of number density of (0.5% Bayol oil/ water/ 1.0 mmole/m<sup>3</sup>, Triton X100, 500->250 rpm)

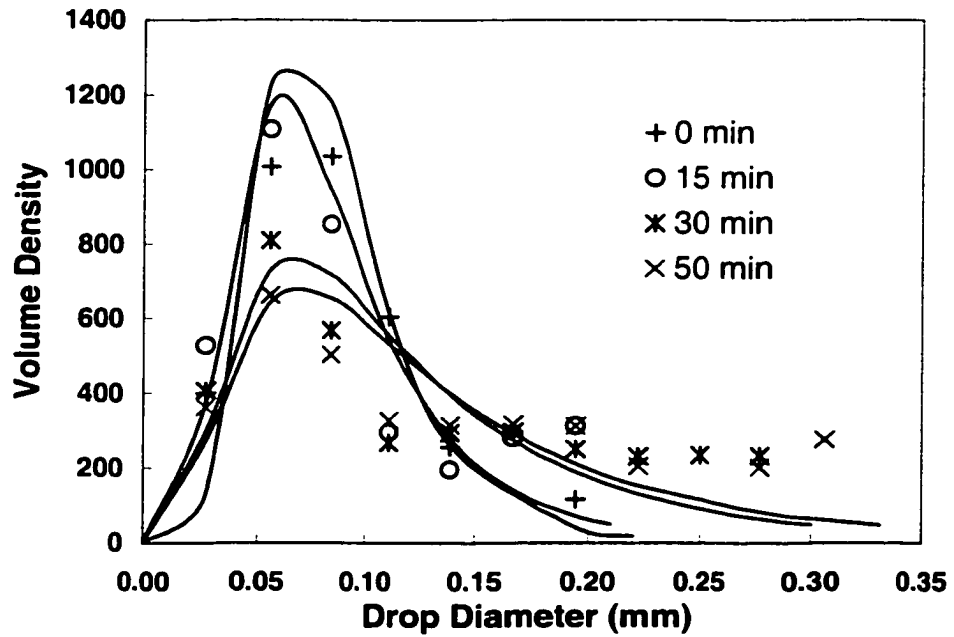


Figure 69. Effect of gravity on evolution of volume density of (0.5% Bayol oil/ water/ 1.0 mmole/m<sup>3</sup>, Triton X100, 500->250 rpm)

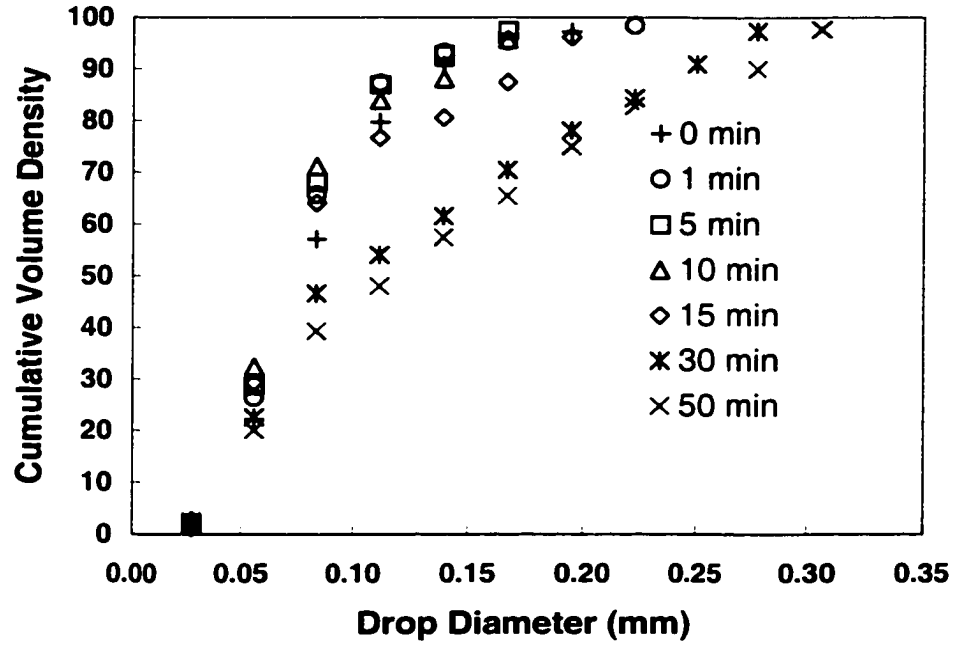


Figure B70. Effect of gravity on evolution of cumulative volume density of (0.5% Bayol oil/ water/ 1.0 mmole/m<sup>3</sup>, Triton X100, 500-→250 rpm)

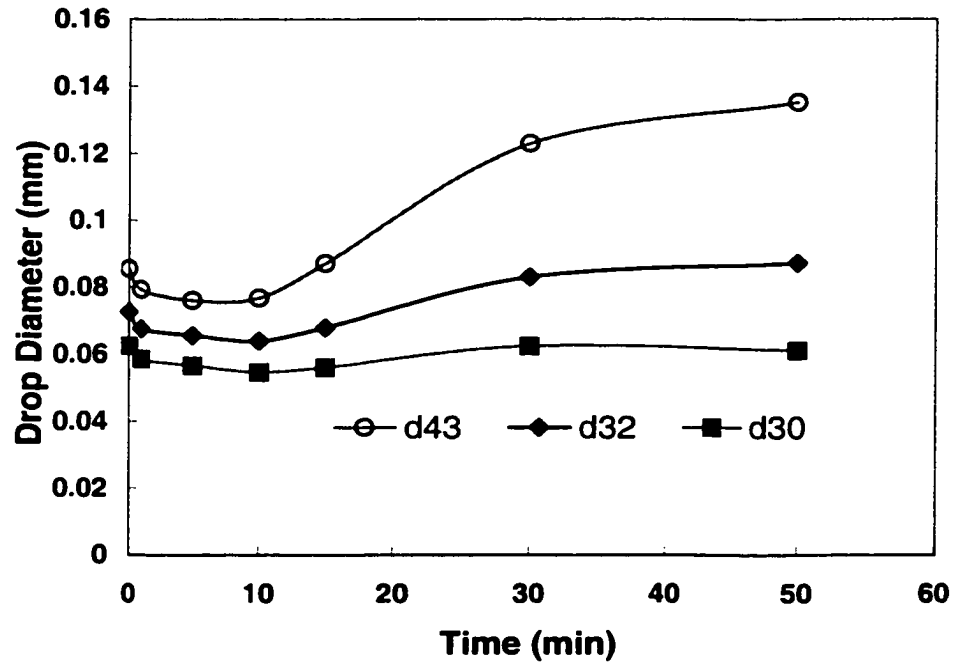


Figure 71. Effect of gravity on evolution of mean drop diameter of (0.5% Bayol oil/ water/ 1.0 mmole/m<sup>3</sup>, Triton X100, 500-→250 rpm)



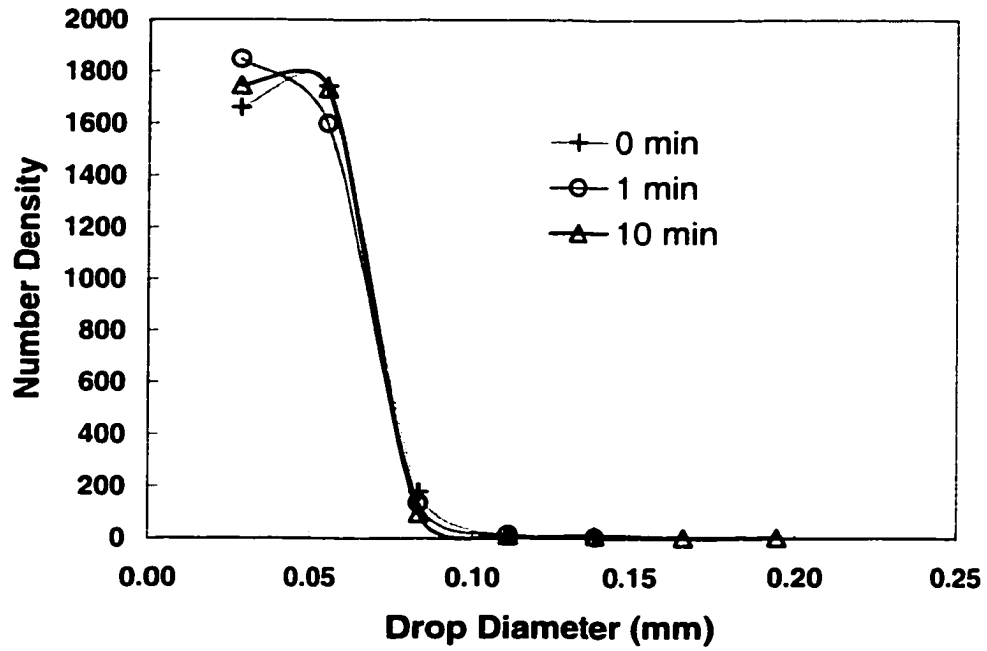


Figure B72. Effect of gravity on evolution of number density of (0.5% Bayol oil/ water/ 4.5 mmole/m<sup>3</sup> Triton X100, 500->250 rpm)

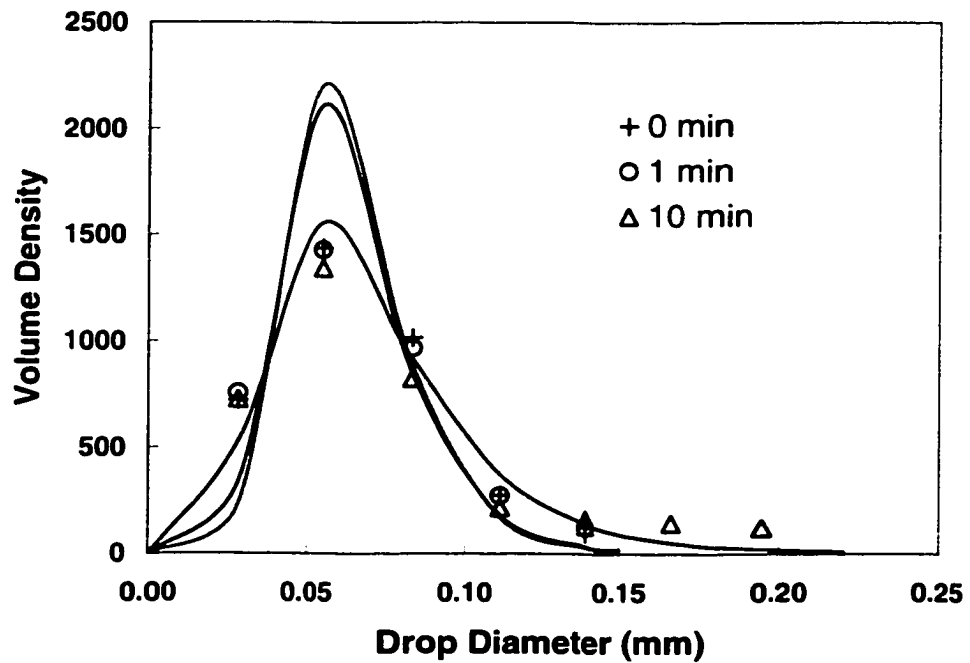


Figure B73. Effect of gravity on evolution of volume density of (0.5% Bayol oil/ water/ 4.5 mmole/m<sup>3</sup>, Triton X100, 500->250 rpm)

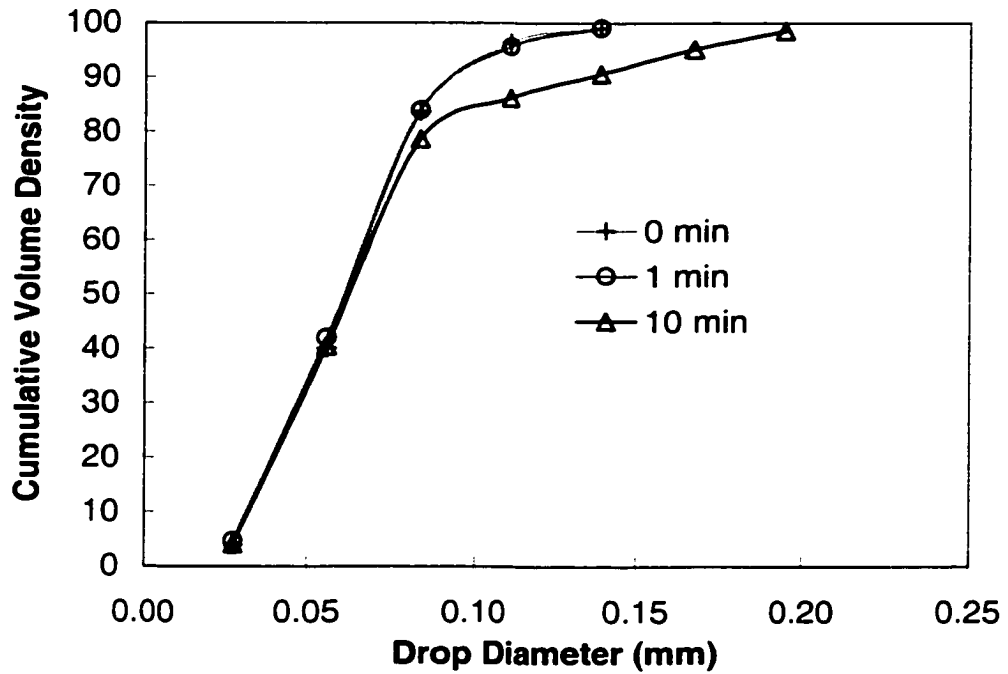


Figure B74. Effect of gravity on evolution of cumulative volume density of (0.5% Bayol oil/ water/ 4.5 mmole/m<sup>3</sup>, Triton X100, 500->250 rpm)

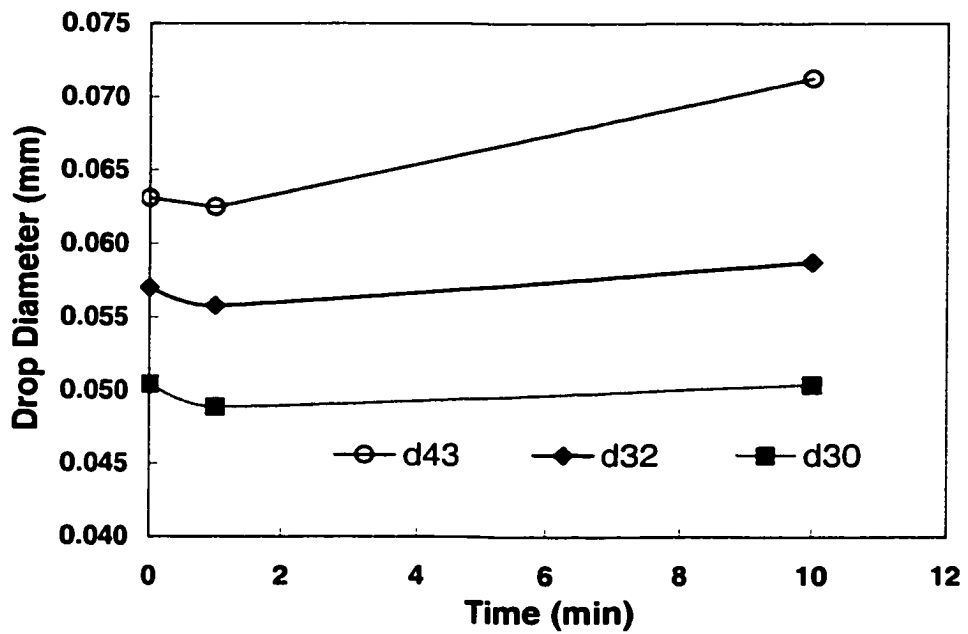


Figure B75. Effect of gravity on evolution of mean drop diameter of (0.5% Bayol oil/ water/ 4.5 mmole/m<sup>3</sup>, Triton X100, 500->250 rpm)

### APPENDIX C

This appendix contains the quasi-steady number density (distributive and cumulative) of the systems investigated.

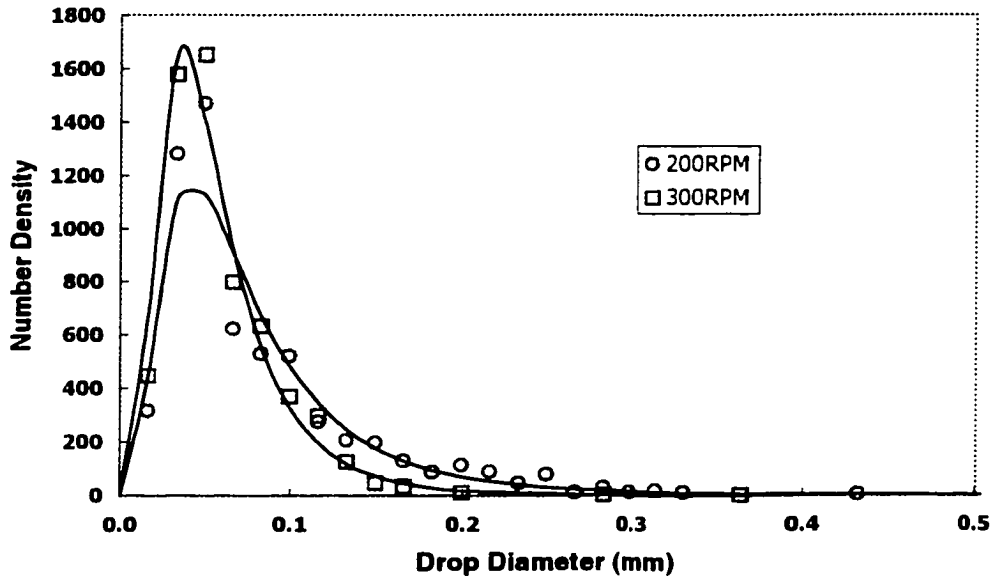


Figure C76. Effect of impeller speed on number density of (0.5% CLB-Bayol oil/ water)

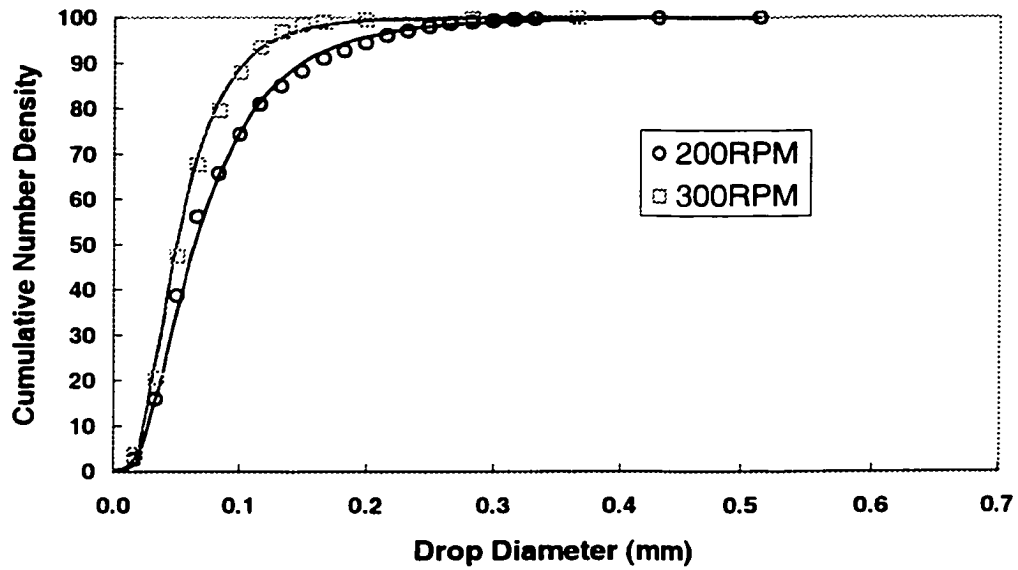


Figure C77. Effect of impeller speed on number density of (0.5% CLB-Bayol oil/ water)

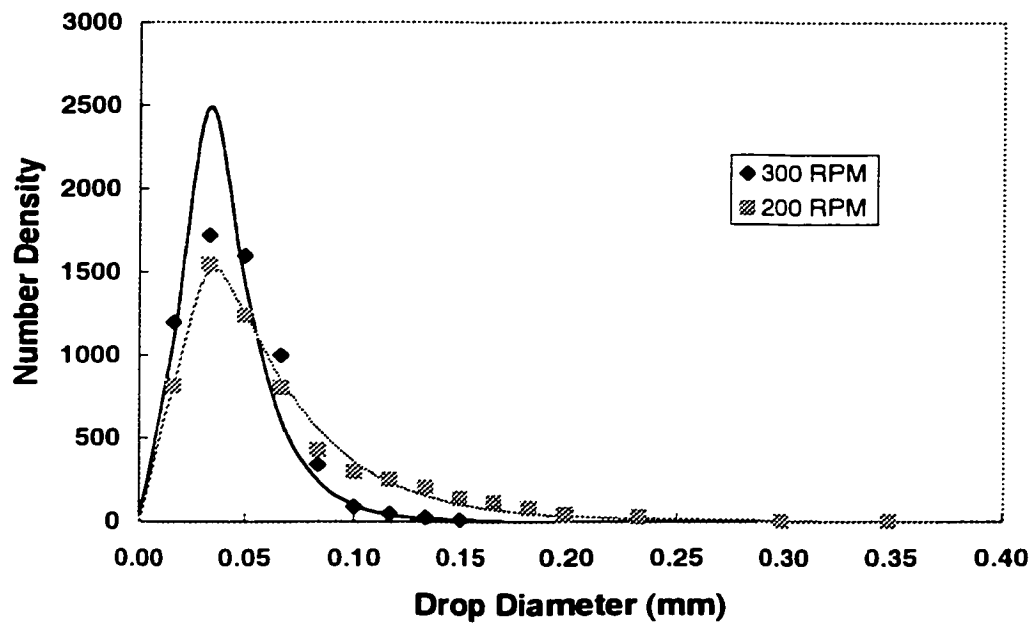


Figure C78. Effect of impeller speed on number density of (0.75% acetophenon/ 0.05 molar NaCl)

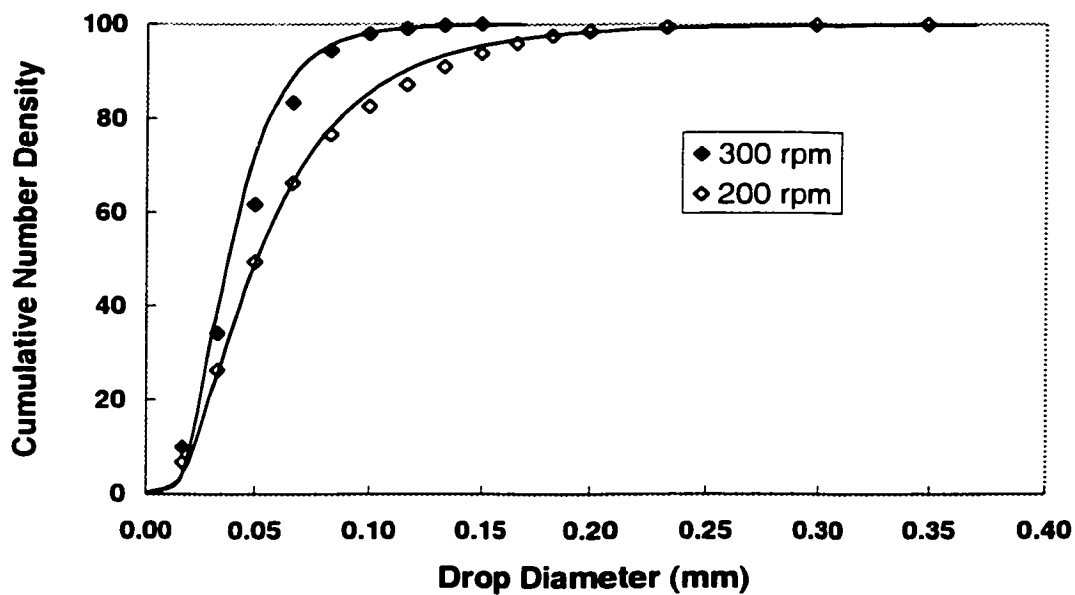


Figure C79. Effect of impeller speed on cumulative number density of (0.75% acetophenon/ 0.05 molar NaCl)

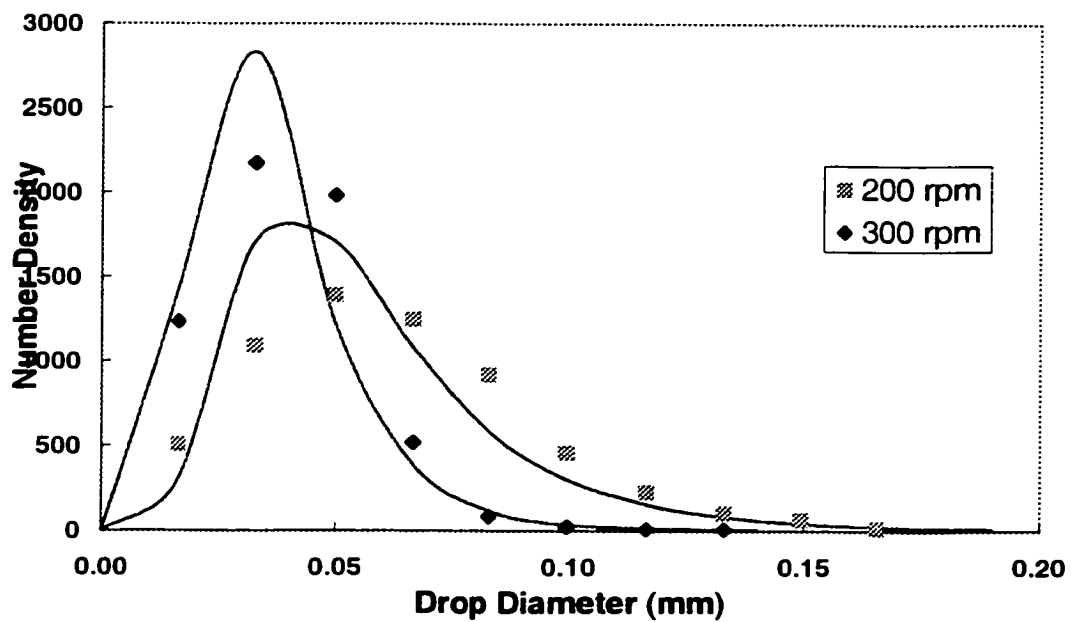


Figure C80. Effect of impeller speed on cumulative number density of (0.75% acetophenon / 0.05 molar NaCl/ 0.1 mmole/m<sup>3</sup> Triton X100)

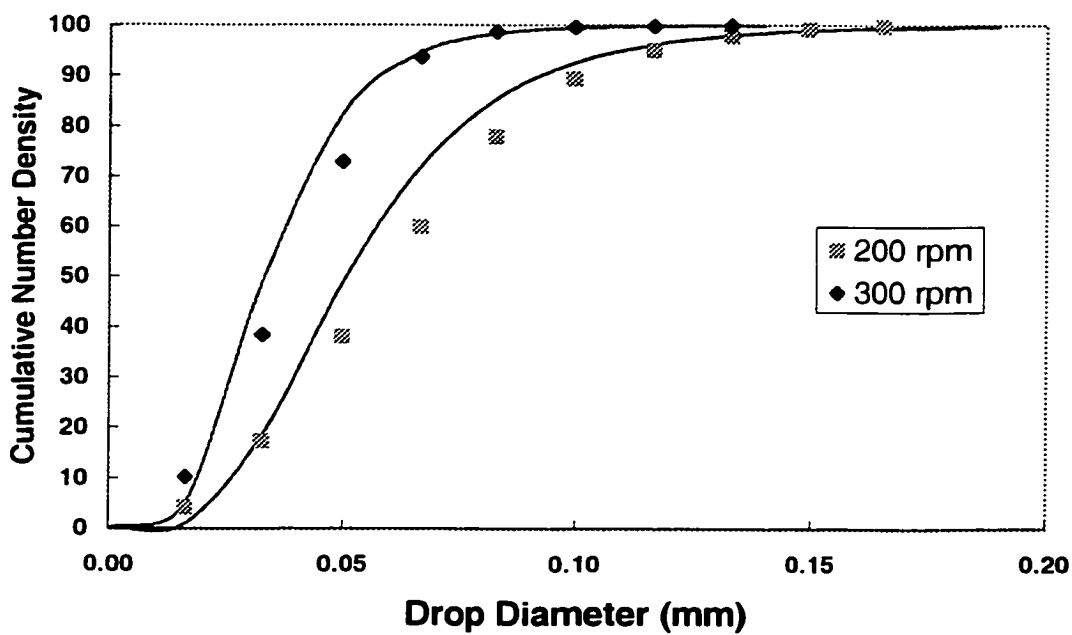


Figure C81. Effect of impeller speed on cumulative number density of (0.75% acetophenon / 0.05M aq. NaCl/ 0.1 mmole/m<sup>3</sup> Triton X100)

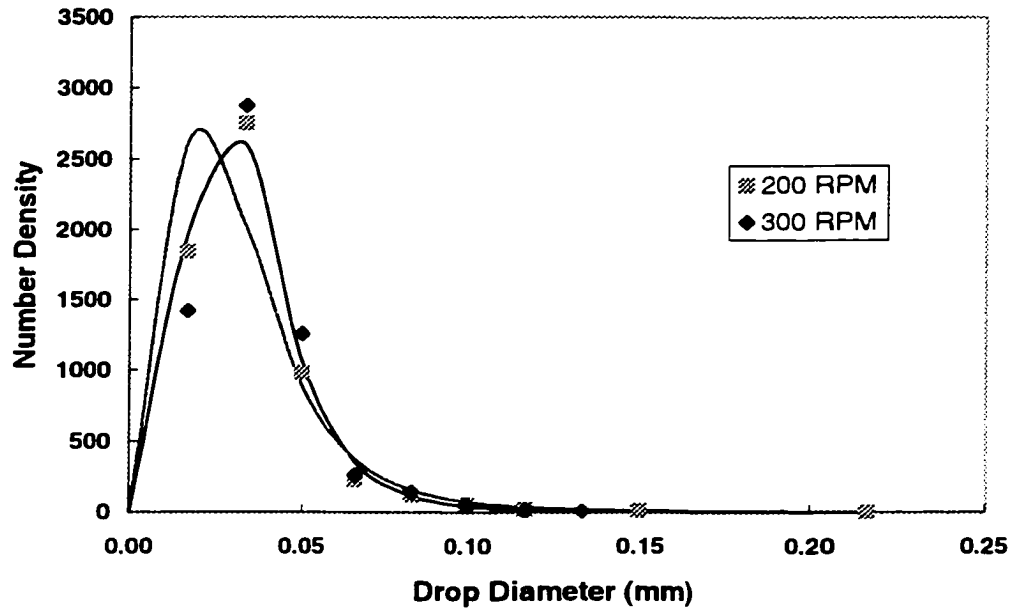


Figure C82. Effect of impeller speed on (0.75% acetophenon / 0.05 mole aq. NaCl / 0.2 mmole/m<sup>3</sup> Triton X100)

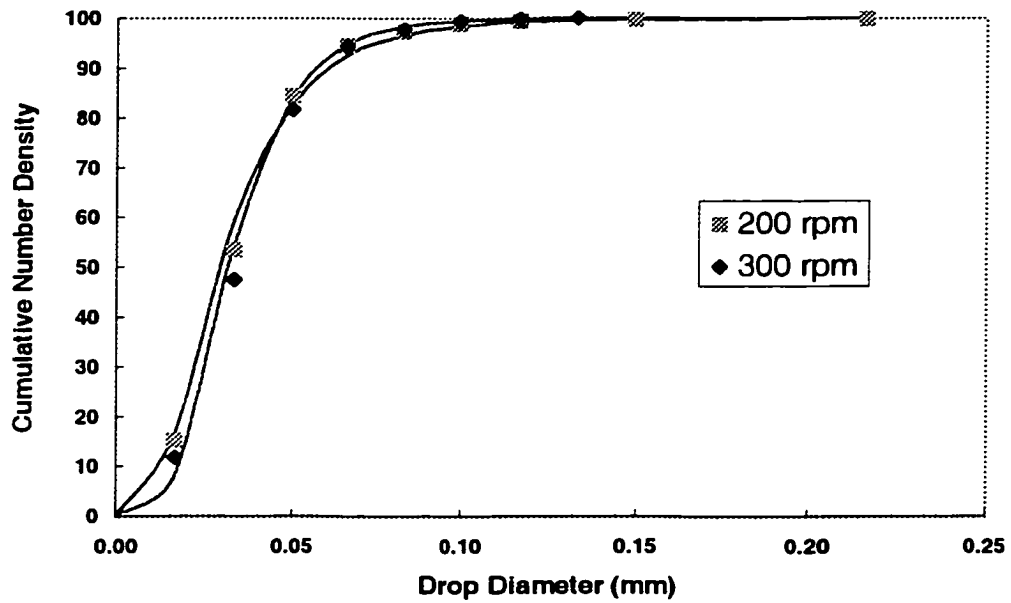


Figure C83. Effect of impeller speed on cumulative number density of (0.75% acetophenon/ 0.05 molar NaCl/ 0.2 mmole/m<sup>3</sup> Triton X100)

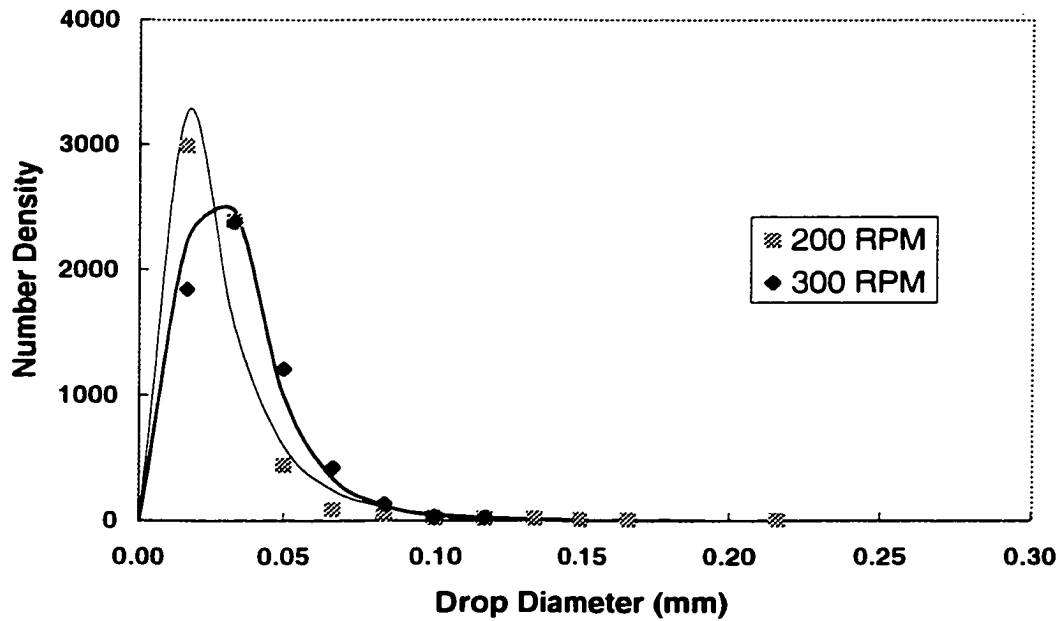


Figure C84. Effect of impeller speed on cumulative number density of (0.75% acetophenon/ 0.05 molar NaCl/ 1.0 mmole/m<sup>3</sup> Triton X100)

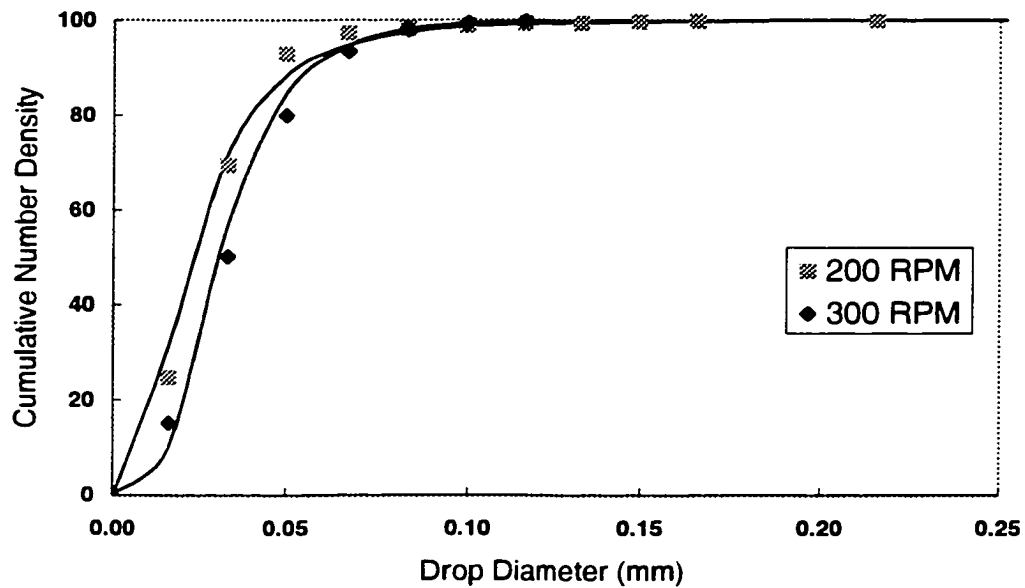


Figure C85. Effect of impeller speed on cumulative number density of (0.75% acetophenon/ 0.05 molar NaCl/ 1.0 mmole/m<sup>3</sup> Triton X100)

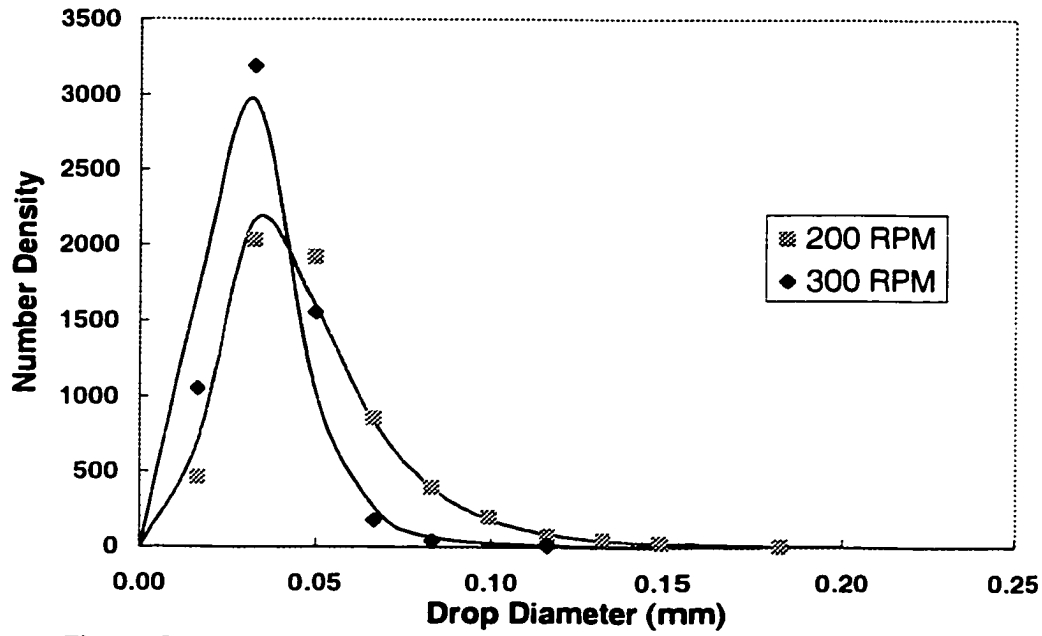


Figure C86. Effect of impeller speed on number density of (0.75% acetophenon/ 0.05 molar NaCl/ 0.1 mmole/m<sup>3</sup> Triton X165)

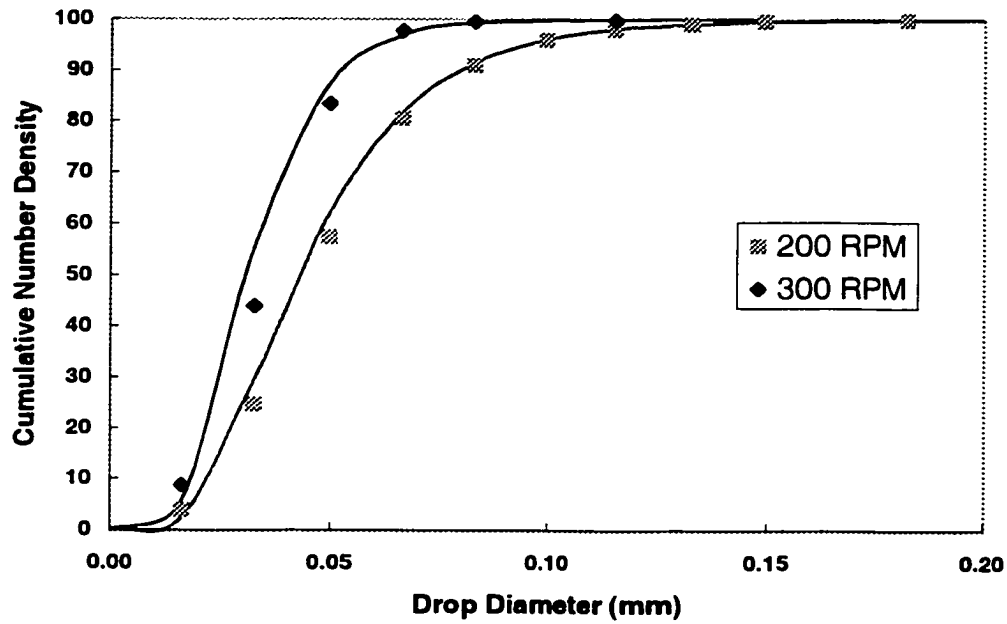


Figure C87. Effect of impeller speed on number density of (0.75% acetophenon/ 0.05 molar NaCl/ 0.1 mmole/m<sup>3</sup> Triton X165)



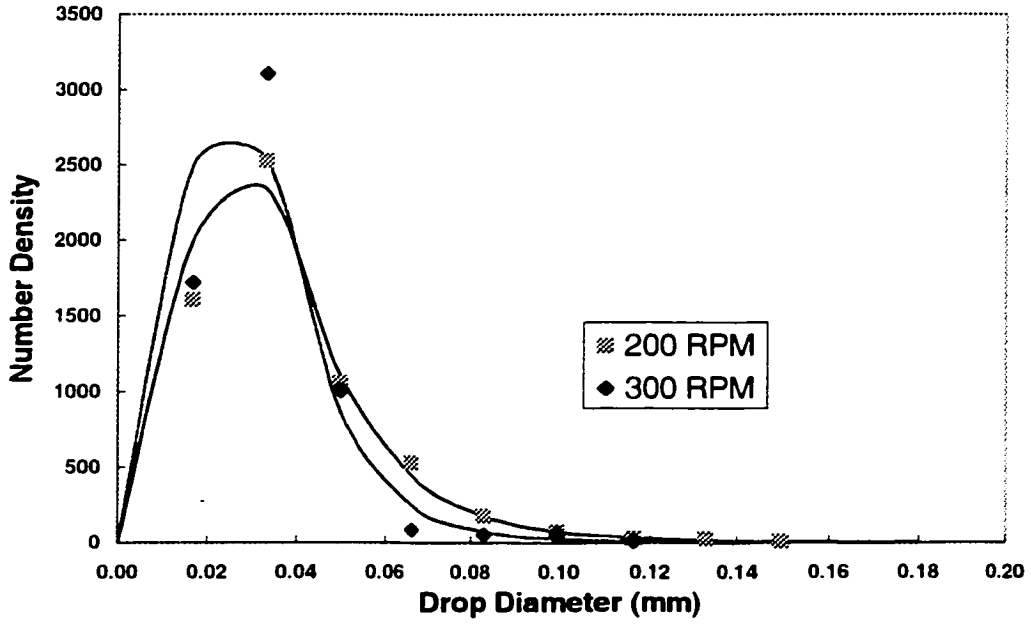


Figure C88. Effect of impeller speed on number density off (0.75% acetophenon/ 0.05 molar NaCl/ 0.2 mmole/m<sup>3</sup> Triton X165)

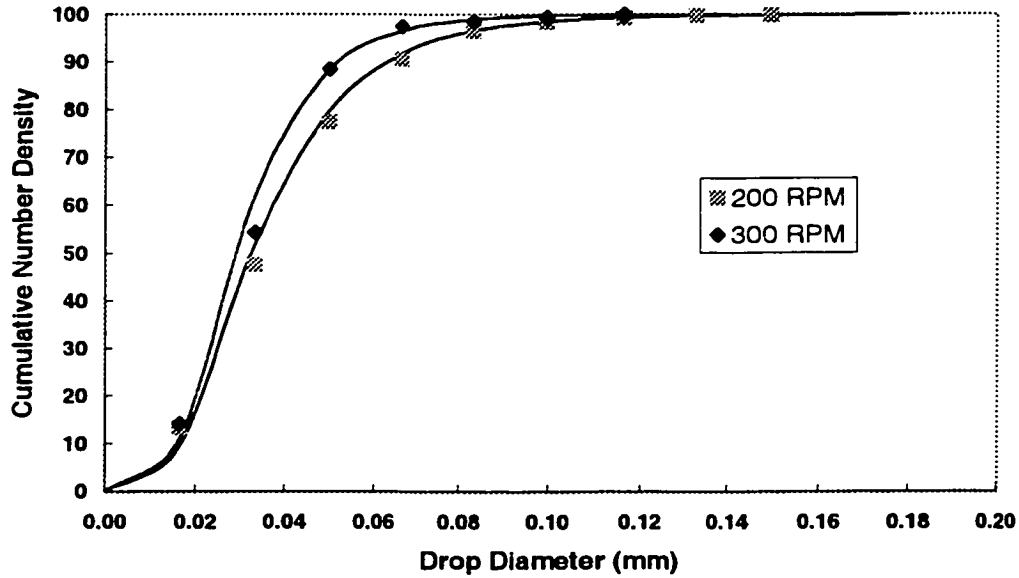


Figure C89. Effect of impeller speed on number density off (0.75% acetophenon/ 0.05 molar NaCl/ 0.2 mmole/m<sup>3</sup> Triton X165)

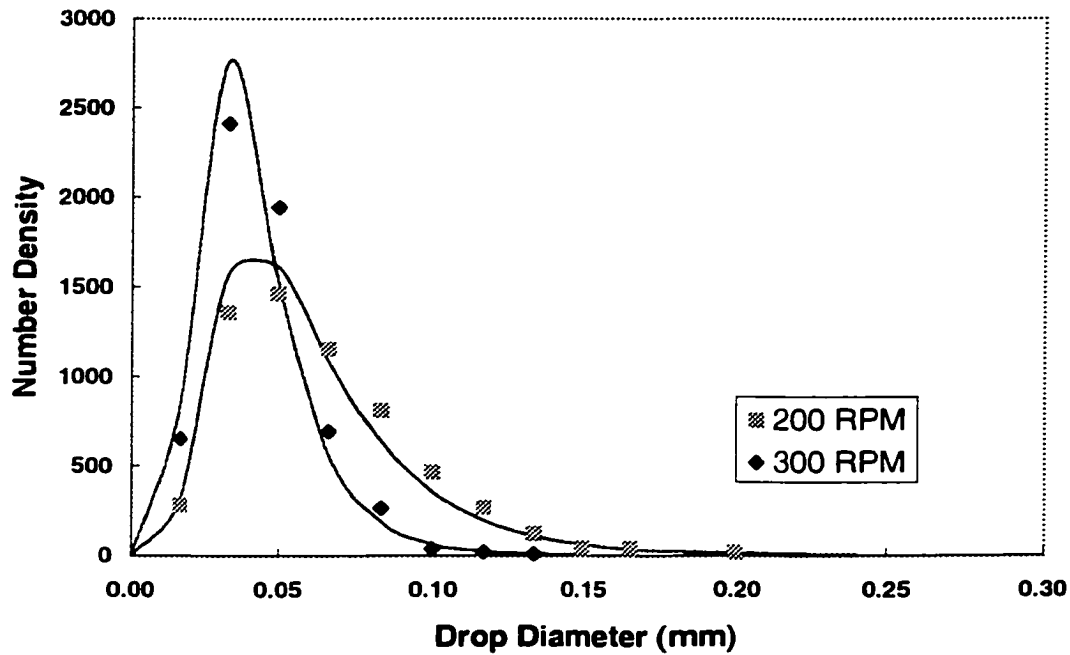


Figure C90. Effect of impeller speed on number density of (0.75% acetophenon/ 0.05 molar NaCl/ 0.1 mmole/m<sup>3</sup> Triton X305)

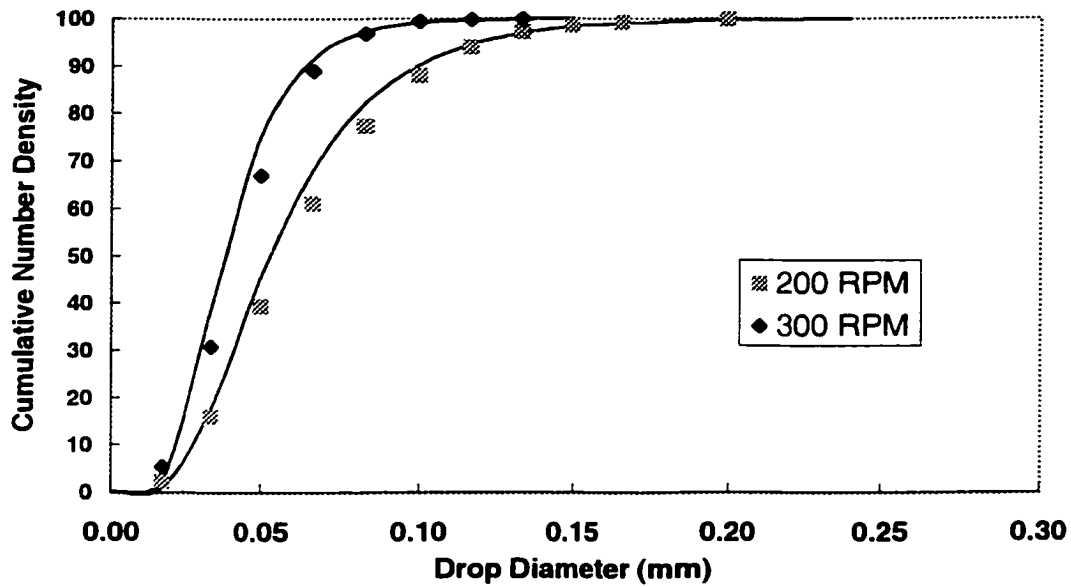


Figure C91. Effect of impeller speed on number density of (0.75% acetophenon/ 0.05 molar NaCl/ 0.1 mmole/m<sup>3</sup> Triton X305)

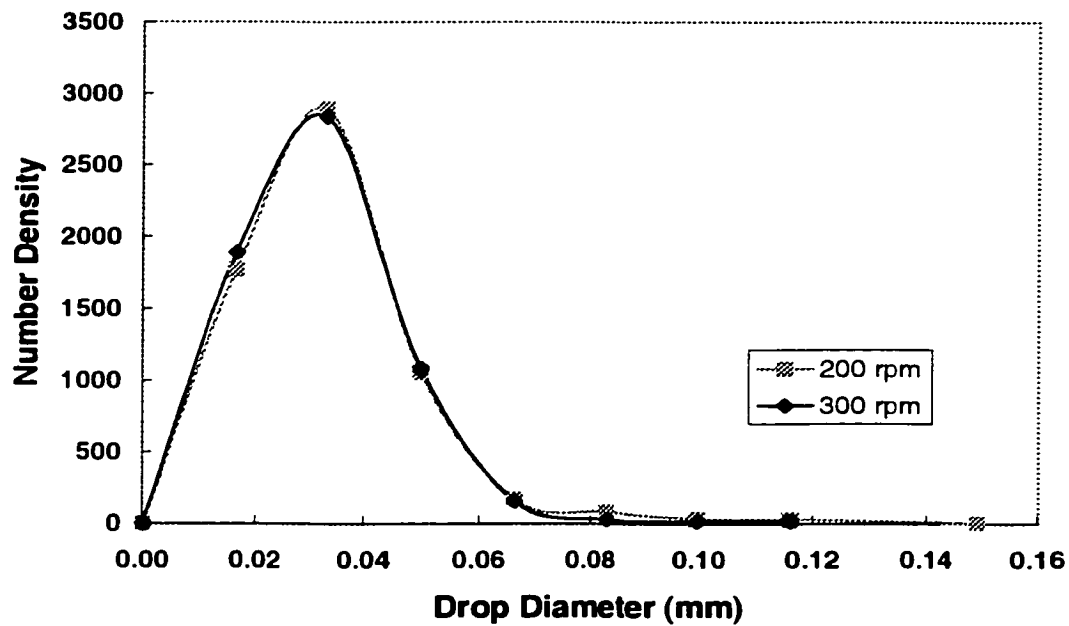


Figure C92. Effect of impeller speed on number density of (0.75% acetophenon/ 0.05 molar NaCl/ 0.2 mmole/m<sup>3</sup> Triton X305)

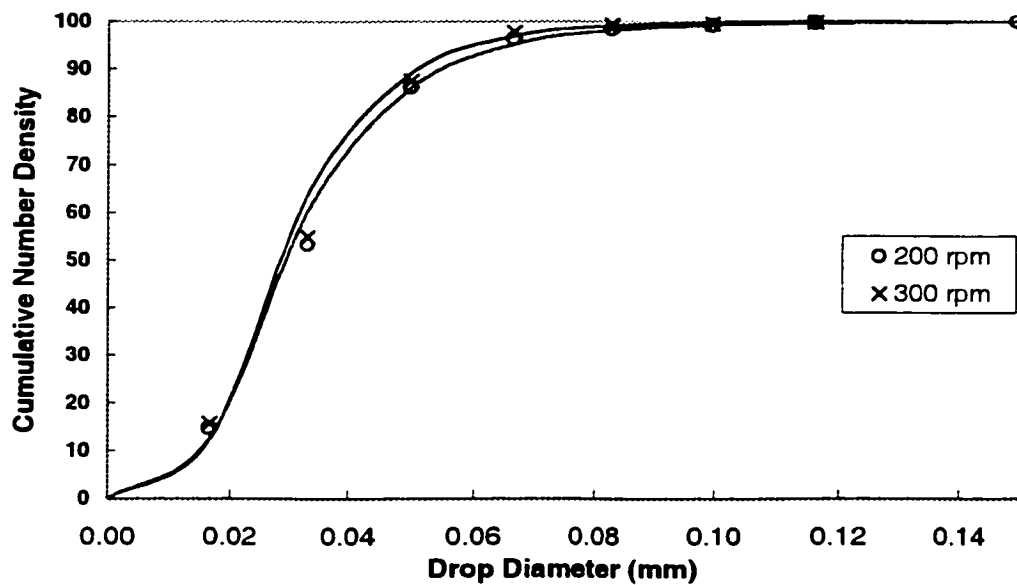


Figure C93. Effect of impeller speed on cumulative number density of (0.75% acetophenon/ 0.05 molar NaCl/ 0.2 mmole/m<sup>3</sup> Triton X305)

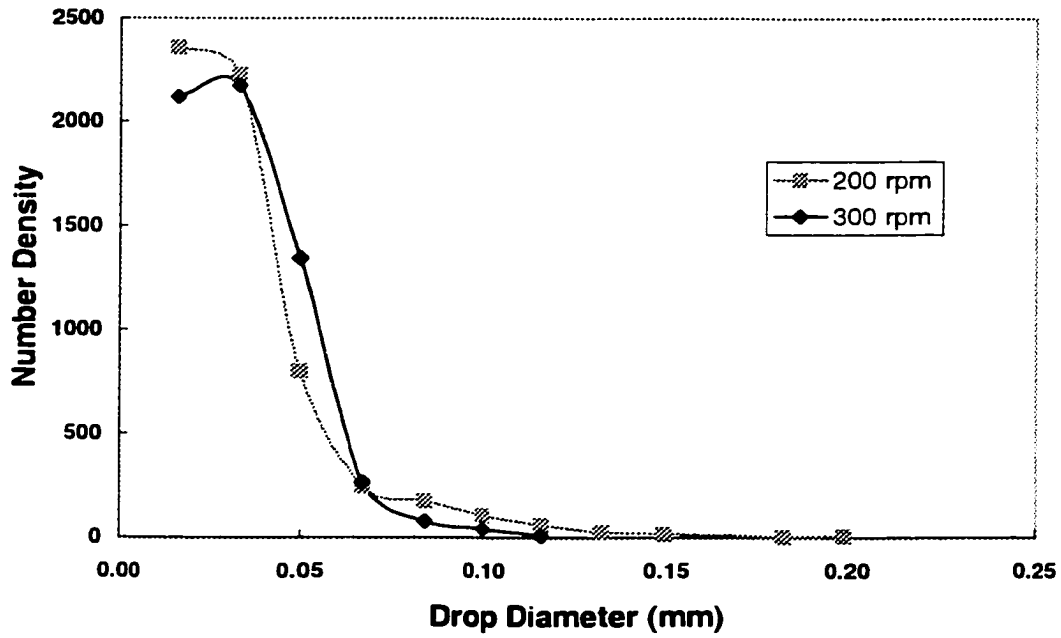


Figure C94. Effect of impeller speed on number density of (0.75% acetophenon/ 0.05 molar NaCl/ 0.1 mmole/m<sup>3</sup> Triton X405)

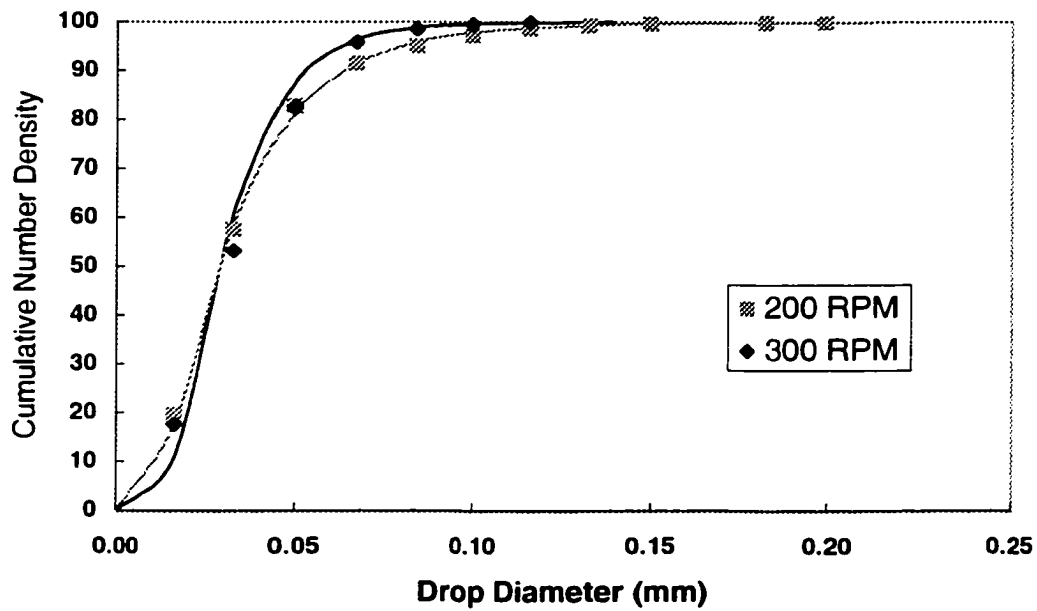


Figure C95. Effect of impeller speed on number density of (0.75% acetophenon/ 0.05 molar NaCl/ 0.1 mmole/m<sup>3</sup> Triton X405)

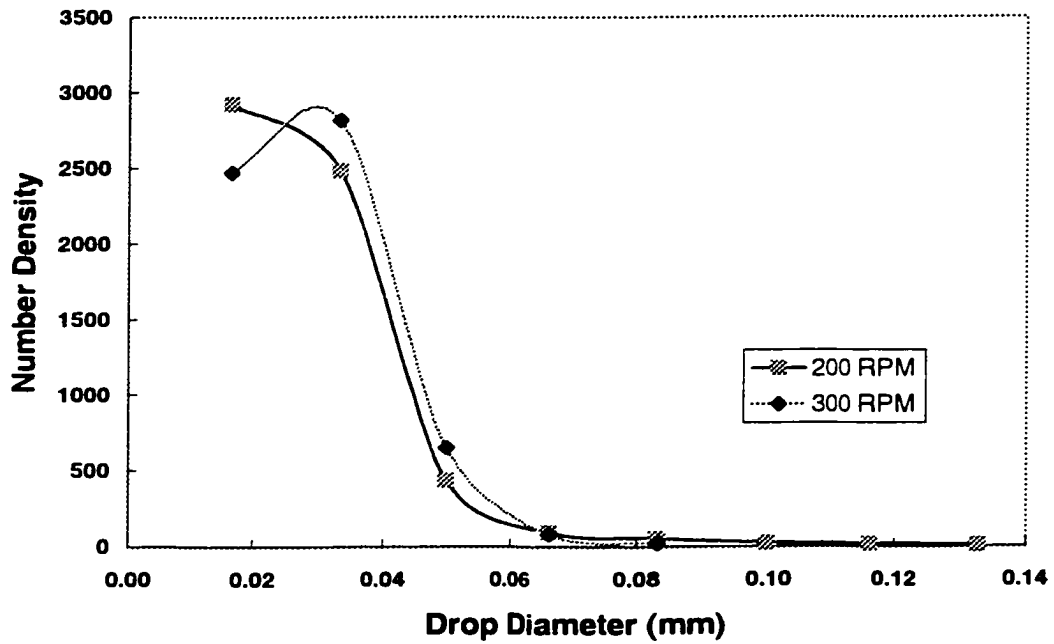


Figure C96. Effect of impeller speed on number density of (0.75% acetophenon/ 0.05 molar NaCl/ 0.2 mmole/m<sup>3</sup> Triton X405)

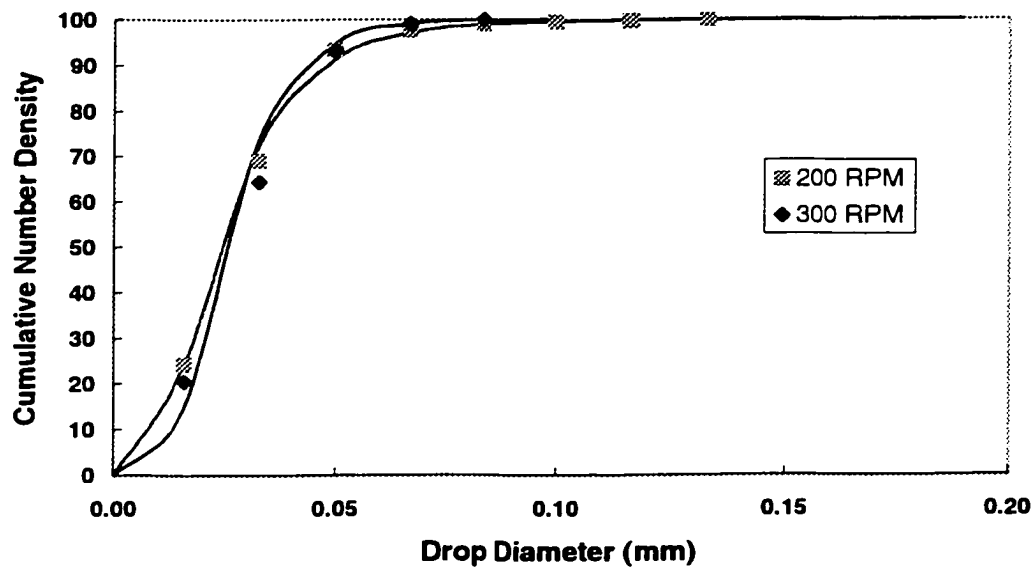


Figure C97. Effect of impeller speed on number density of (0.75% acetophenon/ 0.05 molar NaCl/ 0.2 mmole/m<sup>3</sup> Triton X405)

## APPENDIX D

This appendix contains the quasi-steady drop-volume-density (distributive and cumulative) of the systems investigated.

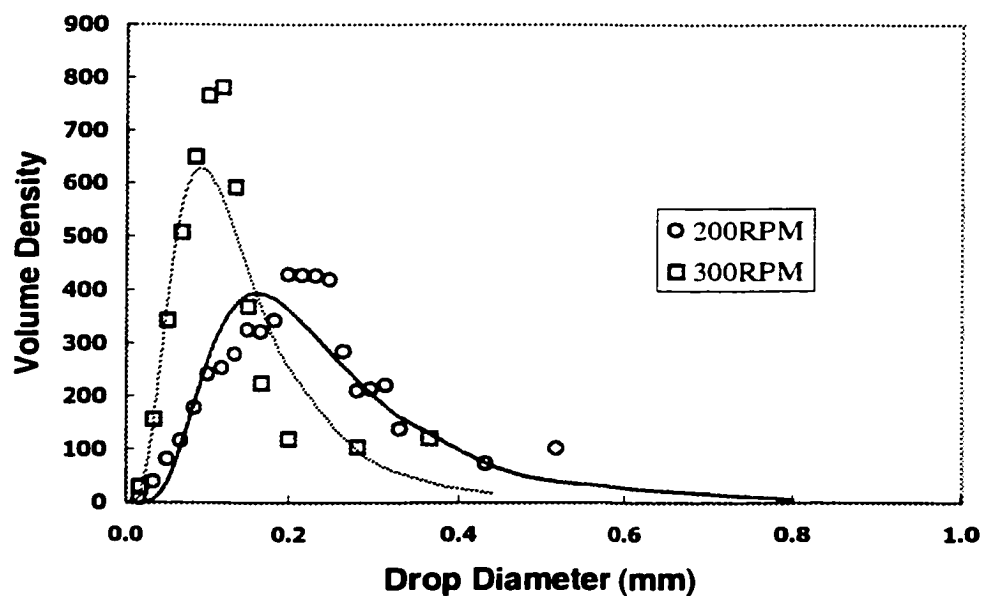


Figure D98. Effect of impeller speed on volume density of (0.5% CLB-Bayol oil / water)

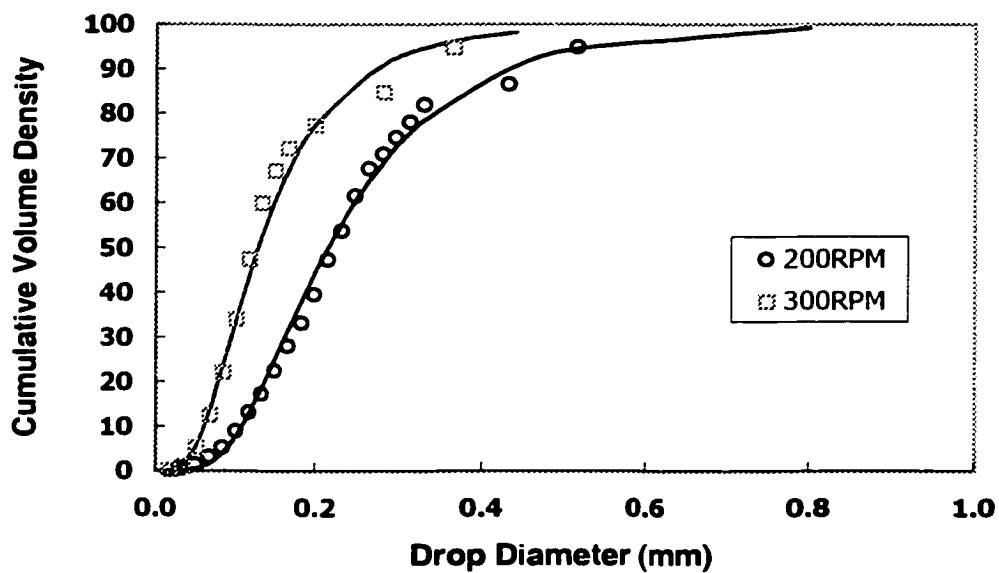


Figure D99. Effect of impeller speed on cumulative volume density of (0.5%CLB-Bayol oil/ water)

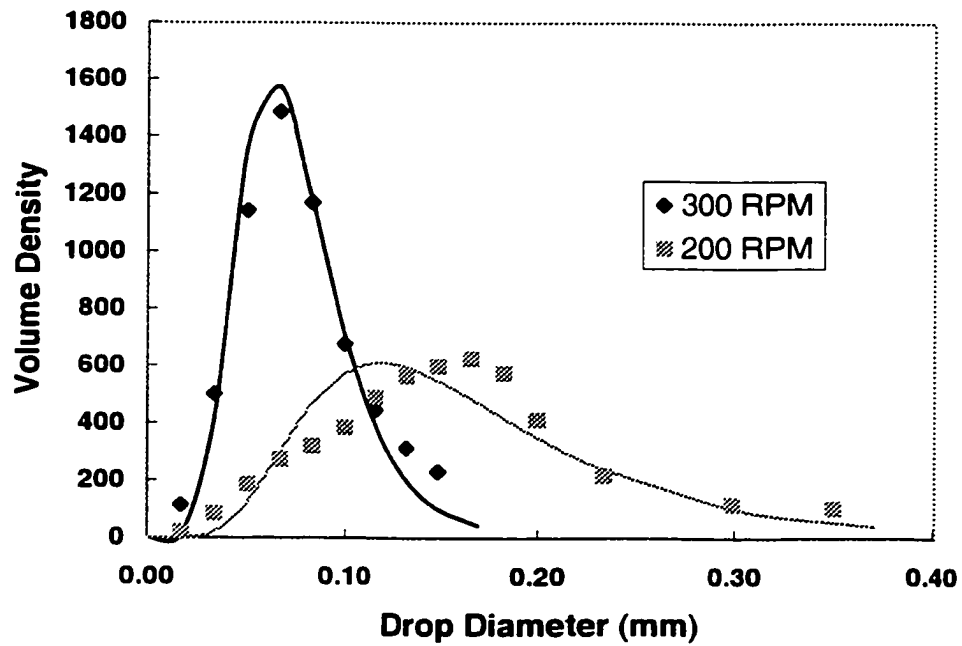


Figure D100. Effect of impeller speed on volume density of (0.75% acetophenon / 0.05M aq. NaCl)

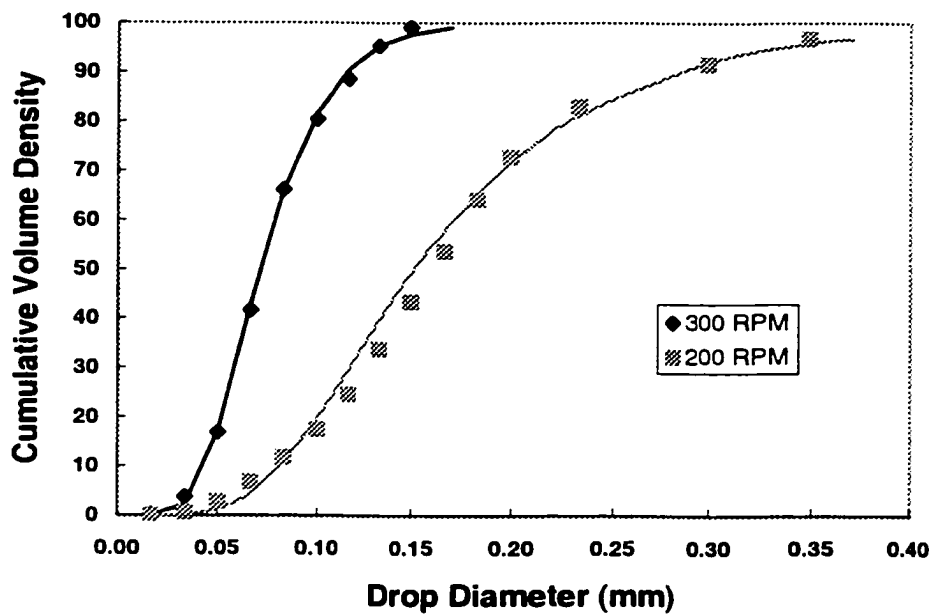


Figure D101. Effect of impeller speed on cumulative volume density of (0.75% acetophenon/ 0.05 M aq. NaCl)

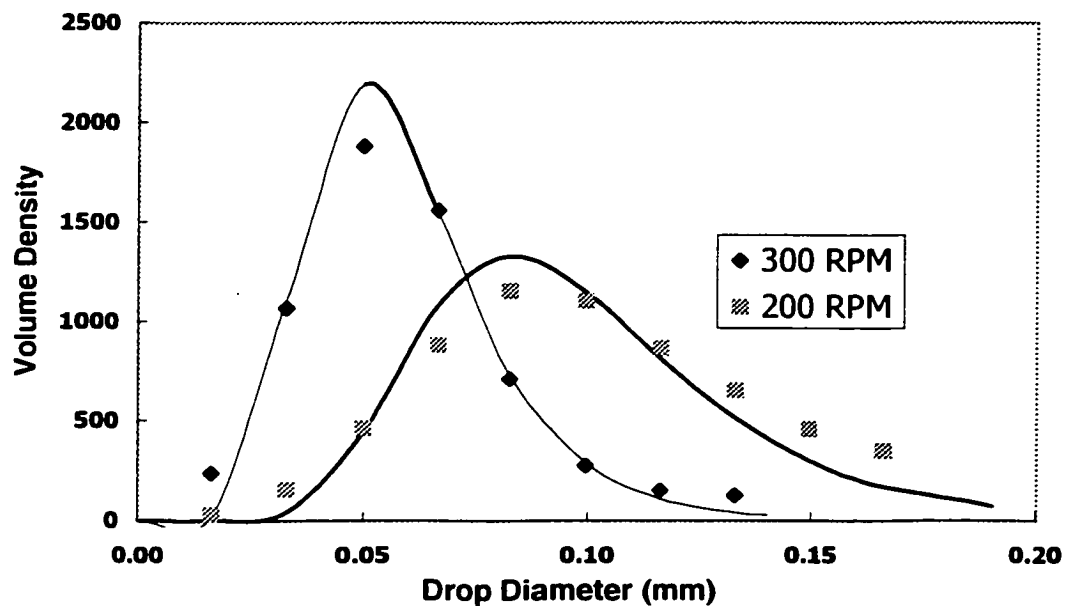


Figure D102. Effect of impeller speed on volume density of (0.75% acetophenon / 0.05 M aq. NaCl / 0.1 mmole/m<sup>3</sup> Triton X100)

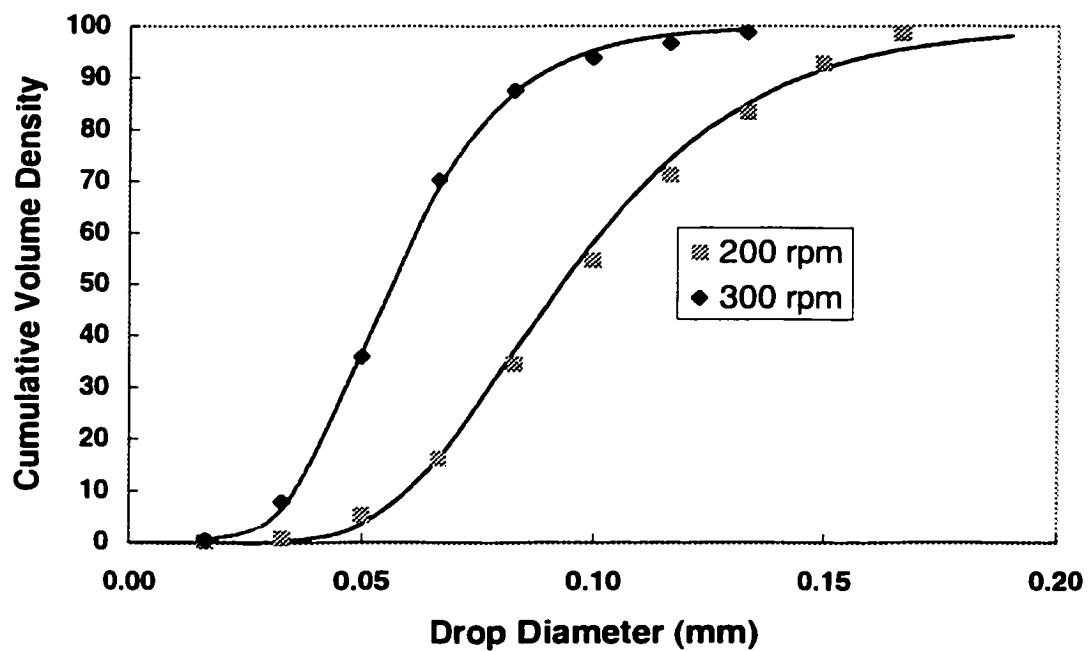


Figure D103. Effect of impeller speed on cumulative volume density of (0.75% acetophenon/ 0.05 M aq. NaCl/ 0.1 mmole/m<sup>3</sup> Triton X100)



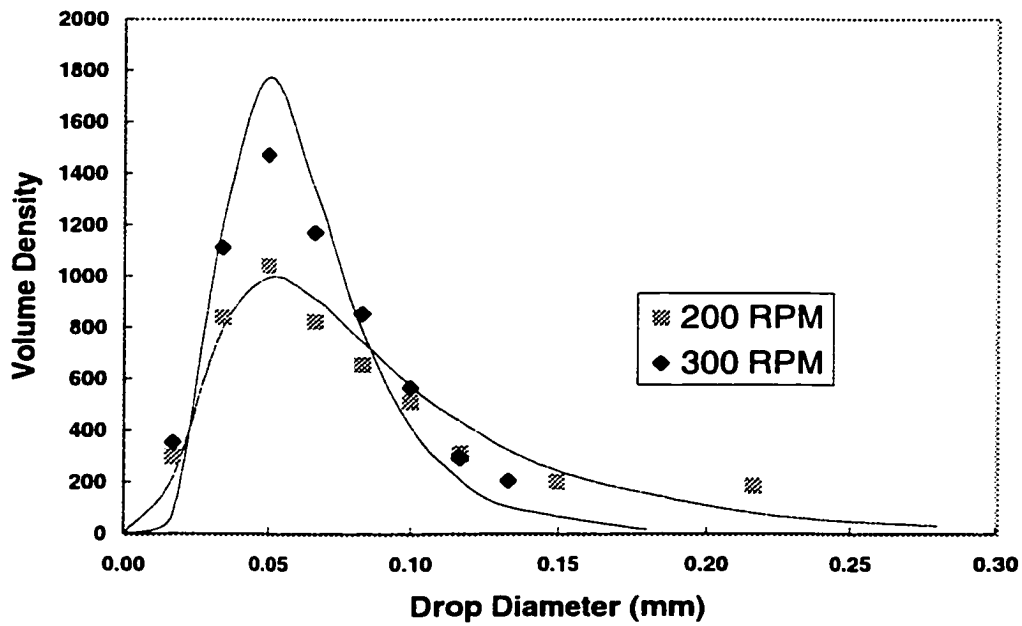


Figure D104. Effect of impeller speed on volume density of (0.75% acetophenon / 0.05 M aq. NaCl / 0.2 mmole/m<sup>3</sup> Triton X100)

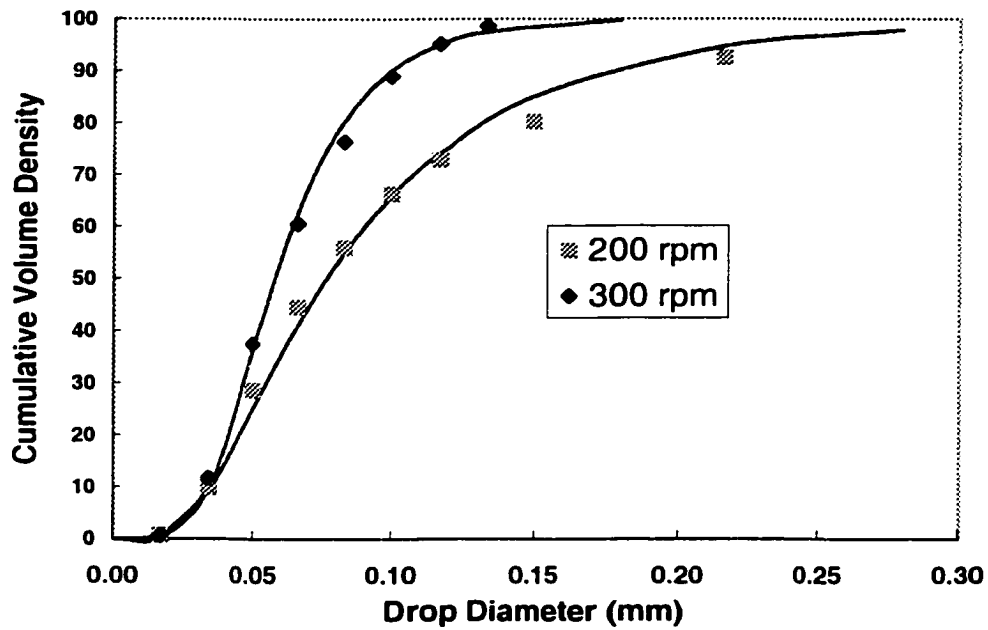


Figure D105. Effect of impeller speed on cumulative volume density of (0.75% acetophenon/ 0.05 M aq. NaCl/ 0.2 mmole/m<sup>3</sup> Triton X100)

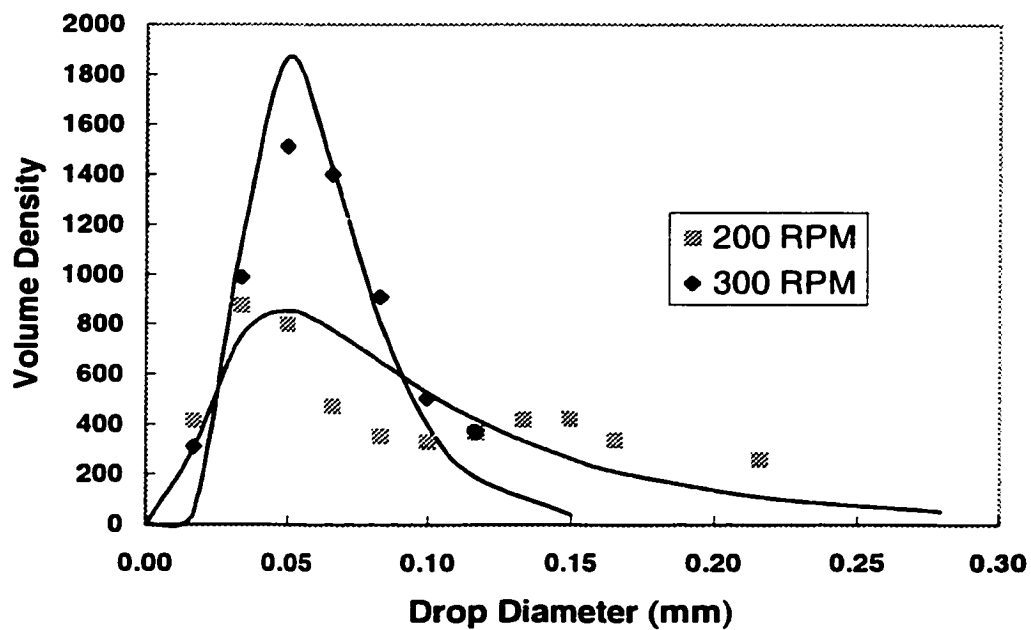


Figure D106. Effect of impeller speed on volume density of (0.75% acetophenon / 0.05 M aq. NaCl / 1.0 mmole/m<sup>3</sup> Triton X100)

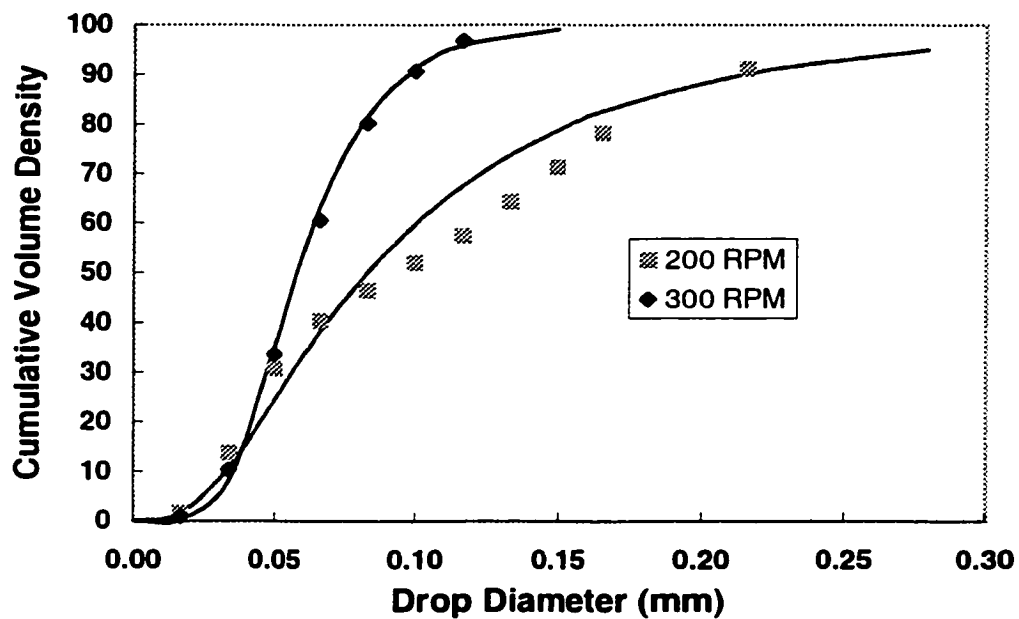


Figure D107. Effect of impeller speed on cumulative volume density of (0.75% acetophenon/ 0.05 M aq. NaCl/ 1.0 mmole/m<sup>3</sup> Triton X100)

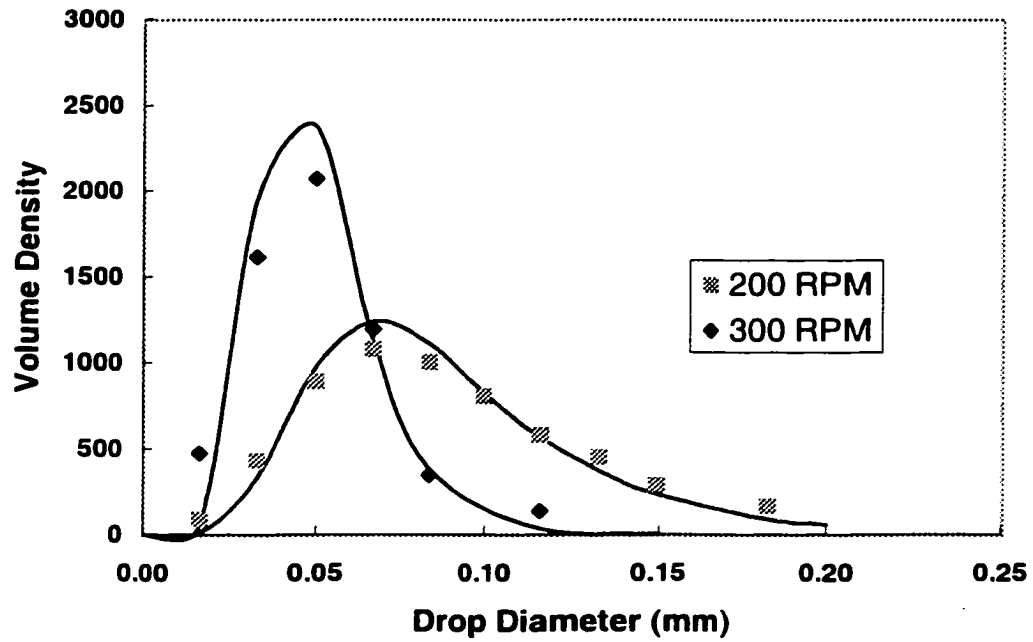


Figure D108. Effect of impeller speed on volume density of (0.75% acetophenon / 0.05M aq. NaCl / 0.1 mMole/m<sup>3</sup> Triton X165)

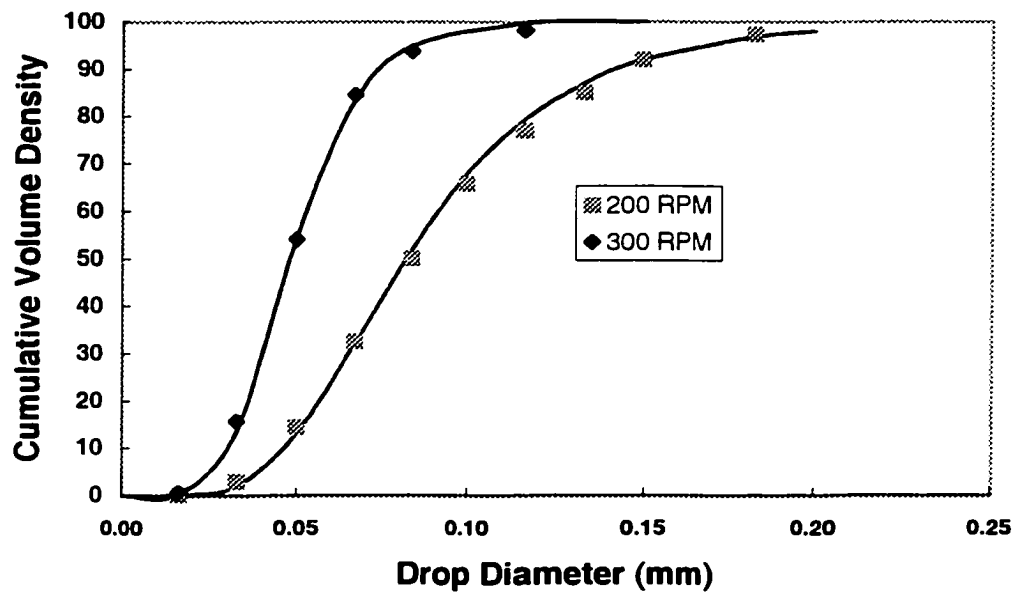


Figure D109. Effect of impeller speed on cumulative volume density of (0.75% acetophenon/ 0.05 M aq. NaCl/ 0.1 mmole/m<sup>3</sup> Triton X165)

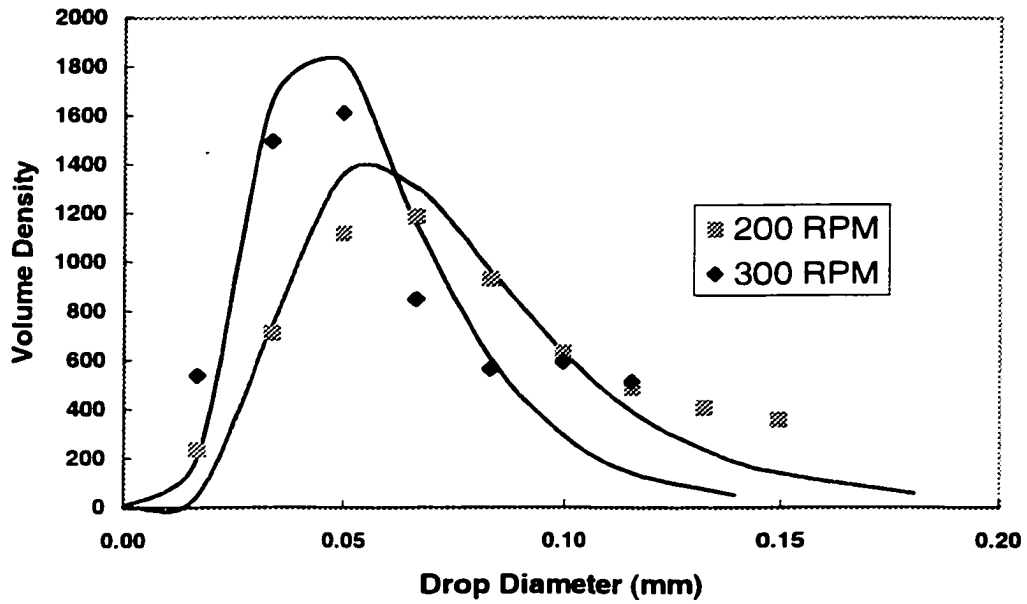


Figure D110. Effect of impeller speed on volume density of (0.75% acetophenon / 0.05 M aq. NaCl / 0.2 mmole/m<sup>3</sup> Triton X165)

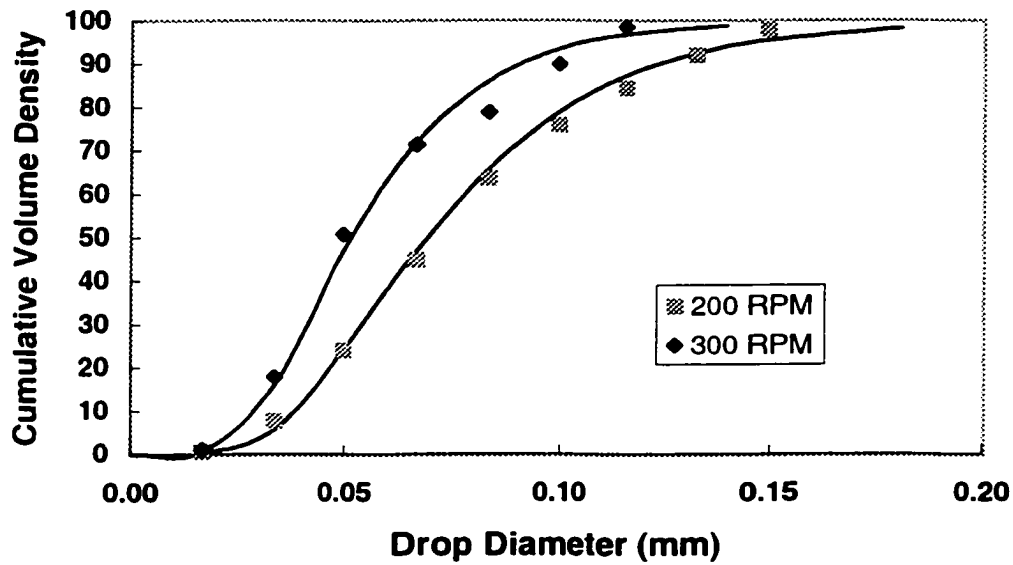


Figure D111. Effect of impeller speed on cumulative volume density of (0.75% acetophenon/ 0.05 M aq. NaCl/ 0.2 mmole/m<sup>3</sup> Triton X165)

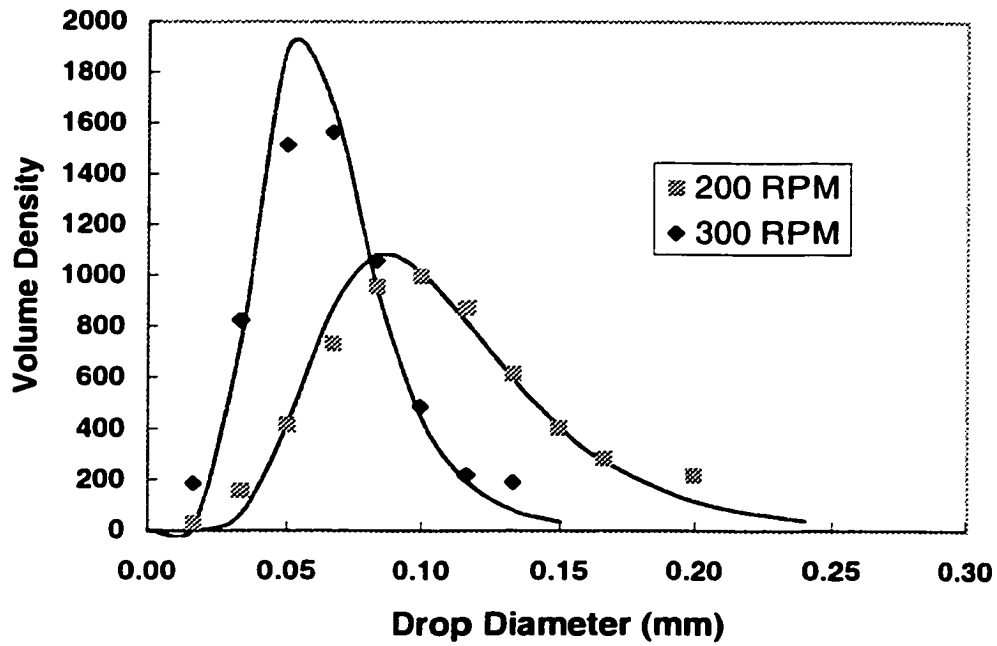


Figure D112. Effect of impeller speed on volume density of (0.75% acetophenon / 0.05 M aq. NaCl / 0.1 mMole/m<sup>3</sup> Triton X305)

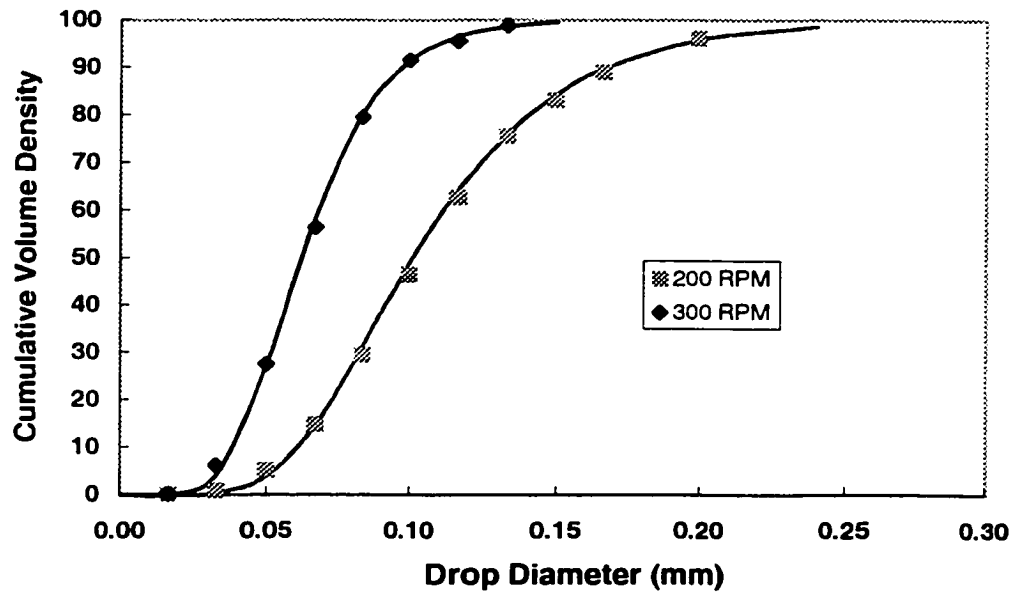


Figure D113. Effect of impeller speed on cumulative volume density of (0.75% acetophenon/ 0.05 M aq. NaCl/ 0.1 mmole/m<sup>3</sup> Triton X305)

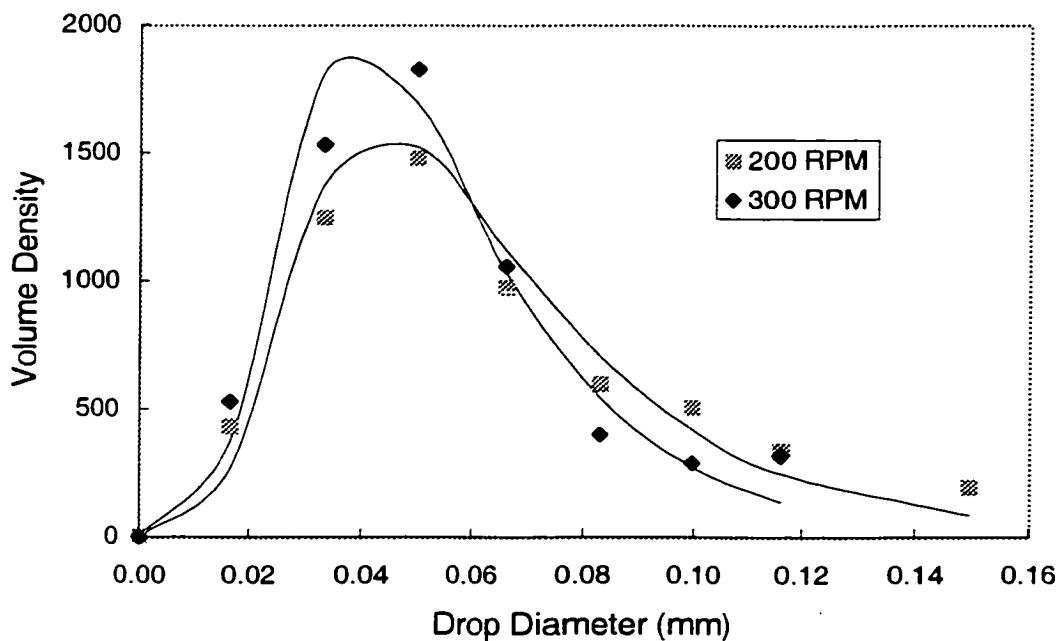


Figure D114. Effect of impeller speed on volume density of (0.75% acetophenon / 0.05 M aq. NaCl / 0.2 mMole/m<sup>3</sup> Triton X305)

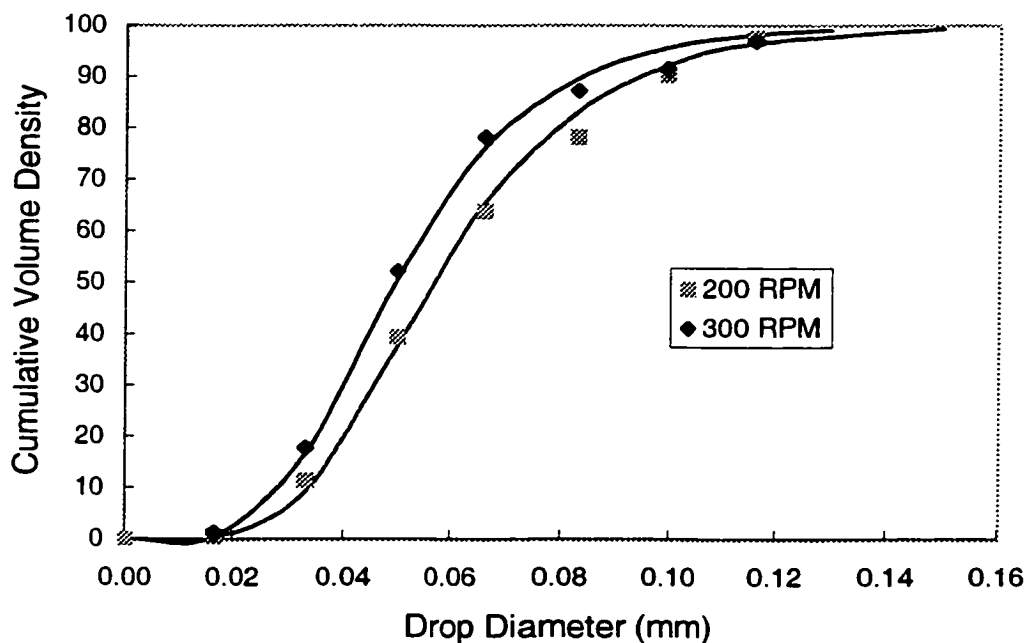


Figure D115. Effect of impeller speed on cumulative volume density of (0.75% acetophenon/ 0.05 M aq. NaCl/ 0.2 mmole/m<sup>3</sup> Triton X305)

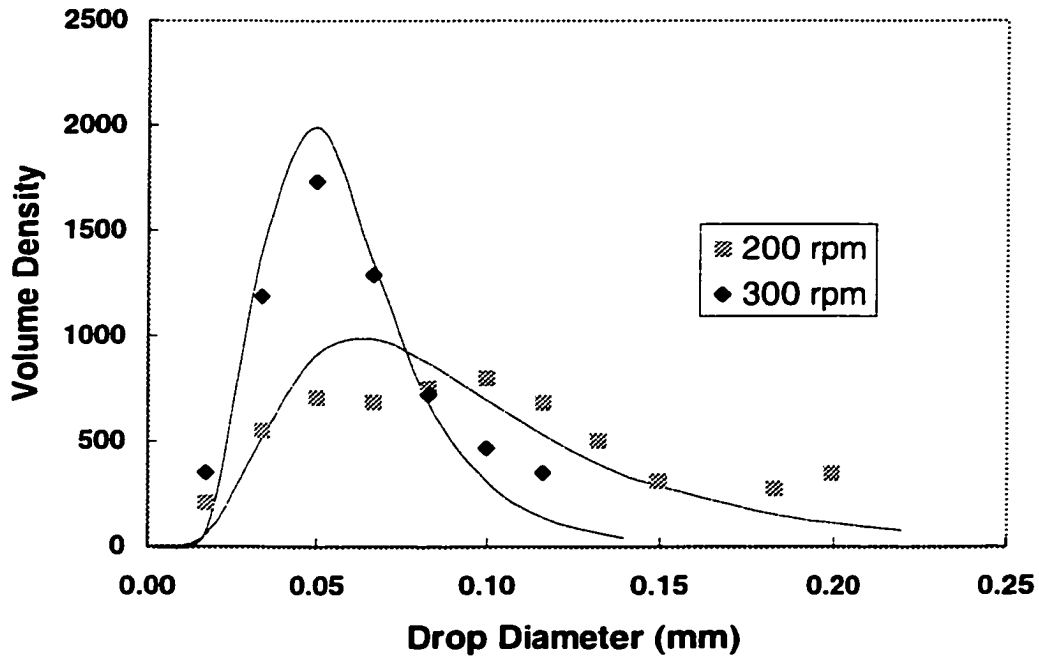


Figure D116. Effect of impeller speed on volume density of (0.75% acetophenon / 0.05 M aq. NaCl / 0.1 mmole/m<sup>3</sup> Triton X405)

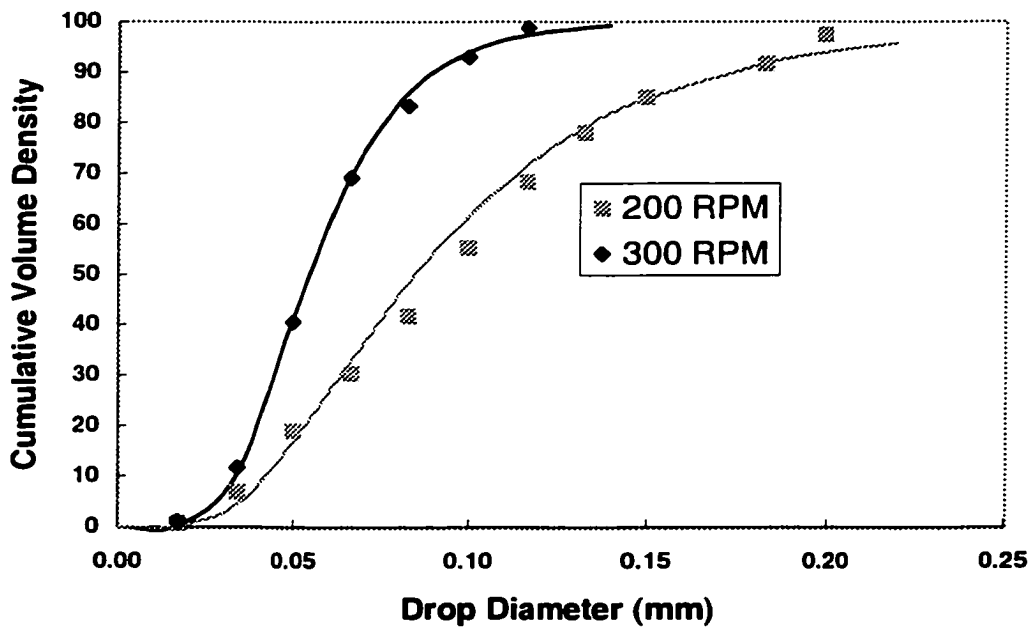


Figure D117. Effect of impeller speed on cumulative volume density of (0.75% acetophenon/ 0.05 M aq. NaCl/ 0.1 mmole/m<sup>3</sup> Triton X405)

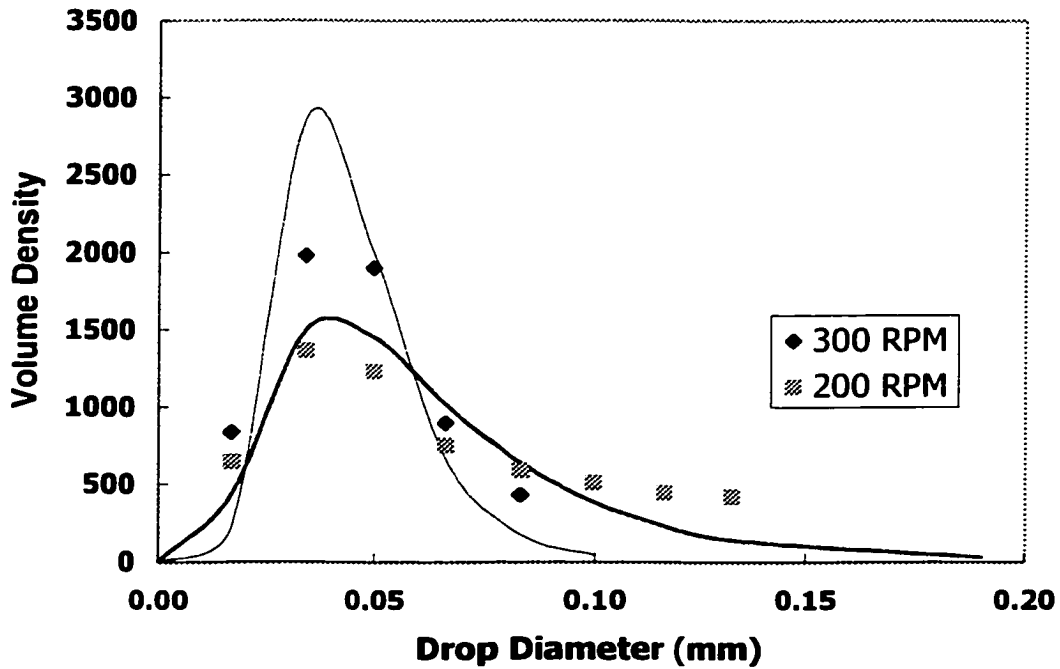


Figure D118. Effect of impeller speed on volume density of (0.75% acetophenon / 0.05 M aq. NaCl / 0.2 mmole/m<sup>3</sup> Triton X405)

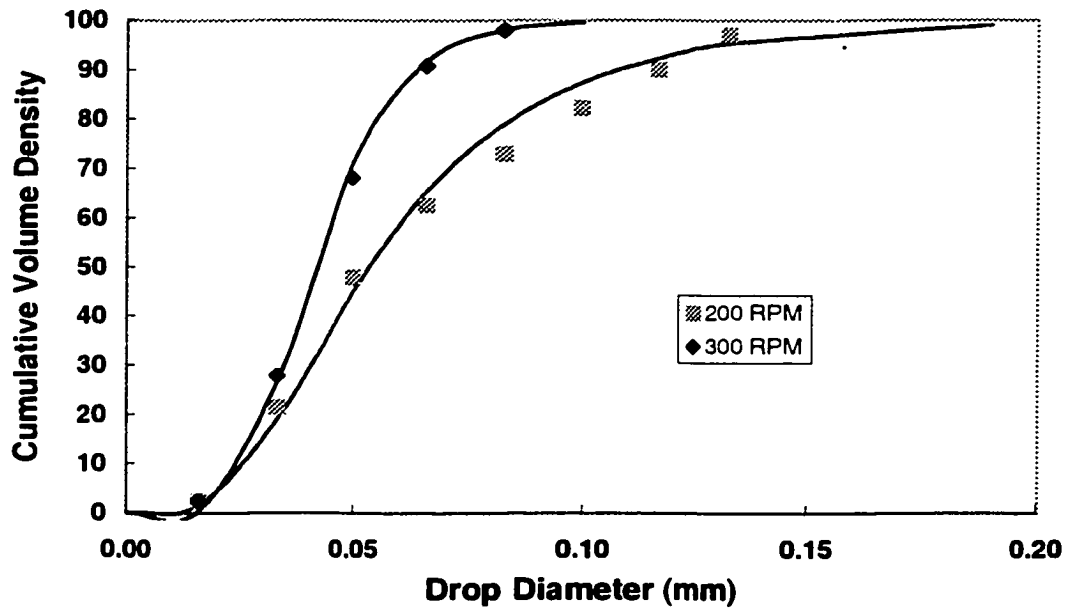


Figure D119. Effect of impeller speed on cumulative volume density of (0.75% acetophenon/ 0.05 M aq. NaCl/ 0.2 mmole/m<sup>3</sup> Triton X405)



## APPENDIX E

This appendix contains the transient drop size (distributive and cumulative) of the systems investigated

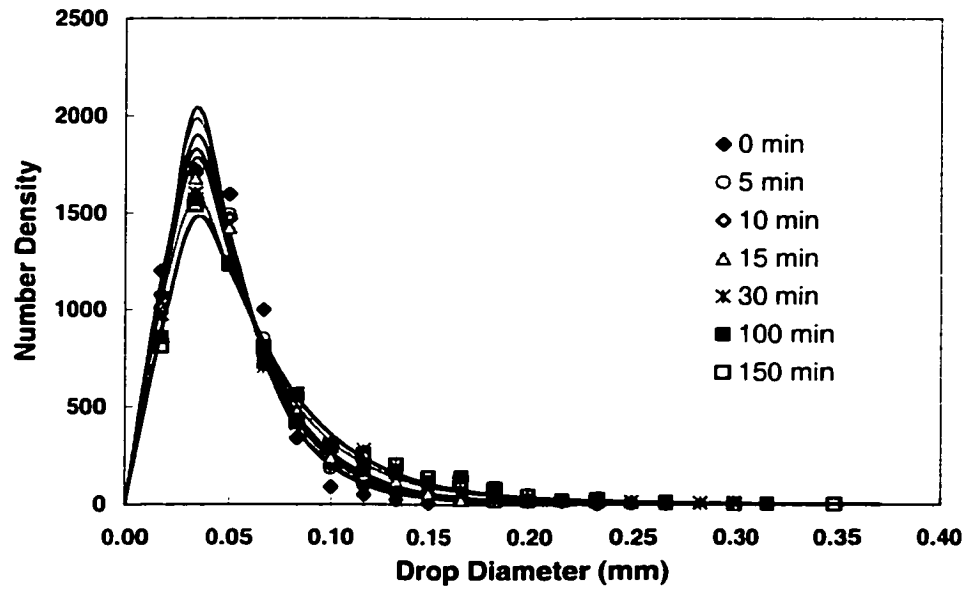


Figure E120. Evolution of number density of (0.75% acetophenon / 0.05 mole aq. NaCl, 300->200 rpm)

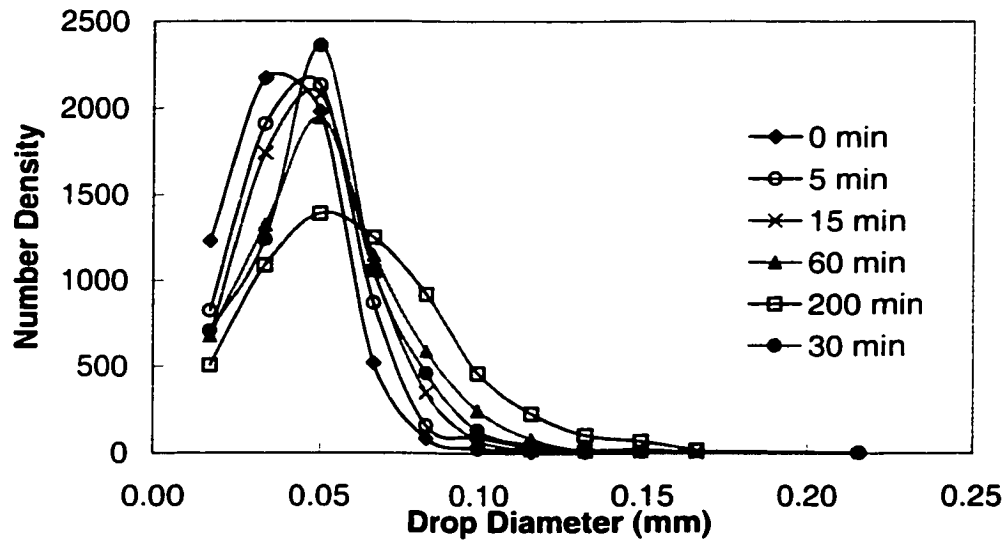


Figure E121. Evolution of number density of (0.75% acetophenon/ 0.05 molar aq. NaCl/ 0.1 mmole/m<sup>3</sup> Triton X100, 300->200 rpm)

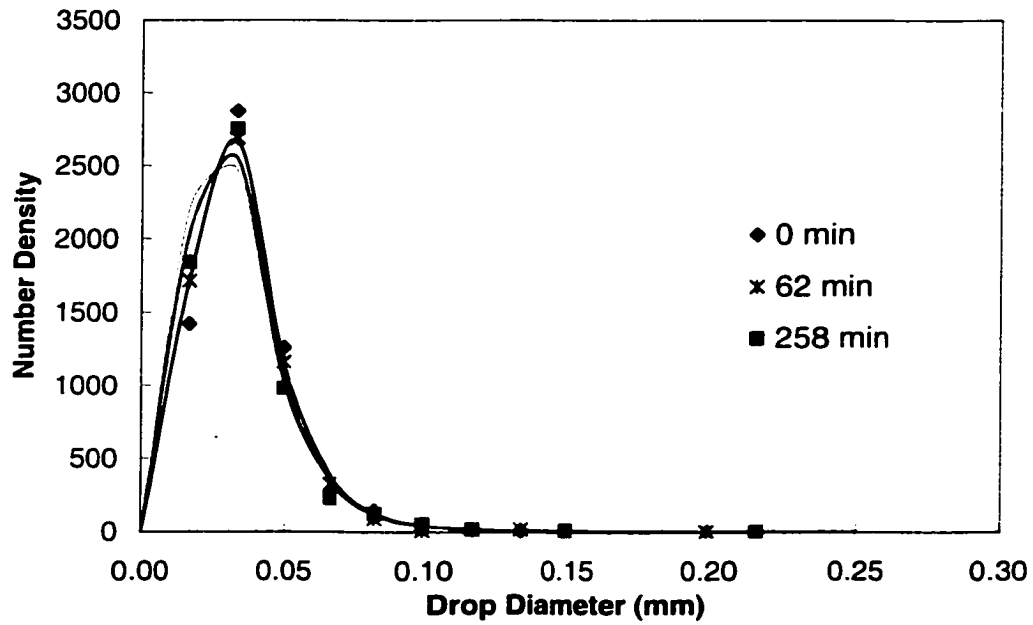


Figure E122. Evolution of number density of (0.75% acetophenon/ 0.05 molar aq. NaCl/ 0.2 mmole/m<sup>3</sup> Triton X100, 300->200 rpm)

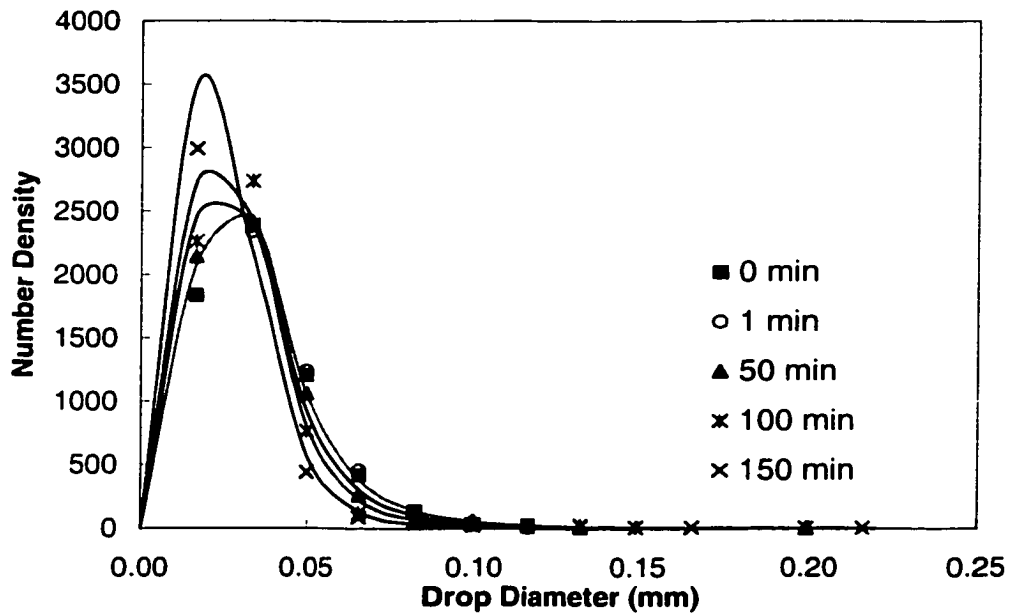


Figure E123. Evolution of number density of (0.75% acetophenon/ 0.05 molar aq. NaCl/ 1.0 mmole/m<sup>3</sup> Triton X100, 300->200 rpm)

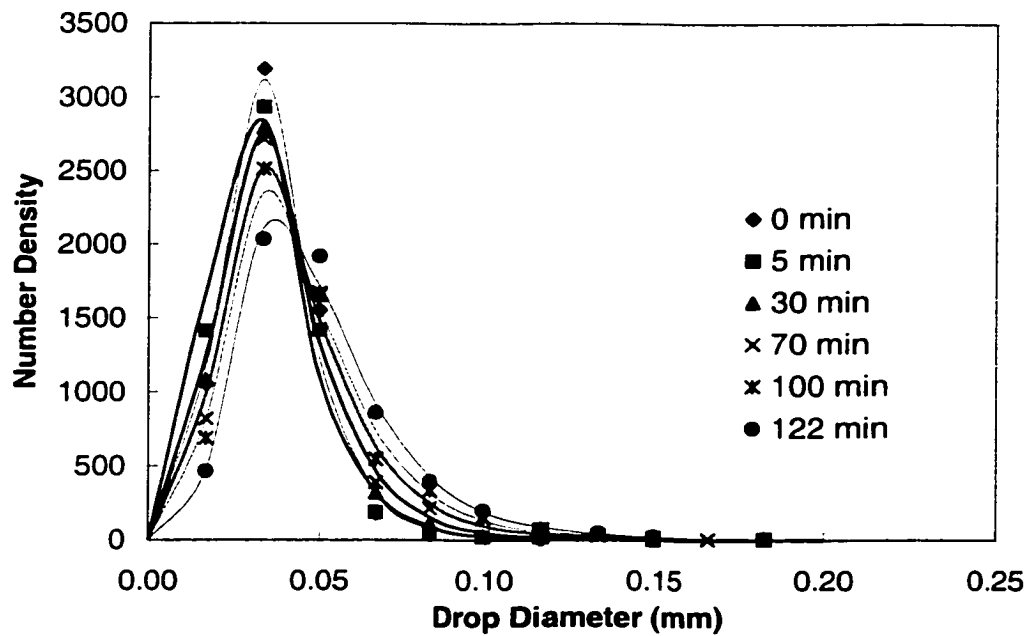


Figure E124. Evolution of number density of (0.75% acetophenon/ 0.05 molar aq. NaCl/ 0.1 mmole/m<sup>3</sup> Triton X165, 300->200 rpm)

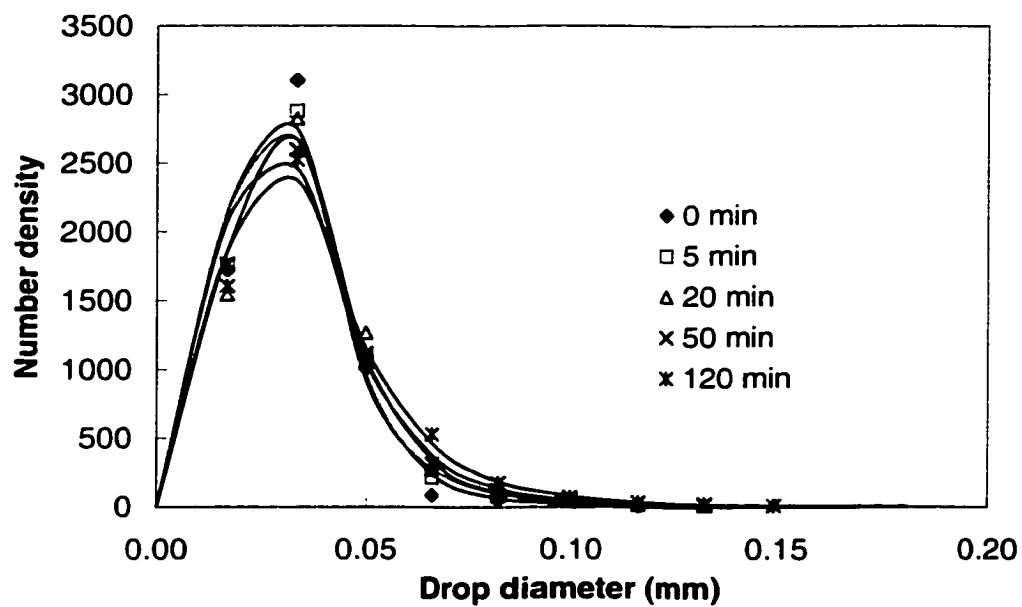


Figure E125. Evolution of number density of 0.75% acetophenon/ 0.05 molar aq. NaCl/ 0.2 mmole/m<sup>3</sup> Triton X165, 300->200 rpm)

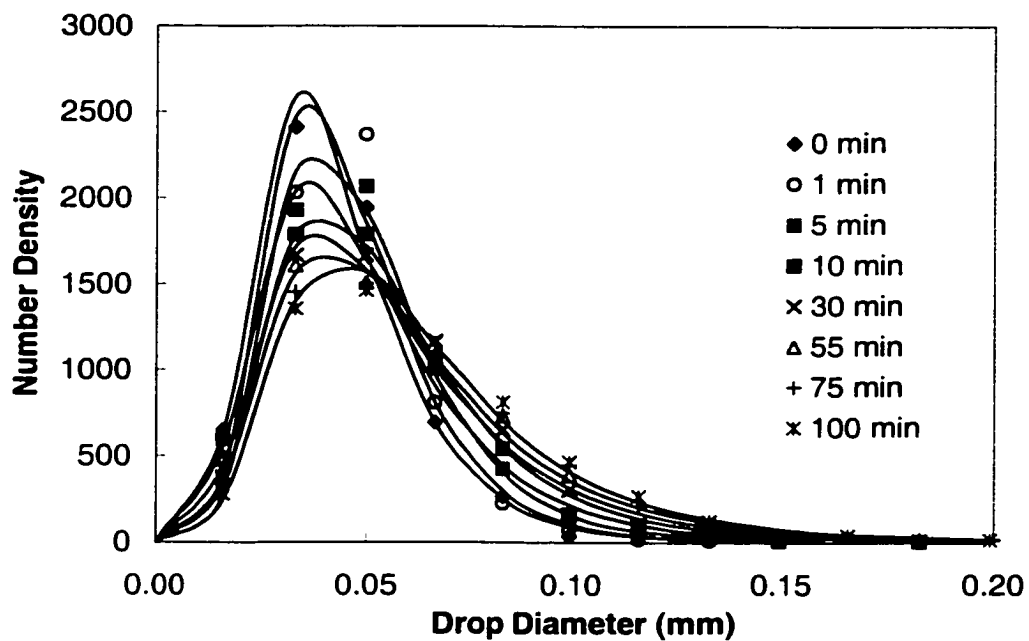


Figure E126. Evolution of number density of (0.75% acetophenon/ 0.05 molar aq. NaCl/0.1 mmole/m<sup>3</sup> Triton X305, 300->200 rpm)

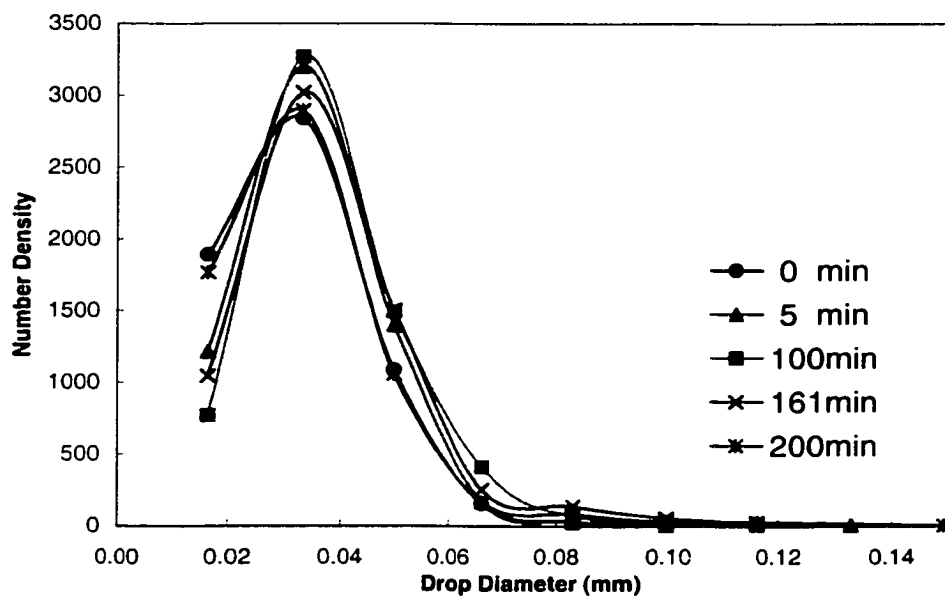


Figure E127. Evolution of number density of (0.75% acetophenon/ 0.05 molar aq. NaCl/ 0.2 mmole/m<sup>3</sup> Triton X305, 300->200 rpm)

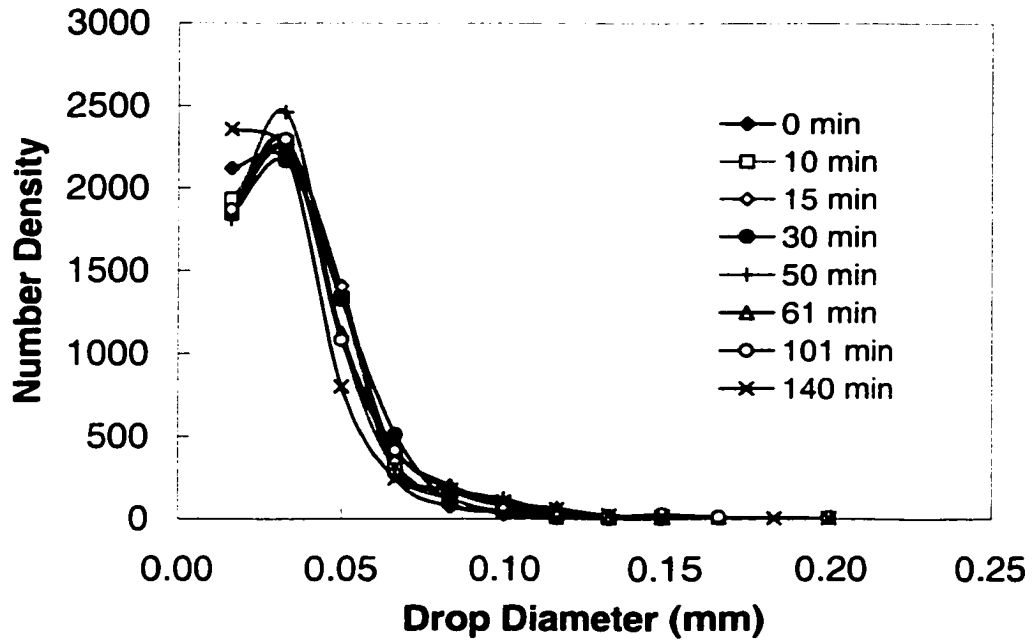


Figure E128. Evolution of number density of (0.75% acetophenon / 0.05 molar aq. NaCl/ 0.1 mmole/m<sup>3</sup> Triton X405, 300->200 rpm)

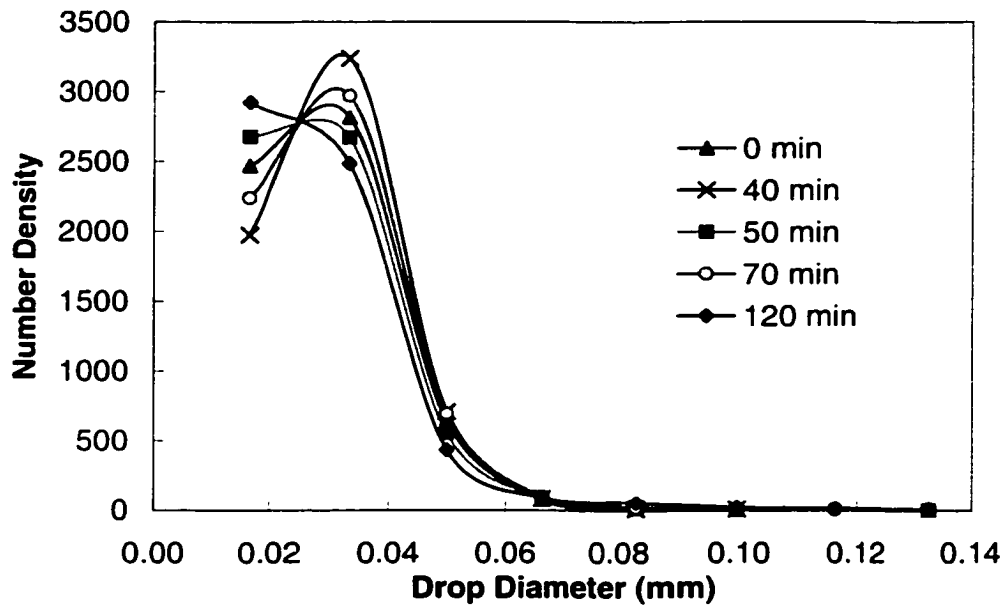


Figure E129. Evolution of number density of (0.75% acetophenon/ 0.05 molar aq. NaCl/0.2 mmole/m<sup>3</sup> Triton X405, 300->200 rpm)

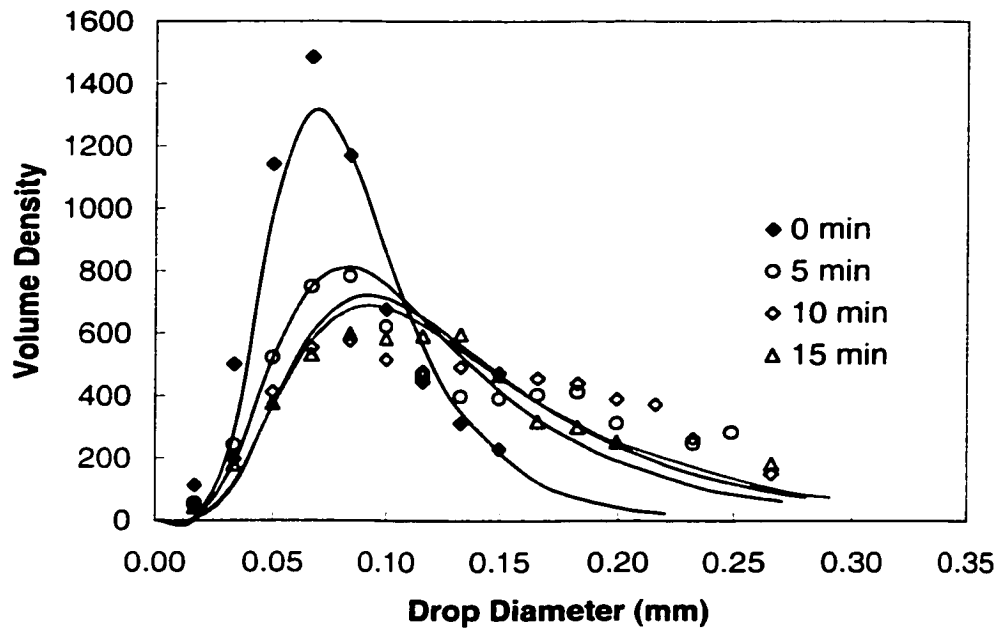


Figure E130a. Evolution of volume density of (0.75% acetophenone/ 0.05 molar aq. NaCl, 300->200 rpm)

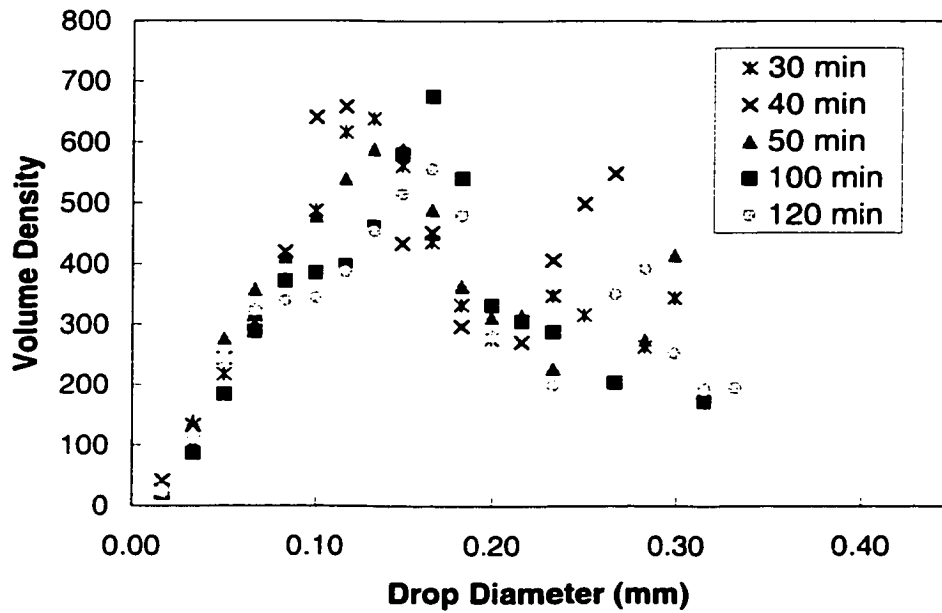


Figure E130b. Evolution of volume density of (0.75% acetophenone/ 0.05 molar aq. NaCl, 300->200 rpm)

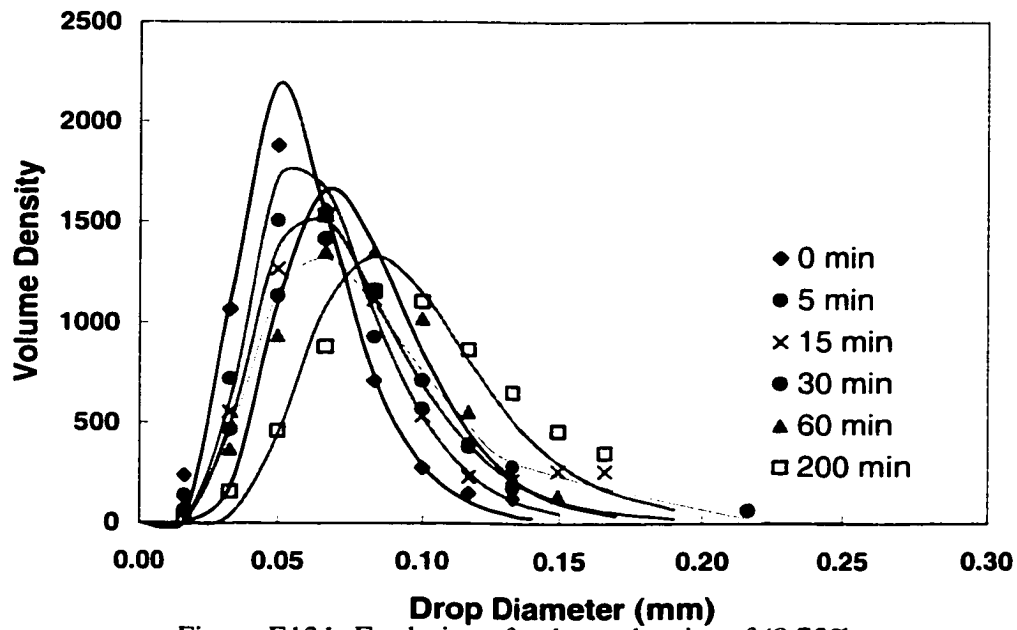


Figure E131. Evolution of volume density of (0.75% acetophenone/ 0.05 molar aq. NaCl/ 0.1 mmole/m<sup>3</sup> Triton X100, 300- $\rightarrow$ 200 rpm)

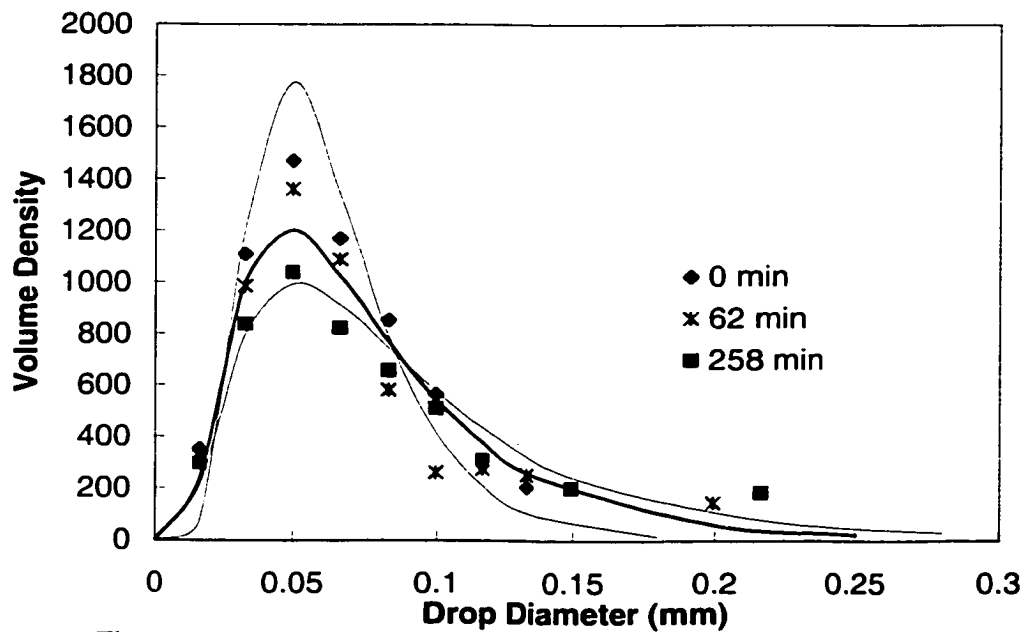


Figure E132. Evolution of volume density of (0.75% acetophenone/ 0.05 molar aq. NaCl/ 0.2 mmole/m<sup>3</sup> Triton X100, 300- $\rightarrow$ 200 rpm)

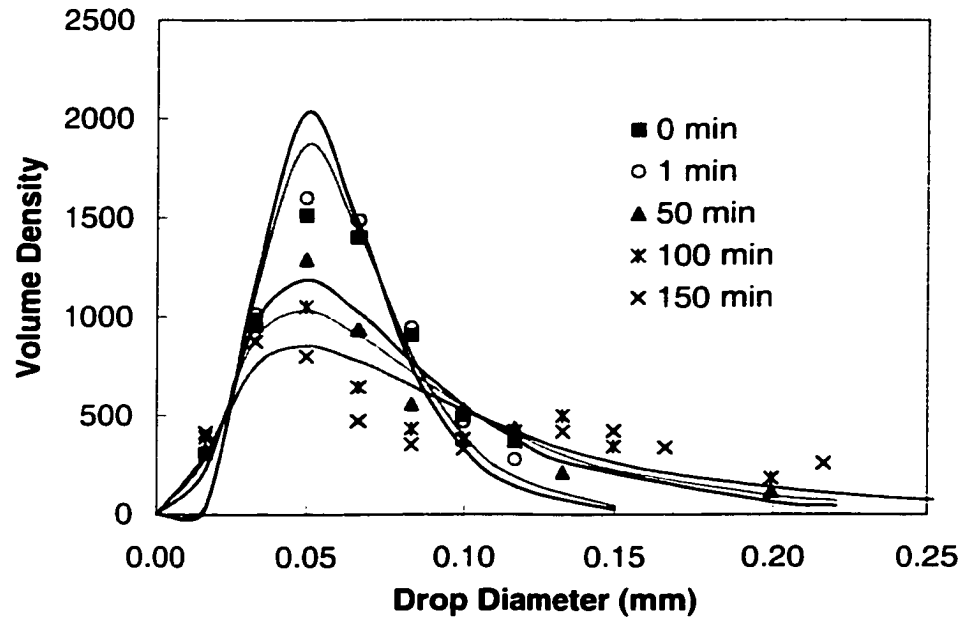


Figure E133. Evolution of volume density of (0.75% acetophenon / 0.05 molar aq. NaCl / 1.0 mmole/m<sup>3</sup> Triton X100, 300->200 rpm)

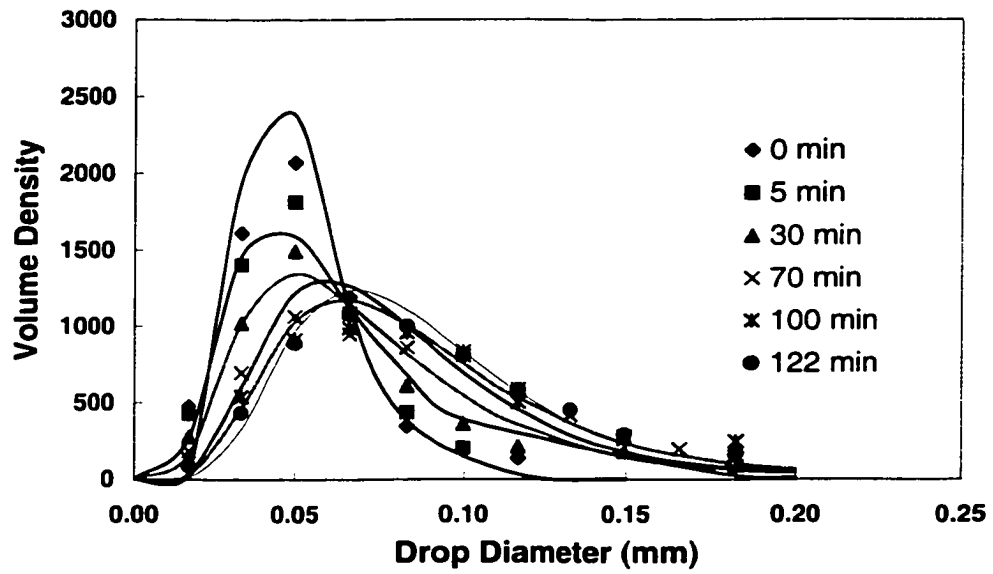


Figure E134. Evolution of volume density of (0.75% acetophenon / 0.05 molar aq. NaCl / 0.1 mmole/m<sup>3</sup> Triton X165, 300->200 rpm)



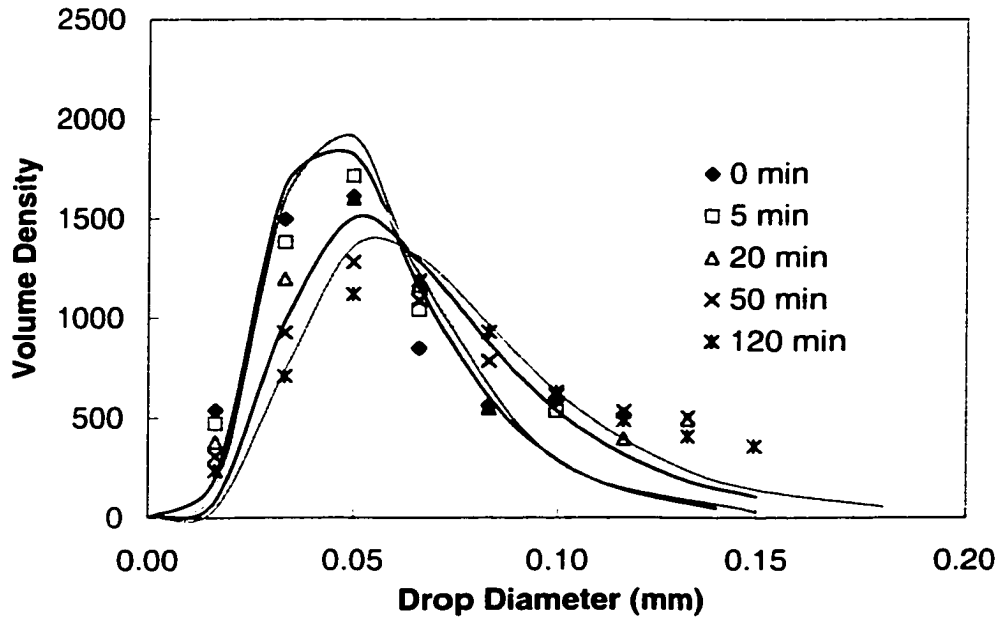


Figure E135. Evolution of volume density of (0.75% acetophenon / 0.05 molar aq. NaCl / 0.2 mmole/m<sup>3</sup> Triton X165, 300->200 rpm)

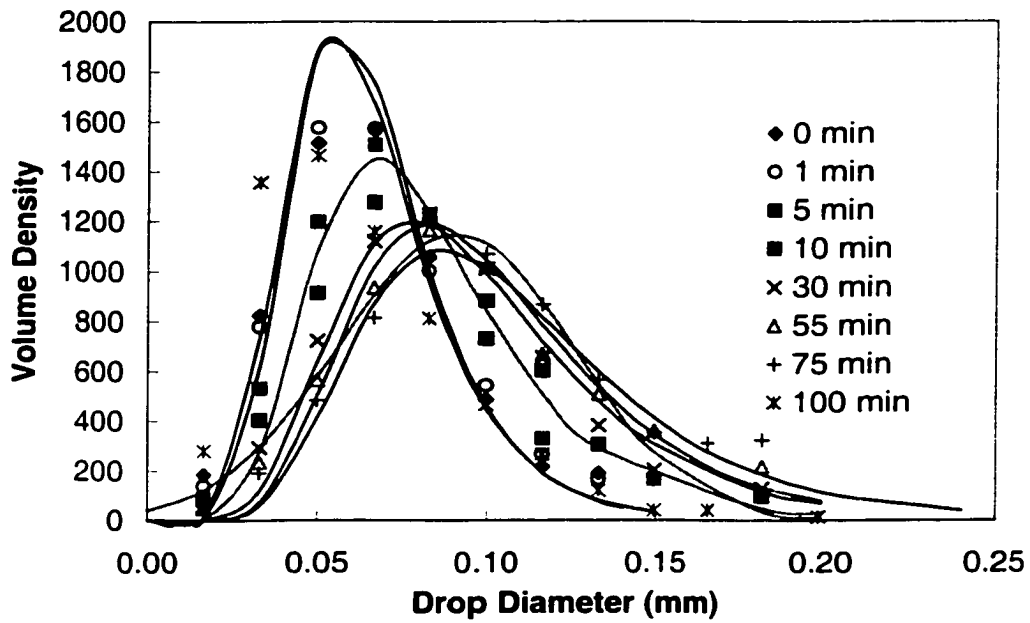


Figure E136. Evolution of volume density of (0.75% acetophenon / 0.05 molar aq. NaCl / 0.1 mmole/m<sup>3</sup> Triton X305, 300->200 rpm)

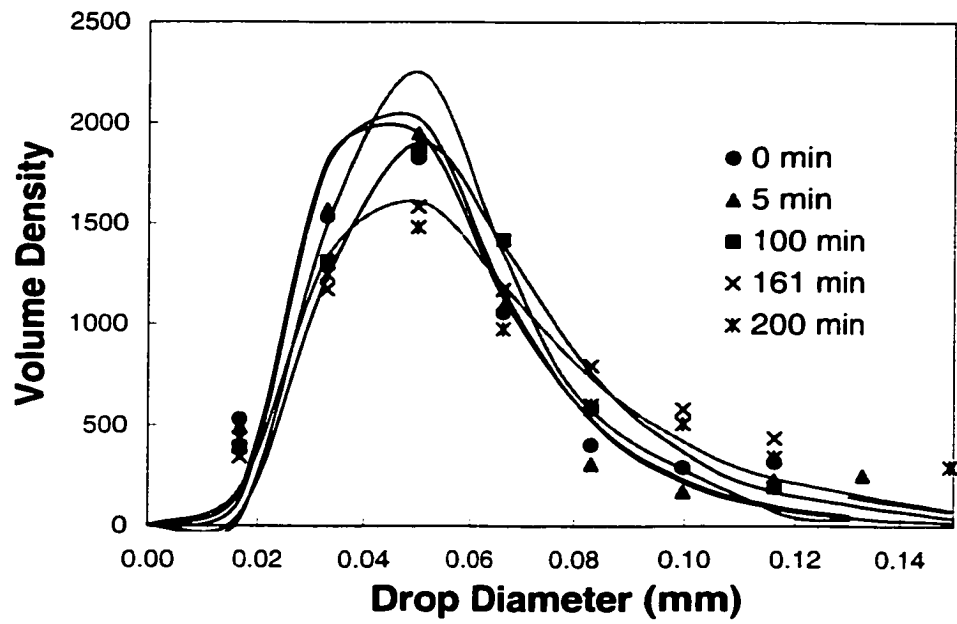


Figure E137. Evolution of volume density of (0.75% acetophenon/ 0.05 molar aq. NaCl/ 0.2 mmole/m<sup>3</sup> Triton X305, 300->200 rpm)

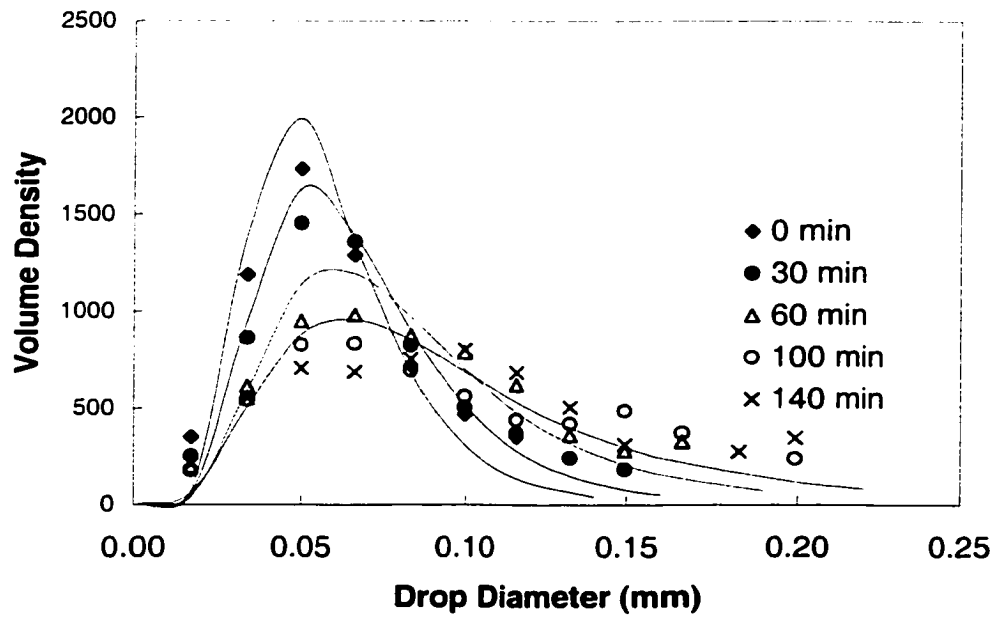


Figure E138. Evolution of volume density of (0.75% acetophenon/ 0.05 molar aq. NaCl/ 0.1 mmole/m<sup>3</sup> Triton X405, 300->200 rpm)

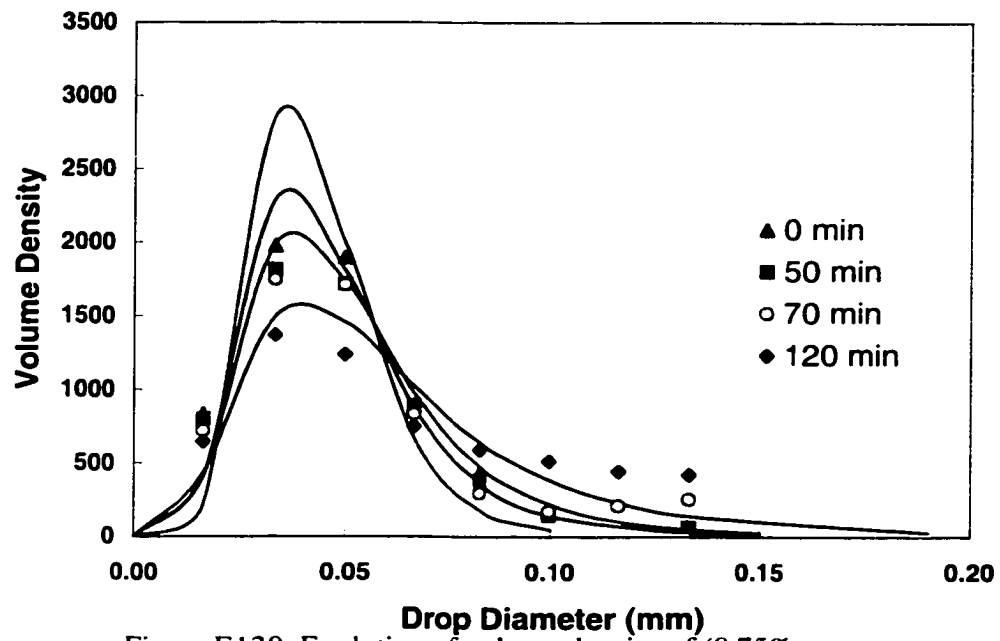


Figure E139. Evolution of volume density of (0.75% acetophenon/ 0.05 molar aq. NaCl/ 0.2 mmole/m<sup>3</sup> Triton X405, 300->200 rpm)

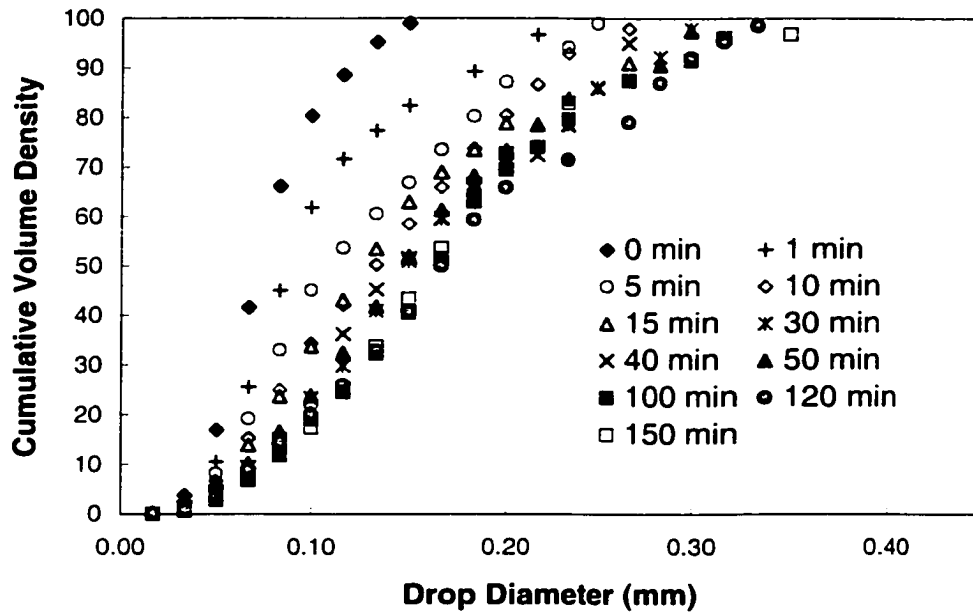


Figure E140. Evolution of cumulative volume density of (0.75% acetophenon/ 0.05 molar aq. NaCl, 300->200 rpm)

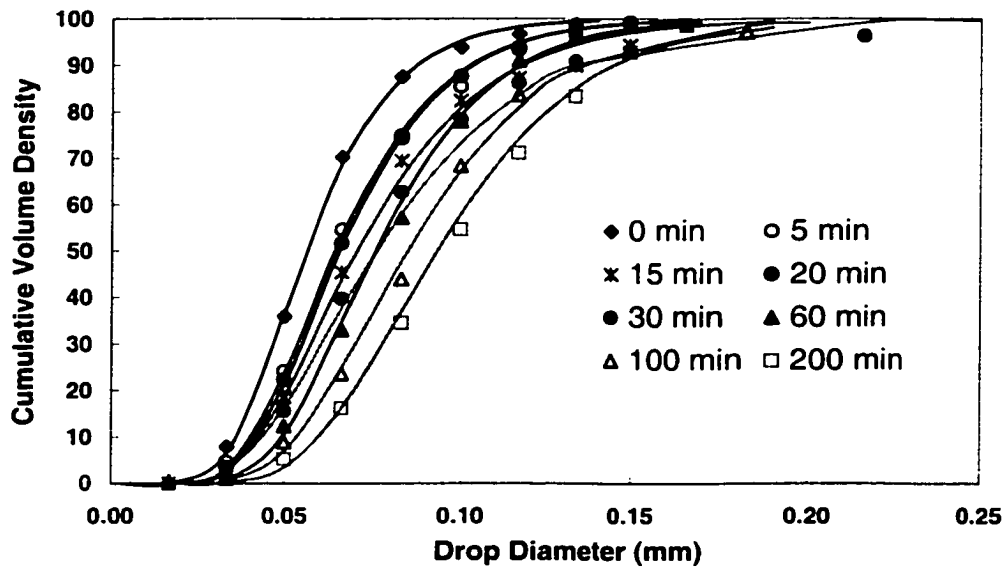


Figure E141. Evolution of cumulative volume density of (0.75% acetophenon/ 0.05 molar aq. NaCl/ 0.1 mmole/m<sup>3</sup> Triton X100, 300->200 rpm)

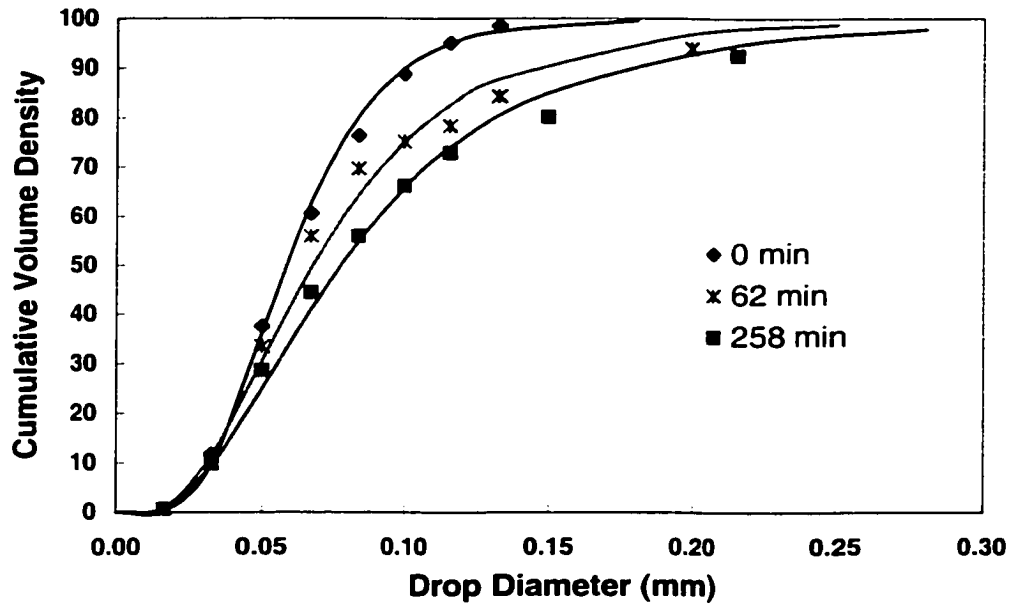


Figure E142. Evolution of cumulative volume density of (0.75% acetophenon/ 0.05 molar aq. NaCl/ 0.2 mmole/m<sup>3</sup> Triton X100, 300->200 rpm)

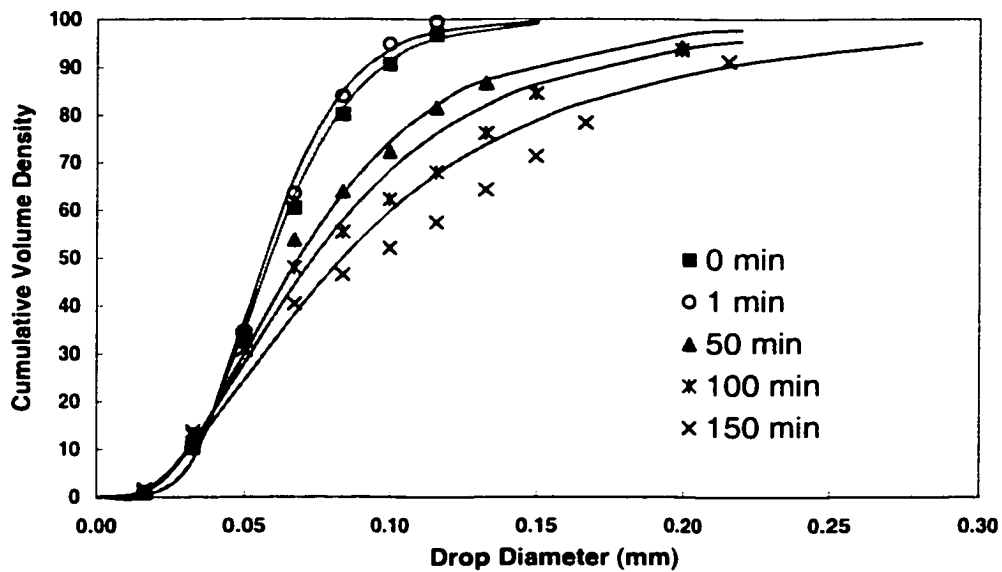


Figure E143. Evolution of cumulative volume density of 0.75% acetophenon/ 0.05 molar aq. NaCl/ 1.0 mmole/m<sup>3</sup> Triton X100, 300->200 rpm)

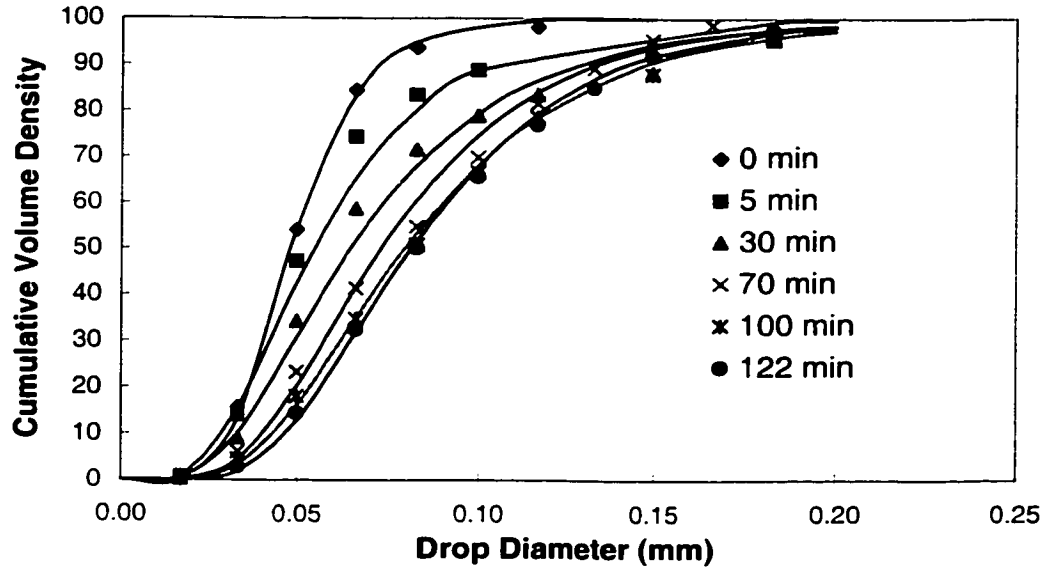


Figure E144. Evolution of cumulative volume density of 0.75% acetophenon / 0.05 molar aq. NaCl / 0.1 mmole/m<sup>3</sup> Triton X165, 300->200 rpm)

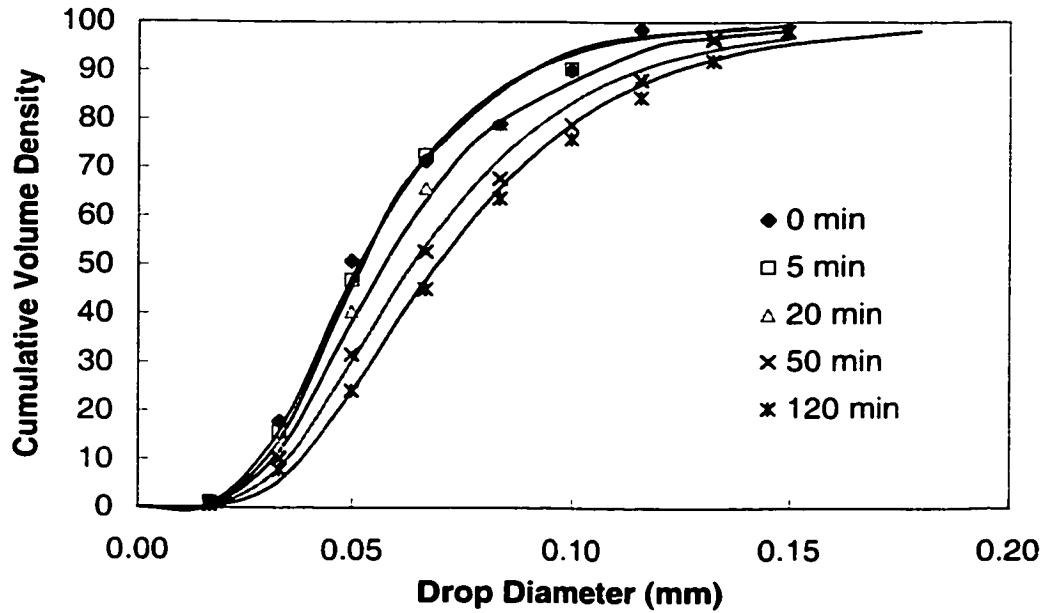


Figure E145. Evolution of cumulative volume density of (0.75% acetophenon / 0.05 molar aq. NaCl / 0.2 mmole/m<sup>3</sup> Triton X165, 300->200 rpm)

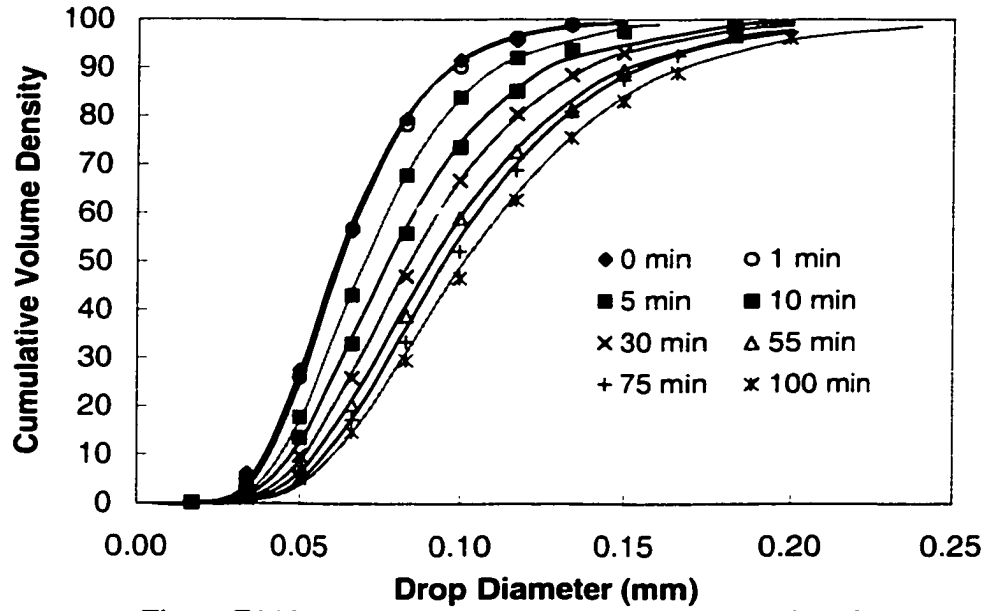


Figure E146. Evolution of cumulative volume density of (0.75% acetophenon/ 0.05 molar aq. NaCl/ 0.1 mmole/m<sup>3</sup> Triton X305, 300->200 rpm)

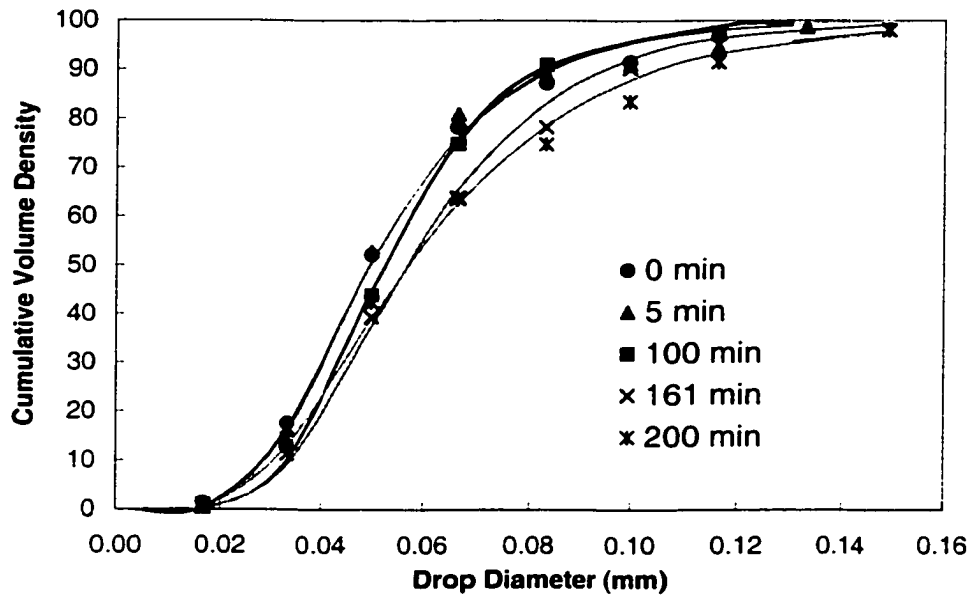


Figure E147. Evolution of cumulative volume density of (0.75% acetophenon/ 0.05 molar aq. NaCl/ 0.2 mmole/m<sup>3</sup> Triton X305, 300->200 rpm)

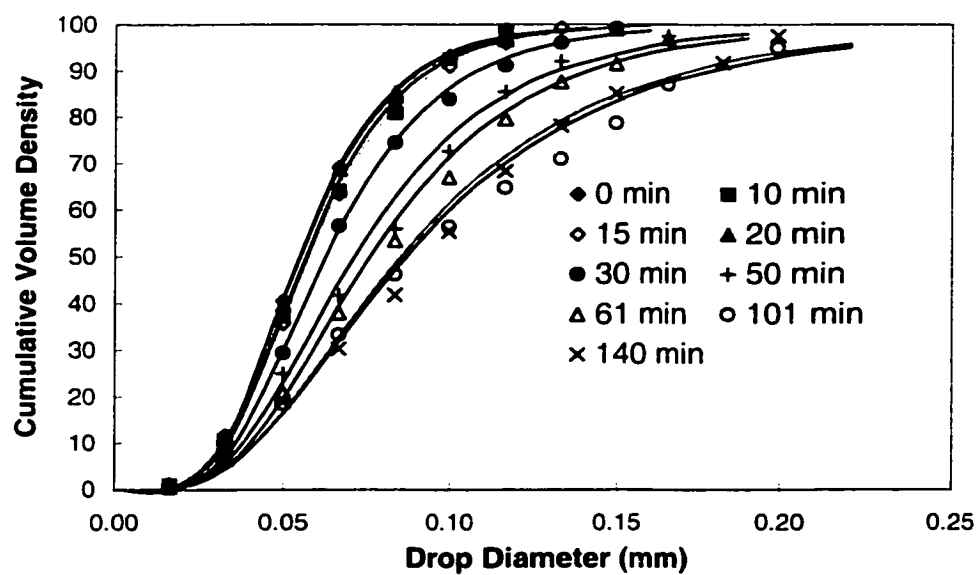


Figure E148. Evolution of cumulative volume density of (0.75% acetophenon/ 0.05 molar aq. NaCl/ 0.1 mmole/m<sup>3</sup> Triton X405, 300->200 rpm)

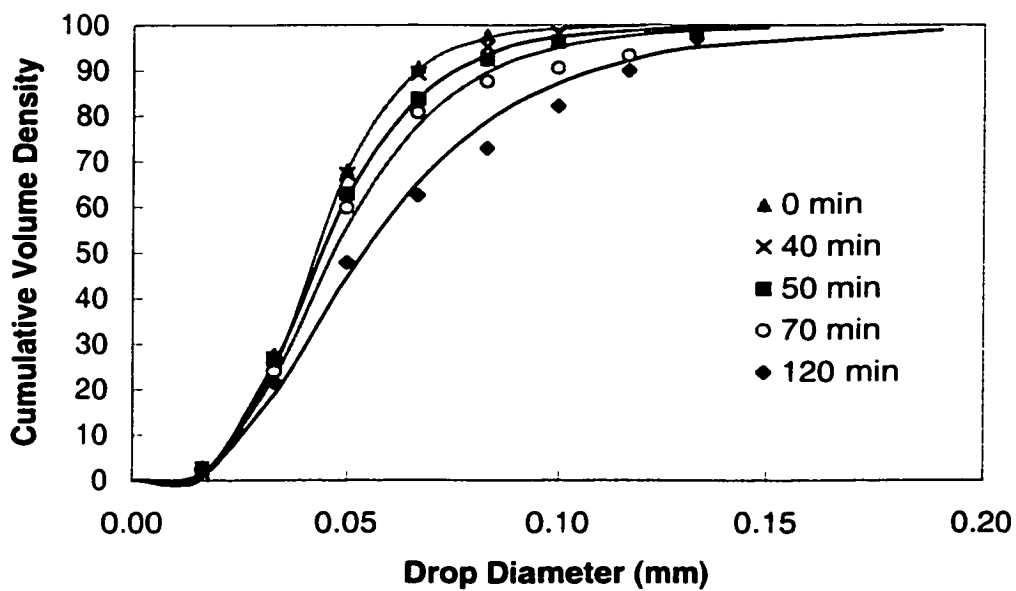


Figure E149. Evolution of cumulative volume density of 0.75% acetophenon/ 0.05 molar aq. NaCl/ 0.2 mmole/m<sup>3</sup> Triton X405, 300->200 rpm)



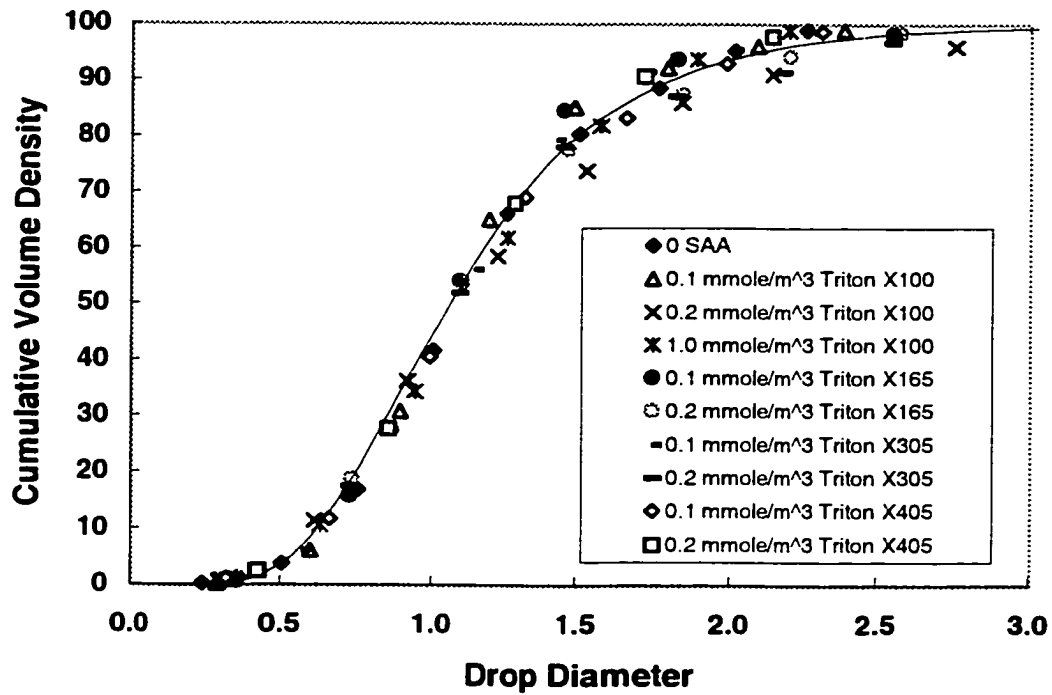


Figure F150. Self-similarity of (0.75% acetophenon/ 0.05 molar aq. NaCl/ Triton, 300 rpm) at quasi-steady

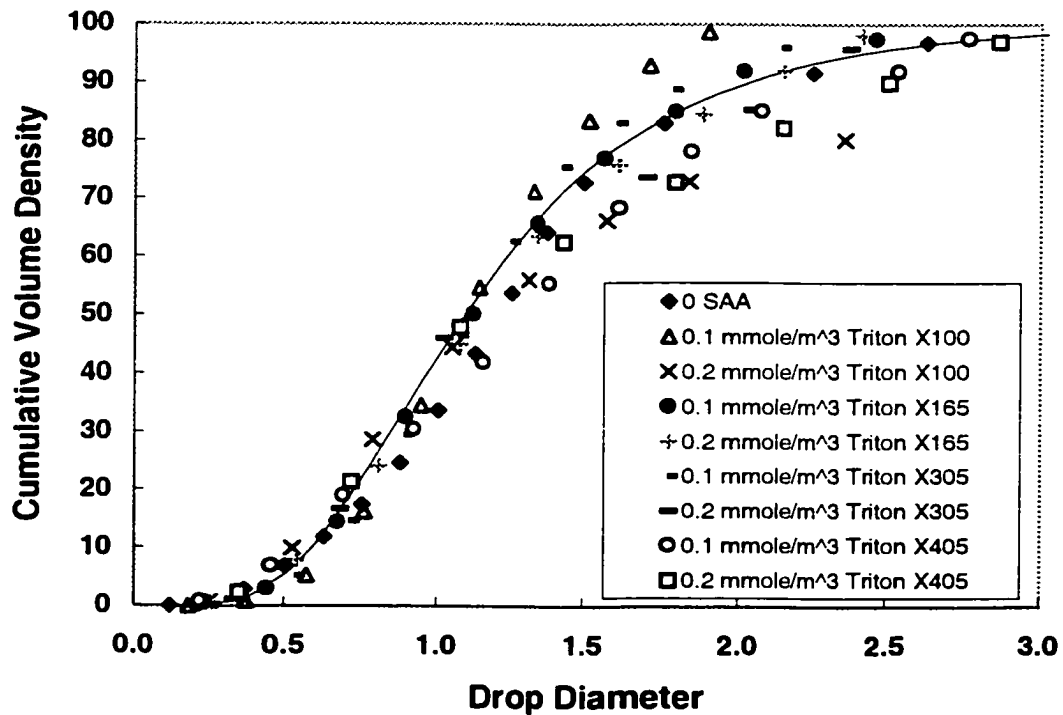


Figure F151. Self-similarity of (0.75% acetophenon/ 0.05 molar aq. NaCl/ Triton, 200 rpm) at quasi-steady

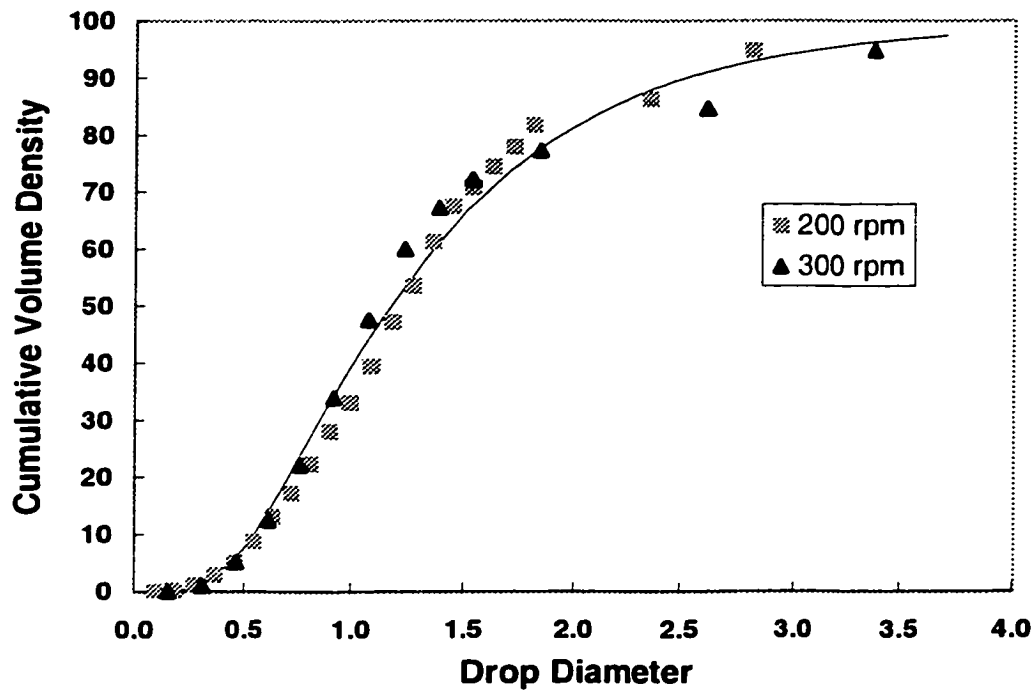


Figure F152. Self-similarity of (0.5% CLB-Bayol oil/water)

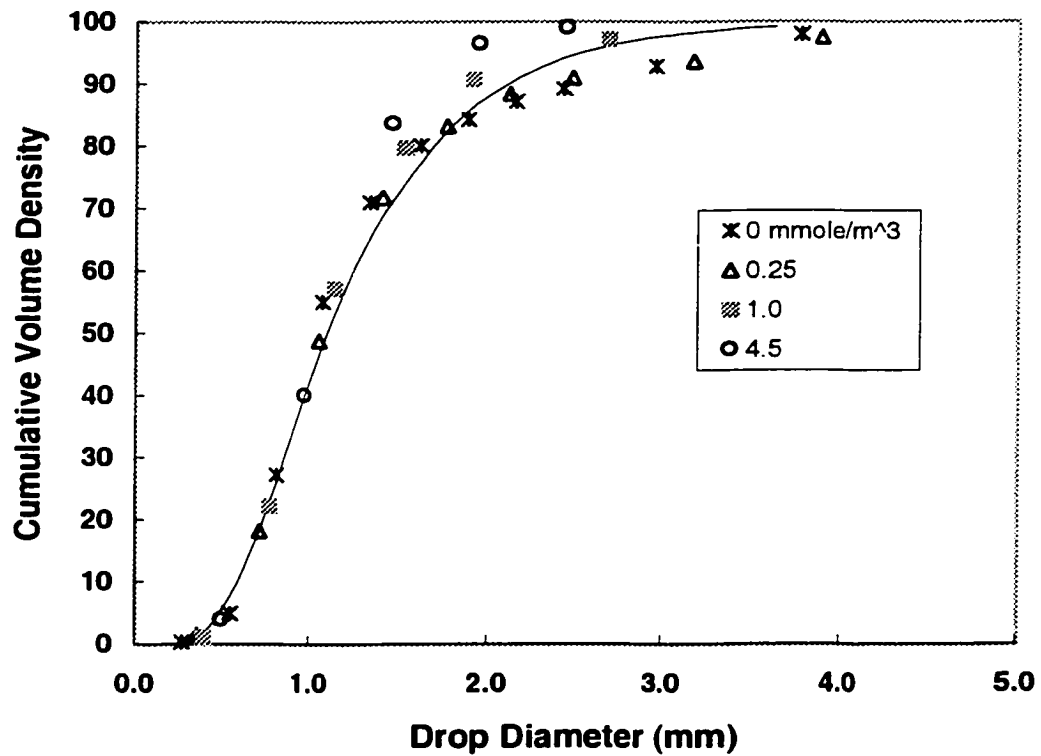


Figure F153. Self-similarity of (0.5% Bayol oil/ water/ Triton X100)

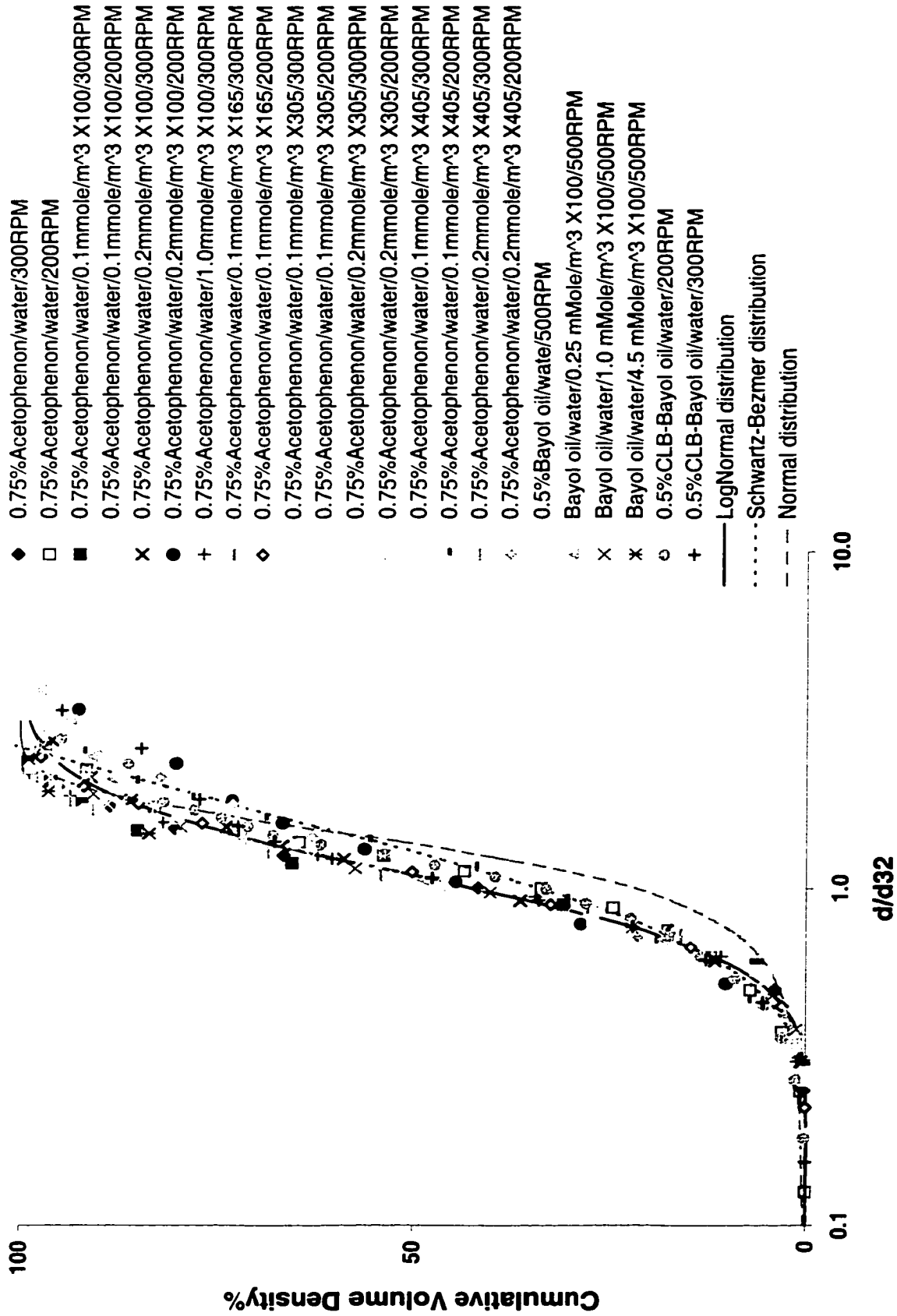


Figure F154. Similarity behavior of all systems studied

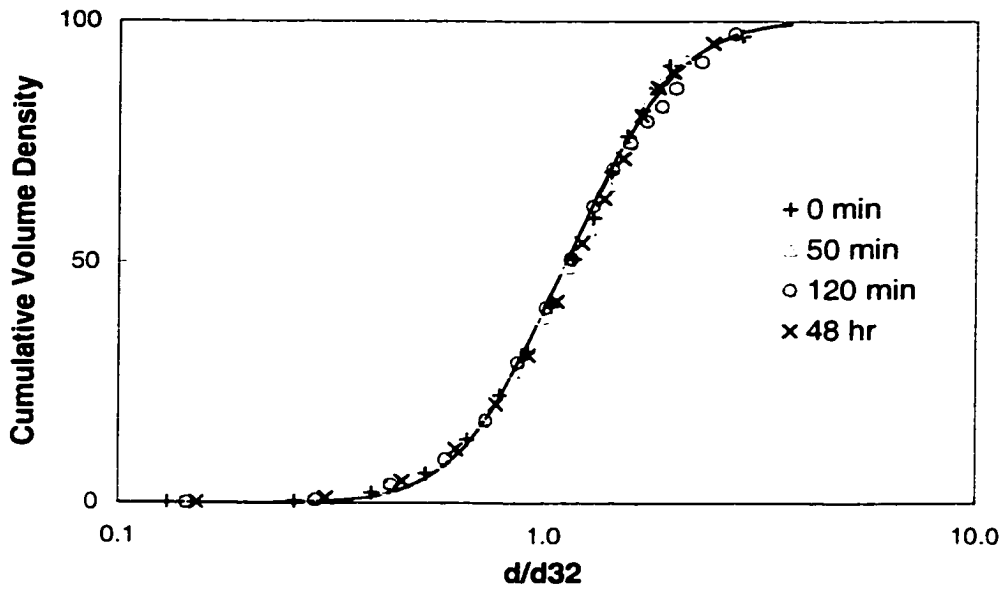


Figure F155. Self-similarity behavior of temporal size distribution of (0.5% CLB-Bayol oil / water / 1.0 mmole/m<sup>3</sup> Triton X100, 250 rpm)

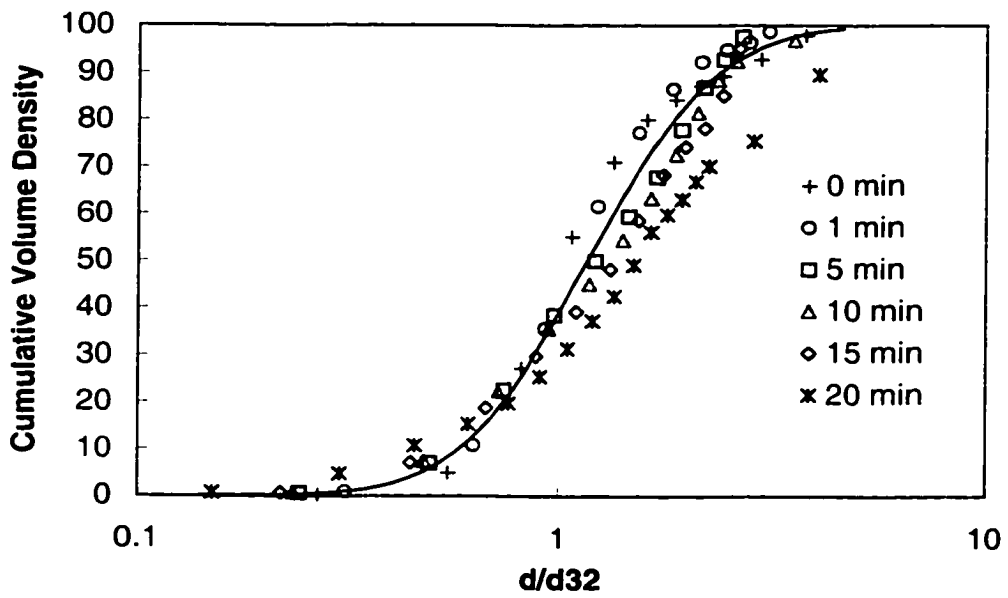


Figure F156. Self-similarity behavior of temporal size distribution of (0.5% Bayol oil / water, 500->250 rpm)

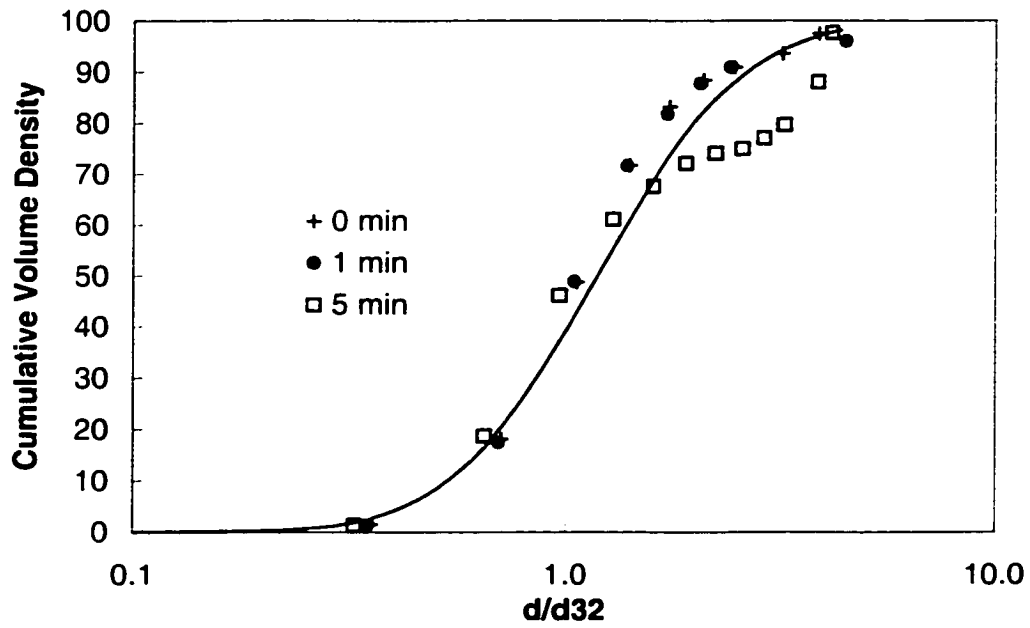


Figure F157. Self-similarity behavior of temporal size distribution of (0.5% Bayol oil / water / 0.25 mmole/m<sup>3</sup> Triton X100, 500->250 rpm)

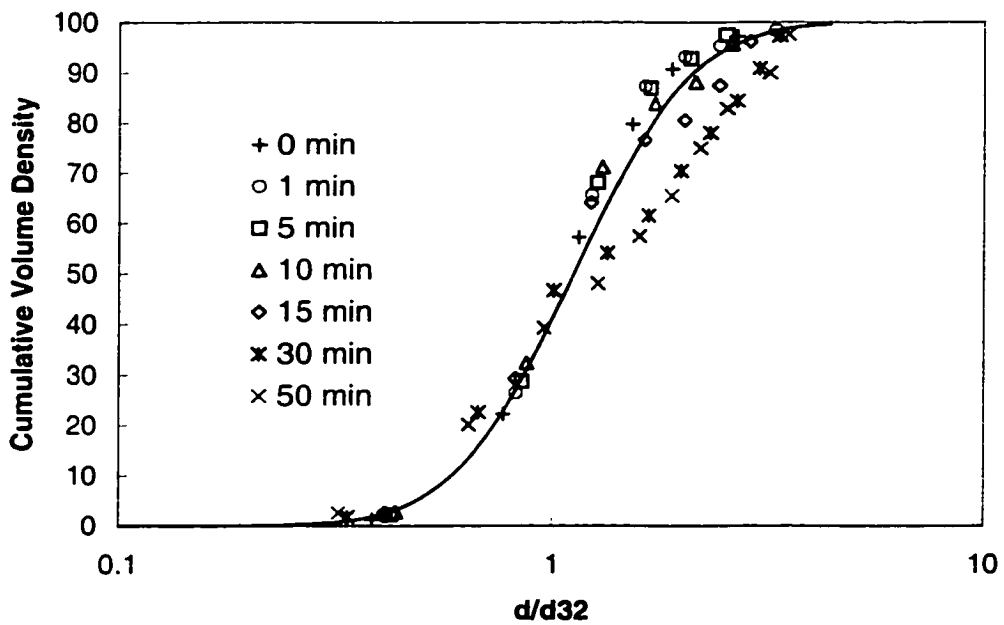


Figure F158. Self-similarity behavior of temporal size distribution of (0.5% Bayol oil / water / 1.0 mmole/m<sup>3</sup> Triton X100, 500->250 rpm)

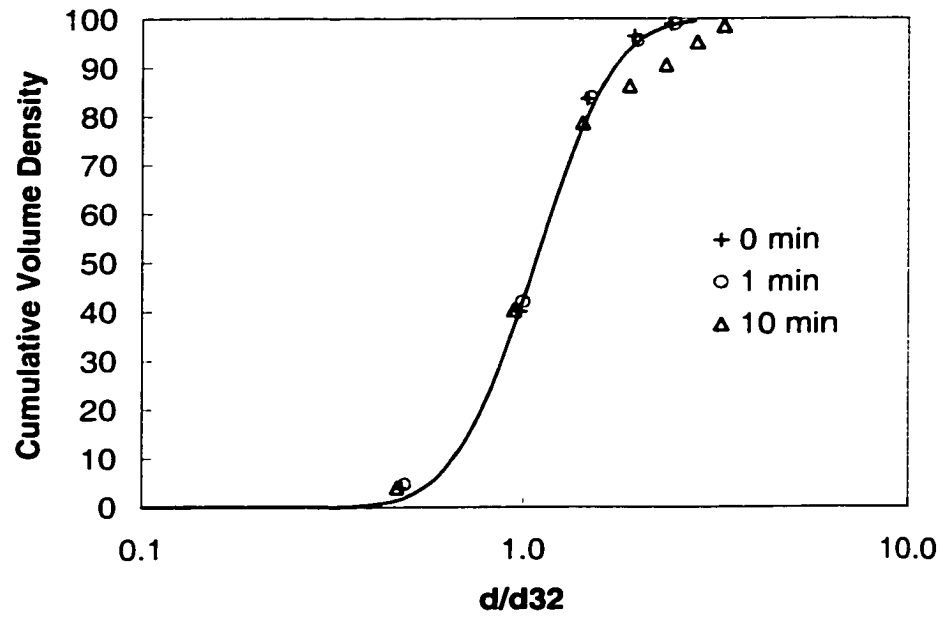


Figure F159. Self-similarity behavior of temporal size distribution of (0.5% Bayol oil / water / 4.6 mmole/m<sup>3</sup> Triton X100, 500-→250 rpm)

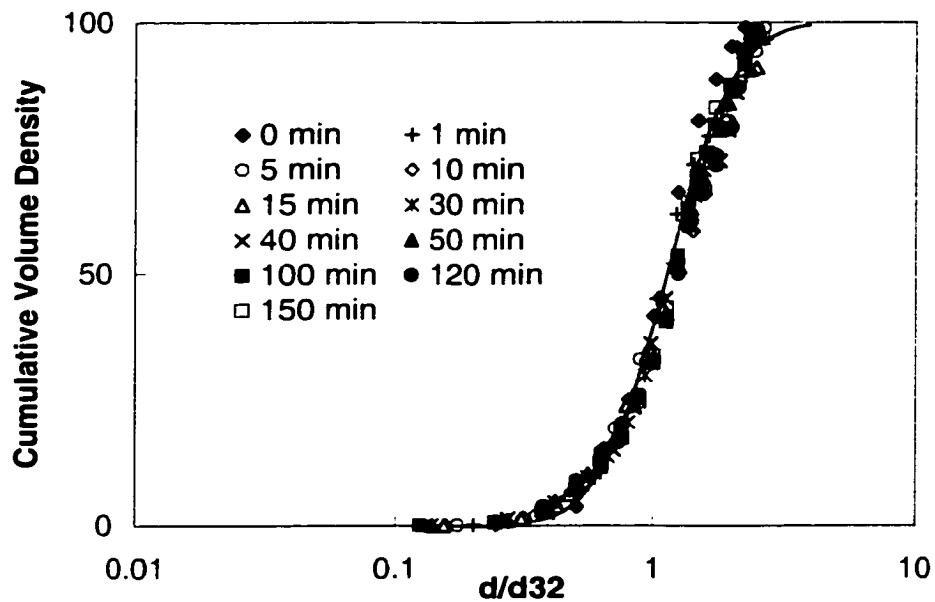


Figure F160. Self-similarity behavior of temporal size distribution of (0.75% acetophenon / 0.05 M aq. NaCl, 300->200rpm)

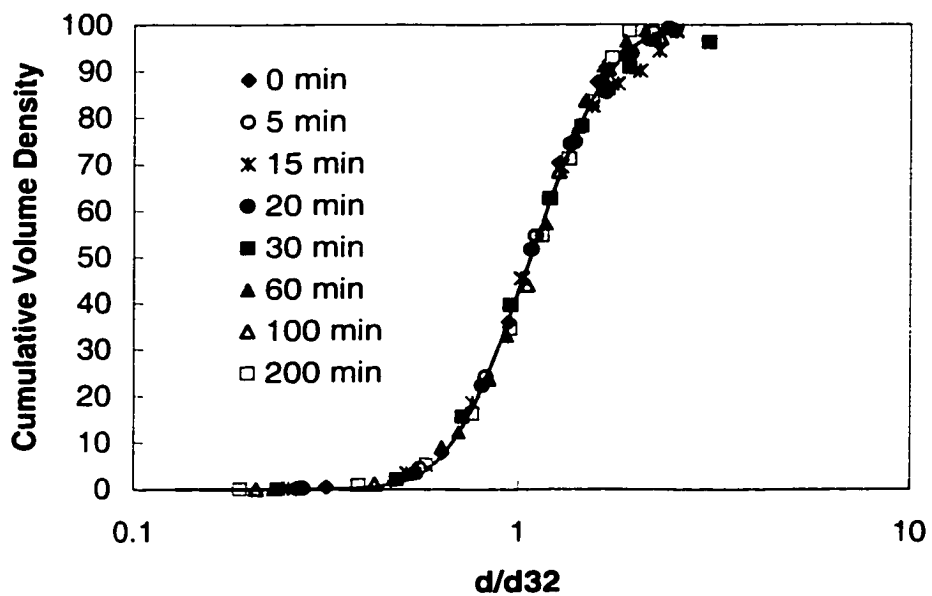


Figure F161. Similarity behavior of temporal size distribution of 0.75% acetophenon / 0.05 M aq. NaCl / 0.1 mmole/m<sup>3</sup> Triton X100, 300->200 rpm)

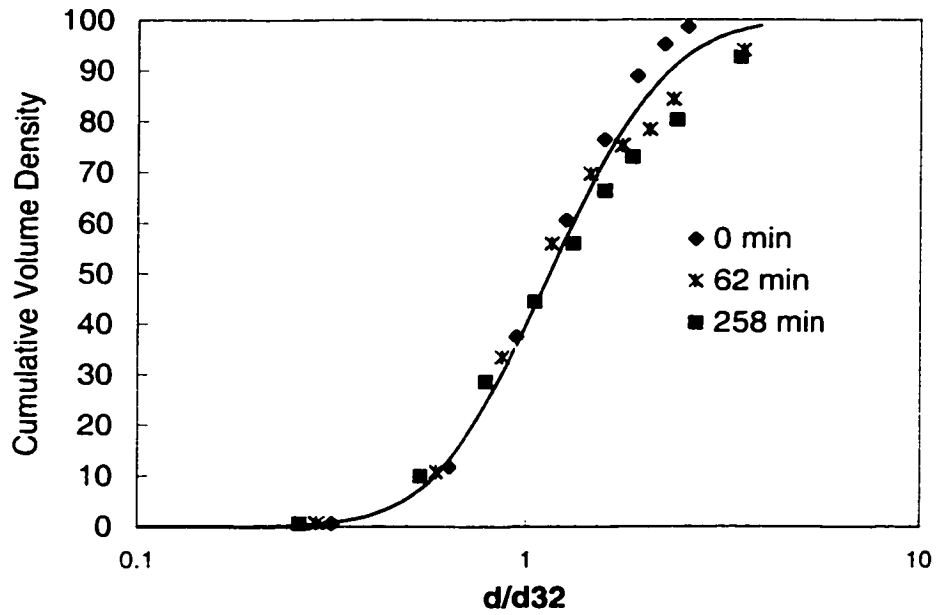


Figure F162. Similarity behavior of temporal size distribution of (0.75% acetophenon / 0.05M aq. NaCl / 0.2 mmole/m<sup>3</sup> Triton X100, 300->200 rpm)

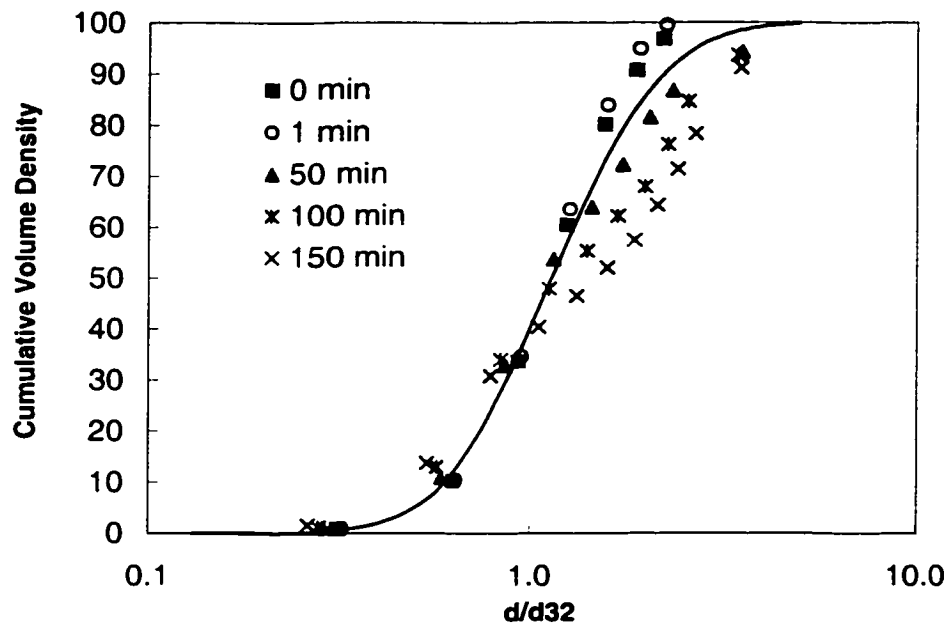


Figure F163. Similarity behavior of (0.75% acetophenon / 0.05 M aq. NaCl / 1.0 mmole/m<sup>3</sup> Triton X100, 300->200 rpm)



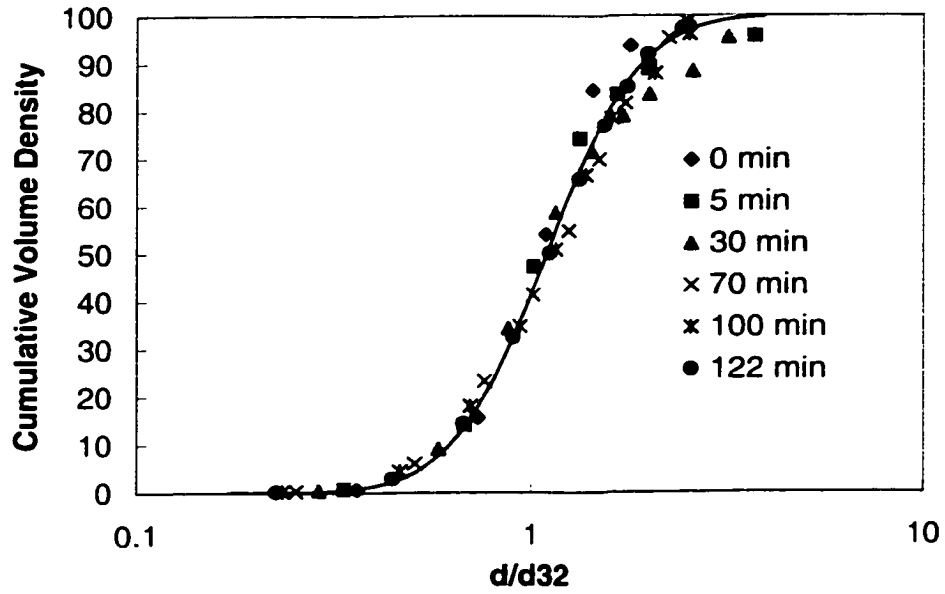


Figure F164. Self-similarity behavior of (0.75% acetophenon / 0.05 M aq. NaCl / 0.1 mmole/m<sup>3</sup> Triton X165, 300->200 rpm)

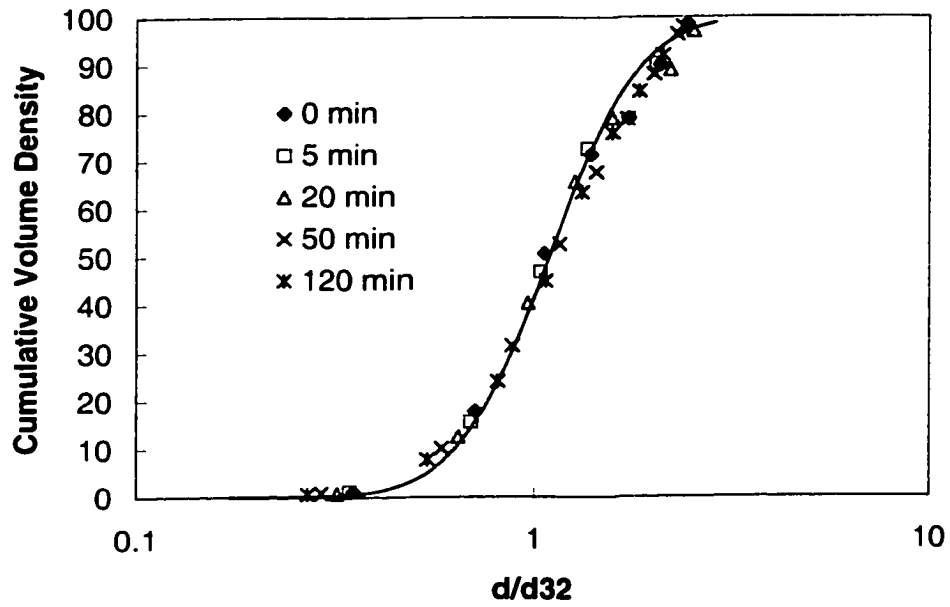


Figure F165. Similarity behavior of temporal size distribution of (0.75% acetophenon / 0.05 M aq. NaCl / 0.2 mmole/m<sup>3</sup> Triton X165, 300->200 rpm)

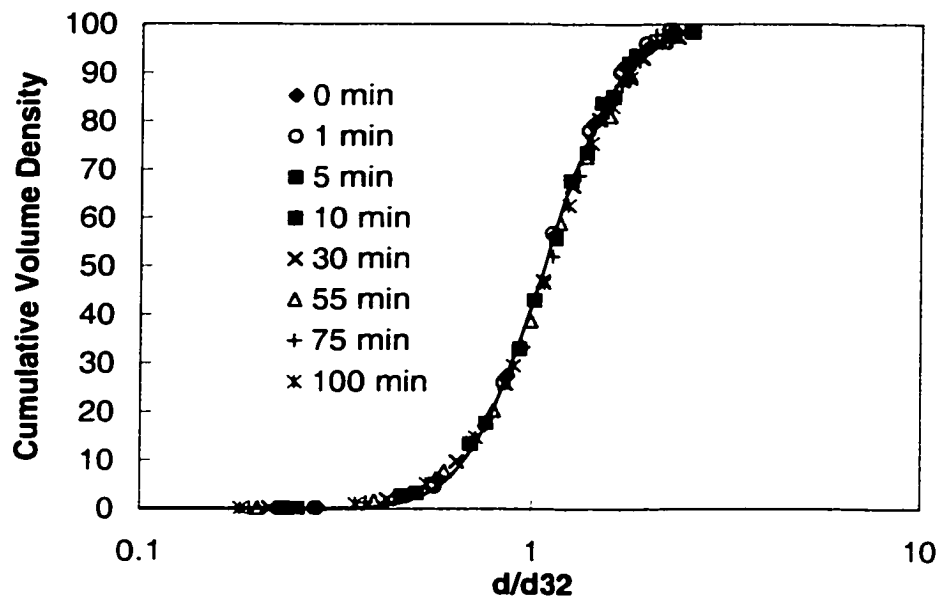


Figure F166. Similarity behavior of temporal size distribution of (0.75% acetophenon / 0.05 M aq. NaCl / 0.1 mmole/m<sup>3</sup> Triton X305, 300- $\rightarrow$ 200RPM)

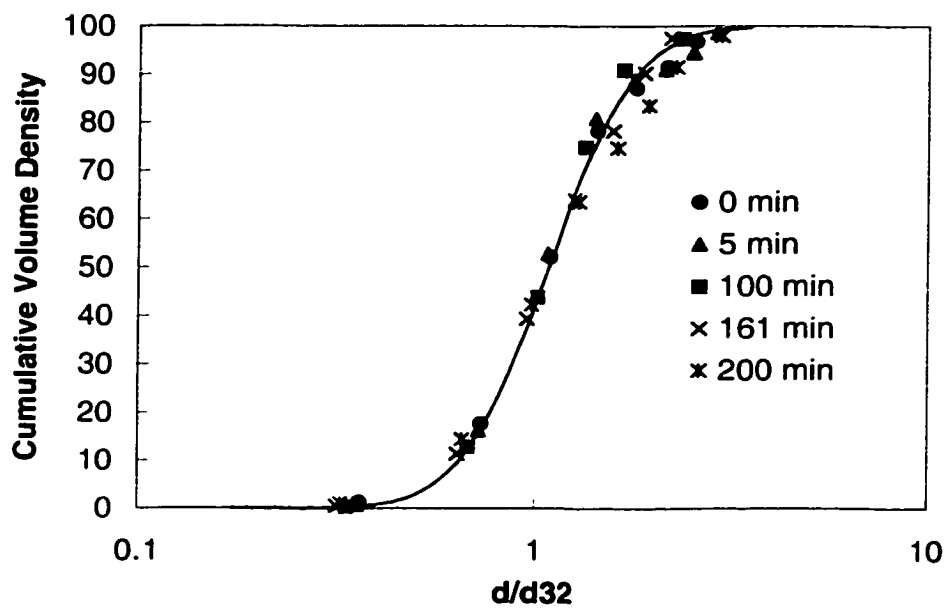


Figure F167. Similarity behavior of temporal size distribution of (0.75% acetophenon / 0.05 M aq. NaCl / 0.2 mmole/m<sup>3</sup> Triton X305, 300- $\rightarrow$ 200 rpm)

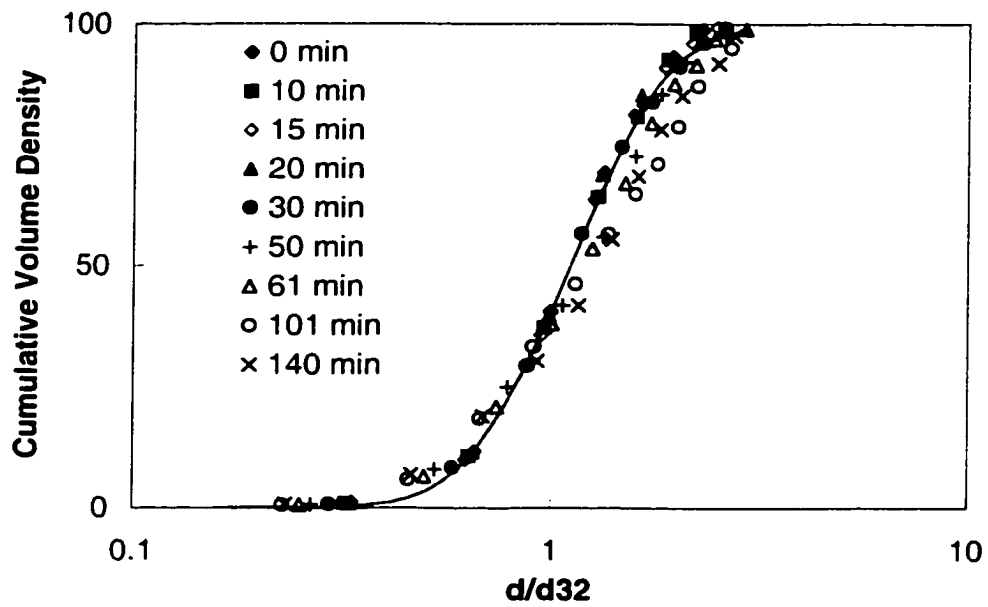


Figure F168. Self-similarity behavior of temporal size distribution of (0.75% acetophenon / 0.05 M aq. NaCl / 0.1 mmole/m<sup>3</sup> Triton X405, 300- $\rightarrow$ 200 rpm)

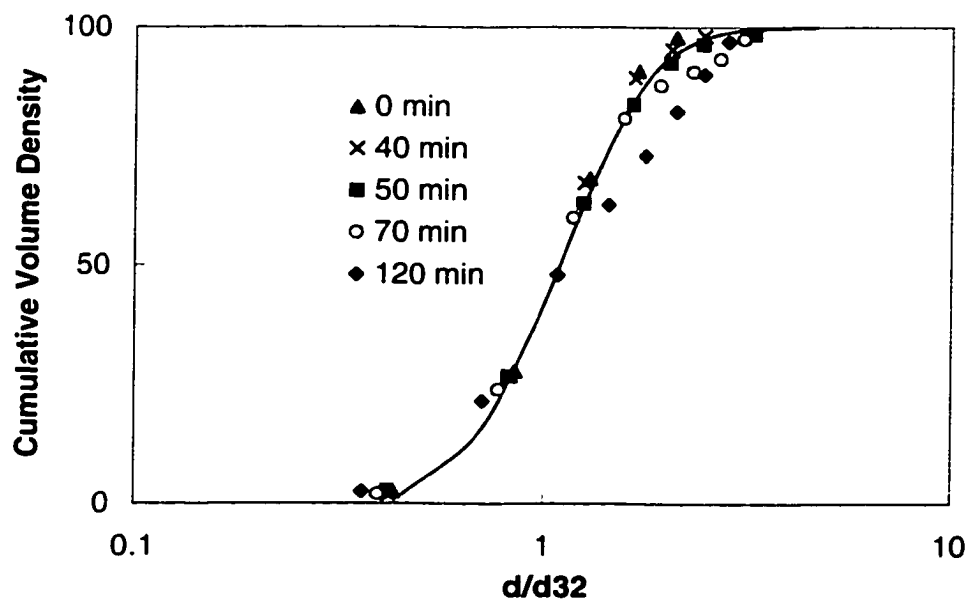


Figure F169. Self-similarity behavior of temporal size distribution of (0.75% acetophenon / 0.05 M aq. NaCl / 0.2 mmole/m<sup>3</sup> Triton X405, 300- $\rightarrow$ 200 rpm)

## APPENDIX G

This appendix contains figures of the transient average drop diameter of the systems investigated.

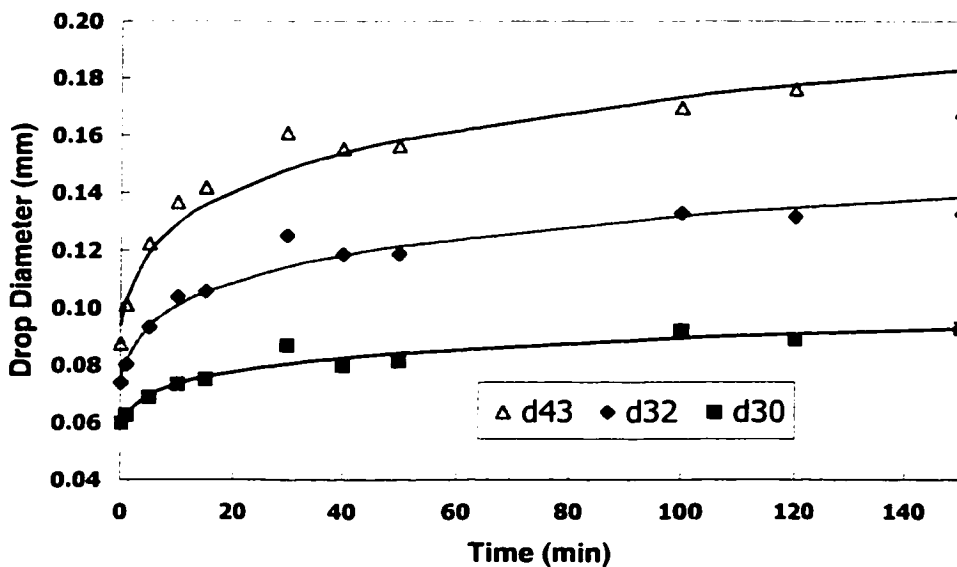


Figure G170. Transient average drop size of (0.75% acetophenon/ 0.05 mole aq. NaCl, 300->200 rpm)

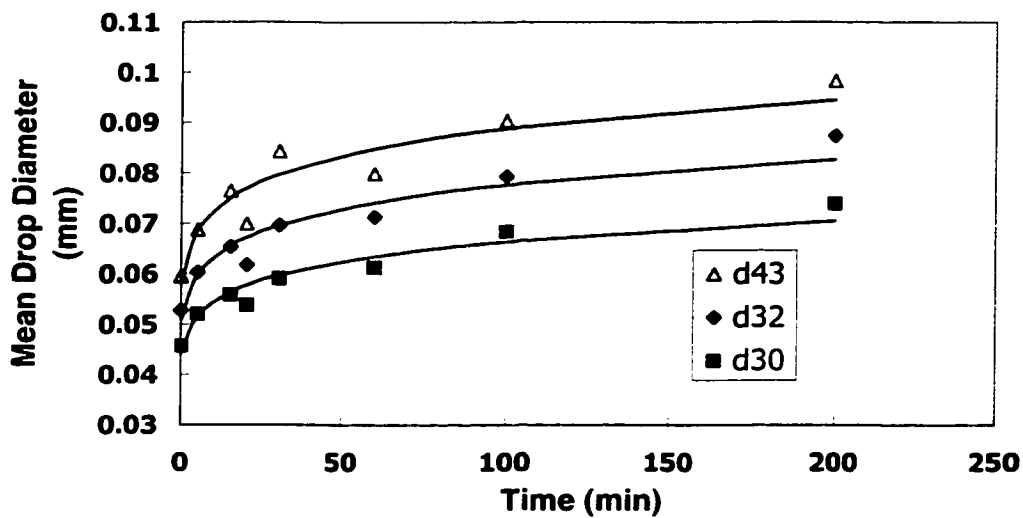


Figure G171. Transient average drop size of (0.75% acetophenon / 0.05 mole aq. NaCl/ 0.1 mmole/m<sup>3</sup> Triton X100, 300->200 rpm)

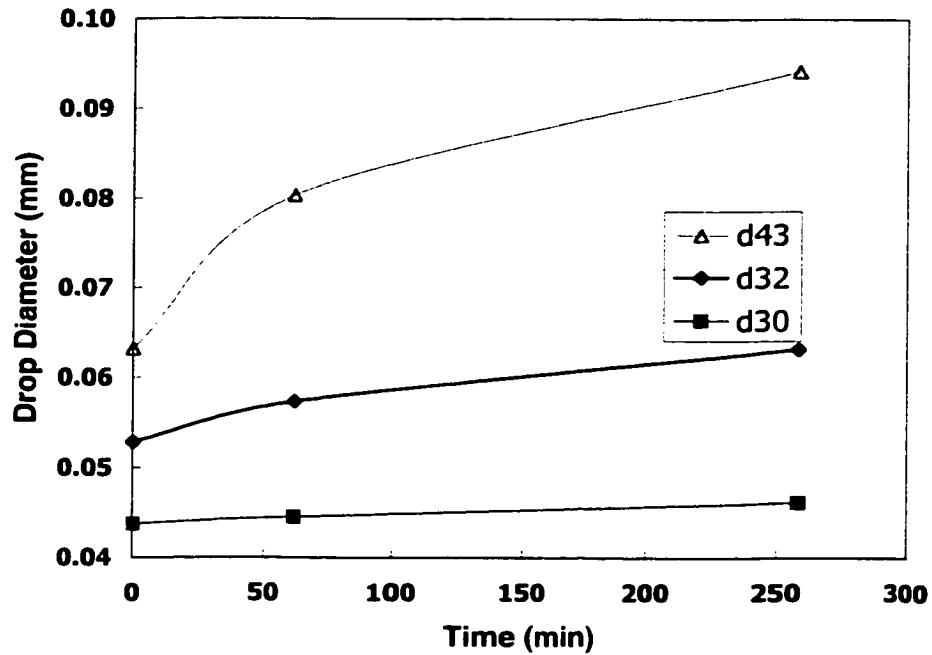


Figure G172. Transient average drop size of (0.75% acetophenone / 0.05 mole aq. NaCl / 0.2 mmole/m<sup>3</sup> Triton X100, 300→200 rpm)

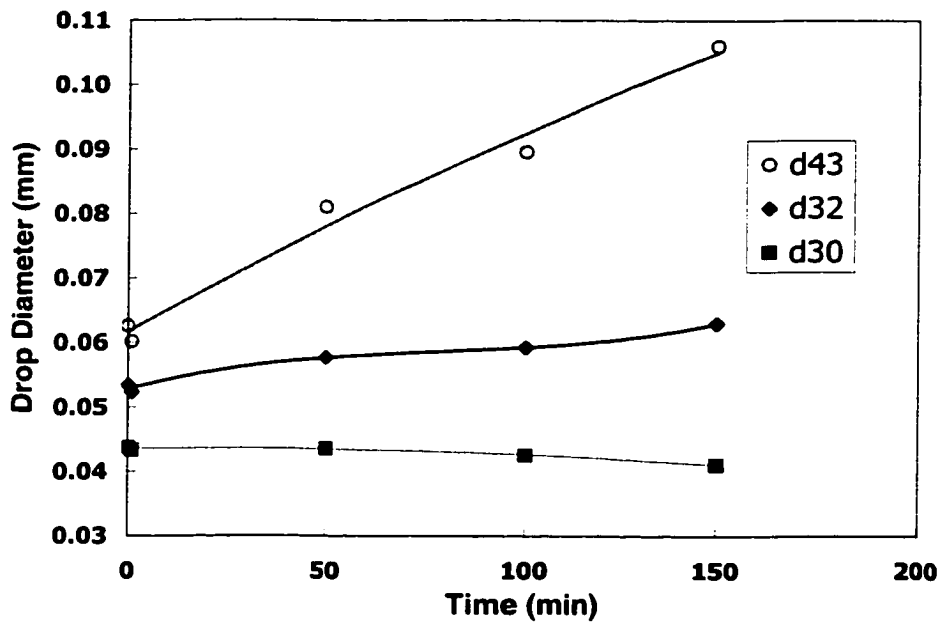


Figure G173. Transient average drop size of (0.75% acetophenone / 0.05 mole aq. NaCl / 1.0 mmole/m<sup>3</sup> Triton X100, 300→200 rpm)

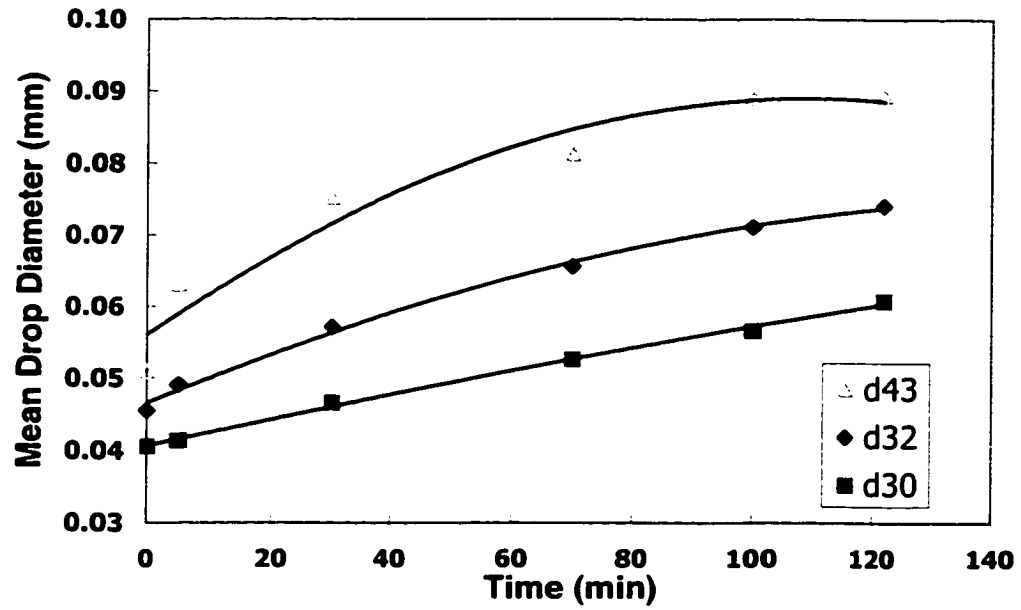


Figure G174. Transient average drop diameter of (0.75% acetophenon /0.05 molar aq. NaCl/ 0.1 mmole/m<sup>3</sup> Triton X165, 300->200 rpm)

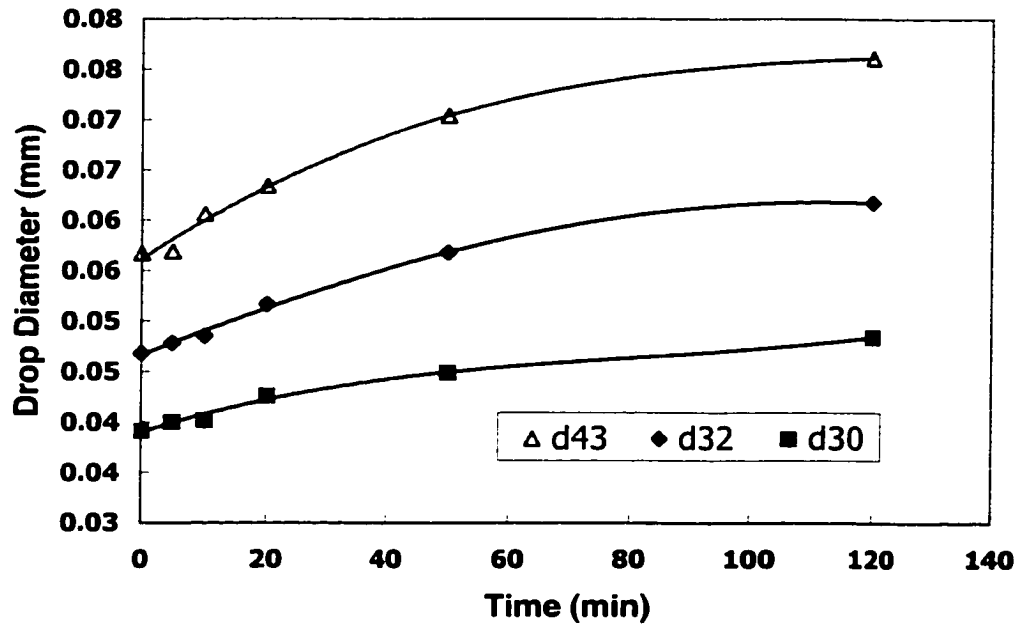


Figure G175. Transient average drop diameter of (0.75% acetophenon /0.05 molar aq. NaCl/0.2 mmole/m<sup>3</sup> Triton X165, 300->200 rpm)

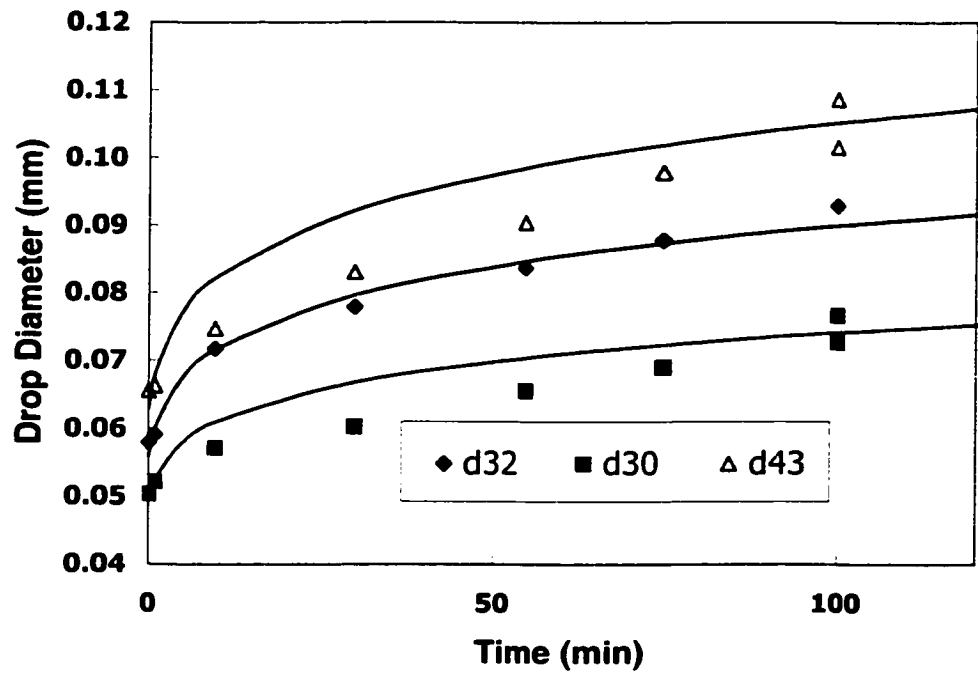


Figure G176. Transient average drop diameter of (0.75% acetophenon / 0.05 molar aq. NaCl / 0.1 mmole/m<sup>3</sup> Triton X305, 300->200 rpm)

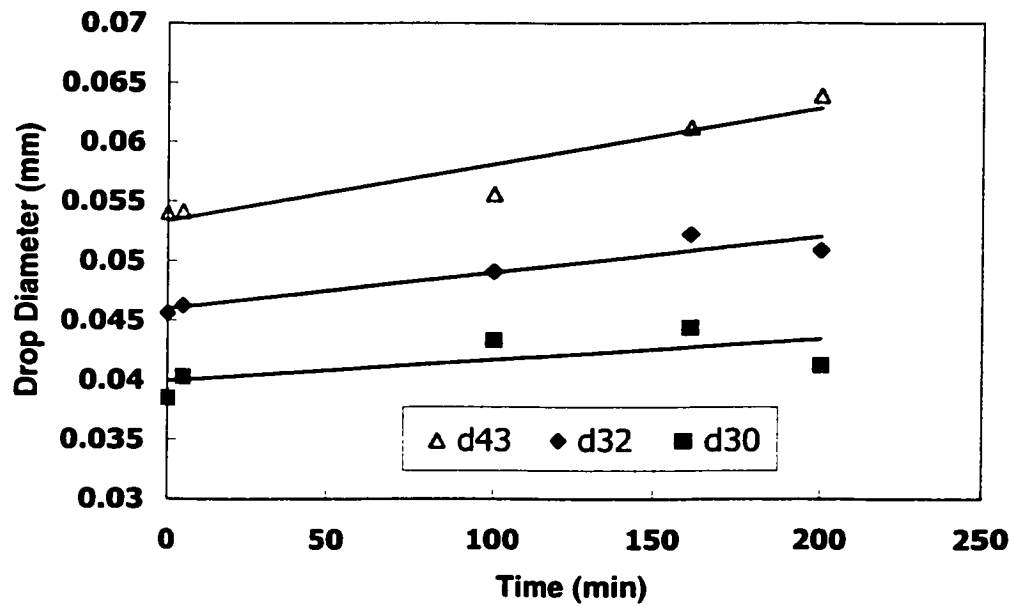


Figure G177. Transient average drop diameter of (0.75 acetophenon / 0.05 molar aq. NaCl / 0.2 mmole/m<sup>3</sup> Triton X305, 300->200 rpm)

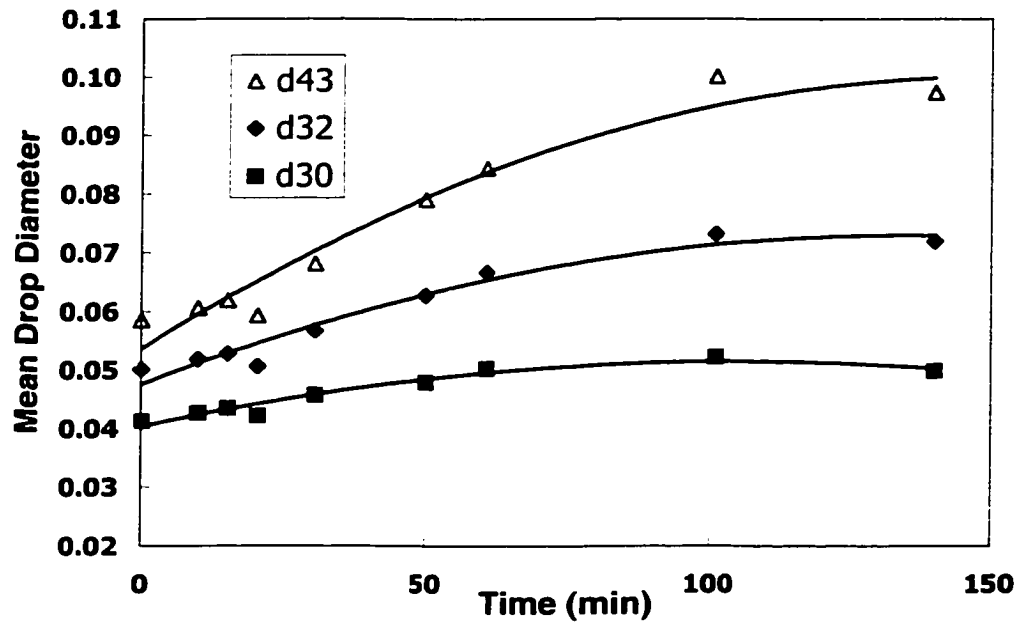


Figure G178. Transient average drop diameter of (0.75% acetophenon/ 0.05 mole aq. NaCl/ 0.1 mmole/m<sup>3</sup> Triton X405, 300->200 rpm)

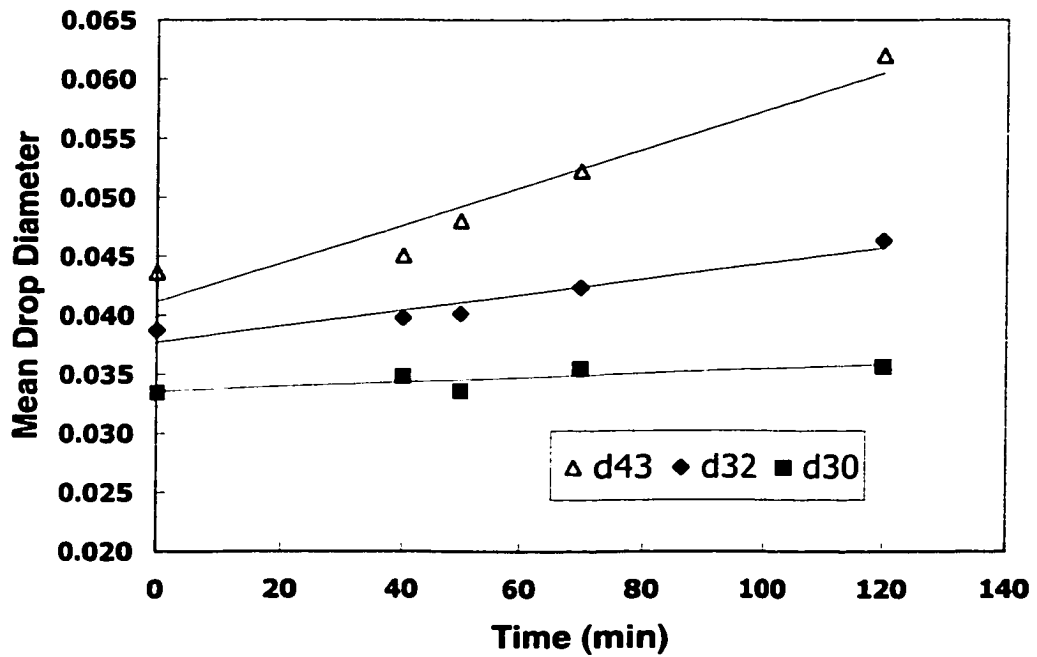


Figure G179. Transient average drop diameter of (0.75% acetophenon/ 0.05 mole aq. NaCl /0.2 mmole/m<sup>3</sup> Triton X405, 300->200 rpm)



## APPENDIX H

This appendix contains the equilibrium and dynamic interfacial characteristics of the systems investigated.

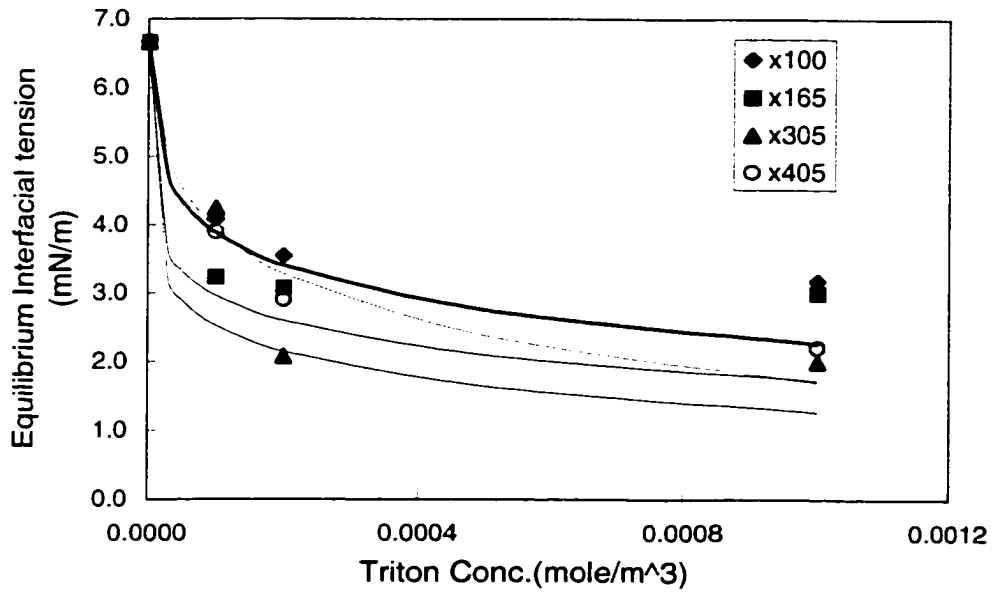


Figure H180. Effect of surfactant concentration on the equilibrium interfacial tension of (acetophenon/ water/ Triton)

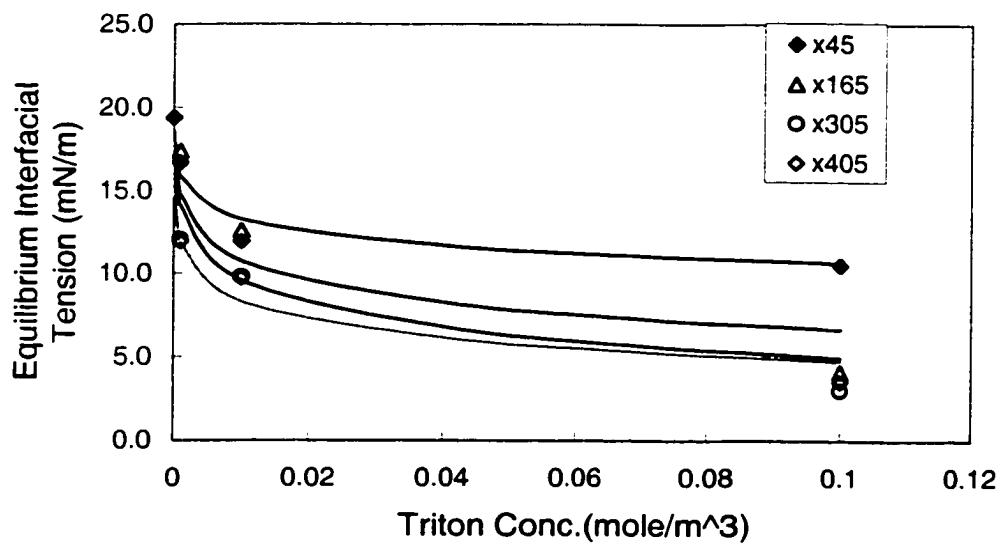


Figure H181. Effect of surfactant concentration on the equilibrium interfacial tension of (Bayol oil/water/Triton)

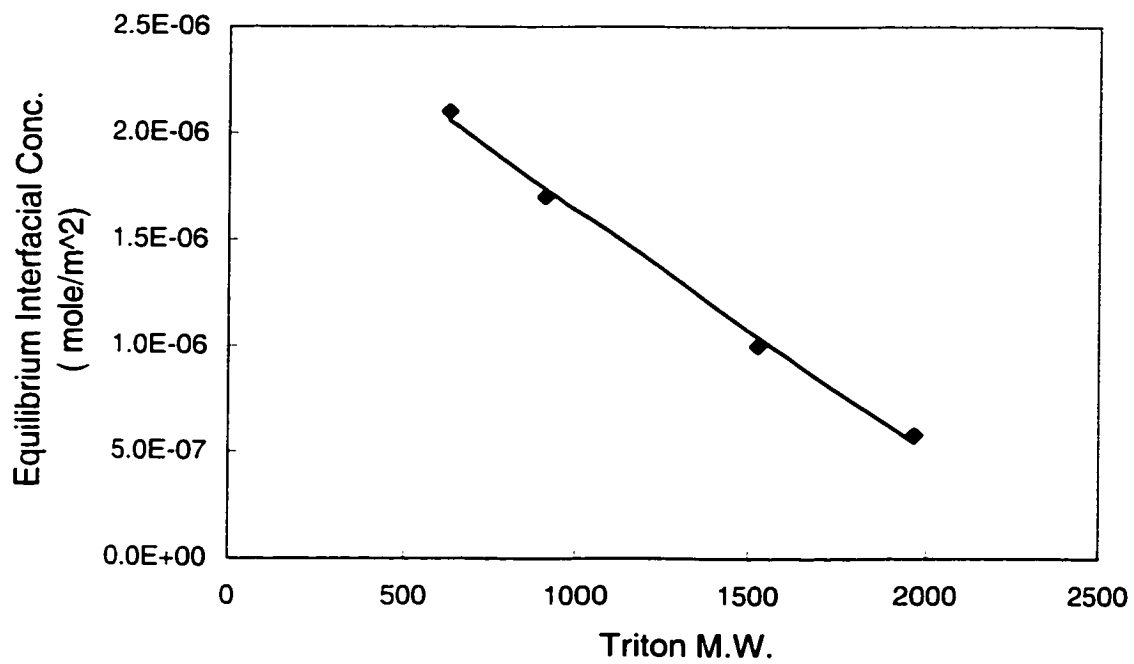


Figure H182. Effect of molecular weight/length on the equilibrium interfacial concentration of (acetophenone/ water/ 0.1 mmole/m<sup>3</sup> Triton)

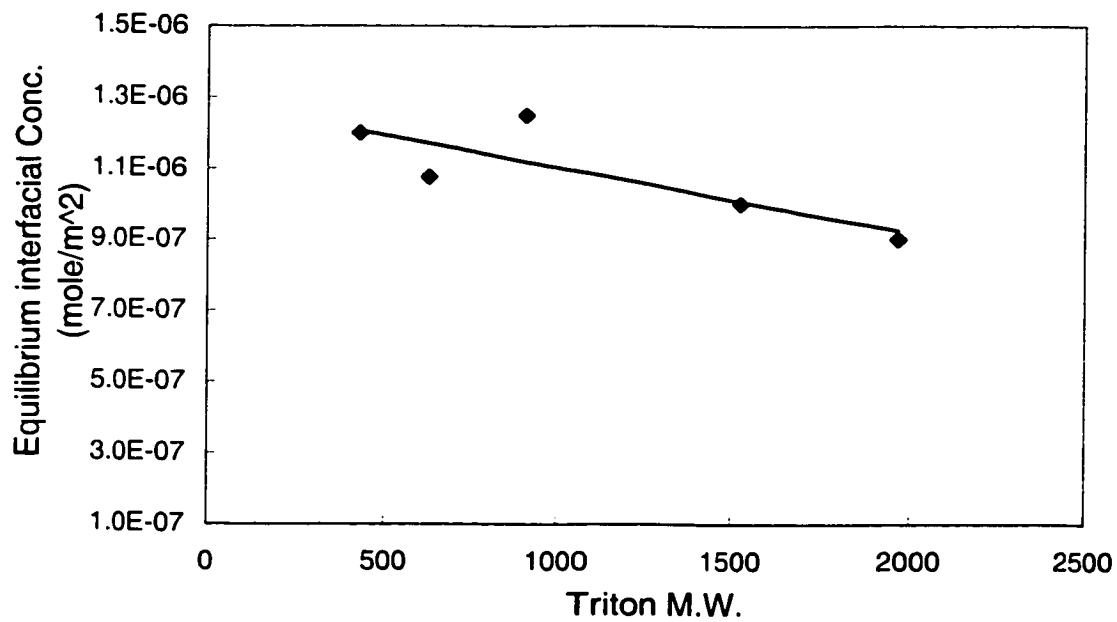


Figure H183. Effect of molecular weight/length on the interfacial concentration of (Bayol oil/ water/ 0.1 mole/m<sup>3</sup> Triton)

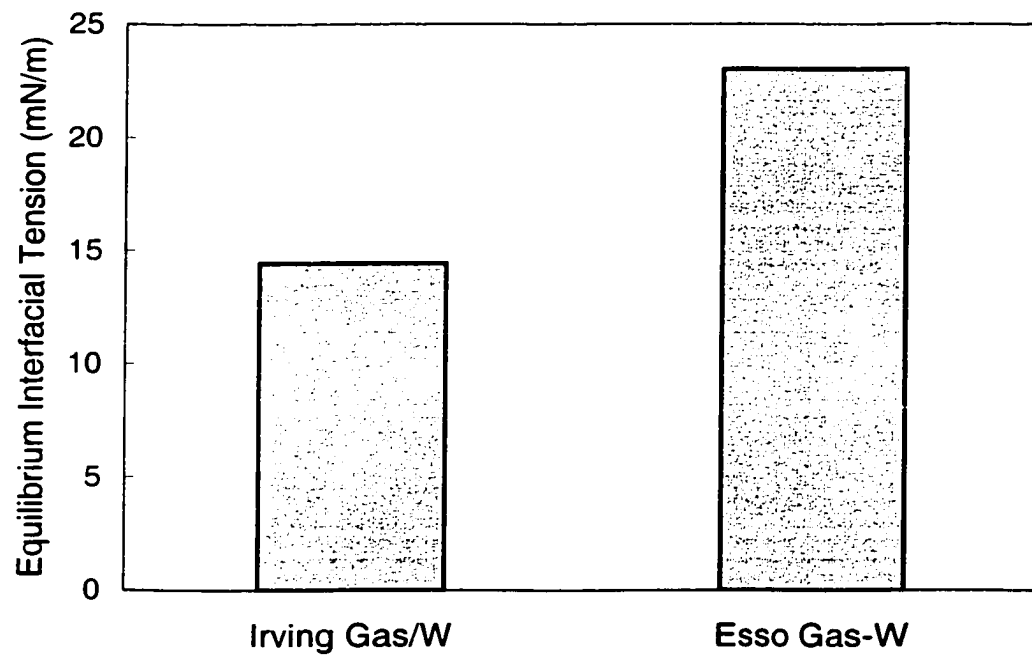


Figure H184. Equilibrium interfacial tension of gasoline/industrial caustics

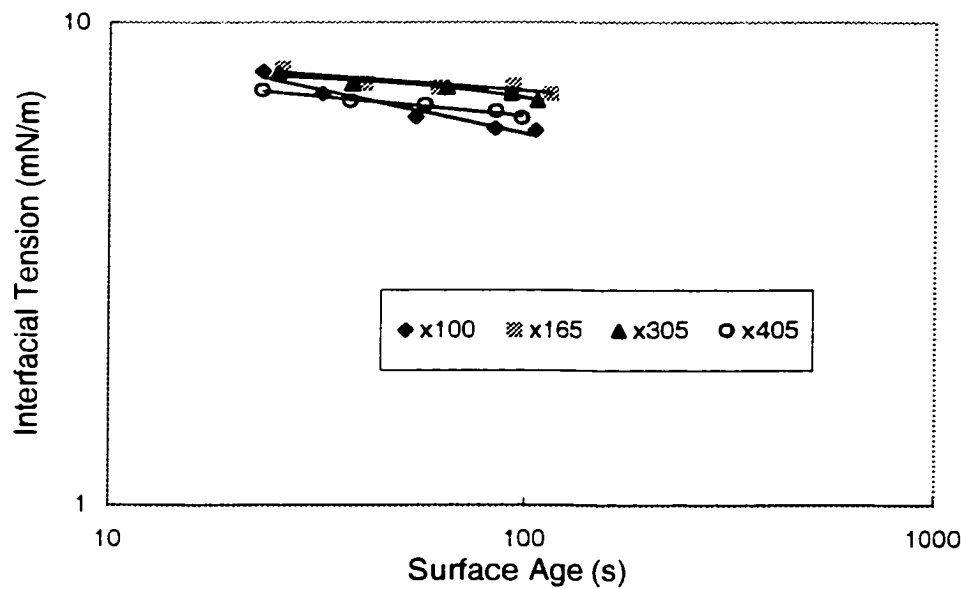


Figure H185. Effect of surfactant molecular weight/length on the dynamic interfacial tension of (acetophenon/ water/ 0.1 mmole/m<sup>3</sup> Triton, drop-volume-technique)

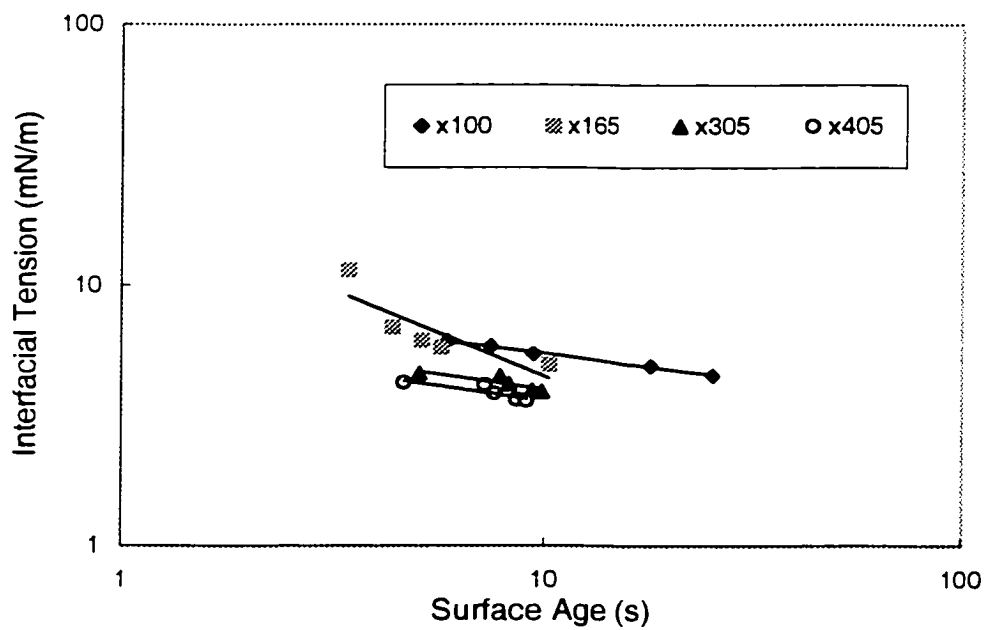


Figure H186. Effect of surfactant molecular weight/length on dynamic interfacial tension of (acetophenon/ water/ 0.1 mmole/m<sup>3</sup> Triton, maximum-drop-pressure-technique)

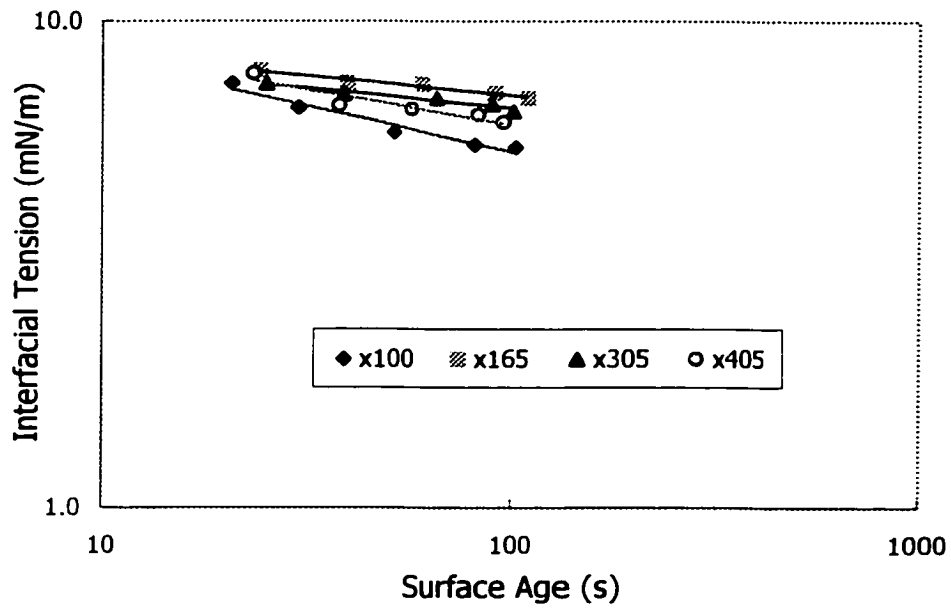


Figure H187. Effect of surfactant molecular weight/length on the dynamic interfacial tension of (acetophenon/ water/ 0.2mmole/m<sup>3</sup> Triton, drop-volume-technique)

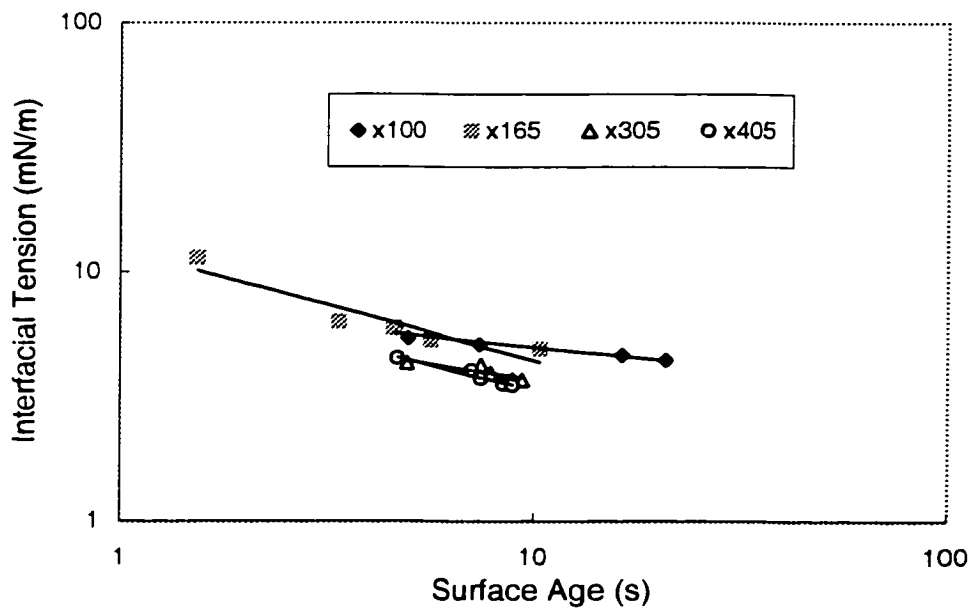


Figure H188. Effect of surfactant molecular weight/length on the dynamic interfacial tension of (acetophenon/ water/ 0.2 mmole/m<sup>3</sup> Triton, maximum-drop-pressure-technique)

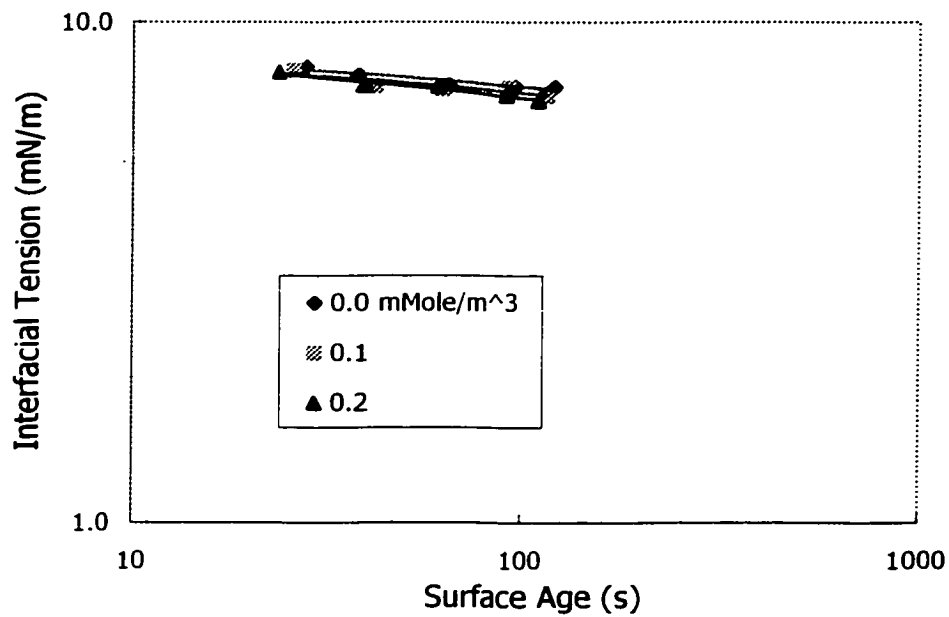


Figure H189. Effect of surfactant concentration on the dynamic interfacial tension of (acetophenon/ water/Triton X165, by drop volume technique)

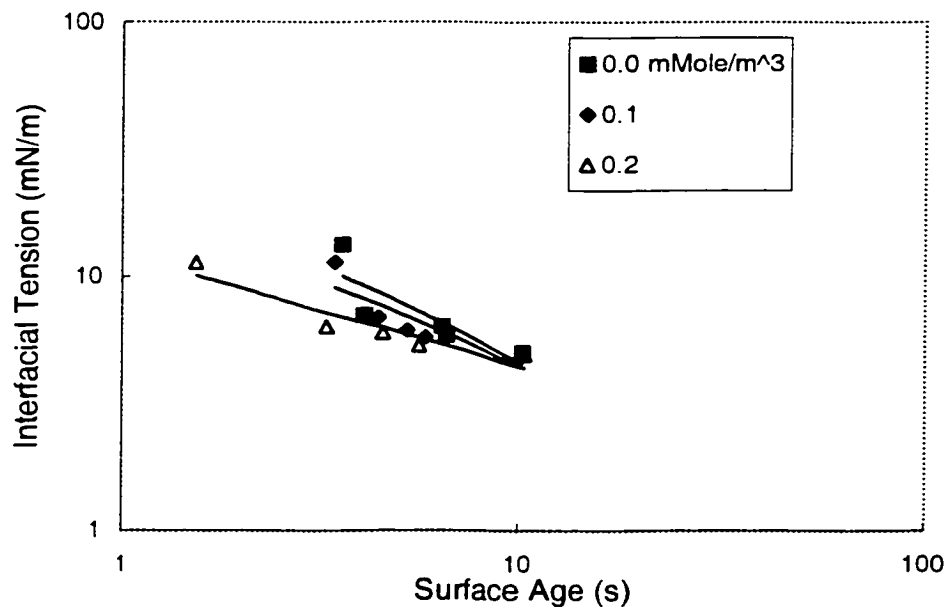


Figure H190. Effect of surfactant concentration on dynamic interfacial tension of (acetophenon/water/Triton X165, maximum-drop-pressure-technique)

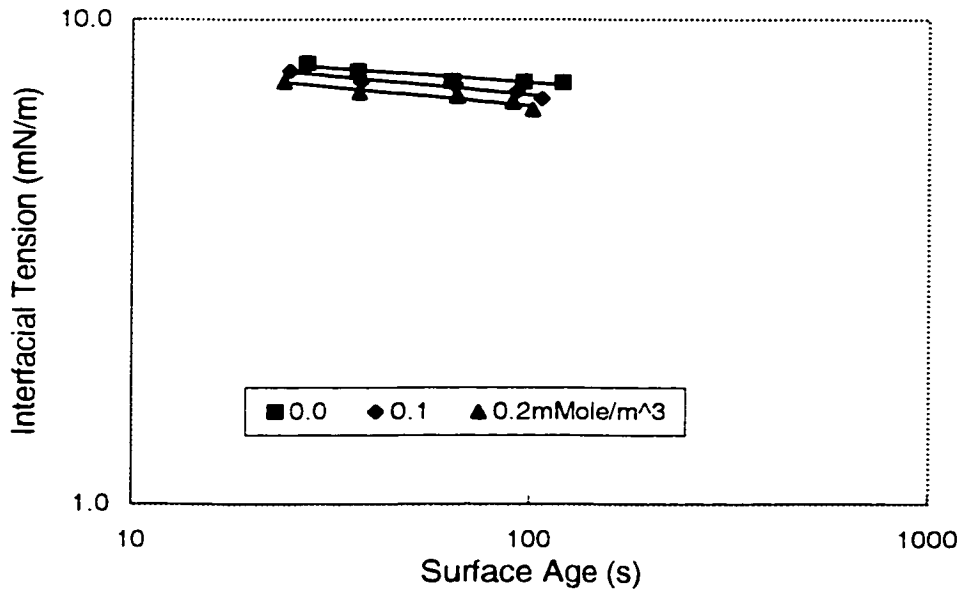


Figure H191. Effect of surfactant concentration on the dynamic interfacial tension of (acetophenone/ water /Triton X305, drop volume technique)

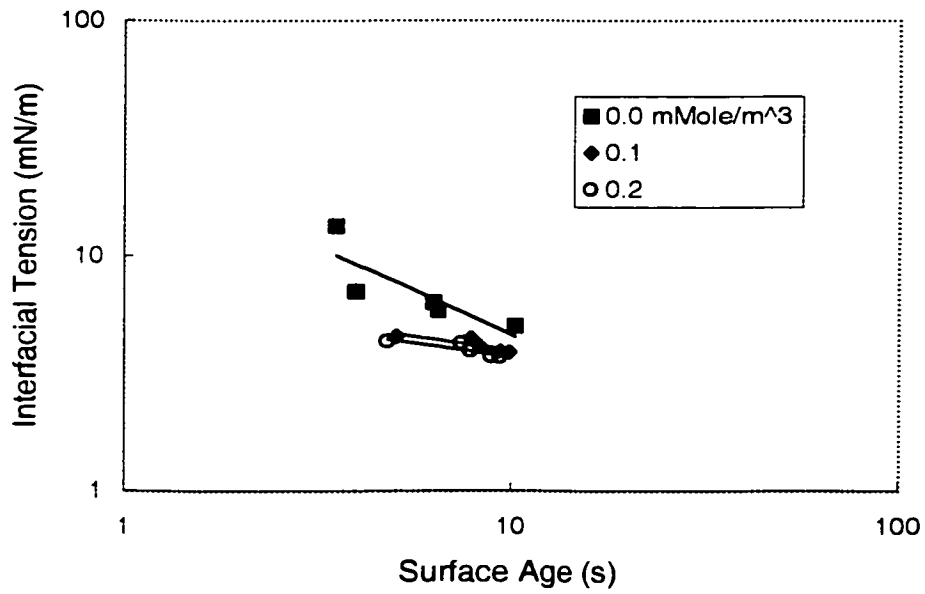


Figure H192. Effect of surfactant concentration on dynamic interfacial tension of (acetophenone/ water/ Triton X305, maximum-drop-pressure-technique)

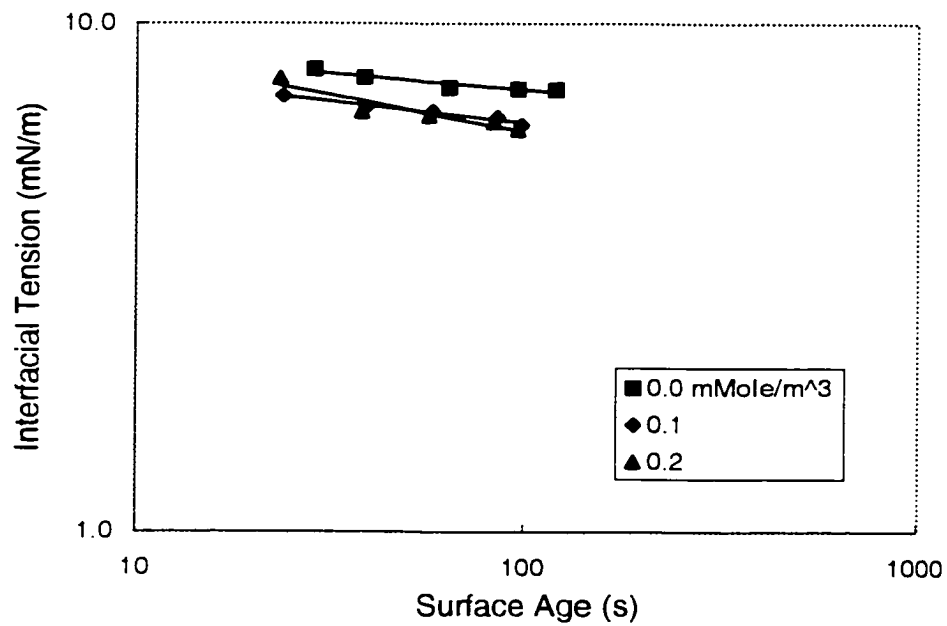


Figure H193. Effect of surfactant concentration on dynamic interfacial tension of (acetophenon/ water /Triton X405, drop volume technique)

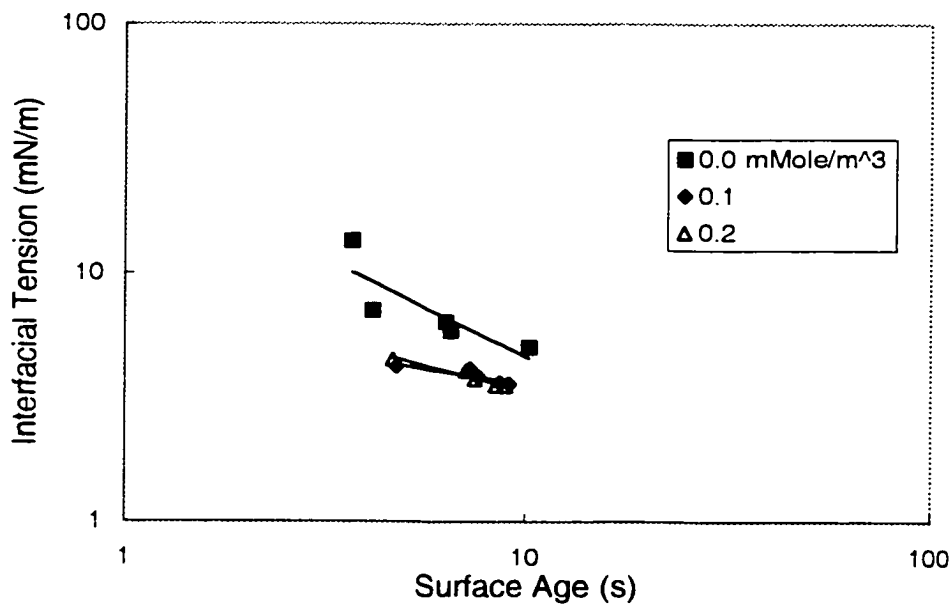


Figure H194. Effect of surfactant concentration on dynamic interfacial tension of (acetophenon/water/Triton X405, maximum-drop-pressure-technique)



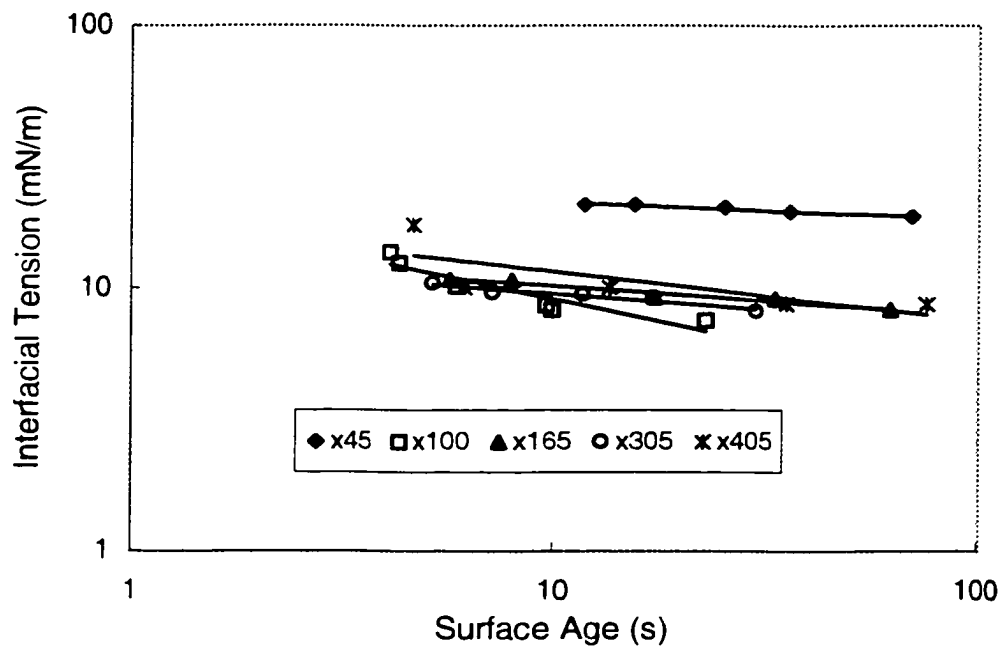


Figure H195. Effect of surfactant molecular weight/length on the dynamic interfacial tension of (Bayol oil / water / 0.1 mole/m<sup>3</sup> Triton, drop-volume-technique)

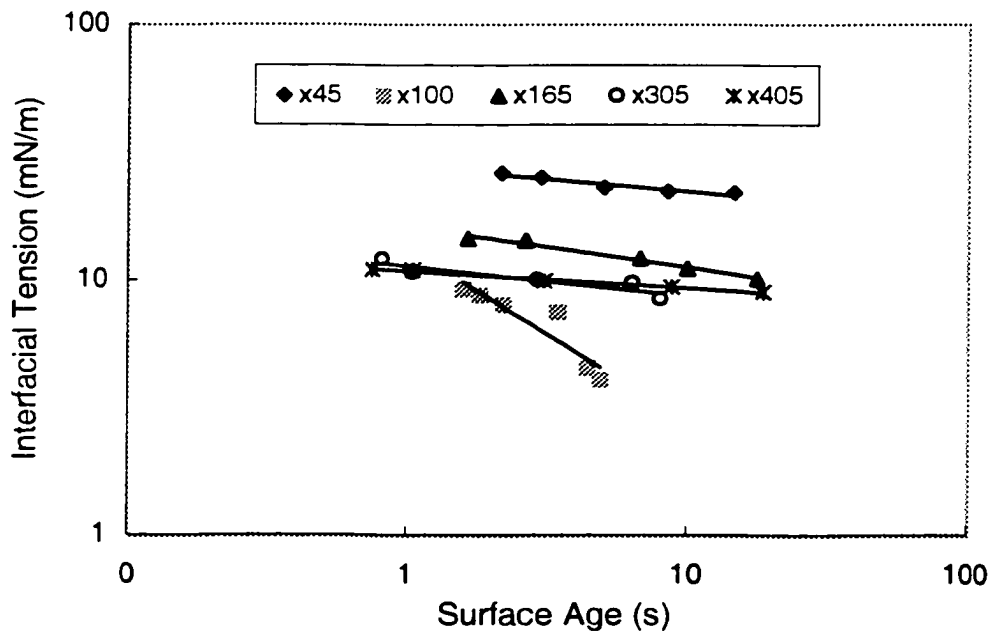


Figure H196. Effect of surfactant molecular weight/length on the dynamic interfacial tension of (Bayol oil / water / 0.1 mole/m<sup>3</sup> Triton, maximum-drop-pressure-technique)

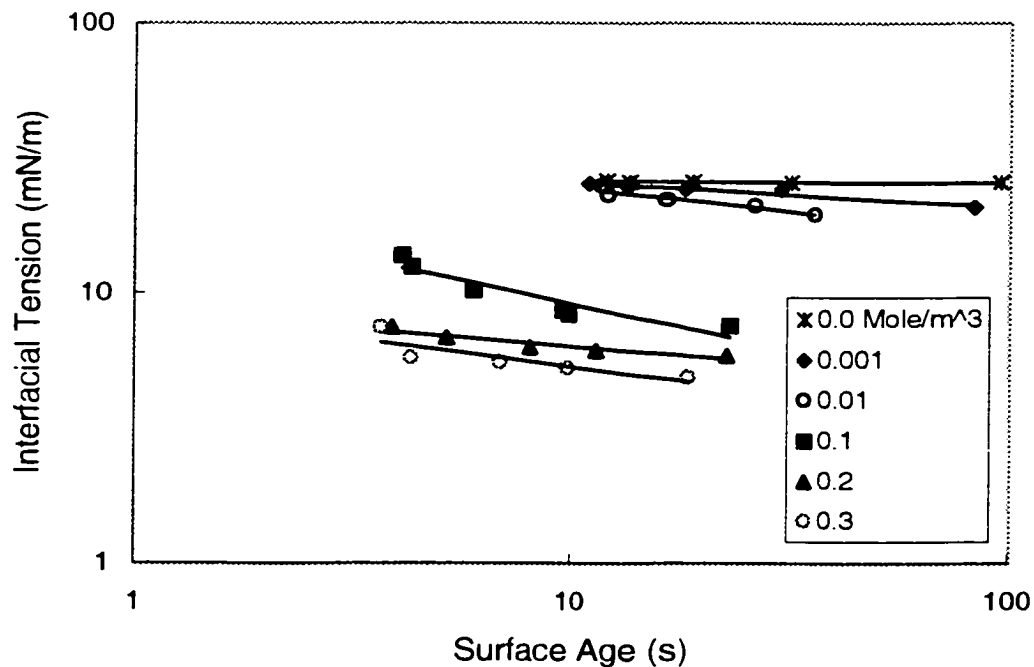


Figure H197. Effect of surfactant concentration on the dynamic interfacial tension of (Bayol oil / water / Triton X100, drop-volume-technique)

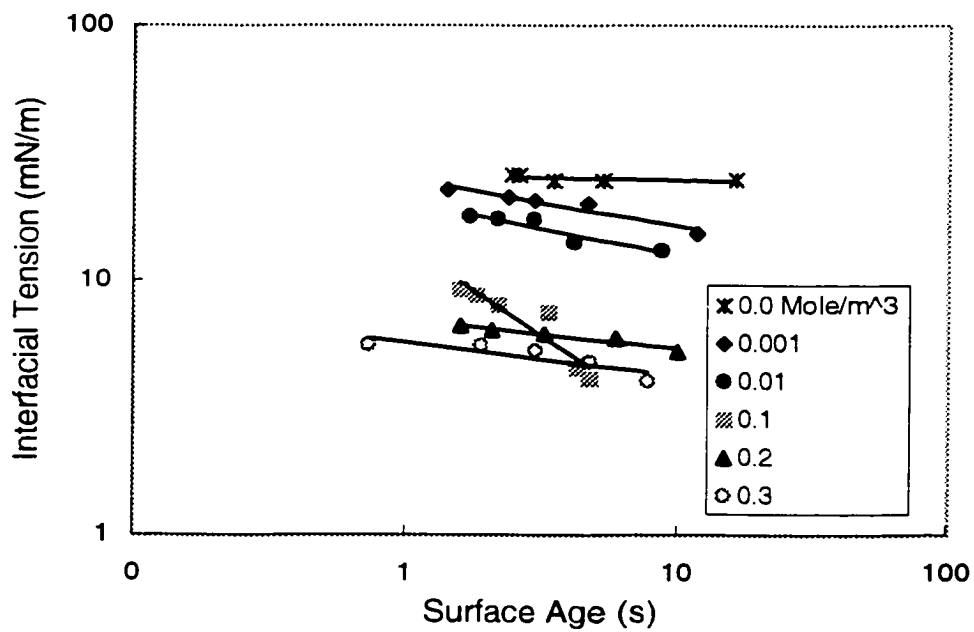


Figure H198. Effect of surfactant concentration on the dynamic interfacial tension of (Bayol oil / water / Triton X100, maximum-drop-pressure-technique)

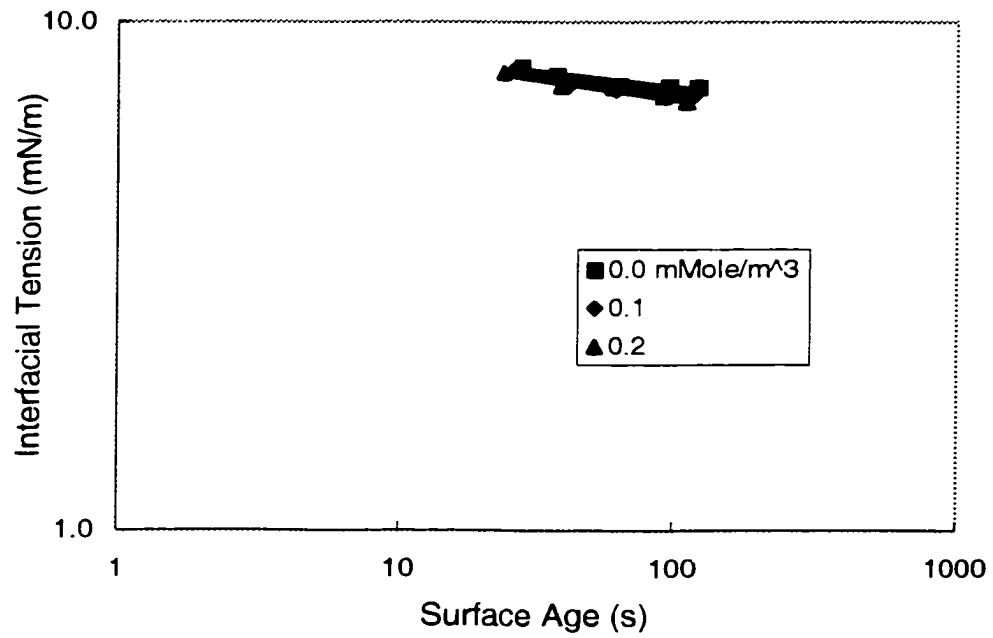


Figure H199. Effect of surfactant concentration on dynamic interfacial tension of (acetophenon / water / Triton X165, drop volume technique)

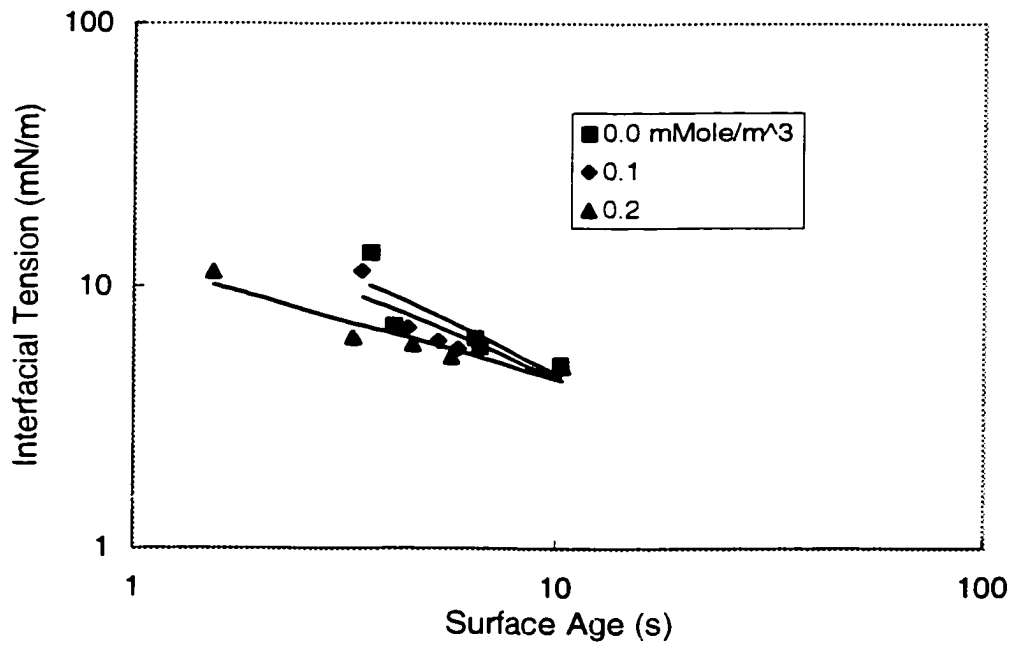


Figure H200. Effect of surfactant concentration on the dynamic interfacial tension of (acetophenon / water / Triton X165, maximum-drop-pressure-technique)

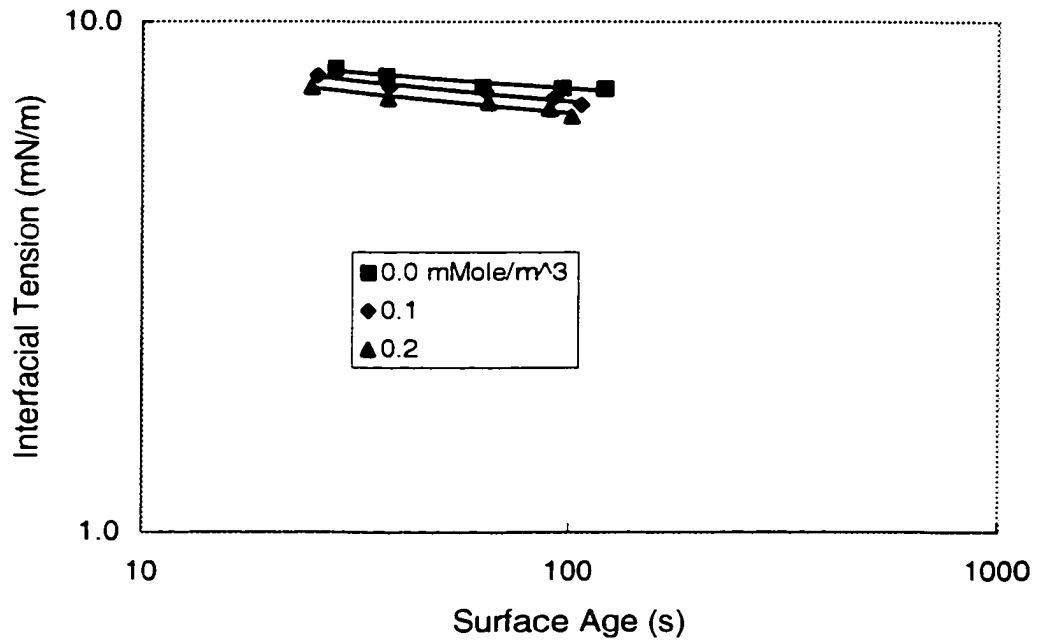


Figure H201. Effect of surfactant concentration on the dynamic interfacial tension of (acetophenone/ water/ Triton X305, drop-volume-technique)

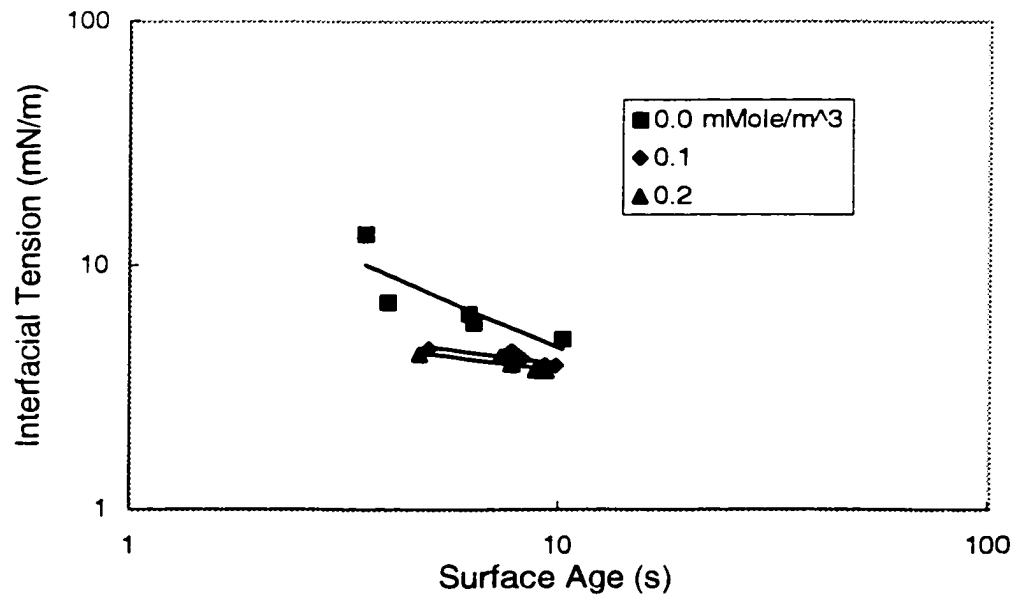


Figure H202. Effect of surfactant concentration on the dynamic interfacial tension of (acetophenone/ water/ Triton X305, maximum-drop-pressure-technique)

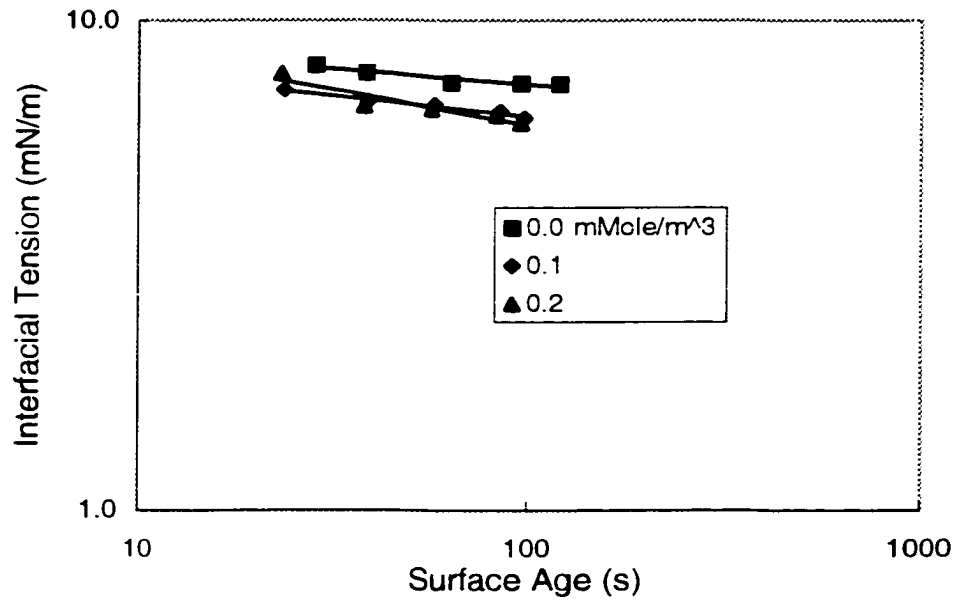


Figure H203. Effect of surfactant concentration on the dynamic interfacial tension of (acetophenon/ water/ Triton X405, drop-volume-technique)

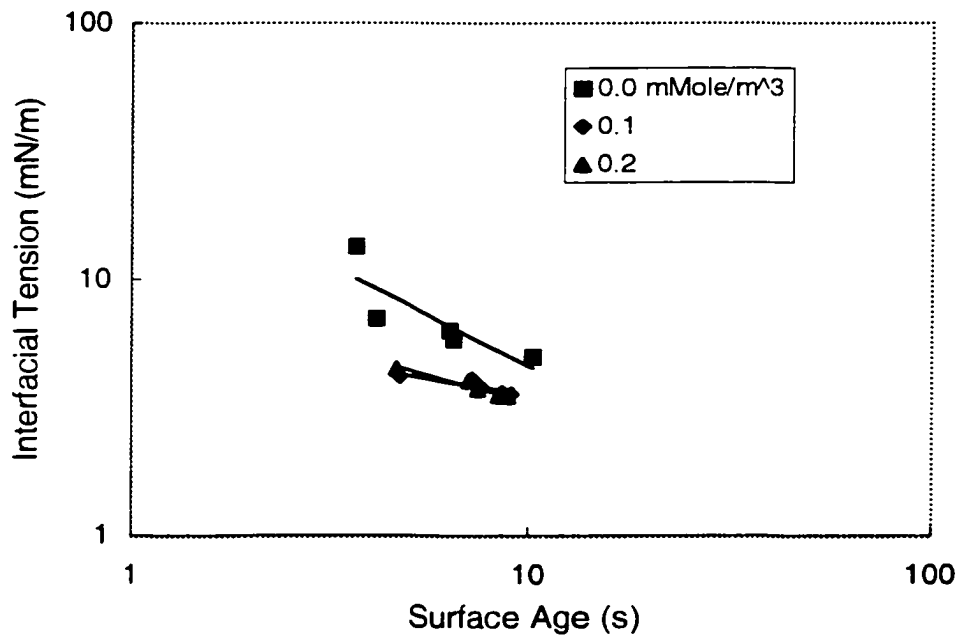


Figure H204. Effect of surfactant concentration on the dynamic interfacial tension of (acetophenon / water / Triton X405, maximum-drop-pressure-technique)

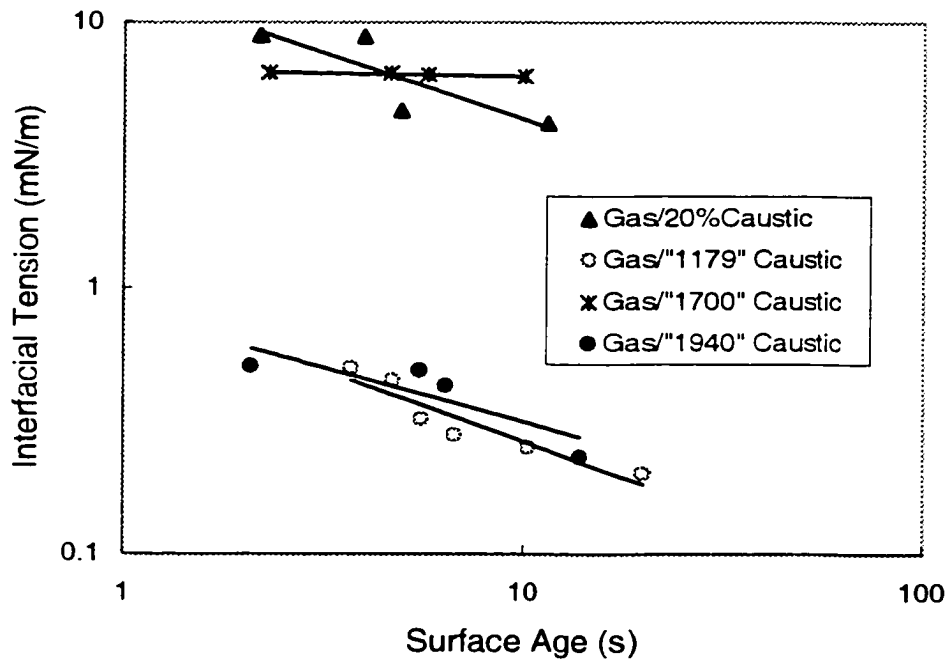


Figure H205. Effect of capacity number on the dynamic interfacial tension of (Irving gasoline/ industrial caustic solution, drop-volume-technique)

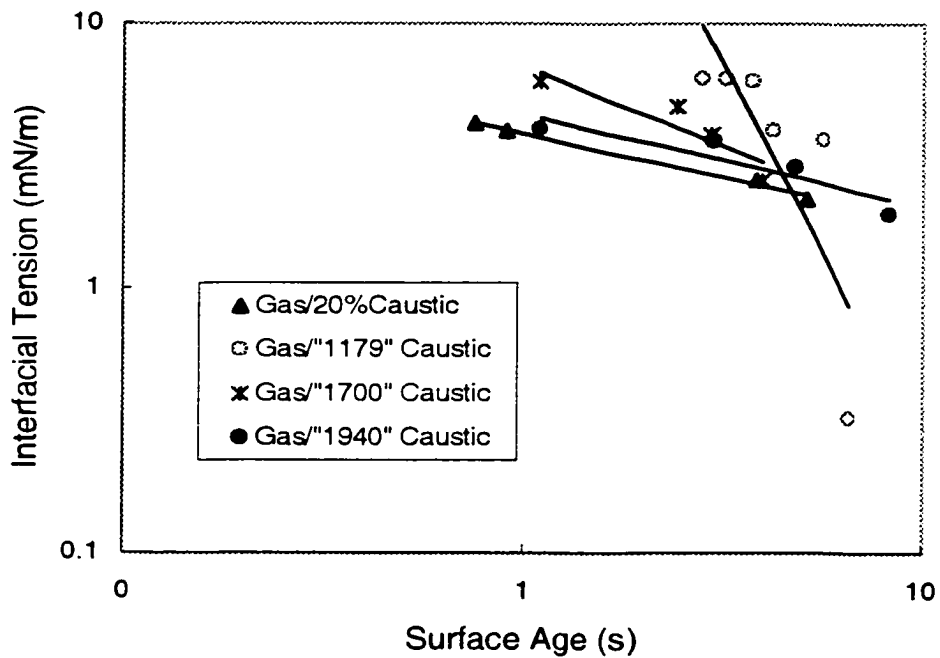


Figure H206. Effect of capacity number on the dynamic interfacial tension of (Irving gasoline/ industrial caustic, maximum-drop-pressure technique)

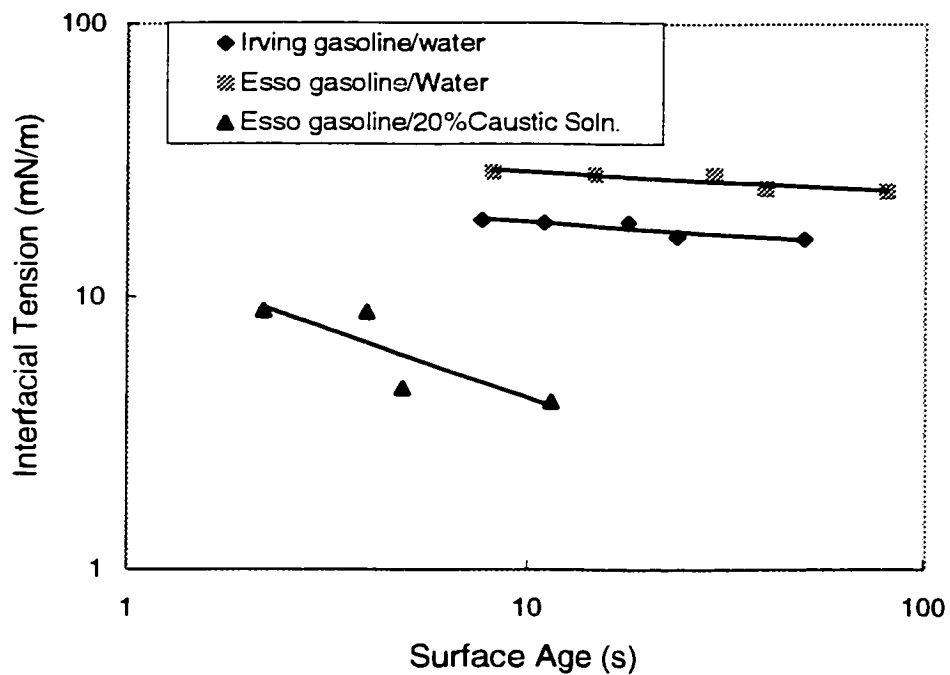


Figure H207. Effect of gasoline type on the dynamic interfacial tension of (gasoline/ aqueous phase, drop-volume-technique)

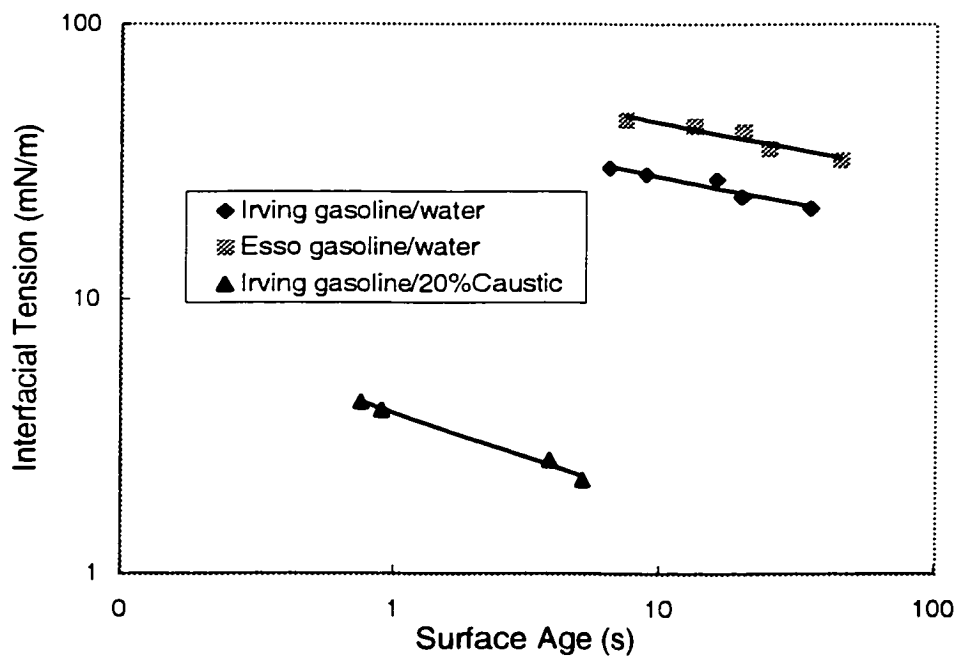


Figure H208. Effect of gasoline type on the dynamic interfacial tension of (gasoline / aqueous phase, maximum-drop-pressure-technique)

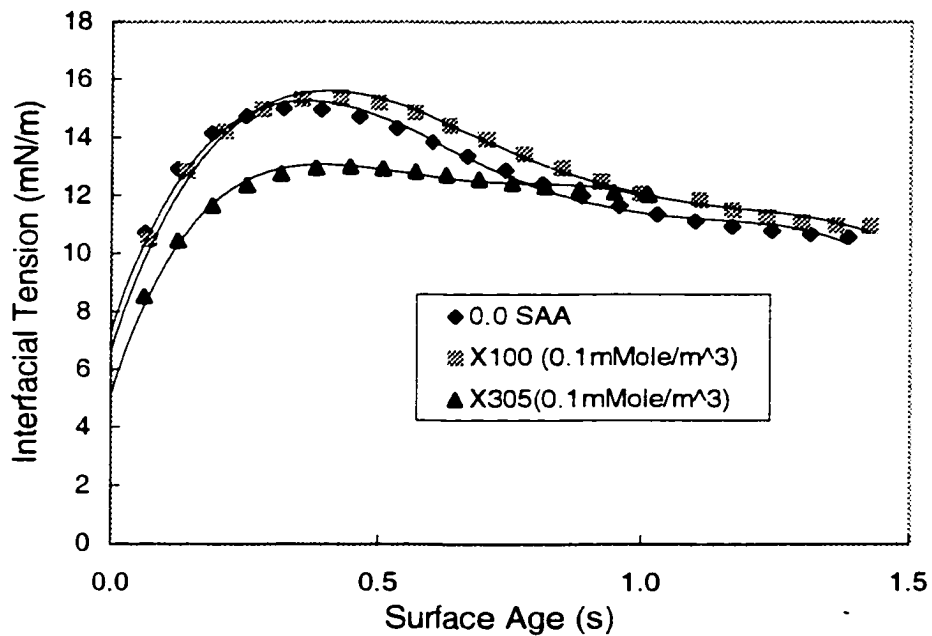


Figure H209. Effect of surfactant molecular weight/length on the dynamic interfacial tension of (acetophenone / water / 0.1 mmole/m<sup>3</sup> Triton , dispersed phase flow rate=0.0442 mL/min, expanding-drop technique)

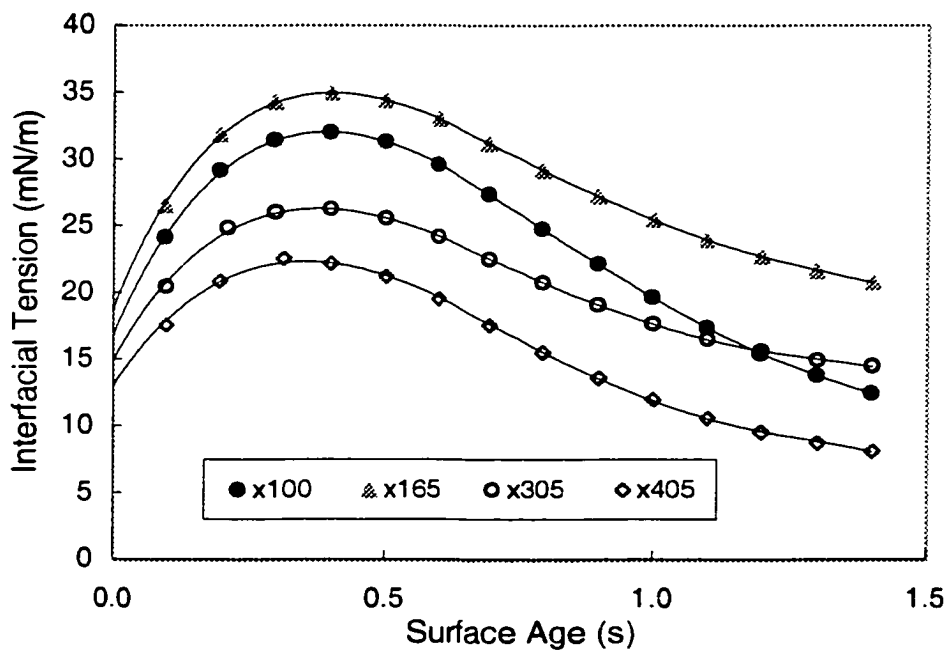


Figure H210. Effect of surfactant molecular weight/length on the dynamic interfacial tension of (Bayol oil / water / 0.1 mole/m<sup>3</sup> Triton, dispersed phase flow rate=0.0316mL/min, expanding-drop technique)



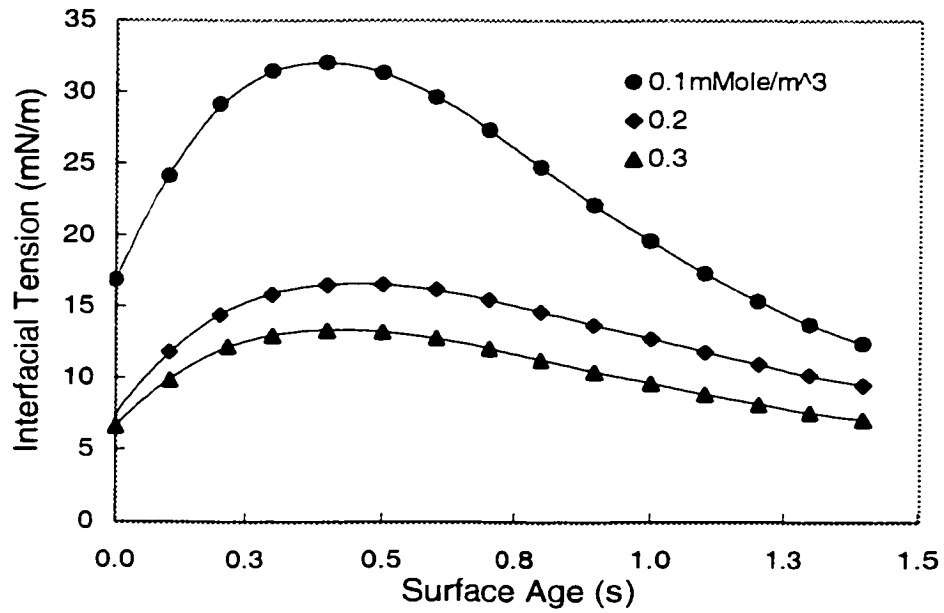


Figure H211. Effect of surfactant concentration on the dynamic interfacial tension of (Bayol oil / water / Triton X100, dispersed phase flow rate= 0.0316mL/min, expanding-drop technique)

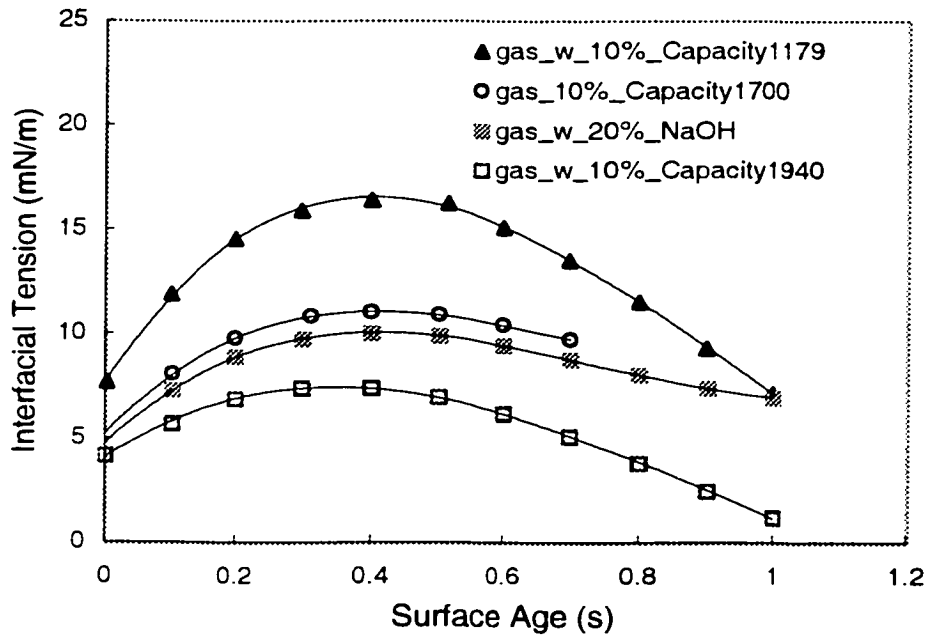


Figure H212. Effect of capacity number on dynamic interfacial tension of (Irving gasoline / industrial caustics, dispersed phase flow rate=0.0316mL/min, expanding-drop-technique)

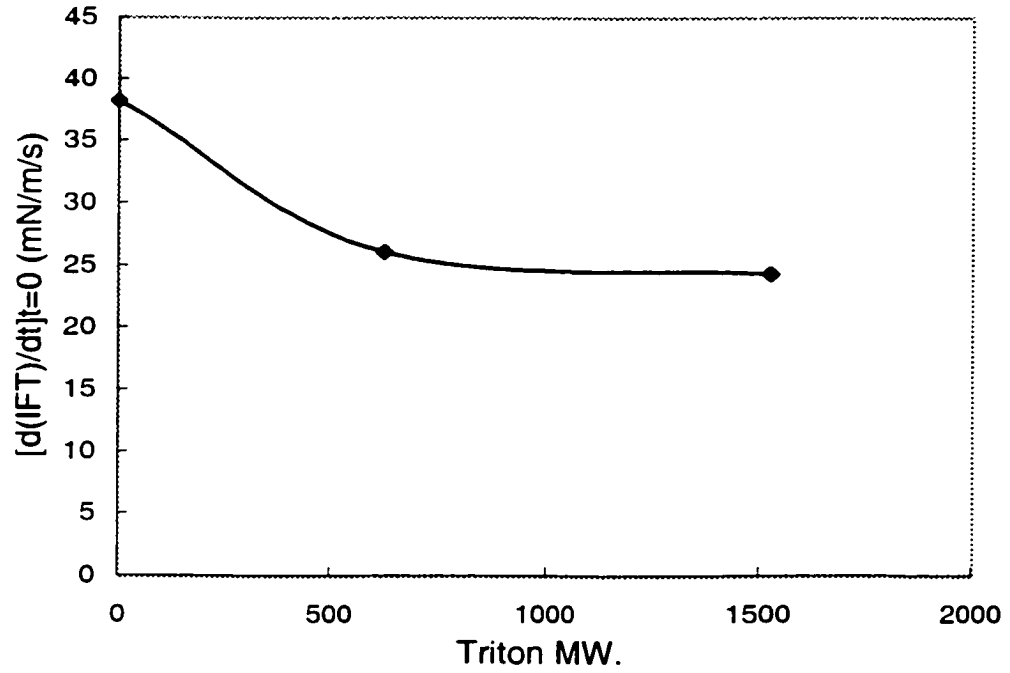


Figure H213. Effect of surfactant molecular weight/length on the initial slope of dynamic interfacial tension vs. time of (acetophenone /water / 0.1 mmole/m<sup>3</sup> Triton, expanding-drop-technique)

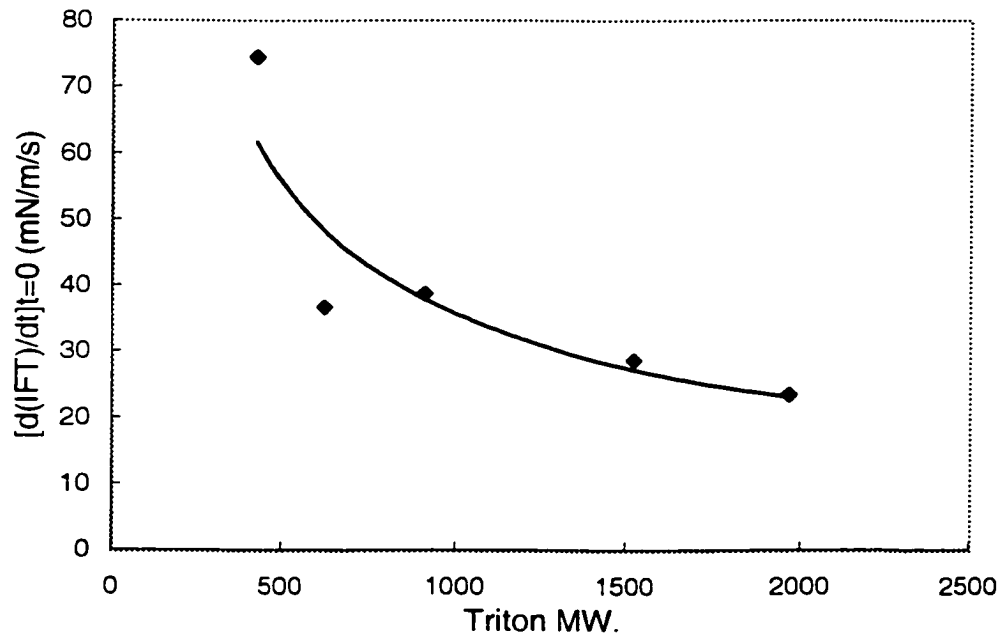


Figure H214. Effect of surfactant molecular weight/length on the initial slope of the interfacial tension vs. time of (Bayol oil /water/ 0.1 mole/m<sup>3</sup> Triton), expanding-drop-technique)

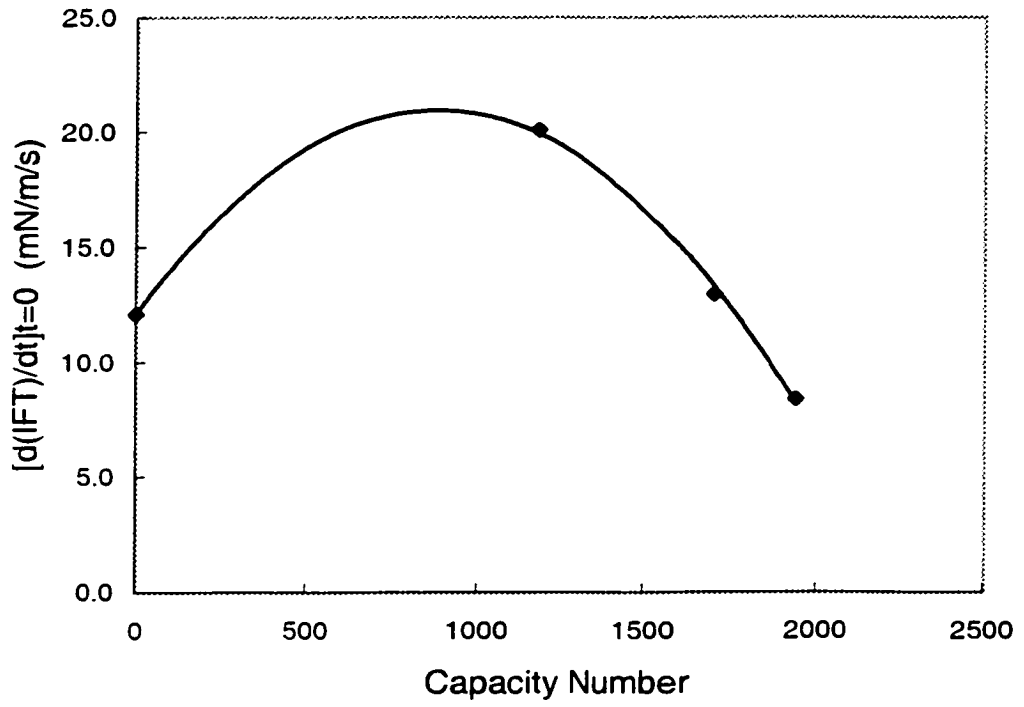


Figure H215. Effect of capacity number of industrial caustic on the initial slope of the interfacial tension vs. time of (Irving gasoline/ industrial caustic, expanding-drop-technique)

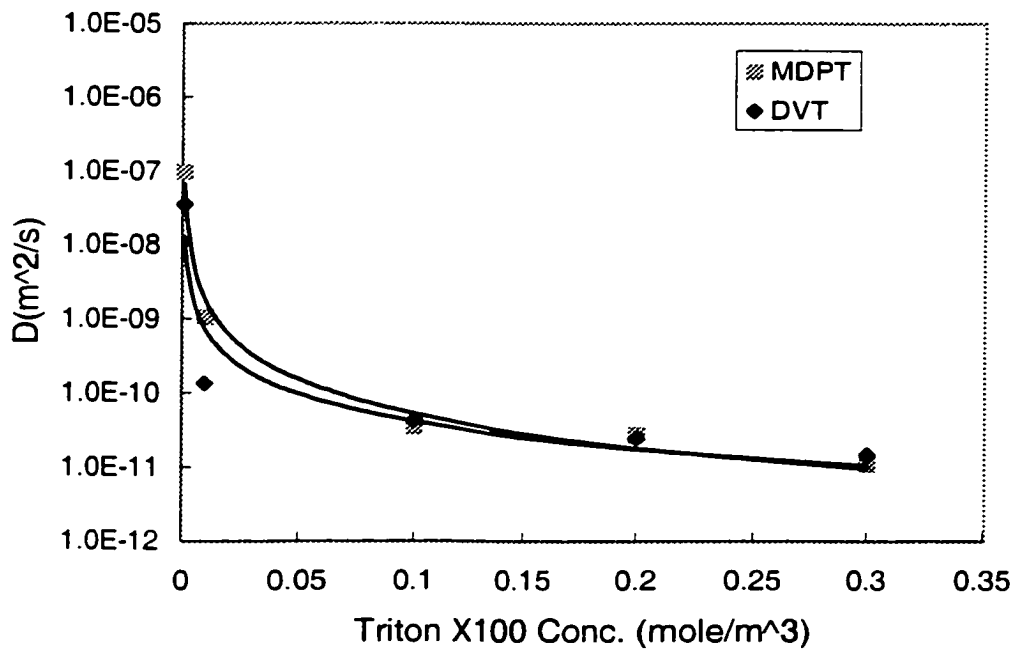


Figure H216. Effect of surfactant concentration on the Triton diffusivity in (Bayol oil/ water/ Triton X100)

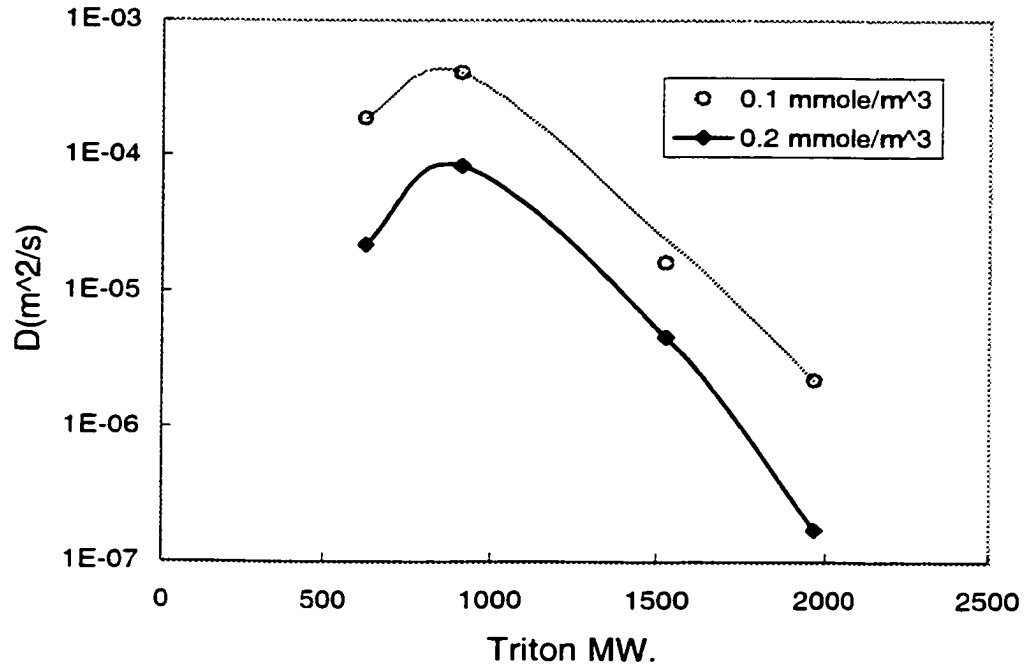


Figure H217. Effect of surfactant molecular weight/ length on the Triton diffusivity in (acetophenon/ water/ Tiron, drop-volume-technique)

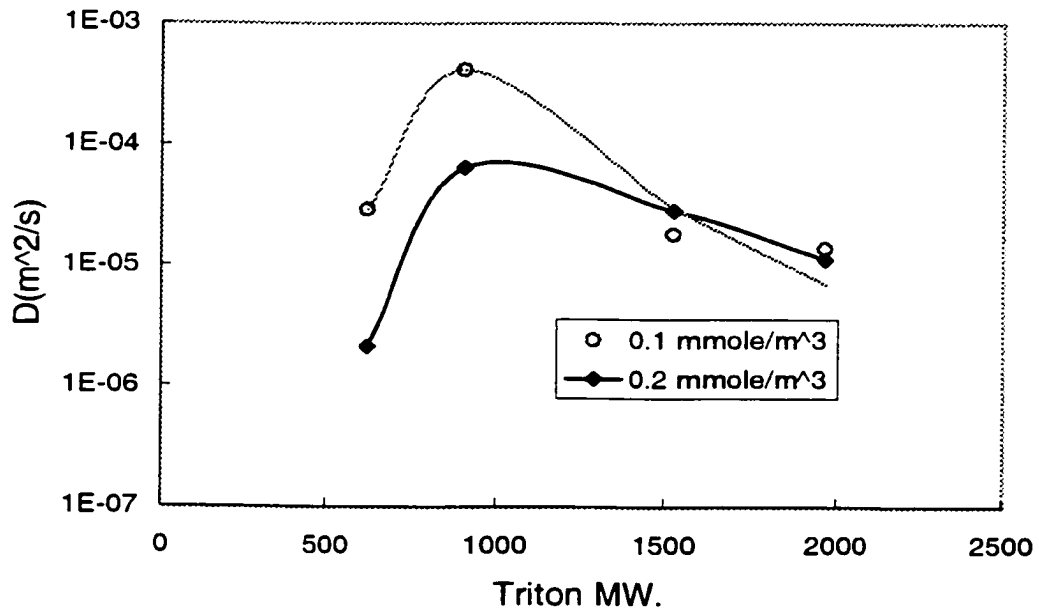


Figure H218. Effect of surfactant molecular weight/length on the SAA diffusivity of (acetophenon/ water/ Tiron, maximum drop pressure technique)

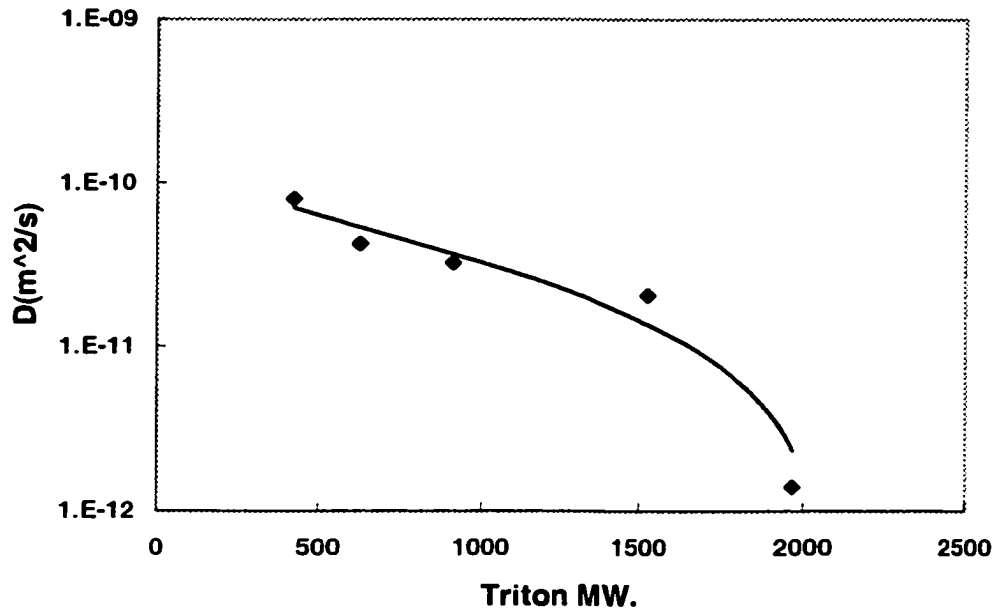


Figure H219. Effect of surfactant molecular weight/length on the Triton diffusivity in (Bayol/ water/ 0.1 mole/m<sup>3</sup> Triton, drop-volume-technique)

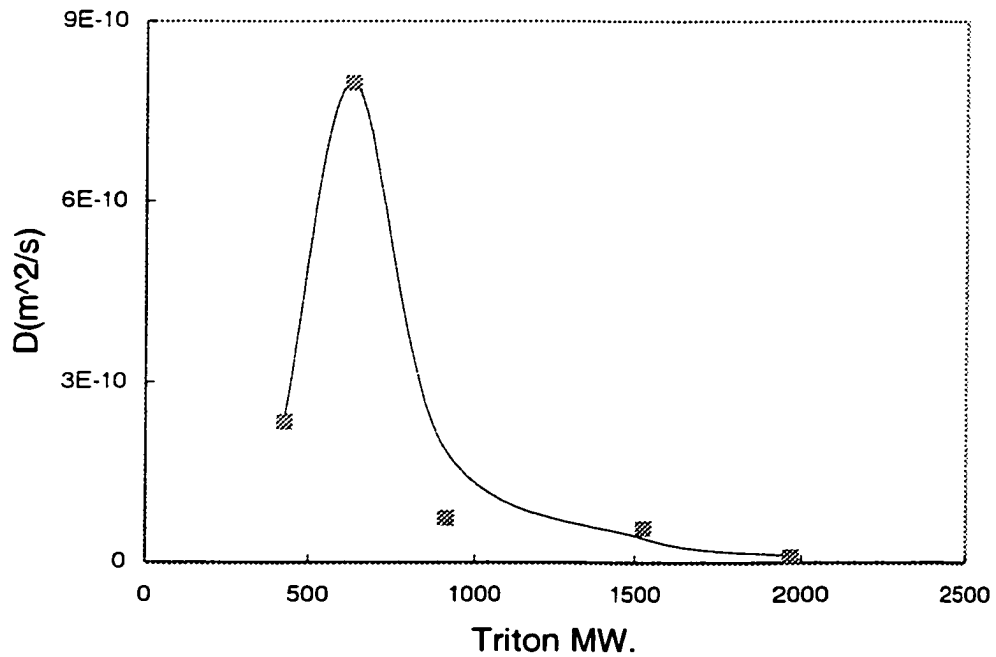


Figure H220. Effect of surfactant molecular weight/length on the SAA diffusivity in (Bayol/ water/ 0.1 mole/m<sup>3</sup> Triton, maximum-drop-pressure-technique)

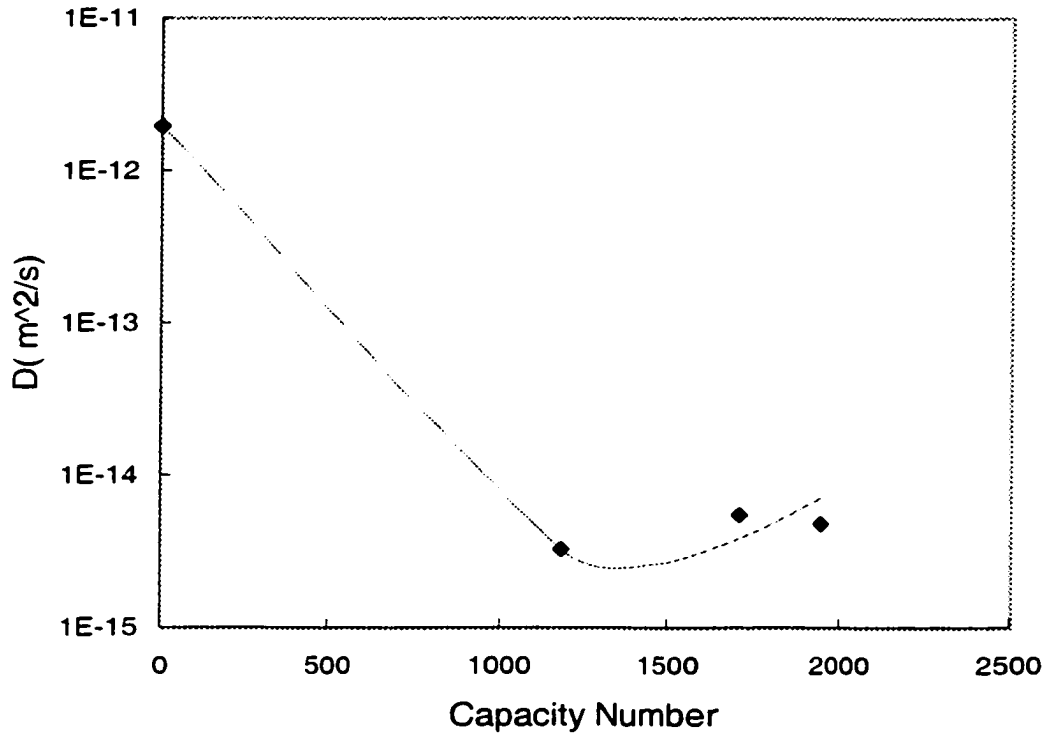


Figure H221. Effect of capacity number of the industrial caustic on the apparent SAA diffusivity in (Irving gasoline/ industrial caustic, maximum-drop-pressure-technique)

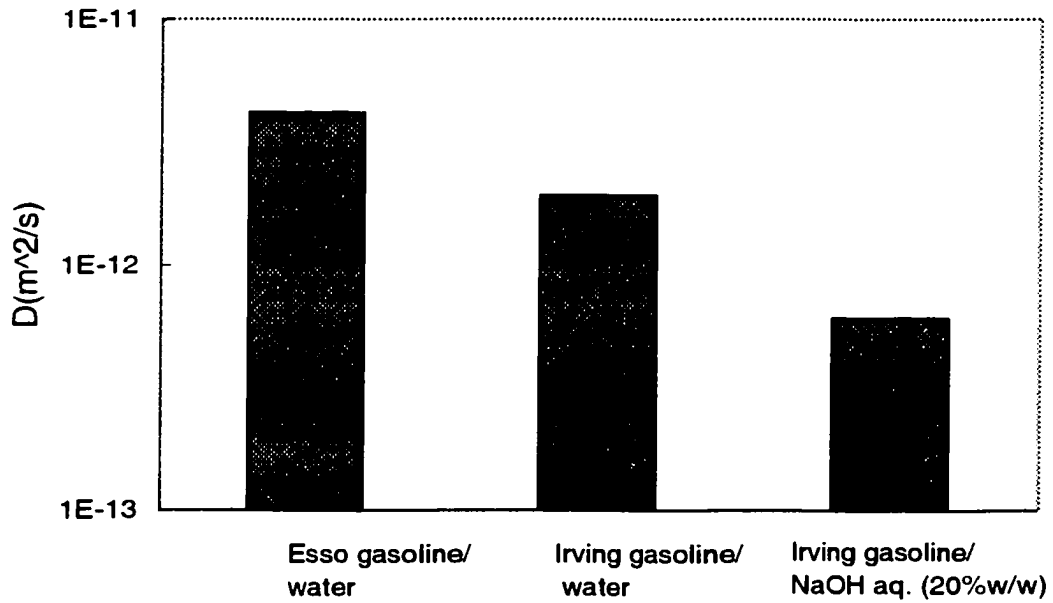


Figure H222. Effect of gasoline type on the apparent SAA diffusivity in (gasoline/ aqueous solution, maximum-drop-pressure-technique)

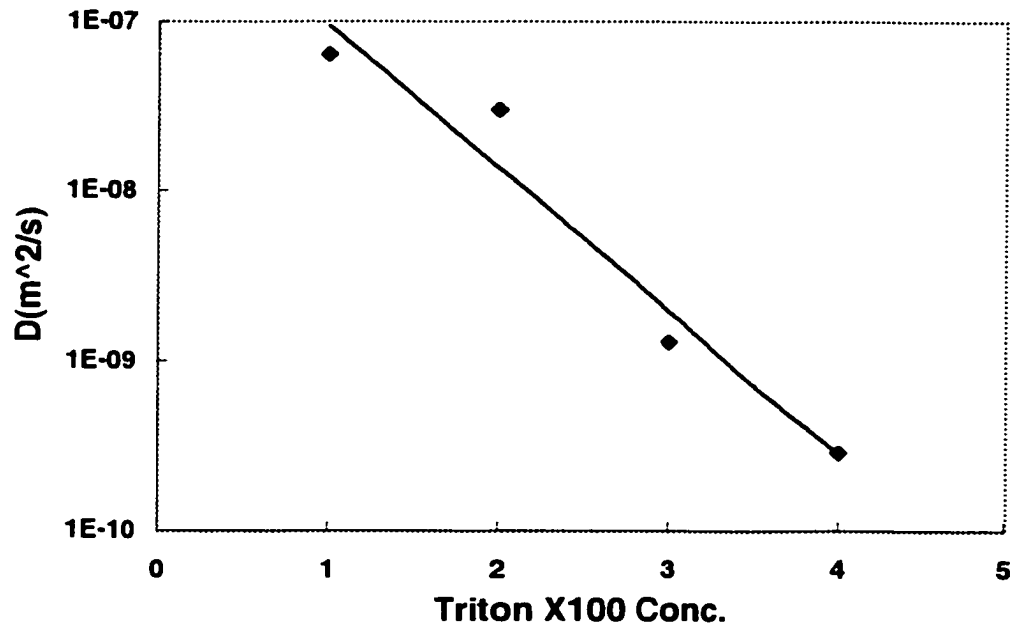


Figure H223. Effect of concentration on the SAA diffusivity in (Bayol oil/ water /Triton X100, expanding-drop technique)

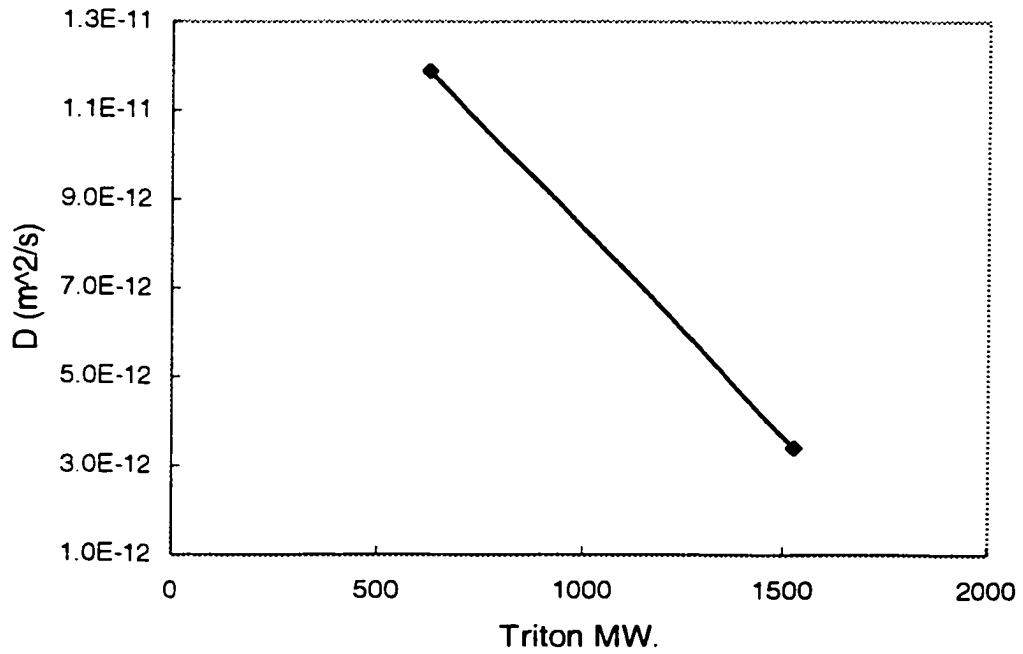


Figure H224. Effect of molecular weight/length on the SAA diffusivity in (acetophenon/ water/ 0.1 mmole/m<sup>3</sup> Triton, expanding-drop technique)



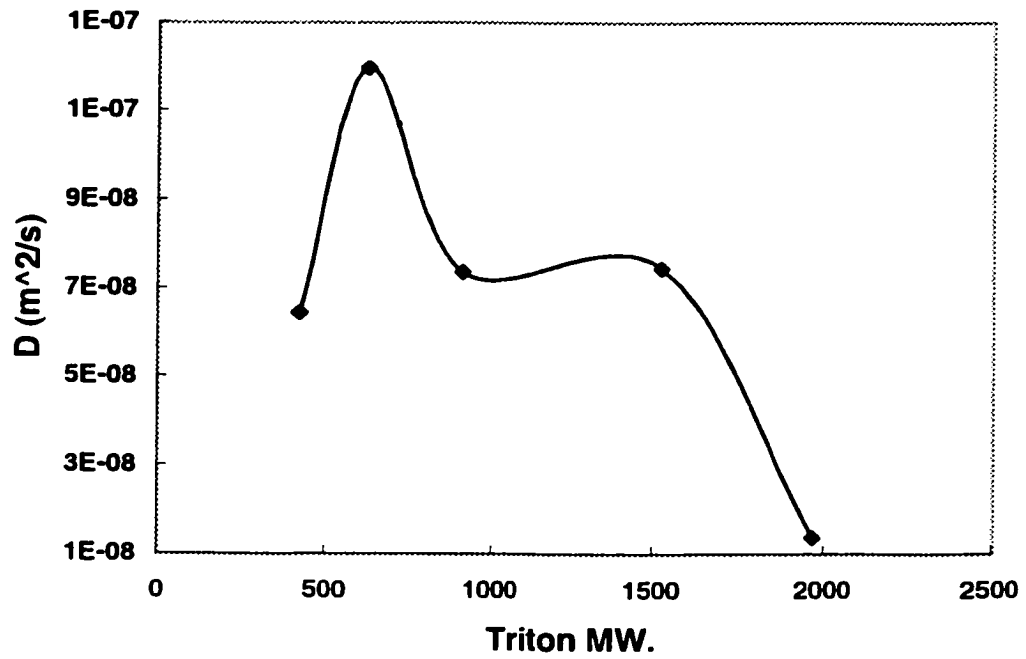


Figure H225. Effect of surfactant molecular weight/length on the SAA diffusivity in (Bayol oil/ water/  $0.1 \text{ mole}/\text{m}^3$  Triton, expanding-drop-technique)

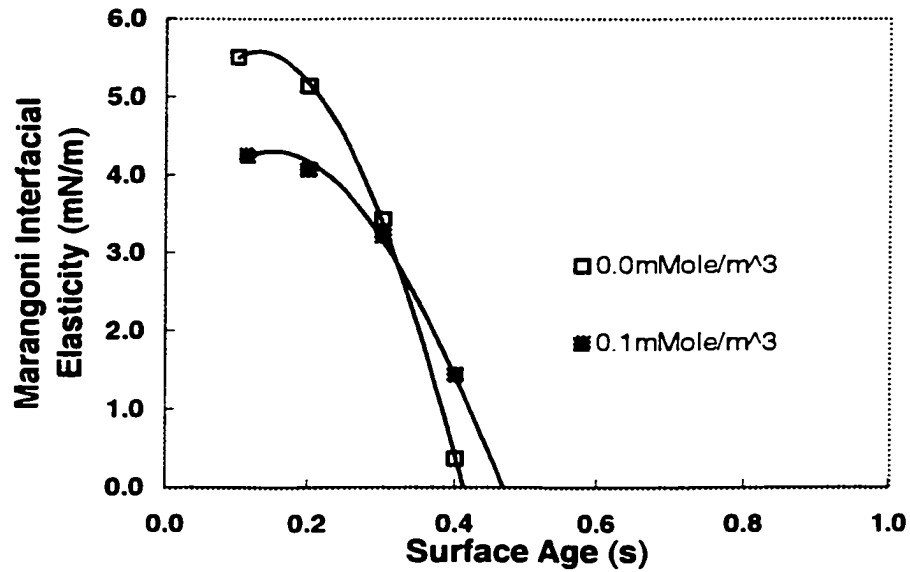


Figure H226. Effect of surfactant concentration on Marangoni interfacial elasticity of (acetophenon/ water/ Triton X305, dispersed phase flow rate= 0.0316 mLitre/min, expanding drop technique)

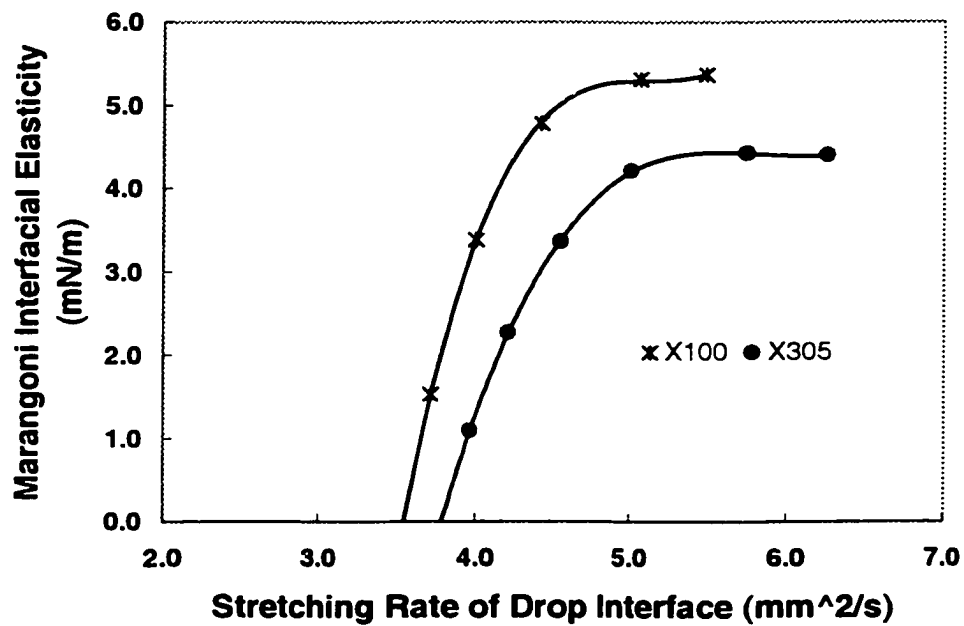


Figure H227. Effect of surfactant molecular weight/length on Marangoni interfacial elasticity of (acetophenon /water/ 0.1 mmole/m<sup>3</sup> Triton, expanding-drop-technique)

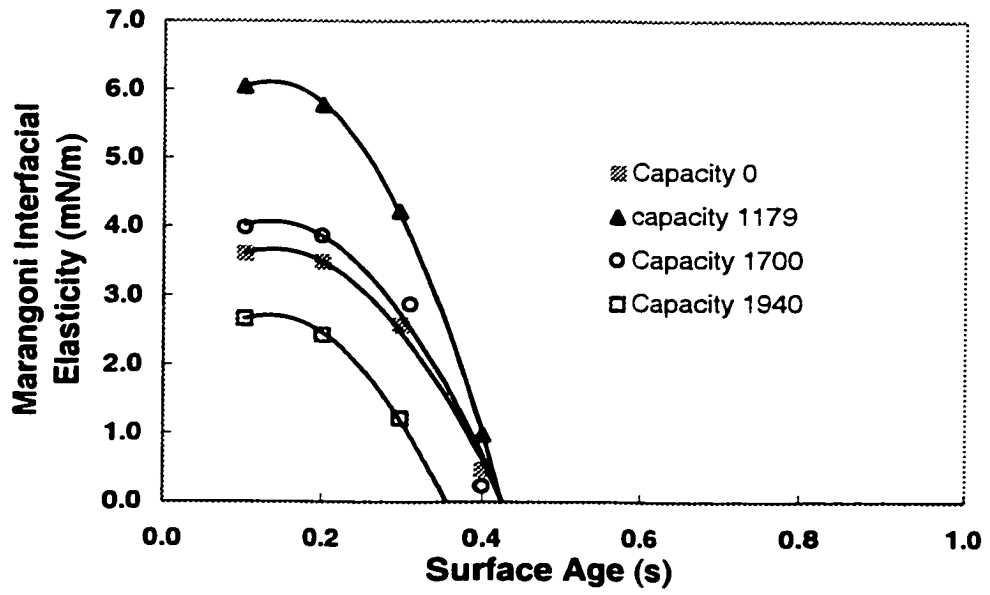


Figure H228. Effect of capacity number on Marangoni interfacial elasticity of (Irving gasoline/ industrial caustic, dispersed phase flow rate = 0.0316 mL/min, expanding-drop-technique)